HAVIC

Hydrogen Aerial Vehicle for Intercity Commuting

DSE Group 16 – Door2Door

Delft University of Technology

TU Delft

This page is intentionally left blank.

Door2Door

Final Report

Group	16
Dirk de Boer	4562771
Tim Koning	4289366
Nick Leenders	4392949
Yari Lo-Fo-Sang	4301013
Omar Mauri	4544765
Matheus Silva	4537823
Tommy Tran	4449142
Thomas Tweedy	4564901
Fleur Verschoor	4467159
Sèra Zalman	4394550

Under the supervision of Pim Groen, Clemens Dransfeld and Yi Zhang

July 2, 2019

Delft, The Netherlands

TU Delft

Preface

The Design Synthesis Exercise (DSE) is the final phase of the TU Delft Aerospace Engineering bachelor programme and Group 16 has been tasked with designing a Door2Door transportation solution. In the last 10 weeks, 10 enthusiastic and sustainably minded aerospace students worked with creativity and the engineering knowledge learned during the Aerospace BSc to attain a innovative product. The HAVIC vehicle acts as a personal car that can drive on the road and fly in the air. This report elaborates the beginning of the conceptual design phase with the mission, subsystems and technical choices.

The Door2Door project group would like to thank Pim Groen, Clemens Dransfeld, and Yi Zhang for their guidance and assistance during the first phase, and all subsequent phases of this project. The group also extends its thanks to Joris Melkert and the OSCC, most notably Sam van Elsloo, for their extensive roles in the planning and organising of the DSE.

List of Symbols

Latin	Description	Unit
a	Acceleration	[m/s^2]
a	Axial Induction Factor	[-]
b	Damping Coefficient	[kg/s]
b	Width	[m]
b	Wingspan	[m]
c	Diameter Core Material	[m]
$\bar{c}$	Mean Aerodynamic Chord	[m]
c_a	Aileron Chord	[m]
c_r	Root Chord	[m]
c_t	Tip Chord	[m]
d	Diameter Sandwich Structure	[m]
d_s	Diameter Shock Absorber	[m]
g	Gravitational Constant	[m/s^2]
h	Height	[m]
i_h	Incidence Angle Horizontal Tail	[°]
k	Spring Constant	[N/m]
k	Wing Fraction	[-]
l_h	Moment Arm Horizontal Tail	[m]
$\dot{m}$	Mass Flow	[kg/s]
n_s	Number of Landing Gears	[-]
q	Dynamic Pressure	[Pa]
s	Distance	[m]
s_s	Length of Shock Absorber	[m]
s_t	Maximum Tyre Deflection	[m]
t	Thickness	[m]
v	Deflection	[m]
v	Humidity Fraction	[-]
w	Width	[m]
A	Area	[m^2]
A	Aspect Ratio	[-]
C	Voltage Gain Constant	[-]
C_f	Skin Friction Coefficient	[-]
$C_{l_{max}}$	Maximum Lift Coefficient 2D	[-]
C_m	Moment Coefficient	[-]
C_n	Normal Force Coefficient	[-]
C_p	Power Coefficient	[-]
C_v	Vertical Tail Volume Coefficient	[-]
C_{D_i}	Induced Drag Coefficient	[-]
C_{D_0}	Zero Lift Drag	[-]
$C_{L_{max}}$	Maximum Lift Coefficient 3D	[-]
D	Drag	[N]
E	Energy	[J]
E	Young's Modules	[GPa]
F	Force	[N]
F_f	Friction Force	[N]
FF	Form Factor	[-]
I	Area Moment of Inertia	[m^4]
J	Mass Moment of Inertia	[kg/m^2]
KE	Kinetic Energy	[J]
$K1C$	Fracture Toughness	[MPa$\sqrt{m}$]
L	Lift	[N]
M	Mass	[kg]
M	Moment	[Nm]
M_f	Maximum Moment Sandwich Material	[Nm]
N	Yawing Moment	[Nm]
N_g	Load Factor Landing Gear	[-]
P	Period	[s]
P	Power	[W]
P_a	Power Available	[W]
P_m	Maximum Load per Landing Gear	[N]
P_r	Power Required	[W]
Q	Heat	[J]
Q	Humid Airflow	[m^3/s]
Q	Interference Factor	[-]
$\dot{Q}$	Heat Flow	[J/s]
R	Reaction Force	[N]
R	Specific Gas Constant	[J/kgK]
Re	Reynolds Number	[-]
S	Surface Area	[m^2]
T	Temperature	[K]
T	Thrust	[N]
U	Flow Velocity	[m/s]
V	Shear Force	[N]
V	Velocity	[m/s]
V_c	Average Voltage Fuel Cell	[V]
W	Weight	[N]
W	Work	[J]
W_{TO}	Take-Off Mass	[kg]

Greek	Description	Unit
α	Angle of Attack	[°]
α	Angular Acceleration	[rad/s^2]
γ	Damping Coefficient	[-]
γ	Specific Heat Ratio	[-]
Γ	Dihedral Angle	[°]
β	Prandtl-Glauert Compressibility Correction Factor	[-]
β	Side Slip Angle	[°]
δ	Theoretical Oswald Efficiency Coefficient	[-]
δ_a	Aileron Deflection	[°]
δ_e	Elevator Deflection	[°]
δ_r	Rudder Deflection	[°]
ϵ	Downwash Angle	[°]
η	Efficiency	[-]
$\ddot{\theta}$	Angular Acceleration	[rad/s^2]
λ	Stoichiometric Multiple	[-]
λ	Taper Ratio	[-]
Λ	Sweep Angle	[°]
μ	Friction Coefficient	[-]
ρ	Density	[kg/m^3]
σ_f	Failure Strength	[MPa]
σ_c	Strength Core Material	[MPa]
σ_y	Yield Strength	[MPa]
τ	Control Surface Effectiveness	[-]
ω	Frequency	[rad/s]

List of Abbreviations

Abbreviation	Description
c.g.	Center of Gravity
tbd	To Be Determined
Al	Aluminium
AoA	Angle of Attack
AFR	Autonomous Flight Rules
APU	Auxilary Power Unit
ATC	Air Traffic Control
ATP	Automated Tape/Tow Placement
CEF	Cost Escalator Factor
CFD	Computational Fluid Dynamics
CFRP	Carbon Fiber Reinforced Polymer
CP	Cruise Propeller
CR	Constraint Based Requirement
CTE	Coefficient of Thermal Expansion
DEP	Distributed Electric Propulsion
DRA	Discontinuous Reinforced Aluminium
DSE	Design Synthesis Exercise
EASA	European Union Aviation Safety Agency
ECMT	European Commission Mobility and Transport
ECSD	European Commission Sustainable Development
FAA	Federal Aviation Administration
FBS	Functional Breakdown Structure
FFD	Functional Flow Diagram
GH2	Gaseous Hydrogen
HAVIC	Hydrogen Aerial Vehicle for Intercity Commuting
HHV	Higher Heating Value
HLP	High Lift Propeller
HS	High Strength
HTOL	Horizontal Take-Off and Landing
IFR	Instrument Flight Rules
Li	Lithium
LE	Leading Edge
LHV	Lower Heating Value
LH2	Liquid Hydrogen
MAC	Mean Aerodynamic Chord
MLI	Multi Layer Insulation
MTOW	Maximum Take-Off Weight
NHTSA	National Highway Traffic Safety Administration
OEW	Operational Empty Weight
OSCC	Ontwerp Synthese Coordinatie Commissie
OSPL	Overall Sound Pressure Level
PEMFC	Proton Exchange Membrane Fuel Cell
PWL	Power Watt Level
QI	Quasi Isotropic
RC	Rate of Climb
RDT	Requirement Discovery Tree
RPM	Revolutions Per Minute
RTM	Resin Transfer Moulding
SED	Specific Energy Density
STOL	Short Take-Off and Landing
TE	Trailing Edge
TOL	Take-Off and Landing
TPM	Technical Performance Measurements
TR	Technical Requirement
TRL	Technical Readiness Level
UD	Unidirectional
UV	Ultra Violet
VFR	Visual Flight Rules
VHF	Very High Frequency
VTOL	Vertical Take-Off and Landing

Executive Overview

This report constitutes the Final Report of the Door2Door project, with the goal to design an aircraft and car hybrid vehicle emitting only water. The result of this goal is the design of the HAVIC.

The Final Report is primarily concerned with the further development of a concept which should meet the system requirements set by the client at the beginning of this project. This concept is worked out in detail to reach the ambitious goal of designing a sustainable flying car.

The Challenge

The goal of this project is to create a new form of transportation to address growing issues with environmental pollution and traffic congestion. The Door2Door project envisions a future where commuters can drive and fly from home to their destinations in a totally green and sustainable way, making pollution and traffic congestion a thing of the past. The client has provided the team with a mission need statement and the team has set forward a project objective, both of which are displayed below:

Mission Need Statement

To design a sustainable vehicle for the future.

Project Objective

To make a design for a water-emission only transportation vehicle for 4 persons that will be able to drive and fly, and which can be manufactured for at most $750,000.

Requirements

To identify the requirements for the Door2Door project, stakeholders are considered and their specific needs are identified. The list of stakeholders includes the client, consumers, and all relevant government organisations. For each of these stakeholders, requirements are identified and a Requirement Discovery Tree (RDT) is made. Further requirements are generated by functional analysis. The requirements are finally split into two categories: Technology-Driven Requirements (TR) and the Constraint-Based Requirements (CR).

The key requirements of the Door2Door project are specified by the client. These are the main driven design constraints that should be accomplished in the final design. These key requirements are listed below.

- The vehicle shall be capable of carrying 4 persons with an average mass of 80 kg
- The vehicle shall produce only water as its waste product
- The vehicle shall have a flying range of 322 km (200 miles) in addition to the driving range of 80 km (50 miles)

Furthermore, the client's initial requirement for Vertical Take-off and Landing (VTOL) capability was renegotiated in a trade-off conducted during the Midterm Review. The decision was then made to design a vehicle capable of travelling medium (intercity) ranges and which can appeal to the personal car and general aviation markets primarily. The vehicle's fixed-wing, Short Take-Off and Landing (STOL) design was based around these decisions.

Intercity Use Case

The intercity use case is designed for people who travel between cities, for example from the Hague to London which is shown in Figure 1. Conventional means of transportation such as the car, train, bus, or airplane could be used for this trip. However, each of these methods of travel involves a long travel time. And crucially, all of these vehicles also have a significant environmental impact and/or limited flexibility. The Door2Door's HAVIC promises to fulfil an intercity trip of this length with the flexibility of a car, the speed of airplane, and no harmful emissions. This use case will compete with personal cars, long range public transport, and regional aviation.

The time saving becomes clear when taking the example of a business person who travels from Delft to London and back twice a week. By airplane this journey takes 1 hour. However, this is excluding the travel time to the airport and the waiting time, which would add another 3 hours to the travel time. With the Door2Door vehicle this journey would only take roughly 2 hours, meaning that the time saving per week is about 8 hours. Using one vehicle for the whole journey also increases flexibility when compared to a standard airplane. It eliminates the need to rent a car or take the train or bus.

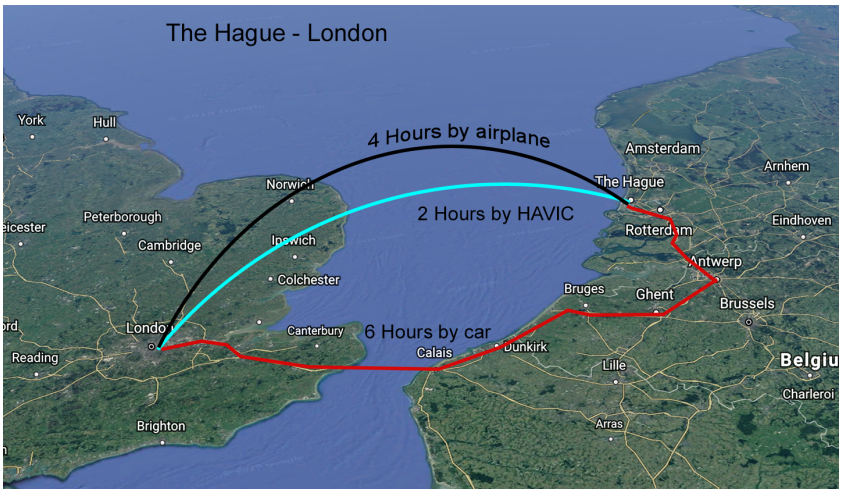

Figure 1: A comparison of travel times between the Hague and London by airplane, car, and HAVIC

Mission Profile

The HAVIC is capable of driving for up to 50 km to its take-off location, taking off and climbing to an altitude of 1.5 km, cruising for 400 km (with reserve fuel for an added 45 minutes of cruise), descending and landing, then driving for another 50 km from the landing strip to its final destination. The significant driving range and reserve fuel allow for flexibility within each trip in terms of allowable proximity to airfields.

Mass and Power Budgets

An iterative design process has been used which yielded into the final mass budget as shown in Figure 2a and all the relevant sizes of the vehicle. The HAVIC's weight estimation converges after 4 iterations with a threshold of 0.5 kg to a *Maximum Take-Off Weight (MTOW) of 1668 kg*, which corresponds to an *Operation Empty Weight (OEW) of 1292 kg*.

The system's primary power budget seen in Figure 2b was calculated by modelling the power required by the propulsion system in each phase of the mission. The vehicle uses a revolutionary distributed electric propulsion system, which is powered by a hydrogen fuel cell.

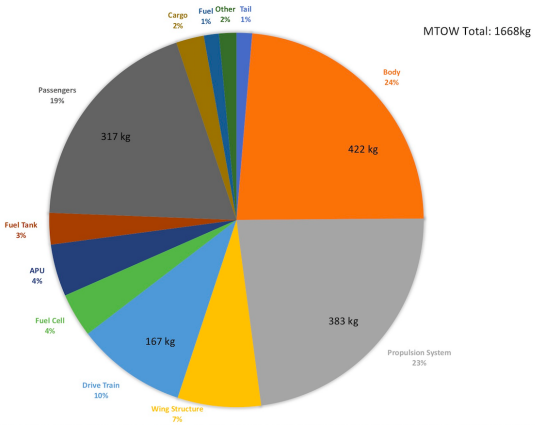

(a) Final overview of the mass of all the subsystems

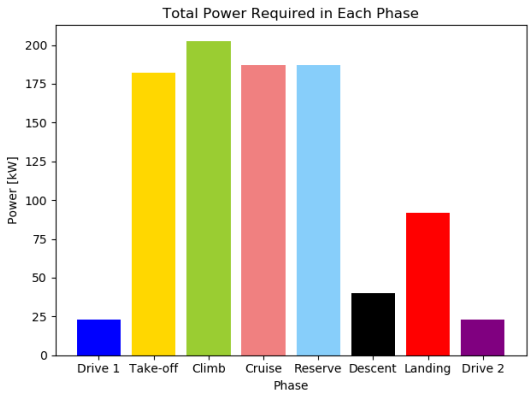

(b) A breakdown of the system's power usage over the course of the entire mission

Final Design Overview

The final design is shown in Figure 3, and a breakdown of the system specifications can be found in Table 1.

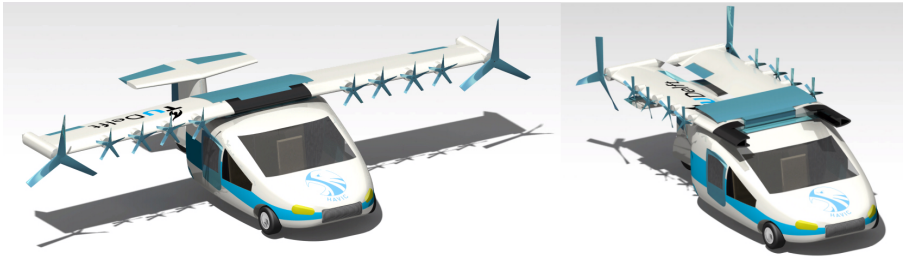

Figure 3: Rendering of the final design of the Door2Door project

Table 1: Specification overview of the HAVIC

Empty Weight	1292 kg
Payload	360 kg
Max. Fuel Weight	21.8 kg
Vehicle Length	5.45 m
Vehicle Width	2.40 m
Capacity	3 passengers + 1 pilot
High Lift Propellers	8 props (574 mm diameter)
Cruise Propellers	2 props (1524 mm diameter)
Engines	8 × Custom H20 (20 kW) and 2 × Custom H60 (60 kW)
Powerplant	2 × Powercell S3 Proton Exchange Membrane Fuel Cell (125 kW)
Fuel Type	Liquid hydrogen
Unit Cost	2.2 million USD
Cruise Speed	250 km/h
Stall Speed	92.4 km/h
Driving Speed	80 km/h
Maximum Acceleration	2.5 m/s^2
Flying Range	400 km
Driving Range	100 km
Cruise Altitude	1219.2 m (4000 ft)
Take-Off Length	428.6 m
Optimum Rate of Climb	430.8 m/min

Future Developments and Recommendations

As this conceptual design phase comes to a close, it is important to consider the next steps to be taken in the preliminary design phase. Plans have been made for extensive verification and validation procedures through aerodynamic modelling of the vehicle, the air duct and distributed electric propulsion specifically, modelling of the air intake and making a prototype, thermodynamic modelling of the tank, and structural analysis on the whole vehicle. In this way the design of the vehicle can be fine-tuned in further design phases. An initial production plan has also been put in place, keeping in mind the project's requirements on sustainability. Lastly, further improvements to the design such as the use of solar panels for charging the Auxiliary Power Unit (APU) have been investigated.

Although this Final Review is only but a small step in the design of a sustainable aircraft, the research and design work done here hopes to inspire future work by showing the possibilities of a hydrogen-powered vehicle.

Contents

1 Introduction

Transport accounts for approximately 23% of worldwide carbon emissions, where road transport alone is responsible for 16.5% of the worldwide carbon emissions [1]. In both air and ground transport, fossil fuels are still widely used and need to be replaced by more sustainable forms of energy. Moreover, congestion is a major problem in large cities and on highways. The average driver in London spends about 74 hours per year in congestion.[1] To counter this phenomenon, more and more roads are built, resulting in even more carbon emissions and pollution of the environment. With this in mind, solutions to these problems are currently being researched extensively. As means of assessment, students from the Aerospace Engineering Bachelor programme at the Delft University of Technology have been tasked with the Design Synthesis Exercise (DSE), in which it was their objective to design a sustainable flying and driving vehicle that can travel from door to door.

This is the beginning of the Door2Door project. The heart of this initiative is the vision to make sustainable travel available for everybody. This form of travelling should adhere to the highest standard of passenger comfort, while not taxing the environment. At the same time, the travel flexibility increases by having one vehicle to transport people over greater distances much faster. It is a versatile vehicle that can be used by business people and families alike. The group aims to explore new and promising techniques and incorporate them in the design. This way the Door2Door project hopes to make a real contribution to the current and future society.

This is the last report of a series comprising a Project Plan, Baseline Report, Mid-term Report and Final Report. During this process, regular meetings with the client have taken place to ensure that all the client's wishes and needs are taken into account. The process started with making a thorough planning for the duration of this project, followed by an extensive literature review and market research. These steps allowed for concept generation, from which one was chosen. This report contains the details on the worked out concepts. The report is structured in 3 main parts: the Project Mission, the Detailed Design and the Further Development.

Chapter 2 describes the definition of the minimum requirements and functionalities of the vehicle. In chapter 3 the market analysis is performed and the set of requirements is finalised. Also, the concepts, concept trade-off method and design strategy are discussed. Chapter 4 elaborates on the design of the wing. In chapter 5 the main body design is explained. Power system design is performed in chapter 6. Chapter 7 an overview of the entire design is provided. The vehicles performance is discussed in chapter 8. Chapter 9 contains all information relating to the sustainability of the Hydrogen Aerial Vehicle for Intercity Commuting (HAVIC). A financial analysis is provided in chapter 10. Compliance with the requirements is checked using a compliance matrix in chapter 11. To endure identification and mitigation of risks, a risk assessment is done in chapter 13. The operations and logistics aspect of the HAVIC are contained in chapter 14. The report is concluded by chapter 15, which states the long term vision, and the conclusion and recommendation.

[1] `http://inrix.com/scorecard/` [cited 08 May 2019]

I

Project Mission

2

Mission Analysis

Creating a new form of sustainable transportation suitable for a family is the goal of this project. The environmental pollution and traffic congestion will be reduced with this Door2Door vehicle that will drive and fly. From this the mission need statement and project objective can be derived.

Mission Need Statement

To design a sustainable vehicle for the future.

Project Objective

To make a design for a water-emission only transportation vehicle for 4 persons that will be able to drive and fly, and which can be manufactured for at most $750,000.

In this chapter the mission analysis is given that includes the explanation of the name, the non labelled requirements and the functional analysis to make a rough sketch of the design.

2.1. Name and Logo

The name Door2Door incorporates the core of the idea: travelling from your starting destination to your final destination in one vehicle. However, this does not say anything about the vehicle itself, as the Door2Door principle might as well be achieved by a bicycle or a car. From the name, it should be clear that it is a flying vehicle. Quickly it was decided that it should refer to a bird, because to be free as a bird represents the ultimate freedom of travelling anywhere at any time.

Another factor that it should contain, is the fact that it is a sustainable vehicle because it runs on hydrogen. Several ideas containing H_2 or hydro were considered, but soon dismissed. Finally, HAVIC was chosen because it is similar to "Havik", which is the Dutch word for Hawk. Also, this allowed us to incorporate the fact that it is sustainable, that it flies and even that it is used for commuting between cities. Once the name was chosen, the logo followed from that and is shown.

HAVIC

Hydrogen Aerial Vehicle for Intercity Commuting

2.2. Stakeholder Requirements

Before starting with the design, it is important to specify the vehicle. What it should be capable of and what it should include. This is stated in the requirements given by the client, requirements identified by the group and requirements that follow from the stakeholders. Stakeholders are assigned and listed below.

1. Client
2. Consumers
3. Air Traffic Control (ATC)
4. General public
5. Government
6. European Aviation Safety Agency (EASA)
7. European Commission: Mobility and Transport (ECMT)
8. European Commission: Sustainable Development (ECSD)
9. Aerospace students

The client gave the Door2Door project multiple requirements to ensure that his vision would be implemented in the vehicle. The requirements shape the vehicle and can be identified as the key requirements related to performance, safety, sustainability and cost. They are defined as follows:

- The vehicle shall be able to transport 4 people with an average mass of 80 kg
- The vehicle shall be capable of carrying 10 kg of luggage per person
- The range shall be 322 km (200 miles) flying with an additional 80 km driving range
- The maximum flying speed shall be at least 241 km/h (150 mph) at cruising altitude
- The maximum driving speed shall be at least 105 km/h (65 mph)
- The cruising altitude shall be between 0.9-1.5 km (3000-5000 ft)
- The vehicle shall have VTOL capabilities
- The vehicle shall only emit water
- The vehicle shall be in compliance with applicable aviation regulations (EASA CS23)
- The noise level shall not exceed 70 dB at 152 m (500 ft)
- Recycling of various components shall be economically viable
- The target manufacturing cost shall not exceed 1.5 times the cost of a small aircraft ($750,000)

2.3. Requirements and Constraints

Besides the clients demands a Requirements Discovery Tree (RDT) is used to identify remaining requirements. This is a tool which hierarchically presents the requirements in an AND tree. A split is made into constrained based requirements as most stakeholders are government related, and into technical requirements that are based on various configurations of the HAVIC including the subsystems. The complete RDT is displayed in Figure 2.1.

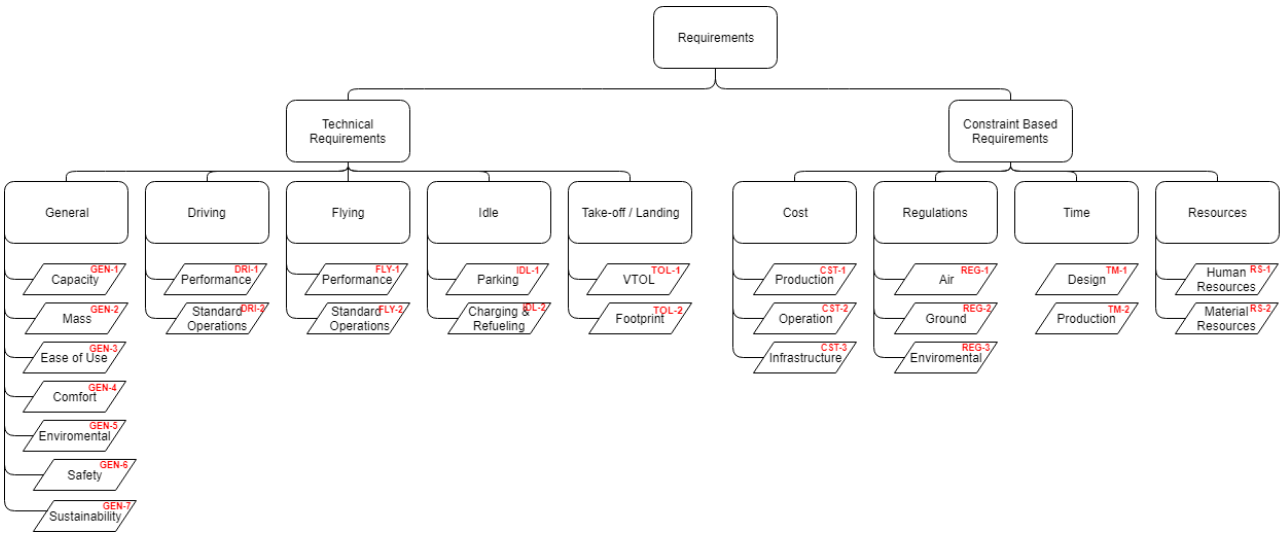

Figure 2.1: Requirement Discovery Tree

Each requirement has an associated identifier which specifies whether it is a technical requirement (TR) or constraint based requirement (CR). Within this division, requirements can further be described as either a performance condition or a theme. This is also indicated in the identifier with an abbreviation. Sub-themes are then stated with numbers. Client requirements are distinguished by a *. The complete list of the requirements that followed from this RDT can be found in the chapter 11.

2.4. Functional Analysis

The client has set the Door2Door project an explicit target for a solution to the future of green air transportation. In order to achieve this, it must be exactly clear what has to be designed so the concept phase can begin.

The first step in this process is to perform a functional analysis and discover all the tasks that the overall system must be able to perform. In order to do this, a general idea of the system is brainstormed, before breaking this down into 4 levels of detail. In this way the most basic level of functions are defined.

For the Door2Door project, the task is to design a vehicle capable of both regular road travel and air travel. It is clear from this that the functions can already be split into two main categories, those related to the flying aspect of the vehicle, and those related to the driving aspect. Furthermore, each of these operational modes require a preparation phase to prepare the vehicle for the varying conditions of flight and road use. So two more categories are derived. Since the vehicle will have distinct hardware both internally and externally during flight and driving, it is important to add a category of functions which allows the vehicle to switch from one operational mode to another and vice versa. Finally when the vehicle has completed the transportation phase of its mission, a final set of functions to 'finish the operation' must be added. This leaves 7 main functional blocks:

1. Operation of Driving Capability
2. Operation of Flying Capability
3. Preparation of Driving Capability
4. Preparation of Flying Capability
5. Conversion from Driving Capability to Flying Capability
6. Conversion from Flying Capability to Driving Capability
7. End of Operations

These 7 main functional blocks can be arranged into a functional flow diagram to show how they interact with each other and are broken down to 3 levels of detail. For a further level of detail the functions can be displayed in a functional breakdown structure.

2.4.1. Functional Flow Diagram

The Functional Flow Diagram (FFD) takes the functional blocks from the previous section and places them in a logical order of operations. For the Door2Door project, it is logical that the user can start by choosing either a driving mode or a flying mode (depending on use case and location where the vehicle was left). After this, they prepare and operate the chosen mode, before converting to a different mode and performing the new operational mode. This is illustrated in the FFD which is displayed in Figure 2.2. Each functional block is then broken down into sub functions which make up that function. Each of these functions are then broken down further so that 3 levels of detail are shown.

In the visual, the large square blocks represent the overall functional blocks, the yellow marked blocks represent sub functions and the blue marked blocks represent the 3rd level sub functions. Since the Door2Door project is a new field, and concepts are yet to be generated, some of the functions are given on a very broad level, this allows room for innovation and concept generation to achieve the functions. The sub functions are defined using logical understanding of both flying and driving: all cars must be able to accelerate, decelerate, turn and stop whilst all aircraft must be able to accelerate, decelerate, take off, cruise, manoeuvre, land and taxi. Furthermore, the sub-functions for the preparation blocks can be defined independently for flight and driving by investigation into pre-flight checks, and standard pre-driving checks such as adjusting mirrors and checking fluid levels.

The coloured arrows on the functional flow represent the different variations of use of the vehicle. Since it is not restricted to the standard drive-then-fly order of operations. It is possible in one use cycle to utilise the vehicle only for driving as such the yellow arrow in the visual bypasses the aircraft use operations. Similarly, if the vehicle was left in an airfield or appropriate take-off location, it is possible to bypass the driving operations (see red arrow). Finally, it is possible for the vehicle to be used in an infinite loop of driving followed by flying, followed by driving etc. This is demonstrated by the green arrow. The true/false blocks represent check gates. When a check has been performed, it must pass a set of predetermined requirements (e.g. there must be $< x >$m of visibility) and only if the check is true will the path be allowed to continue. The flow diagram includes the emergency operations path, which is only traversed in the case of a mid-air emergency (denoted by the blue arrows) and denotes the functions required during a midair incident that requires an emergency landing.

2.4.2. Functional Breakdown Structure

The functional flow diagram shows the logical order of the functions performed by the Door2Door vehicle. However from a design point of view, it is sometimes easier to design and derive requirements if the functions are grouped in different ways. This is where the Functional Breakdown Structure (FBS) comes into play. The FBS shows all the same functions as the FFD but in a tree format rather than a chronological format. This makes it easier to divide the functions into groups. In the FBS, it has been chosen to subdivide the functional blocks into 3 categories: functions which prepare the vehicle for operation, functions which serve to actually operate the vehicle and functions which serve to convert the vehicle between operating modes. These three are displayed as the top level of the FBS Tree. Lastly, a 4th level of detail is added, each blue marked sub function is further divided into base level functions which the system can perform. These are displayed within the green boxes on the visual. The complete FFD and FBS are displayed in Figure 2.2 and Figure 2.3 respectively.

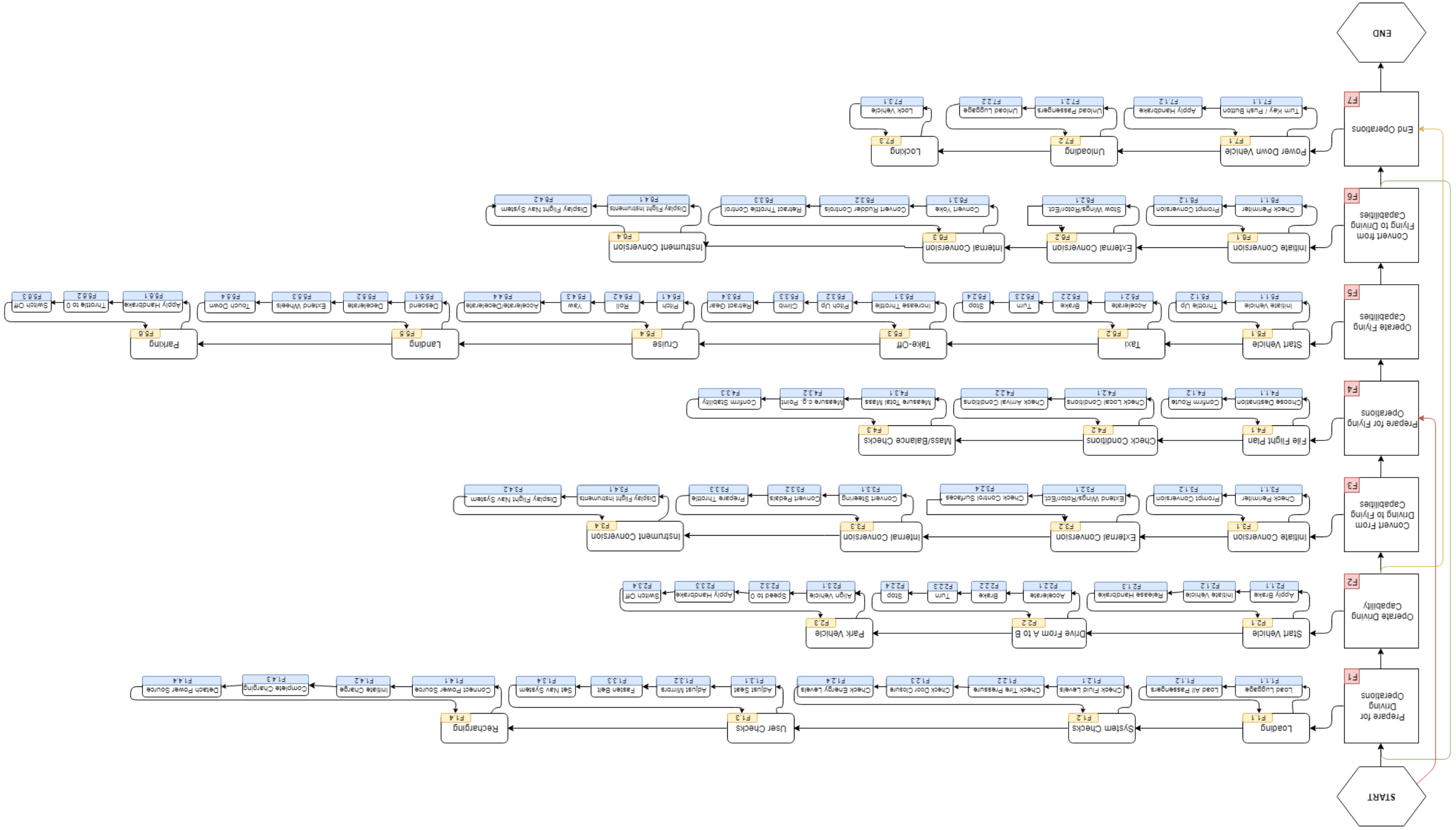

Figure 2.2: Functional Flow Diagram

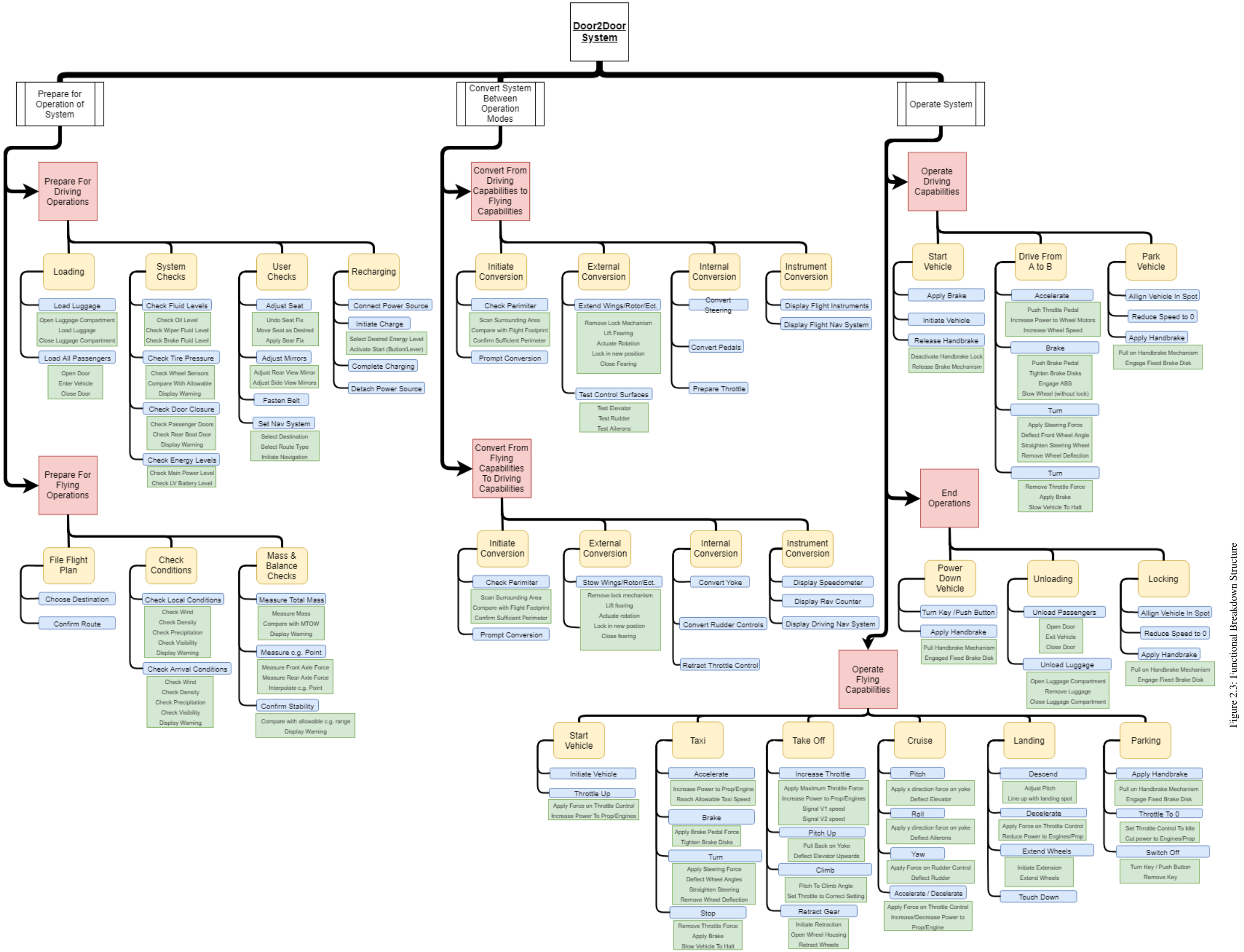

Figure 2.3: Functional Breakdown Structure

3

Concept Development

This chapter elaborates on the process to the final concept selection. First, a market analysis is performed in section 3.1. Next a trade-off between two different use cases is discussed in section 3.2. From the selected use case, a concept is selected in section 3.4 and the potential competitors are discussed in section 3.3. Finally, section 3.5 gives an overview of the characteristics of the winning concept and its requirements. This forms the basis for the continuation of the design process.

3.1. Market Analysis

Market analysis is a quantitative and qualitative assessment which is key to assessing the probability that the product will manage to break into attractive markets. This section identifies the potential markets for this project and discusses the potentials for market entry.

The potential markets will depend mainly on the use case of the vehicle. Since the vehicle shall be able to fly and drive, it must compete with existing vehicles on various markets. The most direct and promising markets for this vehicle are the personal car market, the taxi market and the commercial small aviation market. These markets are discussed and compared to each other by the Competitive Forces Model[1] shown in Figure 3.1. This method treats the intensity of industry rivalry, threat of potential entrants, bargaining power of buyers and suppliers and the threat of substitute goods or services for each market.

Figure 3.1: Competitive Forces Model

3.1.1. Personal Car Market

The personal car market is a very large market. 6.1% of the EU population is employed in the sector and it provides €413 million of tax income for the EU.[2] This market is where most existing flying cars projects are currently trying to break through. Examples of these projects are the AeroMobil[3] and Terrafugia[4]. Vehicles designed for this particular market should be designed for the use case of intracity travel and medium range travel. Breaking into this market can be considered the most difficult. The challenge lies mainly in competing with traditional cars and replacing the traditional, driving car with a flying car as the standard.

[1] https://corporatefinanceinstitute.com/resources/knowledge/strategy [cited 1 May 2019]
[2] https://www.acea.be/press-releases/P10 [cited 2 May 2019]
[3] https://www.aeromobil.com/aeromobil-5_0-vtol/ [cited 1 May 2019]
[4] https://terrafugia.com/transition/ [cited 1 May 2019]

For this market the intensity of industry rivalry can be considered very high. The market has a large number of competing companies building traditional cars, as well as many currently creating concepts for flying cars. Customers often have a quite high brand loyalty and might have difficulties transitioning from their current personal car to a flying car, especially if it concerns a vehicle from a new company that is not operating on the automotive market yet.[5] The fact that the flying car will have a higher cost than traditional cars, further complicates the breakthrough of a flying car into this market. These factors also contribute to the threat of potential entrants. Due to the wide usage of personal cars, a large number of regulations exist, which complicates certification on this market. Wide application of the flying car will most likely require even more government regulations that also have to be taken into account.[6] The bargaining power of buyers is considered low. The group of buyers can be considered as everyone who owns a personal car or is looking to buy one currently, which is a very large group.[7] An individual in this group usually buys one car, which makes the bargaining power of an individual low. Also the bargaining power of suppliers is considered low. Many suppliers for the automotive industry exist, so parts or sub-assemblies are widely available on this market. Lastly, there is a moderate threat of substitute goods/services. Although there are a lot of personal cars available, there are not a lot of flying cars available yet. Early existing designs estimate a quite high selling price.[8] An affordable flying car could have a good chance of a breakthrough in this market.

Concluding, while a breakthrough of a flying car in this market is considered difficult, there is a high number of potential buyers. A reasonably priced, new technology, can have a high potency to breakthrough in the market. A very important factor that needs to be taken into account, is how this flying car will compete with the numerous current designs of flying cars aimed at the personal car market.

3.1.2. Taxi Market

The taxi market is a growing market with a few large companies such as Gett, Uber and Lyft already in existence. These companies strive for fast transportation from A to B for customers at low cost. Vehicles designed for this market should be designed for intracity travel. Recently, the taxi services provided by larger companies have wiped out traditional taxi drivers, mainly due to the present technology which allows the customer to order a cab and pay at any location within a few seconds. The taxi market targets customers who need transportation for short distances especially in a crowded city. In case of large distances, it is cost wise more beneficial to travel by your own car. For example, a transportation with a taxi-service between San Francisco to San Jose, costs about $68.70. In case of travelling with your own car, assuming the average price of $1.075 per liter of fuel and a travel distance of 78 km, the total cost adds up to $5.60. Therefore, it is clear that travelling by car on your own is by far less expensive than the transportation offered by taxi-services.

For this market the intensity of industry rivalry and threat of potential entrants are considered high. The competitiveness between large companies is increasing and with the rapid increase in technology, new companies have the opportunity to enter the market. One consequence of the rising technology is the concept of the flying car which is introduced by Uber under the service name Uber-Air.[9] Uber-Air is expected to launch in 2023. The concept of the flying car will expand the market even further and add an additional transportation option for the customers. The bargaining power of buyers is considered low. There is a large number of potential buyers as taxi services are demanded in crowded areas such as cities. The bargaining power of suppliers is also considered low, since there are a variety of taxi companies competing against each other to offer the lowest price for the customers. The threat of substitute goods/services can be considered low. Currently, there are no substitutes for taxi services that provides the same quality or a higher utility.

In conclusion, even though there has been a rapid increase in technology and the feasibility to produce a flying car which can be put on the market has increased, the concept is still a hard task to accomplish in the modern day. The flying car transportation has to compete with the conventional transportation provided by taxi companies.

[5] https://www.cbtnews.com/automotive-brand-loyalty-important-well/ [cited 9 May 2019]
[6] https://www.wired.com/story/congress-flying-cars-regulation/ [cited 9 May 2019]
[7] https://www.huffingtonpost.ca/2011/08/23/car-population_n_934291.html [cited 9 May 2019]
[8] https://www.businessinsider.com/aeromobil-1-million [cited 9 May 2019]
[9] https://www.ig.com/nl/nieuws-en-trading-ideeen/overig-nieuws/ [cited 1 May 2019]

3.1.3. Commercial Small Aviation Market

The commercial small aviation market has been around for a while and recent innovations of small electric planes are making the industry more sustainable and commercially attractive.[10] A prediction by Airbus states that within ten years, short-haul flights will increase by a factor of 1.8. This is going to require 28,550 more small passenger aircraft over the next 20 years [2], so the commercial small aviation market is rapidly growing. This market is considered as the use case of long range travel. Whenever long range travel is mentioned further on in this section, it refers to this use case of 400-550 km. The challenge for a breakthrough in this market mainly lies in making a four person vehicle efficient for long range travel.

For the commercial small aviation market, the intensity of industry rivalry can be considered reasonably high. Airlines have connected nearby cities with multiple flights per day for a low price, while air charters and private plane owners provide flexible transport between cities. The threat of potential entrants is considered high. Commercial aircraft that operate on long range travel, have a large number of requirements and require extensive certification by airworthiness authorities. Aircraft manufacturers, airlines and air charters have a large expertise in this sector and have build up trust with the costumer. For this market, the bargaining power of buyers is moderate. Currently, the group of buyers in this market is limited to mostly airlines, air charters and some private aircraft owners. Since air charter travellers and private aircraft owners are a relatively small group in society and short-haul flight are rarely taken on a daily basis, the group can be considered medium size when comparing to previous analysed markets [3]. The buyer where the most potential will probably be, is the private owner, because the vehicle is designed for door to door transport. The limited number of passengers is another aspect that makes private owners potential buyers and makes the vehicle less attractive for airlines or air charters. Also the bargaining power of suppliers is low to moderate. There are various suppliers on the market, so most parts and sub-assemblies are widely available.[11] The threat of substitute goods/services can be considered moderate. Various vehicles already exist on the market for long range travel, however there are a lack of vehicles flying on sustainable energy, which makes a sustainable vehicle a relatively untapped market.[12] There is also no product available on the market that offers the multiple uses of both flying and driving that a flying car offers.

Concluding, while there are quite some competitors on this market providing low-cost or flexible travel, there is no service that combines the low costs and flexibility. On top of that, a flying car provides more functionality than a normal aircraft. A huge threat is making a 4-seat vehicle efficient enough to make it viable for long range. If this can be accomplished, the commercial small aviation market can have potential for a flying car.

3.1.4. Summary Potential Markets

All potential markets are compared in Table 3.1 on the competitive forces model and their market size. Although the design may be entering into one of the three markets, the design itself is different compared to the vehicles that are already existing. The design is unique since it produces at most water as an emission, will carry four passengers and is able to fly and drive , which have a significant contribution to the emissions problem and is also able to convert from driving configuration into flying mode. Furthermore, a SWOT has been made which is shown in Figure 3.2.

Table 3.1: Comparative view of potential markets

	Personal Car Market	Taxi Market	Commercial Small Aviation
Intensity of Industry Rivalry	Very high	High	Reasonably high
Threat of Potential Entrants	High	High	High
Bargaining Power of Buyers	Low	Low	Moderate
Bargaining Power of Suppliers	Low	Low	Low to moderate
Threat of Substitute Goods/Services	Moderate	Low	Moderate
Market Size	Very large	Moderate	Large

[10] https://www.electrive.com/2017/11/28/100-seater-hybrid-aircraft-take-off-2020/ [cited 1 May 2019]

[11] https://www.globalair.com/directories/Aircraft-Parts-21.html [cited 9 May 2019]

[12] https://www.marketwatch.com/press-release/more-electric-aircraft-market-2019-global%2Dindustry-overview-by-size-share-trends-technology-drivers-and-challenges-with%2Dregional-forecast-and-to-2023-2019-01-17 [cited 9 May 2019]

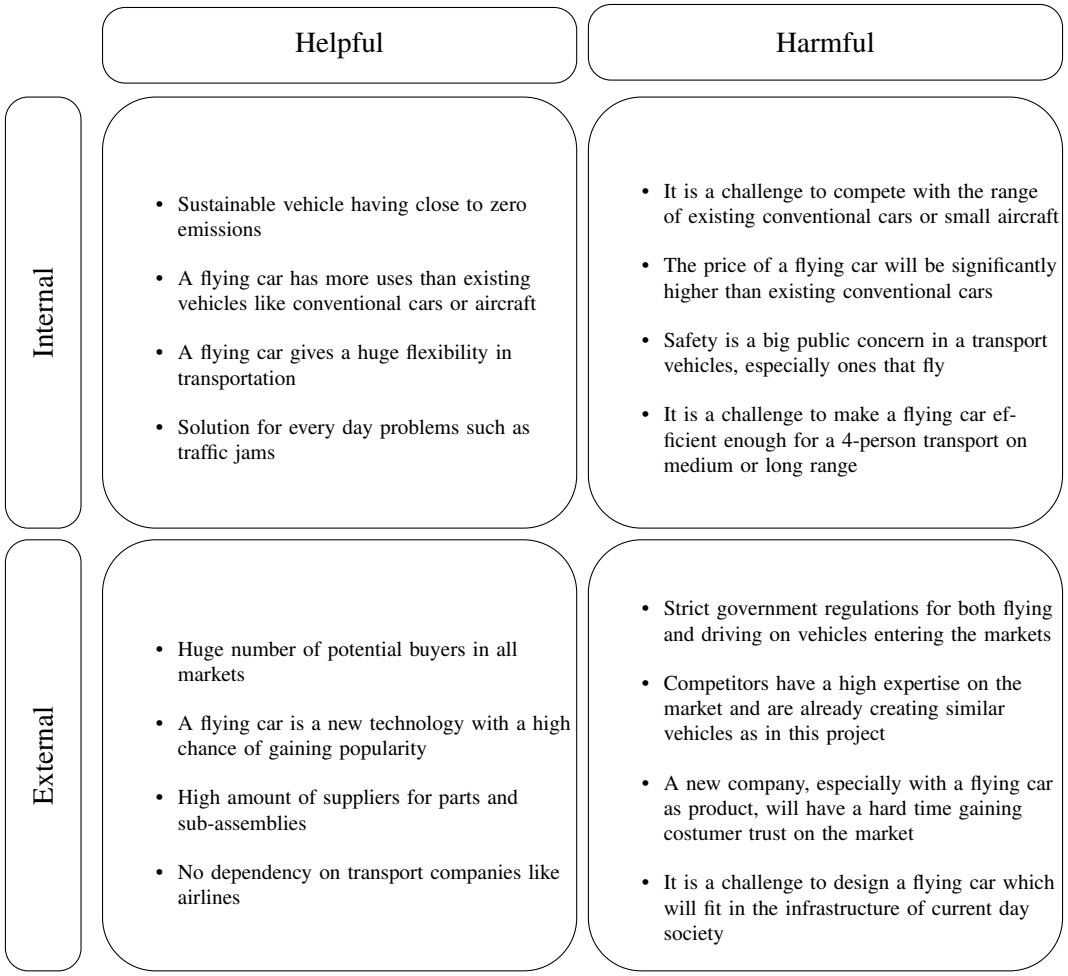

Figure 3.2: SWOT matrix for the market analysis

3.2. Use Cases

While performing the exploratory literature study, it became apparent that not all requirements as stated in section 2.2 and section 2.3 could be satisfied at the same time. That is why two specific use cases are defined, each with their own set of requirements. They are defined as the intercity and intracity use case and explained in the following sections.

3.2.1. Intercity (HTOL)

The intercity use case is designed for people who travel between cities for example from the Hague to London. The conventional transportation vehicles such as the car, train, bus or airplane could be used. However, each of these has a long travel time. They also have a significant environmental impact and limited flexibility. The Door2Door vehicle for the intercity use case would be able to take you literally from Door2Door while providing the flexibility of also having a means of transport at your destination. This use case will compete with personal cars, long range public transport and regional aviation. This yields the following unique requirements:

REQ-UC1-FLY-RANGE: The vehicle shall have a flying range of 400 km

REQ-UC1-DRI-RANGE: The vehicle shall have a driving range of 100 km in addition to the flying range

REQ-UC1-FLY-TOL: The vehicle shall have Horizontal Take-Off and Landing (HTOL)

This use case vehicle would make use of already existing airfields as shown in Figure 3.3a and Figure 3.3b, meaning there is no immediate need for additional infrastructure. Because of the limited size of the vehicle, it can also make use of glider airfields. On the other hand, already busy airfields would have to have time slots

available for the Door2Door vehicles. While this is quite affordable at €2.51 per 1000 kg per take-off [4], it might pose a logistics problem. Once the vehicle becomes widely used, it might be necessary to build extra Take-Off and Landing (TOL) sites, which can be tailored to the Door2Door vehicle.

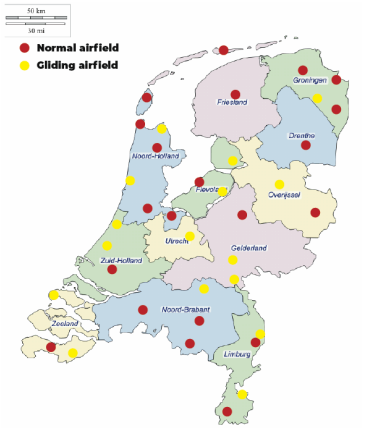

(a) Airfields in the Netherlands

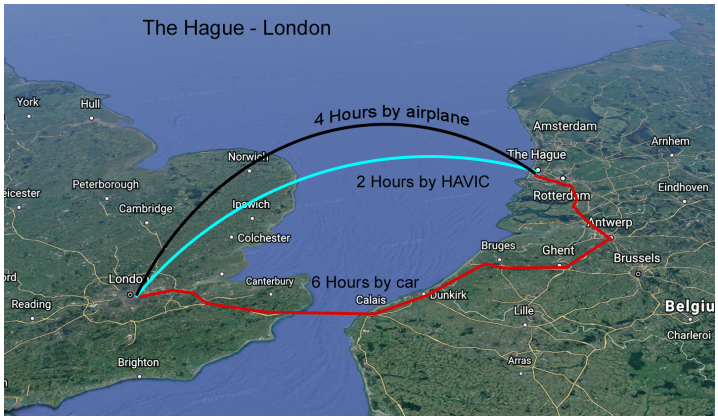

(b) Route from The Hague to London

The time saving becomes clear when taking the example of a business person who travels from Delft to London and back twice a week. By airplane this journey takes 1 hour, however this is excluding the travel time to the airport and the waiting time, which would add another 3 hours to the travel time. With the Door2Door vehicle this journey would only take roughly 2 hours, meaning that the time saving per week is about 8 hours. Also using one vehicle for the whole journey increases flexibility. It eliminates the need to rent a car or transport your car with you.

The vehicle will fly under Instrument Flight Rules (IFR) to maximise its flexibility. Flying IFR means that you are not restricted by environmental conditions such as night time or bad weather. However, this means that contact with ATC is required. Also, it would mean that the user needs to have not only a driver's license but also a pilot's license with an IFR rating.[13] The latter might be costly and difficult to obtain for the users. Additionally, it requires the submission of a flight plan prior to your travel. The vehicle itself shall operate in accordance with the both the applicable road and air regulations.

3.2.2. Intracity (VTOL)

The intracity use case is aimed at people travelling within cities. This vehicle would be ideal for people living and working on opposite sides of town. Congestion is a daily struggle for these users, meaning that they often have long travel times for relatively short distances. Public transport might be a solution, but this is often at the cost of passenger comfort. Additionally, that many non sustainable personal vehicles have a negative environmental impact. The vehicle would have to be adjusted to operate in limited space as cities are often densely populated. This use case would compete with personal cars, public transport and taxi companies. This leads to the following requirements:

REQ-UC2-FLY-RANGE: The vehicle shall have a flying range of 80 km

REQ-UC2-DRI-RANGE: The vehicle shall have a driving range of 20 km in addition to the flying range

REQ-UC2-FLY-TOL: The vehicle shall have Vertical Take-Off and Landing (VTOL)

The current infrastructure is not ready to accommodate air travel within the city. For the Door2Door result, one would have to be able to take off and land close to the destination, such that the driving distance is minimised. This would require the placement of helipads and heliports throughout the city. As a test case, TOL sites were placed on map of the city centre of Rotterdam, the result can be seen in Figure 3.4. The red circles represent a 1 km radius, which means that a large part of Rotterdam is covered using this placement. Some existing infrastructure might be converted for the Door2Door purpose, such as parking lots or train stations.

[13] https://epicflightacademy.com/vfr-pilot-rating-vs-ifr-pilot-rating/ [cited 23 May 2019]

Traffic studies could be used for the ideal placement of the TOL sites. Even if the TOL site is not immediately available, the waiting time will be limited because TOL can take place at a rapid pace.

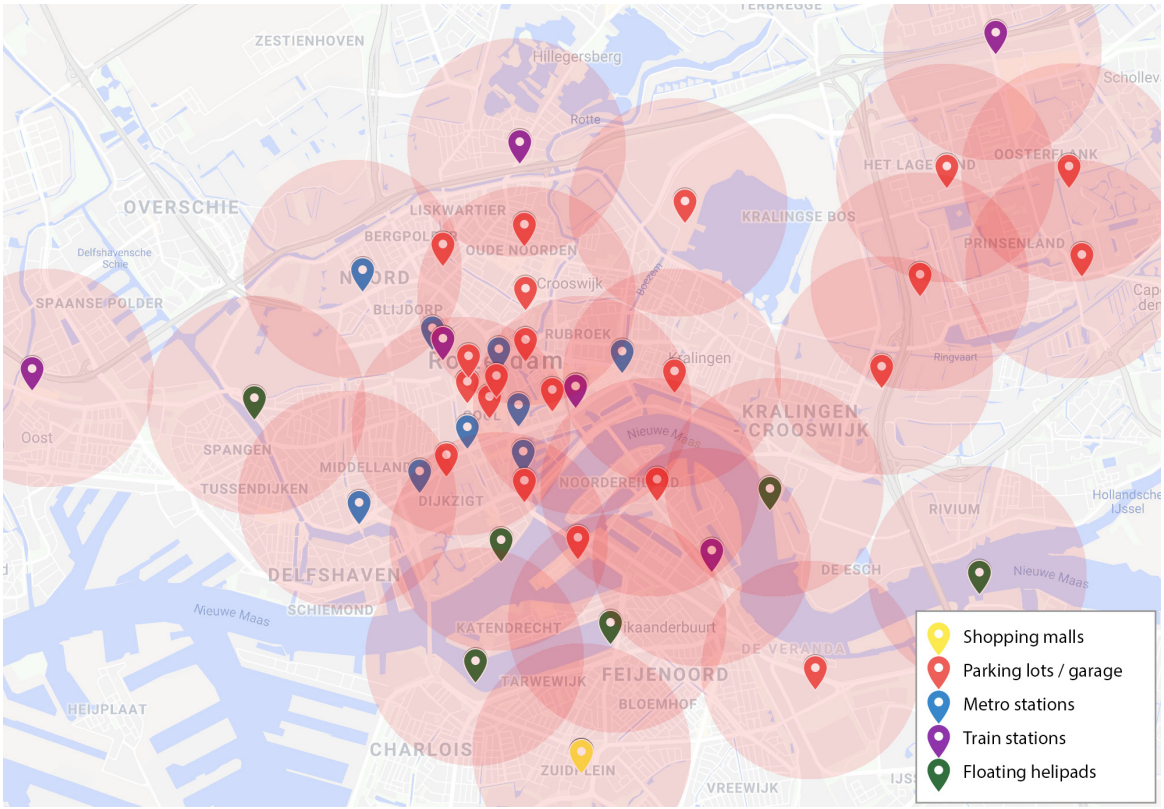

Figure 3.4: Helipad placement in Rotterdam

The time saving for this use case will be maximised during rush hour. The test cases were set in varying environments such as Los Angeles or Sydney, to test the robustness of the use case. A time saving of around 25% resulted. The strength of this use case is the frequency that it will be used, which will probably be multiple times a day. You may use it to get to work, but also to get groceries or visit friends.

This vehicle could be operated under Visual Flight Rules (VFR) when it is first introduced. This limits flexibility greatly, as there are strict visual requirements. Once this vehicle gains ground and technology advances, the vehicle might be automated. Automation would increase efficiency and might allow for less strict license rules. However, fully automated manned aircraft are still heavily debated and still have a long way to go for certification.

3.2.3. Trade-Off

In order to perform the trade-off between the two use cases, 12 criteria were selected. These were assigned a weight between 1-10. For the assignment of weights, the importance to the project and the design as a whole of each criterion was considered. For the scoring of the use cases, a fixed point system of 10 points per criterion was used. All scores are multiplied with the weight and summed to the final score. The scores, weights and final scores are displayed in Table 3.2 and Table 3.3.

1. *Existing TOL Sites*: This criterion is used as a measure for the extra infrastructure required by the use case.
2. *Area used by TOL Site*: For this criterion the area used by a complete TOL site is taken into account.
3. *Reduction in Emissions*: Reduction in emissions is a sustainable aspect of this trade-off. In both use cases the vehicle itself would be designed to emit only water vapour.
4. *Noise Pollution* : For both use cases it was assumed that they would comply with the regulations concerning noise levels, so the location of TOL sites became the deciding factor.
5. *Flexibility*: The flexibility of the use cases was measured based on how easy one could decide to travel somewhere.

6. *Total Power Usage*: The power usage of both systems is compared primarily from initial basic calculations, but also from basic engineering knowledge.
7. *Total Energy Usage*: The total energy usage is derived from the power.
8. *Time Saving*: Most relative time savings on a weekly basis.
9. *Competitors*: The number of existing competitors in the same market.
10. *Potential Customers*: The number of potential customers for a use case.
11. *Regulation*: Both the VTOL and HTOL have to comply with the regulations set by the Federal Aviation Administration (FAA) and the National Highway Traffic Safety Administration (NHTSA), but the feasibility of compliance to these regulations can be compared.
12. *Technical Readiness Level (TRL)*: This criterion will compare the technical readiness for both use cases.

Table 3.2: Use case trade-off table

Category	Existing TOL Sites	Area used by Site	Reduction in Emission	Noise Pollution	Flexibility	Energy Usage
Weight	5	4	8	4	10	10
Use Case 1 (VTOL)	2	7	6	1	7	3
Use Case 2 (HTOL)	8	3	4	9	3	7

Category	Time Savings	Power Usage	Competitors	Potential Customers	Regulations	TRL
Weight	10	4	8	10	6	3
Use Case 1 (VTOL)	6	2	3	7	4	4
Use Case 2 (HTOL)	4	8	7	3	6	6

Table 3.3: Result of the use case trade-off

Category	Final Result
Intracity (VTOL)	438
Intercity (HTOL)	482

In Table 3.3, it can be seen that the intercity use case came out the trade-off as a winner. The intercity use case is superior because it will fit better into current society. No additional infrastructure has to be built and the technology required is more mature than for the intracity. Also, noise pollution from the intercity cause would cause far less annoyance as it would operate from airfields and fly at a higher altitude. This vehicle will most likely be a fixed wing vehicle, while the intracity case would use a rotorcraft. Since fixed wing vehicles are more efficient, it scores better on power and energy usage. The intercity has a unique market, while the intracity would have to compete with similar initiatives such as Uber Elevate and Volocopter. Also, since the flying operations will be similar to those of existing aircraft, a lot of regulations are already in place to accommodate for this. Overall, the intercity case is more feasible at the moment. This means we will only work further on this use case, while also keeping the knowledge gained from the intracity use case.

3.3. Competitors

In the HTOL use case, many different competitors already exist in the form of small aviation aircraft, however, none these aircraft are not able to drive on the road, nor are they sustainably powered. Aeromobil[14] and Terrafugia[15], shown in Figure 3.5 and Figure 3.6 are direct competitors in this use case, capable of flying and driving, but are both powered by fossil fuels and can only carry up to two persons at a time. The Door2Door project aims to design a vehicle capable of flying and driving, transporting four passengers including luggage, while using a sustainable power source.

[14] https://https://www.aeromobil.com/evolution//[cited 1 July 2019]
[15] https://terrafugia.com/transition/[cited 1 July 2019]

Figure 3.5: The Aeronobil 3.0

Figure 3.6: The Terrafugia Transition

3.4. Concepts

For the chosen intercity use case, three concepts were developed further and considered in a final trade-off. With the specific requirements the concepts are designed to achieve a 400 km flying range with Short Take-Off and Landing (STOL) capabilities. For these HTOL specification, a fixed-wing is needed and applied to all of the concepts. To generate enough lift in this short take-off airstrip, a new sort of propulsion is considered; distributed propulsion. Having several small diameter, high Revolutions Per Minute (RPM) electric propellers placed along the leading edge of a wing surface increases the flow velocity over the wings and generates more lift for a given airspeed and wing area. Because the small RPM propellers do not produce enough thrust, two larger diameter, lower RPM propellers (called cruise propellers) are added to generate the majority of the thrust during cruise where very high lift coefficients are not necessary. This design choice was quintessential for guaranteeing STOL capabilities for these aircraft without sacrificing range or requiring very large wing surfaces (which would have increased the road area of the vehicle when in driving mode). Three different concepts are described below, including the Eagle, the Surfboard and the Canard.

3.4.1. Eagle

This first concept is called the Eagle and has a traditional aircraft configuration with two large main wing surfaces near its midpoint and a T-tail in the back with two horizontal tail surfaces and one vertical tail surface. This can be seen in Figure 3.7. Propulsion is achieved through four small High-Lift Propellers (HLP) propellers along each of the main wings, and one larger Cruise Propeller (CP) near the tip of each wing. This placement of the cruise propellers was found to be the most efficient, as it has aerodynamic benefits. The transformation to a road vehicle is accomplished through movement and rotation of the two main wings on rails onto the roof of the vehicle. The drivetrain has only three wheels (two at the front and one at the back) to reduce weight and cross-sectional area.

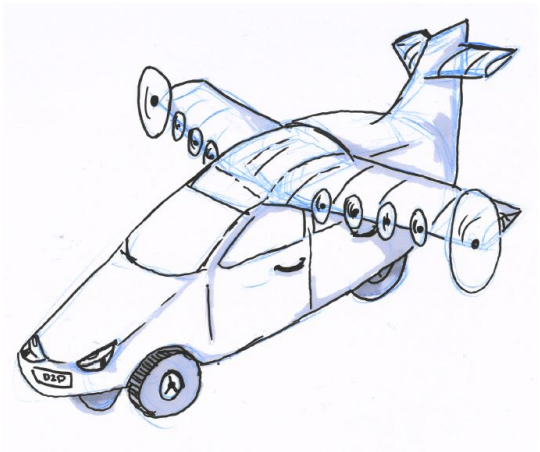

Figure 3.7: An illustration of the Eagle concept

This concept has the benefits of an efficient propeller configuration, a relatively small road area and a relatively low complexity transformation system. Its drawbacks include negative lift generation at the tail surface (for stability), and inferior rolling stability on the road due to the tricycle layout.

3.4.2. Surfboard

This vehicle also has a mostly traditional aircraft configuration with one large main wing surface above the cabin and an H-tail in the back with one horizontal tail surface and two vertical tail surfaces as can be seen in Figure 3.8. Propulsion is achieved through eight HLP along the main wing, and two CP near the ends of the wing. The transformation to a road vehicle is accomplished through the rotation of the entire wing surface about an axis on top of the roof of the vehicle. The ends of the wing then fold over about two joints to shorten wingspan and improve visibility in the driving configuration. The drivetrain has four wheels as a regular car. This concept has the benefit of an efficient propeller configuration. Its drawbacks include negative lift

generation at the tail surface (for stability), a relatively large road area, and a complex wing folding mechanism.

3.4.3. Canard

This vehicle has a canard configuration, meaning its main wing surfaces are behind the centre of mass of the vehicle and the horizontal tailplane is near the front of the vehicle (making it a Canard surface), which is shown in Figure 3.9. This allows the vehicle to maintain longitudinal stability while producing positive lift at both wing surfaces, which is more efficient than producing negative lift at the tail. Yaw control is achieved through differential thrusting of the distributed propellers, of which there are three on each Canard surface and four on each of the main wings. The vehicle also has a single cruise propeller at the back, which is less aerodynamically efficient and produces less total thrust than having two cruise propellers on the wings. The transformation to a road vehicle is accomplished through the retraction of the canard into the front of the vehicle and the rotation of the main wings about pin joints on the roof of the vehicle.

This concept has the benefit of positive lift generation at the canard surface, and a relatively small road area. Its drawbacks include no vertical tail surface for yaw stability and control, and an inefficient propeller configuration.

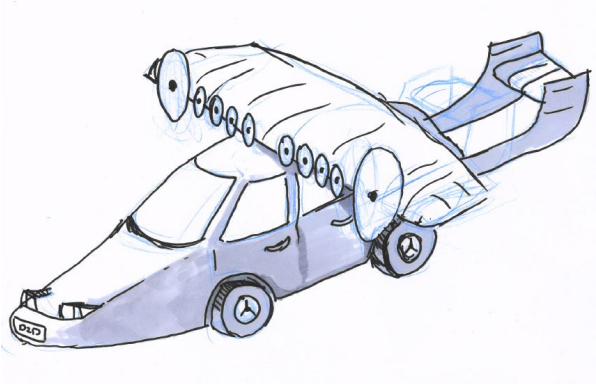

Figure 3.8: An illustration of the Surfboard concept

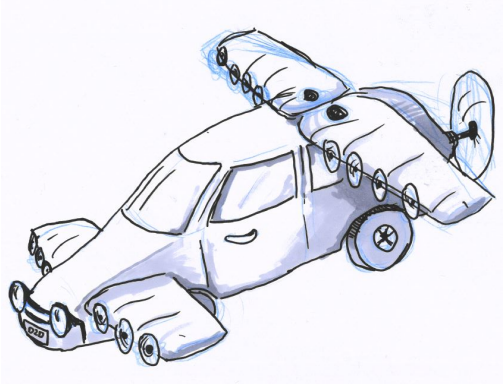

Figure 3.9: An illustration of the Canard concept

3.4.4. Trade-Off

The concept trade-off is a very important procedure in the design process. Not only does the trade-off give a basis for the final design, but it also allows for discussion of the advantages and disadvantages of each concept. This enables the team to get an overview of the concepts and ensures that beneficial parts of each design will be considered even once the trade-off is complete. In order to keep the trade-off method as fair as possible a strict set of six criteria is set. A fixed-point system is used so every concept can be ranked out of ten regardless of the score of the other concepts.

1. *Mass*: Total mass is taken into account including the expected structural mass increase from the mechanical complexity of design e.g. joints adding weight.
2. *Ease of Design*: This criterion takes into account the complexity of the folding/retracting mechanisms used in the concept as well as the existing knowledge the group has on the design.
3. *Power Usage*: To make a quantitative analysis, the maximum power usage in kW/kg of two similar vehicles was considered: AeroMobil 4.0 at 0.23 kW/kg and a Cessna 172 at 0.1 kW/kg. The comparison was done using interpolation with the same maximum power as a 172 Cessna achieving a 10 and the same score as the AeroMobil achieving a 0.
4. *Road Size*: The road size is important for the ease of use for the customer, for example when handling and parking a smaller vehicle gives better results. The lower bound for the length was taken as the length of an average American car parking space, 4.2 m. The upper bound was the length of an average stretched limousine, 9.14 m. The lower bound of the width was the width of a limousine 1.98 m and the upper bound the width of an American car parking space, 2.6 m.
5. *Energy Usage*: The energy needed to fly a range of 400 km and drive 100 km is calculated and compared.
6. *Take-off Speed*: Lower take-off speed typically results in a shorter take-off distance, positively influencing the chance of meeting the STOL requirement. Furthermore, a low take-off speed could lead to an easier construction of future infrastructure.

Finally one of the three concepts considered is chosen as a basis for the final design of the vehicle. However, this does not mean the other two concepts are completely discarded. Beneficial parts of the designs that have not been chosen are still taken into the final design, so the final vehicle still contains subsystems from designs that are not chosen. When determining the trade-off criteria and assigning them weights, the main factor considered was the feasibility of the design for the given requirements. The weight of each criterion is determined not only by the influence it has on the feasibility of the design, but also by the accuracy of the values that are currently available for the comparison between designs. Table 3.4 shows the result of the final trade off. The concept with the highest score is the Eagle concept and is therefore chosen as a basis for the final design.

Table 3.4: Trade-off between the three concepts

Criteria	Road Size	Ease of Design	Energy Usage	Power Required	Take-Off Speed	Total
Weight	10	9	7	6	4	36
Eagle	9	6	5	9	8	265
Surfboard	6	3	4	8	8	195
Canard	6	4	4	8	6	196

3.5. Design Strategy

Taking the previously chosen concept as a starting point, the design strategy could be developed. The initial design stayed close to the concept as shown in Figure 3.7. The only difference was that the cruciform tail was replaced by a T-tail, leaving more space for the wings when in driving configuration.

3.5.1. Design Iteration Method

The design of one subsystem has a great influence on the design of another subsystem. This is the reason for this project to use an iterative design method. This ensures that when a parameter changes in one of the subsystems, it automatically changes in the code that determines the parameters for another subsystem. A schematic overview of how this project's code works is shown in Figure 3.10.

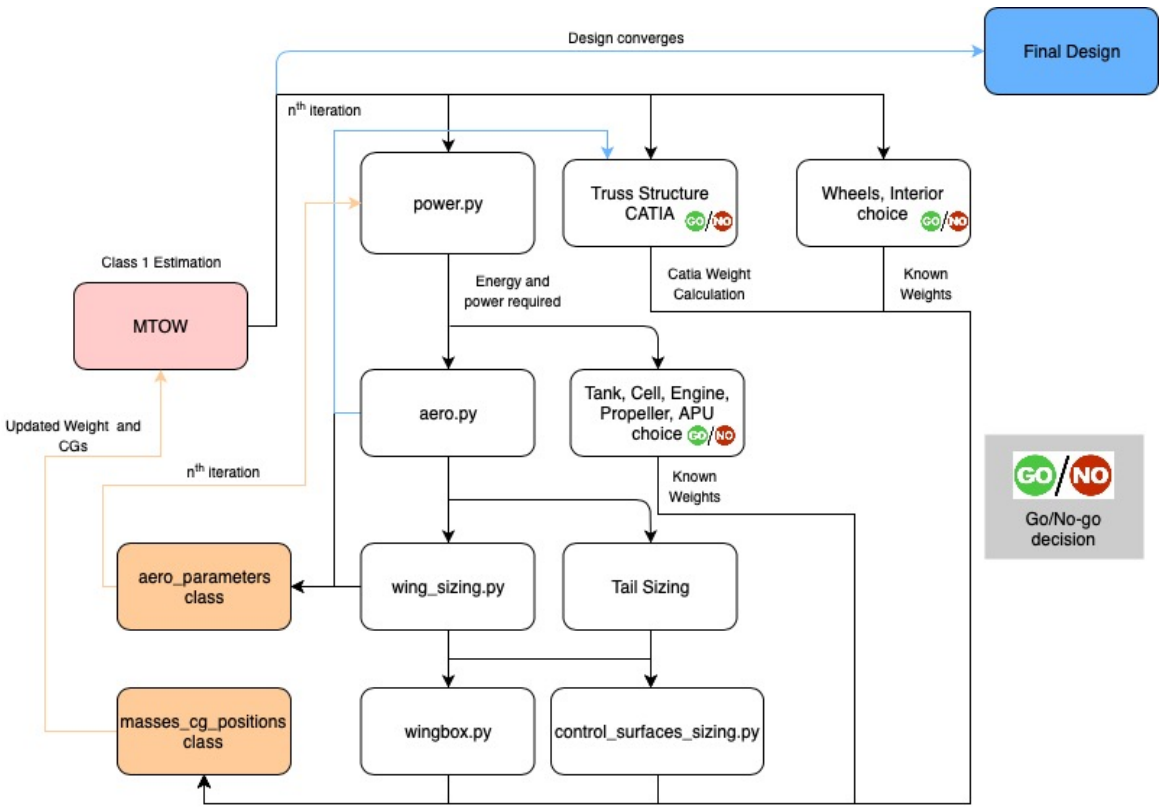

Figure 3.10: Diagram that illustrates the design iteration method

The iteration starts with a Maximum Take-Off Weight (MTOW) which is obtained by a Class I weight estimation. Some initial estimates are then taken for the masses and center of gravity (c.g.) locations of subsystems, which are placed in the $masses\_cg\_positions$ class. Initial estimates are taken for the aerodynamic values as well and inserted in $aero\_parameters$. The program is now runned and sends these parameters to $power.py$, which contains the given flight profile and calculates the required energy and power that is needed by the vehicle. Now $aero.py$ calculates the required lift and aerodynamic properties needed for this power and energy. The wing planform is then determined in $wing\_sizing.py$. All the parameters obtained from these calculation are stored in $aero\_parameters.py$. $wingbox.py$ can now determine the dimensions of the wing box and the tail is sized from these calculations as well after which $control\_surfaces\_sizing.py$ calculates the dimensions and locations of the rudder, aileron and elevator. The weights from the components is calculated and stored in $masses\_cg\_positions$.

At the same time a truss structure in CATIA is provided with the weights and aerodynamic loads in limiting flight conditions, where CATIA then calculates if the structure can withstand these loads. A go/no-go decision is then made that depending if the structure can withstand the loads. If it cannot, the truss structure needs to be redesigned until it can withstand the loads. If it can, the mass of the structure is updated in $masses\_cg\_positions$.

Since the design is using existing parts, the specifications of these parts are put into the program where it checks if these parts meet requirements of the energy, power or loads, from which another go/no-go decision is taken. In case of a No-go decision, another part has to be chosen that meets these requirements. In case of a Go decision, the masses are put in $masses\_cg\_positions$. This program will be ran until the MTOW converges. All the design parameters can now be put into the final design. Once a change has to be made to the design, the process can be easily repeated with this iterative design method.

3.5.2. Materials Choice

In order to ensure a successful design in the field of the Materials & Manufacturing, the goals and scopes are determined at the start of the process. From this four main steps are established:

1. Determine the material (family) for the main components
2. Determine the manufacturing methods for the main components. This is documented in the production plan in section 15.2
3. Integrate sustainability into the material choice and manufacturing methods, which will be further discussed in chapter 9
4. Update the weight estimate by implementing the chosen materials into the CATIA model

The main components are the following:

- *Frame*, the skeleton of the vehicle which has a double function as the air frame and the chassis
- *Hydrogen tank*, this should take into account all safety measures
- *Skin*, includes the fuselage and the wings
- *Mechanisms*, this includes all mechanisms required for the wing folding
- *Wing box*, the wing box is broken into two parts and it should still withstand all loads
- *Interior*, this should be designed for maximum safety and passenger comfort

The final goal is to have a material choice and manufacturing method for all main components. Additionally, a cost estimate will be produced and the sustainability aspect is elaborated upon. The process is done is co-operation with various departments. For the frame, tank, skin, mechanisms, and wing box the structures department is involved, as this department sets the requirements on the mechanical material properties. Additionally, the ground system, power & propulsion, and the aerodynamics engineers are involved when a material is chosen for their department. Special attention is reserved for the material of the fuel tank, as this poses a challenge. All material properties are taken from the database provided by CES edupack [5].

The very first pioneers flew on aircraft made of wood. They later transitioned to metals, and currently another transition to composites is taking place [6]. In 2011 and 2013 the Boeing 787 Dreamliner and the Airbus A350

XWB were introduced, both of which having over 50% of their weight composed of composite material[16][17]. For most of the structural components of the Door2Door vehicle, a composite and a metal option are considered. Depending on the specific requirements for that part, a material (family) was chosen. Composites are desirable for their specific properties, as they tend to be lighter than metal alloys. Apart from their low density, they also save weight in their joining. For example in the Boeing 787 Dreamliner, 50,000 rivets were saved per airplane [18]. One of the main disadvantages of composites is that damage such as delamination is not visible from the exterior. Also, they are not as extensively tested as metal alloys are, and thus their behaviour is not yet predictable. Composite structures might require an integrity inspection after a collision, even when there is no external damage visible. Techniques for inspection include ultrasonic measurements, acoustic emission analysis, and thermography [7]. Another difference between metals and composites is their manufacturability, which is elaborated upon in section 15.2

3.6. Concept Development Recap

From the market analysis it followed that two different use cases are feasible for the Door2Door hydrogen vehicle: the short range VTOL use case and the medium range STOL use case. Ultimately the medium range STOL use case was chosen to further develop. Three concepts were generated which differ in wing stowing mechanism, empennage design, and drivetrain. These concepts all considered DEP as their propulsion type powered by a sustainable fuel source. Out of the three concepts, the Eagle concept was chosen after an extensive trade-off. The main attributes of the Eagle concepts are its Distributed Electric Propulsion (DEP) system, sustainable fuel source, backwards rotatable wings, traditional T-tail, and a three-wheel configuration.

From chapter 4 onwards, the Eagle concept will be referred to as the HAVIC and the design process from Eagle to HAVIC will be laid out.

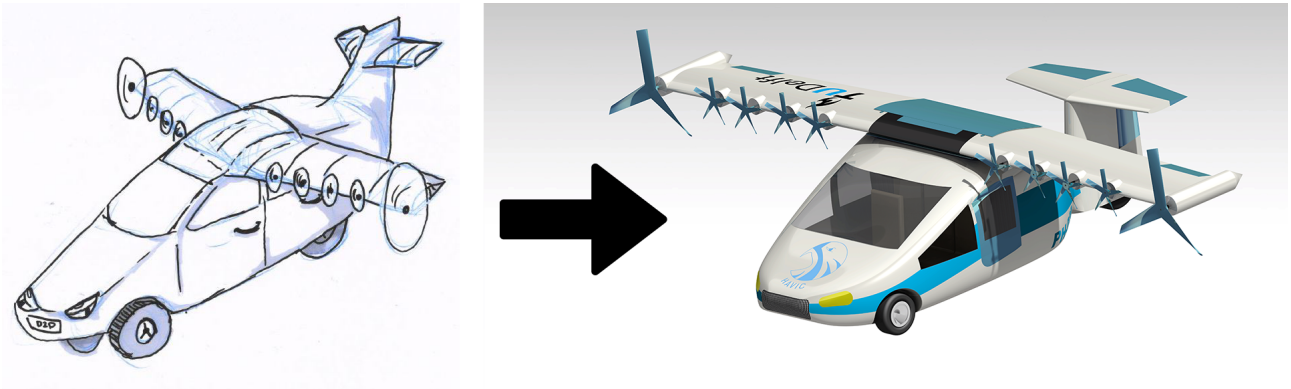

Figure 3.11: From Eagle to HAVIC

[16] https://www.azom.com/article.aspx?ArticleID=7858 [cited 15 June 2019]
[17] https://www.sciencedirect.com/topics/engineering/boeing-787-dreamliner [cited 15 June 2019]
[18] https://www.thoughtco.com/boeings-787-dreamliner-820385 [cited 13 June 2019]

II

Detailed Design

4

Wing Design

In this part, the details of the HAVIC's design are presented together with the design process itself. This chapter concerns the wing design specifically. Design methods and trade-offs are shown in this chapter, while the final results of the wing design are presented in chapter 7. The components of the wing that are being discussed are the distributed propulsion on the wing in section 4.1, the aerodynamic design, including the wing planform and airfoil choice in section 4.2, the wing box design in section 4.3, the wing folding mechanism in section 4.4, and finally the aileron sizing in section 4.5.

4.1. Propulsion System

In order to maximise flexibility, STOL capabilities are desirable. This requires either that the HAVIC is capable of accelerating to a high take-off speed very quickly or that the aerodynamic surfaces of the aircraft produce enough lift to take off at relatively low speeds. The former is a challenging goal to reach with fully electrically-powered propulsion. The latter is also difficult to achieve with a wingspan that is limited by road regulations, but distributed electric propulsion has shown promising results for such an application in NASA studies.[1]

Distributed electric propulsion typically involves placing several small diameter, high RPM propellers along the leading edge of the wing. These propellers act to speed up the flow over the airfoil, which in turn increases lift generation for a given airspeed. Computational Fluid Dynamics (CFD) simulations and experiments performed by NASA have shown this technique to achieve lift coefficients as high as 5.5 for flapped wings (up from 2.5 without power). The downside of this configuration is that small diameter, high RPM propellers are less efficient in generating thrust than large diameter, low RPM propellers.[2] It was therefore chosen to place the so-called HLP along the leading edge of the middle part of the wing to facilitate TOL and two larger CP at the wing tips to improve cruise efficiency.

An estimate for the speed increase and thrust generated by each propeller was performed using a simple actuator disk model [8]. The actuator disk model is based on the following assumptions: no frictional drag, constant pressure increment or thrust per unit area over the disk, continuity of velocity through the disk, an infinite number of blades and homogeneous, and incompressible, steady-state fluid flow.

[1] https://aero.larc.nasa.gov/files/2012/11/Distributed-Electric-Propulsion-Aircraft.pdf [cited 17 May 2019]
[2] https://web.mit.edu/16.unified/www/FALL/thermodynamics/notes/node86.html [cited 21 May 2019]

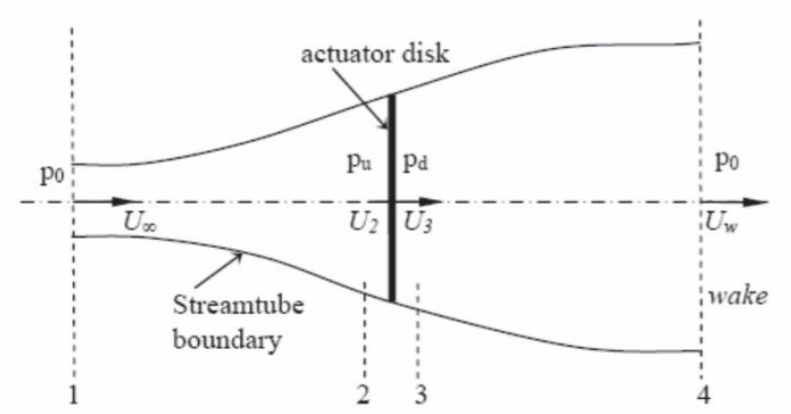

Figure 4.1: Illustration of the actuator disk model, with four stations defined (1: free-stream region, 2: just before the blades, 3: just after the blades, and 4: wake region) [8]

According to this model as shown in Figure 4.1, the flow speeds at stations 3 and 4 can be expressed as in Equation 4.1, Equation 4.2, using the definition of the axial induction factor a given.

$$U_R = U_\infty(1-a) \qquad (4.1) \qquad\qquad U_w = U_\infty(1-2a) \qquad (4.2)$$

$$a = \frac{U_\infty - U_R}{U_\infty}$$

Equation 4.3 is used to find the power output of the rotor, making use of the earlier results for Equation 4.1 and Equation 4.2. This represents the power transferred to the fluid.

$$P = TU_R = \frac{1}{2}A\rho\left(U_\infty^2 - U_w^2\right)U_R = P = 2\rho A U_\infty^3 a(1-a)^2 \qquad (4.3)$$

In order to find the power which must actually be provided to the propellers, the propeller efficiency must additionally be accounted for. This can be accomplished through an algorithm based on the momentum theory [9]. Through this method, propeller efficiencies are calculated separately for the (HLP) and the (CP) for each flight condition (i.e. altitude and velocity). The power fed to the propulsion system can then be calculated as $P_{in} = P_{out}/\eta_{prop}$, with P_{out} being calculated with Equation 4.3. Propeller efficiency and wake velocity values for the different mission phases are provided in Table 4.1 below.

Table 4.1: Propeller values at different mission phases

	V_∞ [m/s]	$V_{wake,HLP}$ [m/s]	$V_{wake,CP}$ [m/s]	η_{HLP} [-]	η_{CP} [-]	T_{HLP} [N]	T_{CP} [N]
Take-Off	30.8	54.2	30.8	0.81	0.87	2537.9	0.0
Climb	45.0	54.8	45.0	0.85	0.89	1165.9	0.0
Cruise	69.4	76.2	74.7	0.86	0.90	1089.3	1492.8
Reserve	69.4	76.2	74.7	0.86	0.90	1089.3	1492.8
Descent	31.0	31.0	39.3	0.80	0.87	0.0	1134.7
Landing	39.0	56.0	39.0	0.83	0.88	1928.8	0.0

With the required power known, the required current that has to flow from the fuel cell to the electric motor can be calculated. This current is needed to size the power cables and determine the mass of these cables. For the HLP and CP, a maximum current of 285 ampere and 342 ampere is found respectively. Larger diameter cables are needed when the current is higher. For the HLP a cable density of 0.723 kg/m is found and for the CP a density of 0.844 kg/m.[3] These suited cables will have a combined mass of 23 kg. During further development of the design, this aspect will be elaborated upon.

The thrust or driving force required for a given mission phase is calculated as the sum of the drag acting on the entire vehicle, the friction force acting on the vehicle (if the wheels are touching the floor), and the

[3] https://en.wikibooks.org/wiki/Engineering_Tables/Standard_Wire_Gauge [cited 18 June 2019]

force required to accelerate the vehicle (if the vehicle is accelerating, e.g. during take-off) as can be seen in Equation 4.4.

$$T = D + F_f + ma = D + mg\mu + ma \tag{4.4}$$

During take-off, the HLPs and cruise propellers are throttled to their maximum power to produce the thrust needed and to increase the lift generation. In the ascend to cruise altitude, the power levels are tuned to provide maximum rate of climb. During landing, the power levels of the propellers are once again tuned to provide the necessary lift, but decrease the thrust production of the propellers, such that the speed can be lowered to a minimum. In any other flight condition, the HLPs power is lowered to a minimum as it is most efficient to use the CPs to provide the required thrust.
Upon iteration of the thrust and power and calculations and integration with the other subsystems, the required power for the CP and HLP is calculated and available electric engines are selected. It is chosen to have individual electric motors driving each propeller, as opposed to having engines which drive more than one propeller. This results in a simpler shaft and gear box design, allows for the HLP and CP to be throttled separately, gives greater redundancy for single points of failure, and yields smaller engines which can be placed within the wing box in the case of the HLP. The CPs' engines are placed in a nacelle on top of the wing.

The diameters of the CP and HLP and resulting propeller configurations are also optimised. A smaller diameter for either the HLP or the CP results in a greater number of propellers distributed along the wing. This improves the clearance of the wings but also decreases propulsive efficiency and thus increases the power required. The resulting specifications of the propulsion system are presented in Table 4.2 below. This includes the electric engines which are kept in nacelles along the wing. These engine specifications are elaborated upon in chapter 6.

Table 4.2: Final specifications of the propulsion subsystem

	HLP	CP
Propeller	MH114 Airfoil	MH117 Airfoil
Number of Propellers [-]	8	2
Propeller Diameter [m]	0.576	1.524
Number of Blades [-]	5	3
Mass per Propeller [kg]	16.36	30.0
Engine	Custom H20	Custom H60
Maximum Power [kW]	20.0	60.0
Torque [Nm]	80.12	237.4
Shaft Diameter [cm]	2.09	3.59
Length [mm]	133	209
Diameter [mm]	200	280
Mass per Engine [kg]	8.2	30.0

4.2. Aerodynamic Characteristics

In this section, the choice of wing aerodynamic parameters and reasoning for these are given. In subsection 4.2.1, the wing size and shape are found and stated. Later on, in subsection 4.2.2, the process of finding an airfoil and its result are given.

4.2.1. Wing Planform

The wing area and shape are very limited due to size constraints in driving configuration: the maximum possible span is 8.8 m and the root chord can not be larger than 1.2 m, as the wings have to fit side by side and the HAVIC is 2.4 m wide. Furthermore, as the propellers are in front of the leading edge, it would be beneficial for the leading edge to be straight to make sure thrust is pointing forward.

The required area is mainly determined by the weight and take-off speed and is restricted by the size constraints. As the high weight in combination with the small possible wing size would lead to high take-off velocities, STOL would not be possible anymore. For this reason, a combination of propellers is placed just in front of the leading edge to accelerate the airflow and increase the velocity the airfoil feels, increasing lift. This is mostly

achieved by the 8 HLP, plus 2 CP on the wingtips. The extra velocity over the wing is found by a simplified disk analysis given in section 4.1, but NASA has also done computational modelling on this.[4] As not all portions of the wing contain propellers, the average velocity over the wing is a weighted combination between the wake behind the HLP, the wake behind the CP and the areas with no wake, as can be seen in Equation 4.5.

$$V_{wing} = k_{noprops}V_{\infty} + k_{CP}V_{CP} + k_{HLP}V_{HLP} \tag{4.5}$$

Finally, using this, the current estimate of the MTOW and a estimate of the C_{Lmax}, the wing area can be found using Equation 4.6.

$$S = \frac{1.1MTOW}{\frac{1}{2}\rho V_{w_{take-off}}^2 C_{L_{max}}} \tag{4.6}$$

As lift increases with the square of velocity, it would be better to calculate the lift per section and then sum them. However, since the calculation is reversed (the required lift is known and the areas have to be found), this cannot be done. The method of Equation 4.5 and Equation 4.6 is conservative, resulting in an underestimated lift and a larger surface area than needed. Checking the actual lift after finding the area and iterating optimise the result. After that, with this wing area and the average cruise weight, the design lift coefficient can be found using Equation 4.7.

$$C_{L_{design}} = \frac{1.1(\frac{1}{2}W_{Cruise_{start}} + \frac{1}{2}W_{Cruise_{end}})}{\frac{1}{2}\rho V_{w_{cruise}}^2 S} \tag{4.7}$$

With the set wing area, the dimensions can be altered with optional taper, sweep, twist, dihedral and high lift devices. The choices made for the HAVIC vehicle are elaborated below.

When the tip chord is smaller than the root chord, the wing shape is closer to the optimal elliptical wing shape, making it aerodynamically more efficient and increasing the Oswald efficiency [10]. However, a *tapered wing* needs a larger root chord length for having the same Mean Aerodynamic Chord (MAC), which is limited by size constraints. Furthermore, the Leading Edge (LE) will not be straight anymore, but will be rotated back slightly. This is not optimal as the thrust is most efficient when it is pointing exactly forward. A normal taper ratio is for this reason not applicable for the HAVIC, but a taper in combination with sweep is.

Backward *sweep* is mostly used for aircraft that experience highly compressible flow over the wings. The sweep is applied to reduce the drag and avoid shockwaves. The cruise Mach number for the HAVIC is below 0.25, making it reasonable to assume incompressible flow. Backward sweep is for this reason not an beneficial option. As already mentioned before, the thrust should point forward, where the propeller axles and their engines are placed in the wings, which limits the LE to be straight. As the required wing area is a rectangle of 8.8 m by 1.08 m, it is decided to add a small taper ratio of 0.87 to increase aerodynamic efficiency. The root chord is designed to be a little smaller than 1.2 m to add a margin. Forward sweep will be applied to have a straight LE. The precise parameters can be found in Table 4.3.

Twist is not used as a twisted wing would be very complex to fit on the roof in driving configuration

Dihedral is not used as the wing should rest on the horizontal tail in driving configuration. A dihedral will lead to a very high or very low tail, as well as a roof shaped to the dihedral of the wing.

The LE is occupied by the propellers, so no *high lift devices* are possible here. However, the Trailing Edge (TE) of the wings is still free. For this reason, it is decided to put plain flaps to increase the lift coefficient at take-off, climb and landing. The hinge for plain flaps is generally located at approximately 0.7c, so it is chosen for the design as well. The flaps run from $b = 1.4$ to $b = 3.0$, with appropriate gaps with the fuselage and the aileron to avoid undesired interference. The increase in $C_{L_{max}}$, the lift curve slope and the flap drag coefficient that hold for this type of flap can be found using Equation 4.8, Equation 4.9 and Equation 8.11.
$F_{flap} = 0.0144$, $\Delta C_{l_{max}} = 0.9$ and S_{flap} is all area in front of the flaps, making the ratio $\frac{S_{flap}}{S_{ref}} = 0.36$

$$\Delta C_{L_{max}} = 0.9\Delta C_{l_{max}} \frac{S_{flap}}{S_{ref}} cos(\Lambda_{hingeline}) \tag{4.8}$$

[4] https://aero.larc.nasa.gov/files/2012/11/Distributed-Electric-Propulsion-Aircraft.pdf [cited 17 May 2019]

$$C_{L_{\alpha_{flapped}}} = C_{L_{\alpha_{clean}}} \tag{4.9}$$

With these parameters and options for the wing, the final wing planform can be obtained with the corresponding dimensions in Table 4.3.

Table 4.3: Wing parameters

Parameter	Value	Unit
S	9.53	[m^2]
b	8.8	[m]
$\bar{c}$	1.08	[m]
λ	0.88	[-]
$\Lambda_{c/4}$	0.63	[°]
Twist	0	[°/m]
Γ	0	[°]
$\Delta C_{L_{max}}$	0.29	[-]
Airfoil	NACA 63(3)-618	[-]

Research shows that ice on wings results in drastic lift decrease and drag increase.[5] For this reason, a deicing system should be put along the leading edge of the wing to make sure the vehicle can fly in icy conditions. Heat could come from the engines, fuel cells or a separate heater, decided upon in a later phase of design.

4.2.2. Airfoil Choice

In this phase of design, the airfoil is picked from the NACA databases. For later design phases, it would be better to optimise the shape of the airfoil for this vehicles purpose to minimise the drag. Initially, lifting line theory was considered to estimate the drag coefficient over the range of lift coefficients of the wing. Firstly, the zero lift drag is found from a database,[6] then the induced drag is found. Rather than finding the Oswald efficiency $\frac{1}{1+\delta}$ seen in Equation 4.10 from Equation 4.11, it can be found from Figure 4.2, as it is mostly influenced by the aspect and taper ratio as shown [10].

$$C_{D_i} = \frac{C_L^2}{\pi A}(1+\delta) \tag{4.10}$$

$$\delta = \sum_{n=2}^{N} n\left(\frac{A_n}{A_1}\right)^2 \tag{4.11}$$

As these estimations do not take into account the Reynolds number and Mach number, it is better to use finite-wing estimations which do take Reynolds number, compressibility, and wing geometry into account. For this reason, many different airfoils were looked at using Javafoil to model the behaviour in different conditions. Parameters such as the aspect ratio, Mach number, Reynolds number, viscosity, and density are put into the model and changed per iteration. A selection was made by looking at their maximum lift coefficient and design lift coefficient and comparing these to the required values. After this, six NACA 4 digit and six NACA 6 digit airfoils were left. Then a decision had to be made to either use the 4 or 6 digit airfoils for the trade-off. The 4 digit airfoils generally have a higher maximum lift coefficient, but also a higher drag coefficient, while for the 6 digit airfoils the opposite holds. In the end it was chosen to go for the 6 digit airfoils. The main reason for this, is that the total wing drag values are lower, even though the wing areas are higher due to a lower maximum lift

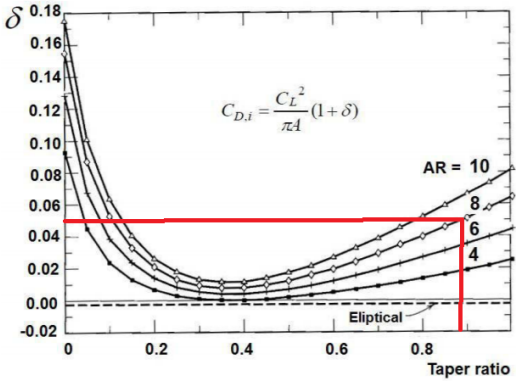

Figure 4.2: Estimate of δ from literature [10]

[5] http://www.flightlearnings.com/2012/11/01/general-effects-of-icing-on-airfoils/ [cited 15 May 2019]
[6] http://airfoiltools.com/search/index [cited 15 May 2019]

coefficient. Furthermore, the wing areas do not exceed the size constraints. In Table 4.4, the different airfoil types and some important parameters of these are indicated, after which is explained for which airfoil is chosen.

Table 4.4: List of NACA 6 digit airfoils

Airfoil	$\frac{t}{c}$	$C_{L_{AOA=0}}$	$C_{L_{max}}$	$\alpha_{C_{L_{max}}}$	$C_{D_{min}}$	C_L at $C_{D_{min}}$	$\frac{C_L}{C_D}_{max}$	$C_{M_{cruise}}$	C_D at $C_{L_{design}}$
63(2)-615	15	0.50	1.30	10.5	0.007	0.15	36.0	-0.08	0.027
63(3)-418	18	0.34	1.32	12.5	0.005	0	35.0	-0.06	0.028
63(3)-618	18	0.40	1.42	13	0.008	0.10	33.5	-0.05	0.029
64(3)-618	18	0.52	1.37	11	0.006	0.10	28.6	-0.09	0.028
65(1)-412	12	0.34	1.00	9	0.007	0.10	37.8	-0.06	0.032
65(2)-415	15	0.35	1.10	10	0.005	0.10	38.9	-0.07	0.028

A larger thickness to chord ratio is optimal as the structure can be made lighter and the engines can fit more easily into the airfoil. A $C_{L_{AOA=0}}$ that is closest to the design lift coefficient is optimal, such that only a small angle of attack is needed in cruise. $C_{L_{max}}$ is one of the most important parameters, as a high $C_{L_{max}}$ is beneficial for the STOL configuration as a smaller take-off velocity would be required. A higher $\alpha_{C_{L_{max}}}$ is beneficial as it would make it harder to stall the aircraft. The smaller the minimum drag coefficient, the better because it lowers the minimum drag. The closer the lift coefficient at minimum drag is to the design lift coefficient, the better, as this results in less drag. A higher optimum lift over drag ratio is beneficial for low drag but high lift. The closer to zero the airfoil moment coefficient, the better, as it is easier to counteract the moment. The lower the drag coefficient at the design lift coefficient, the better, as this would directly result in less drag. Keeping all these things in mind, it was decided to go for the NACA 63(3)-618, as it has a relatively high maximum lift coefficient, but still acceptably low drag. After choosing this airfoil, the chamber, thickness and their locations were changed slightly to see if these would result in beneficial effects. However, in the end it is found that these generally have negative effects.

4.3. Wing Box Design

Since the vehicle should be able to transform from a plane to a car, the wings are not fixed in position. This feature makes for a more complex design for the wings and therefore the wing box. This section will cover the steps taken in order to design and size the wing box to support all the loads in the structure.

4.3.1. Wing Loading

In order to determine the wing box sizing, it is important to accurately calculate the forces that act on the wing. Since the two wings are not connected in the centre due to the rotating mechanism, it is possible to assume that the wing behaves similarly to a cantilever beam with a length of 3.2 m (the span of the wing, without the central portion of the vehicle). All the forces can then be positioned along the span of the wing to calculate the reaction forces acting at the hinge. Then finally the shear and moments acting along the wing can be determined. The free body diagram of the wing seen from above and from the front is shown in Figure 4.3.

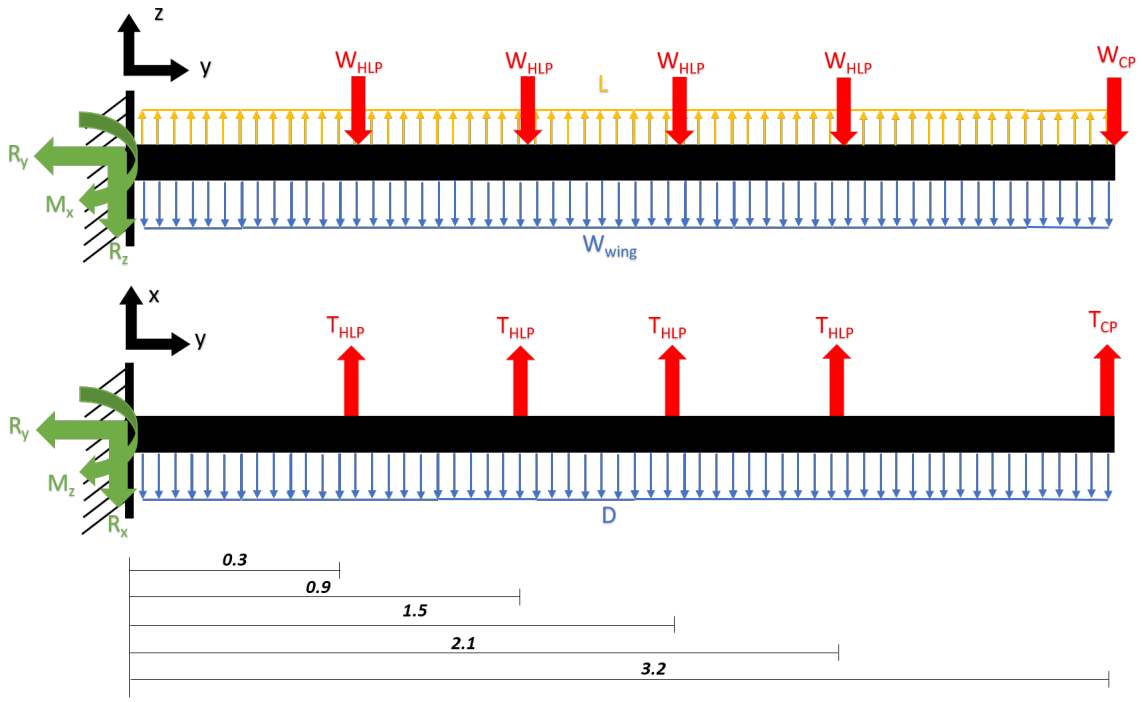

Figure 4.3: Free body diagram of the wing

The dimensions and units of each force are shown in the Table 4.5. These are for the simple horizontal flying condition where $L = W$.

Table 4.5: Magnitude of forces acting on wing

Parameter	Value	Unit
L	2504.3	[N/m]
D	406.5	[N/m]
W_{wing}	229.9	[N/m]
W_{HLP}	313.9	[N]
W_{CP}	657.3	[N]
T_{HLP}	136.2	[N]
T_{CP}	746.4	[N]

Next the reaction forces and moments can be determined using simple static analysis. Firstly it is intuitive that:

$$\sum F_y \Rightarrow R_y = 0$$

The remaining 4 reaction forces and moments can be determined from the following relationships:

$$\sum F_z \Rightarrow R_z = L \cdot 3.2 - W_{wing} \cdot 3.2 - W_{CP} - 4 \cdot W_{HLP}$$

$$\sum F_x \Rightarrow R_x = D \cdot 3.2 - T_{CP} - 4 \cdot T_{HLP}$$

$$\sum M_x \Rightarrow M_x = L \cdot 3.2 \cdot 1.6 - W_{HLP} \cdot 0.3 - W_{HLP} \cdot 0.9 - W_{HLP} \cdot 1.5 - W_{HLP} \cdot 2.1 - W_{CP} \cdot 3.2 - W_{wing} \cdot 3.2 \cdot 1.6$$

$$\sum M_z \Rightarrow M_z = D \cdot 3.2 \cdot 1.6 - T_{HLP} \cdot 0.3 - T_{HLP} \cdot 0.9 - T_{HLP} \cdot 1.5 - T_{HLP} \cdot 2.1 - T_{CP} \cdot 3.2$$

It is possible to solve for the reactions using the above relationships. These have to be found for different load cases to test the extreme values that the wing box has to be designed for. The first is the static condition, in this scenario, L, D and all thrusts are set to 0. The second case is the maximum load factor case, in this scenario the Lift is set to equal 3.5 the weight. Finally, the engine failure case is tested, where L=W but all thrusts are set to equal 0. The final reaction forces and moments for each load case are found and outlined in Table 4.6.

Table 4.6: Calculated reaction forces and moments for the wing structure

Reaction	Static Case	Maximum Load Factor Case	Engine Failure Case	Unit
R_y	0	0	0	[N]
R_z	-2501.55	25547.0	5512.3	[N]
R_x	0	9.7	1300.8	[N]
M_x	-4551.8	40326.0	8270.4	[Nm]
M_z	0	-960.74	2081.3	[Nm]

The next step is to calculate the internal shear and moments within the beam. Due to the changing forces and moments along the beam, these forces will be a function of the distance along the beam. In the case where a point force is acting, a switch that can be integrated is required. In this scenario, a Mcauley step function is used. This is represented by the square brackets in the equation. If the contents of the brackets is > 0 then the switch is on. If the contents of the bracket is < 0 then the switch is off and the bracket will equal 0. Equation 4.12 shows the relationship between the y position and shear in the z direction. Equation 4.13 shows the same but for shear in the x direction.

$$V_z = R_z + W_{wing} \cdot y - L \cdot y + W_{HLP}[y-0.3]^0 + W_{HLP}[y-0.9]^0 + W_{HLP}[y-1.5]^0 + W_{HLP}[y-2.1]^0 \quad (4.12)$$

$$V_x = R_x + D \cdot y + T_{HLP}[y-0.3]^0 + T_{HLP}[y-0.9]^0 + T_{HLP}[y-1.5]^0 + T_{HLP}[y-2.1]^0 \quad (4.13)$$

The next stage is to find the relationship between the internal moment and the span-wise y position. Mcauley step functions can be integrated as is shown in [11]. Equation 4.14 shows the internal moment as a function of the y-position for moments about the x-axis. Equation 4.15 shows the internal moment function for moments about the z-axis.

$$M_{I_x} = M_x - R_z \cdot y + \frac{L \cdot y^2}{2} - \frac{W_{wing} \cdot y^2}{2} - W_{HLP}[y-0.3]^1 - W_{HLP}[[y-0.9]^1 - W_{HLP}[y-1.5]^1 - W_{HLP}[y-2.1]^1 \quad (4.14)$$

$$M_{I_z} = M_z - R_x \cdot y + \frac{D \cdot y^2}{2} - T_{HLP}[y-0.3]^1 - T_{HLP}[y-0.9]^1 - T_{HLP}[y-1.5]^1 - T_{HLP}[y-2.1]^1 \quad (4.15)$$

The graph in Figure 4.4 shows the plotted internal shear and moments as a function of the spanwise location. The blue line represents the static condition, the orange line shows the maximum load factor condition and the green line shows the Engine failure condition. It is clear that for bending around the x-axis, the maximum load factor is critical condition, and for bending around the z-axis, the engine failure condition is critical. So for computation of the wing box design, only these load cases will be reasoned.

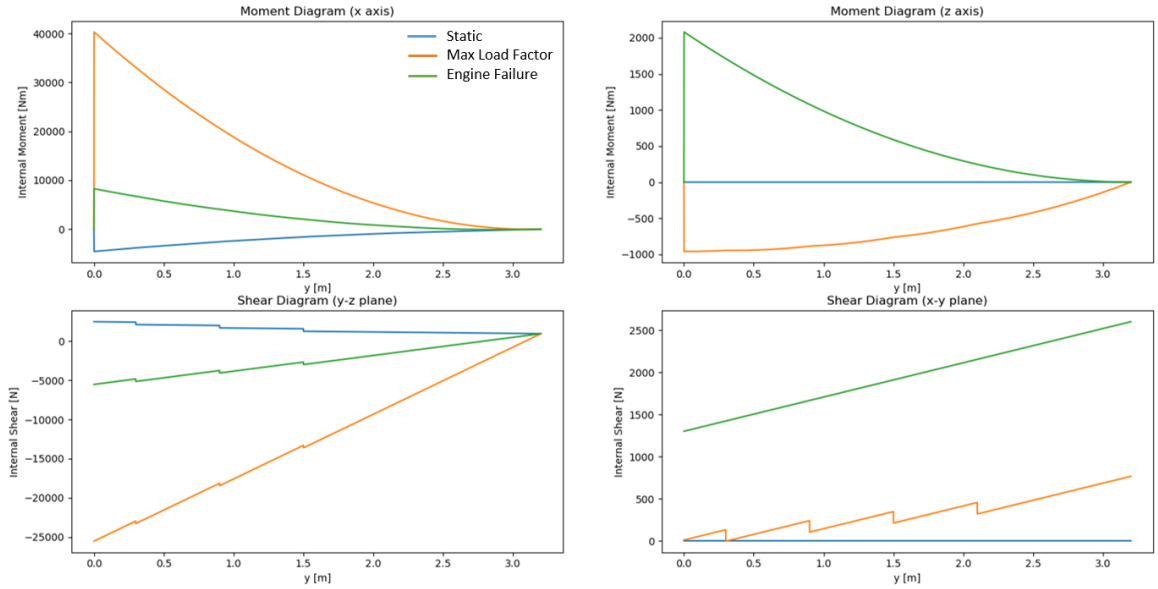

Figure 4.4: Shear and moment diagrams for 3 load conditions

The loading of the wing box directly influences its design. The wing box must take all the loads in the wing and be able to resist the deflection caused by the bending and also withstand the bending stresses caused by such moments. A limit on deflection has been set at 4 cm. This number was extrapolated from existing aircraft knowledge based on deflection as a function of wingspan. This means that the wing box must allow no more than a 4 cm deflection from the horizontal plane at any point along the wing span.

To simplify the process of the wing box design, it is logical to start from a rectangular wing box of constant cross section. The wing box can be designed in this case and then iterated to save weight. The deflection for a constant moment of inertia wing box can be determined by Equation 4.16 [12].

$$M = -\frac{1}{EI}\frac{d^2v}{dy^2} \tag{4.16}$$

This can be twice integrated to solve for deflection:

$$v = -EI\int\int M$$

The first integration of the moment equations results in the equations below. The integration constant can be equated to 0 since $v'(0) = 0$

$$\int M_{I_x} = M_x \cdot y - \frac{R_z \cdot y^2}{2} + \frac{L \cdot y^3}{6} - \frac{W_{wing} \cdot y^3}{6} - W_{HLP}\frac{[y-0.3]^2}{2} - W_{HLP}\frac{[y-0.9]^2}{2} - W_{HLP}\frac{[y-1.5]^2}{2} - W_{HLP}\frac{[y-2.1]^2}{2} \tag{4.17}$$

$$\int M_{I_z} = M_z \cdot y - \frac{R_x \cdot y^2}{2} + \frac{D \cdot y^3}{6} - T_{HLP}\frac{[y-0.3]^2}{2} - T_{HLP}\frac{[y-0.9]^2}{2} - T_{HLP}\frac{[y-1.5]^2}{2} - T_{HLP}\frac{[y-2.1]^2}{2} \tag{4.18}$$

The second integration of the moment equations results in the equations below. The integration constant can again be equated to 0 since $v(0) = 0$.

$$\int\int M_{I_x} = \frac{M_x \cdot y^2}{2} - \frac{R_z \cdot y^3}{6} + \frac{L \cdot y^4}{24} - \frac{W_{wing} \cdot y^4}{24} - W_{HLP}\frac{[y-0.3]^3}{6} - W_{HLP}\frac{[y-0.9]^3}{6} - W_{HLP}\frac{[y-1.5]^3}{6} - W_{HLP}\frac{[y-2.1]^3}{6} \tag{4.19}$$

$$\int\int M_{I_z} = \frac{M_z \cdot y}{2} - \frac{R_x \cdot y^3}{6} + \frac{D \cdot y^4}{24} - T_{HLP}\frac{[y-0.3]^3}{6} - T_{HLP}\frac{[y-0.9]^3}{6} - T_{HLP}\frac{[y-1.5]^3}{6} - T_{HLP}\frac{[y-2.1]^3}{6} \tag{4.20}$$

4.3.2. Wing Box Cross Section Design

As described above and is depicted in Figure 4.3 and Table 4.5, the wing needs to be able to withstand strong loads. In order to size a wing that is able to do so, limiting design cases shall be considered. To start, an assumption will be that the loads are all carried by the wing box inside the wing and this wing box shall be optimised to have a lowest mass as possible and certainly should not exceed the first mass estimate of the wings. To size the wing box inside the wing, some sizing constraints have to be raised. One of these constraints will be the airfoil itself. The Aerodynamics department has chosen a certain airfoil as can be read in subsection 4.2.2

Next to this wing box, the electric motors, power cables, and flaps also need to fit in the wing. With the chosen airfoil, fitting the electric motor without interfering with the airfoil becomes impossible. The radius and length of the electric motor is simply too large. This issue can be solved by adding a nacelle on the airfoil at the specific locations of the electric motor. This manufacturing concern will be elaborated further in this chapter. To avoid increasing the chord length of the airfoil at the locations of the electric motors, the motors should be fitted lengthwise in the airfoil. As the electric motors are 13 cm in length a chord-wise position of around 20 cm behind the leading edge is chosen. This location will have to be chosen in a iterative manner as the electric motors will be connected to the front spar of the wing box.

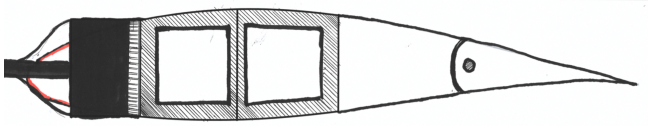

Figure 4.5: Sketch of a cross section of the wing showing the wing box, electric motor and flap

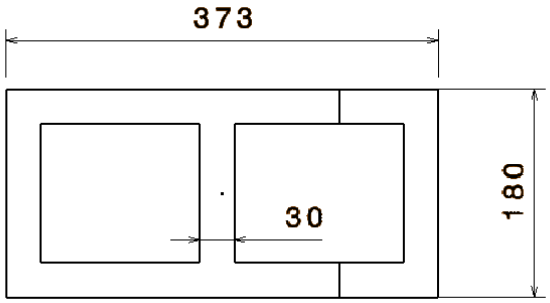

Figure 4.6: A cross section of the wing box at the root

The wing box is chosen as a rectangle at the root as this is beneficial for the calculation time of the project group and this choice is not seen as a large disadvantage to the design of the wing box. With this in mind, the height of the wing box can be found at each chord position of the airfoil. At 21.2 cm from the leading edge, the distance between the upper and lower airfoil is 18.0 cm. The width of the wing box will be 37.3 cm and this will leave enough space for flaps in the wing at 70% of the chord-length, so 80.5 cm from the leading edge. Power cables and hydraulic system that will have to power the electric motors, flaps and ailerons will go through the wing box and will have an approximate combined radius of 5 cm for the power cables and 5 cm for the hydraulic tubing. This is illustrated in Figure 4.5 and Figure 4.6. To check if this will fit, the thickness of the wing box spars need to be determined.

Material choice plays an important role in the thickness and mass of the structural element. Material properties are of major influence in the final wing box properties and therefore have to be chosen carefully. From literature research two options are taken into account, one metal and one composite combined with honeycomb material. Properties can be found in table Table 4.7 [13]. The E-modulus is found by applying the rule of mixtures while neglecting the honeycomb material [14]. The loads will be transferred by the composite solely and the honeycomb is for stiffening the wing box and for making the wing box less prone to column buckling. A lay up of 90 / 20 / 90 / -20 / 90 is found to be optimal for our case, as that will represent a ratio complying with the loads acting on the wing in the various directions. This lay up orientation is depicted in Figure 4.7, where

90 °is representing the direction parallel to the wingspan. With the help of the E-modulus and by changing the thickness of the spars, a first estimate on the mass can be made. This first mass estimate is based on a deflection constraint of 1.3% of the wingspan at the tip of the wing, which is typical for these kind of wingspans. [7] By changing the thickness, the area moment of inertia changes and therefore the bending stiffness of the wing box. The first mass estimate is also included in Table 4.7.

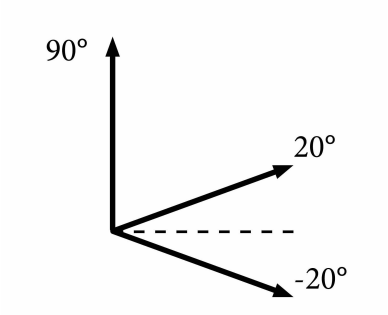

Figure 4.7: Illustrating the lay up orientation

Table 4.7: Wing box material properties

	Aluminium 7075 T6	**HS Carbon Fibre (Honeycomb core)**
Mass [kg]	160	120
Density [kg/m^3]	2800	1550
Fatigue strength [MPa]	160	1185
Manufacturability	Good	Good
Cost [€/kg]	€3,50	€33, -

Based on the properties described in Table 4.7, the Carbon High Strength (HS) in combination with a Para-aramid paper honeycomb core are chosen as the materials for the wing box and wing. This material choice will result in a reduction in mass, while not conflicting with other aspects such as being able to be manufactured. The accessibility of the electric motors can become an issue when using adhesive and composite material for the wing box. Electric motors will need to be inspected and therefore a three part configuration of the wing is chosen. The middle part will consist of of three spars, fully extending from the root to the tip. The front spar will continue even further from the root to the folding and attaching mechanism in a C-shape as depicted in Figure 4.16 and Figure 4.9. The middle part of the wing will form the wing box and the other parts will be either riveted or attached via hinges to the wing box. The leading edge part, which will consists out of the nacelles for the electric motor, will be riveted to the wing box to ensure accessibility when needed. To make sure the flaps are able to rotate downward during the landing phase, these flaps shall be attached via hinges to the wing box. These flaps will be operated via a fly-by-wire system, powered via the hydraulic system. This will be further elaborated upon in a later development phase.

To design the wing box for the loads that will occur during flight, another design case will have to be considered. The bending moments due to the lift and drag are found to be the limiting cases. To find the maximum bearable moment of a sandwich structure, Equation 4.21 [15] can be used. The σ_{fatigue} is the fatigue tensile stress of the material, M is the (maximum) bending moment at the root of the wing, y is the lateral distance from the location where the moment is acting to the composite material and I_{xx} is the area moment of inertia around the x axis where only the composite material is included. Taking a safety factor of 2.5 into account, which is normal for designing with composites. In addition another design safety factor of 10 is used. This will allow the team to reduce mass at a later stage as not all loads and buckling is taken into account. The team is aware that a buckling analysis must be done at a later design stage, as this is vital in a design with composites. For a preliminary concept, a bending moment analysis with these safety factors is adequate.

[7] https://www.comsol.com/paper/download/114853/atmeh_paper.pdf [cited 22 June 2019]

$$\sigma_{fatigue} = \frac{M \cdot y}{I_{xx}} \tag{4.21}$$

This maximum bending calculation is performed at different span positions of the wing: at the root, at 1/3 of the span and at 2/3 of the span. With this information different thicknesses are chosen over the span of the wing, resulting in a reduced mass. The outcome of the variance in thicknesses along the span position can be read in Table 4.8 and a schematic drawing can be seen in Figure 4.8.

Table 4.8: Wing box material properties

	Wall Thickness	**Core Thickness**	**Thickness Airfoil**
Section 1 [mm]	30.00	24.0	2
Section 2 [mm]	19.35	17.6	2
Section 3 [mm]	10.00	9.0	2
Total Mass [kg]	36	-	24

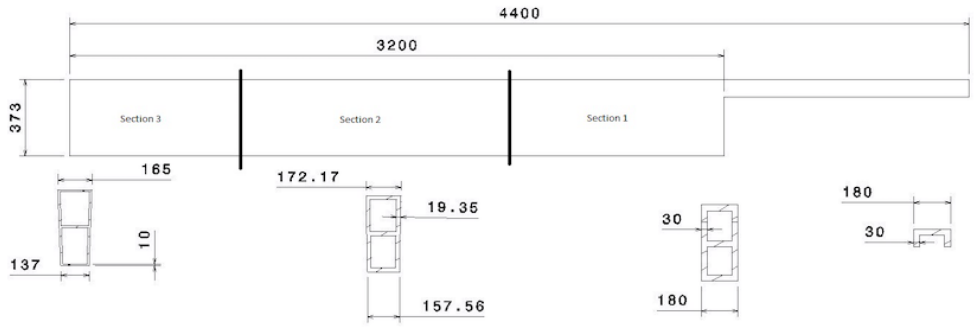

Figure 4.8: Technical Drawing of the wing box and the section division

To verify the wing box design, a CATIA model was made. This model can be used to verify both the mass and the loading case, as described in chapter 12. Two risk items have not been discussed yet, but have been taken into account. The risk on lightning strike impact is a risk to seriously consider. There is research being done on reducing impact of a lightning strike when using carbon wing boxes. When a slim copper mesh will be placed in between the carbon and paint layer, this will conduct the electricity and mitigate the risk of having critical damage after a lightning strike.[8] De-icing is also an aspect that will have to be taken into account. Although the HAVIC is not flying at high altitudes, it can still face freezing temperatures. To deice the wings, an electric deicing system can be used. This new technology uses electrical energy to heat carbon fibres and therefore heat the wing. In this way the deicing system can also be load carrying.[9]

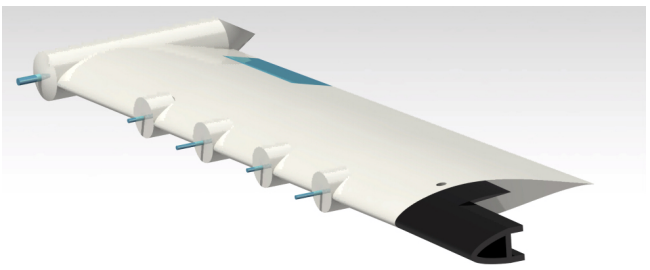

Figure 4.9: A CATIA visualisation of one of the wings of the HAVIC

[8] https://www.aerospacemanufacturinganddesign.com/article/amd0715-aerospace-lighting%2Dprotection-aircraft-structures/ [cited 20 June 2019]

[9] https://www.dlr.de/dlr/en/desktopdefault.aspx/tabid-10081/151_read-31938/gallery/33356 [cited 20 June 2019]

The final design of the wing in size would be a total width of 373 mm with a height of 180 mm. There are 3 spars, varying in thickness at three different span-wise locations. In Table 4.8 these thicknesses are displayed. Section 1 is referring to the part starting from the root to 1/3 of the span of one of the wings, section 2 is the section from 1/3 to 2/3 and section 3 is the last section. There are both flaps and ailerons located on the wing. The flap starts at 0.2 m measured from the root and has a area of 0.52 m^2. The aileron starts at 2 m from the root and has an area of 0.3 m^2. There is enough space in the aileron to fit these surfaces. Figure 4.9 gives a final overview of the wing design of which the wing box plays a vital role.

4.3.3. Wing Box Analysis

Once the design of the wing box has been finalised it is possible to perform an analysis on the design to ensure the bending and flutter characteristics are acceptable. As previously stated, a maximum allowable wing tip deflection of 5 cm was selected. It is now possible to perform a bending analysis on the wing box using Equation 4.19 and Equation 4.20. However in this case, the moment of inertia term in the equation is not constant, but is a function of wing span. This is due to the changing cross section of the wing box. In order to account for this, a program is set up which splits the wing box into discretised short sections of constant cross section. The analysis is performed on each section, with the results of that section forming the boundary conditions of the following section. The analysis is performed on the final wing box design and the slope and deflection at each point along the wing span are plotted in Figure 4.10 for each of the 3 previously specified load cases.

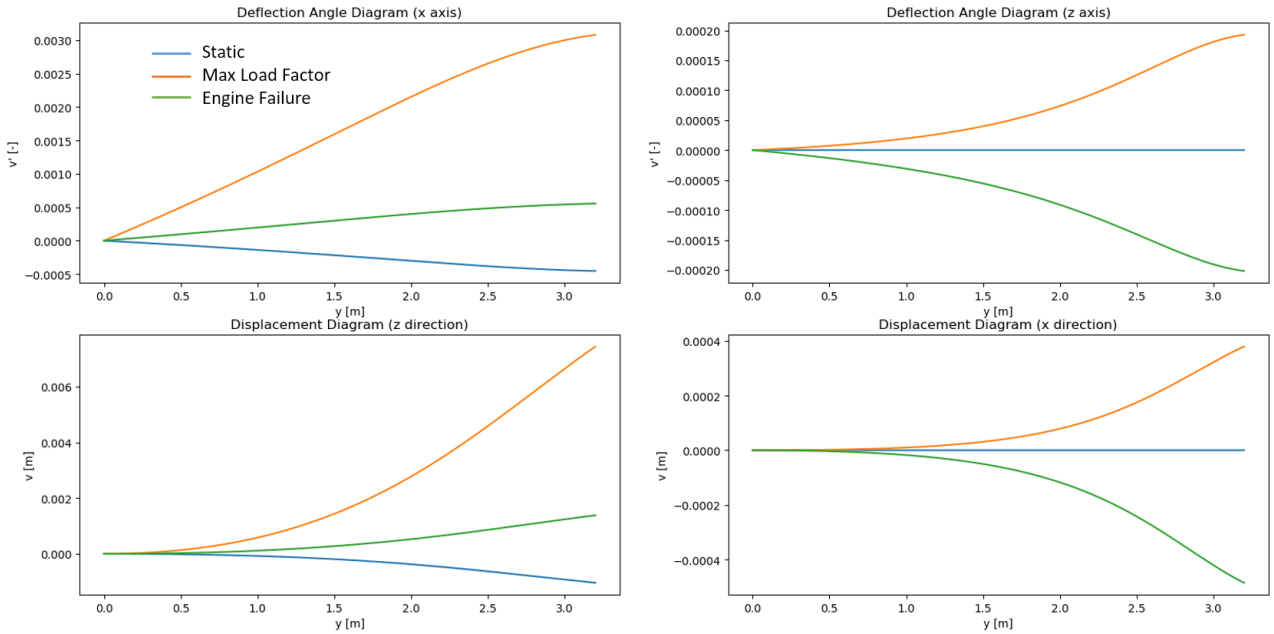

Figure 4.10: Slope and deflection of the wing box in each of the 3 load cases

It can clearly be seen that the deflection is below the 4 cm threshold. This is because the limiting factor for the design of the wing box was the bending stress and not the deflection. The maximum deflection in the z-direction is approximately 7 mm and the maximum deflection in the x-direction is approximately 0.5 mm. This confirms that the wing box has been designed correctly and the requirement is met.

The other analysis to consider is the flutter of the wings. This can be calculated at a basic level by considering the natural frequency of the beam simplification. This can be calculated for both distributed loads and point loads by using standard formulas. The natural frequency of a cantilever beam with a point force is given by Equation 4.22 and for a distributed load is given by Equation 4.23 [16].

$$\omega = \frac{1}{2\pi}\sqrt{\frac{3EI}{FL^3}} \tag{4.22}$$

$$\omega = 0.56\sqrt{\frac{3EI}{qL^4}} \tag{4.23}$$

The lift and weight of the wings are combined into a single distributed load. Using these formulas, the natural frequency is calculated for each individual source of vibration. The displacement against time for a duration of 1 second is plotted using a standard damping coefficient, γ, of 0.3 and Equation 4.24. The amplitude for each individual source of vibration is taken to be the displacement at the span-wise location where the force is acting, taken from Figure 4.10.

$$v = e^{-\gamma t} A \sin \omega t \tag{4.24}$$

Finally, all the sources of vibration were superimposed to give the final flutter of the wing. This is plotted for a time of 1 second and is shown in the bottom figure of Figure 4.11.

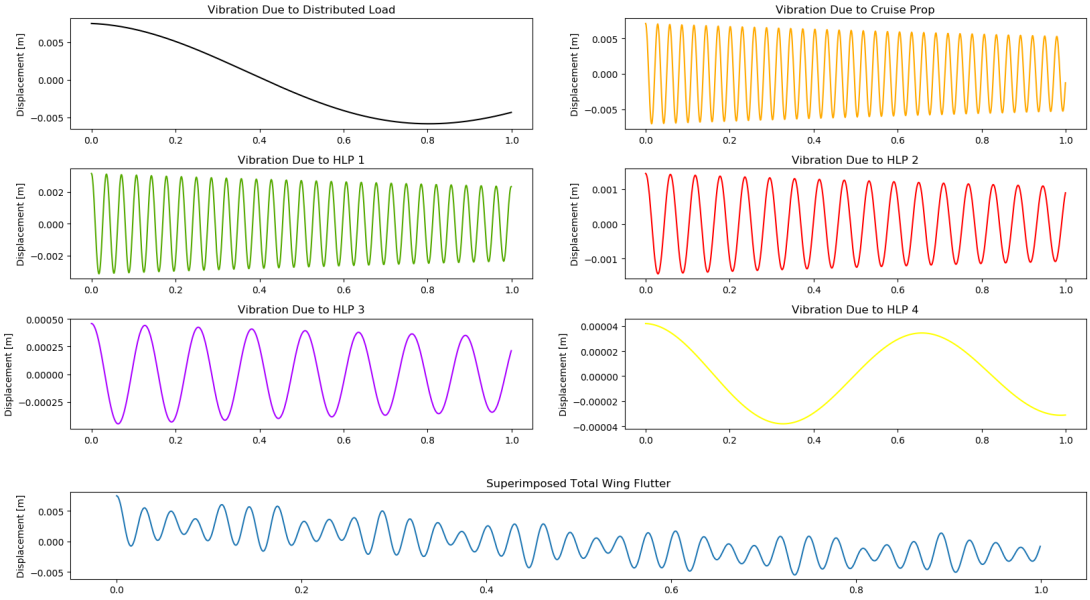

Figure 4.11: Individual components and total superimposed wing flutter

4.4. Wing Folding Mechanism

One of the main features of the HAVIC is its ability to convert between a flying and a driving configuration. The wings are able to rotate from the extended position, to be stowed along the length of the vehicle which is shown in Figure 4.12. This allows the width of the vehicle to be reduced to just 2.4 m allowing it to drive on the road easily. This section will look at the specific mechanism which allows for this conversion.

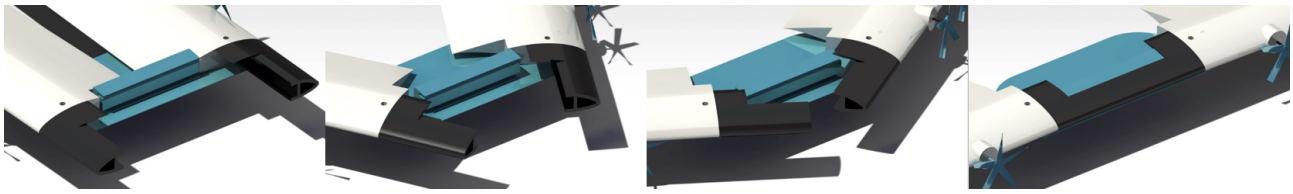

Figure 4.12: Render of the wing rotating mechanism (aerodynamic fairing is hidden)

4.4.1. Wing Turning Geometry

Before a specific mechanism can be designed, the top level movement of the wing must be designed. The following constraints are set on the wing geometry for rotation:

- The wing will extend 4.4 m from the centre line of the vehicle in open position
- The wing will not extend beyond 1.2 m of the centre line in closed position
- The leading edge will sit at 2.3 m from the front of the vehicle in open position
- The wing will not cross over the centre line at any point during the rotation
- The rotation hinge will be within the wing box section of the chord

Taking into account all these constraints, the hinge is placed at 850 mm from the centre line in the y-direction and 250 mm from the leading edge in the x-direction. The whole wing profile continues for 100 mm beyond the hinge location after which only the leading edge skin (aerodynamic purposes) and front C spar (structural purposes) extend to the centre line. The geometry is shown in Figure 4.13

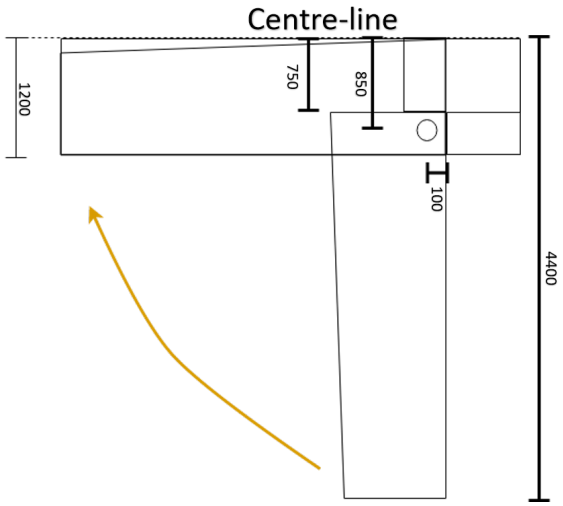

Figure 4.13: Wing rotation geometry

4.4.2. Folding Actuation

The actuation mechanism must be able to generate enough torque to rotate the wing around the hinge. For this a servo will be used. Primarily a geared servo will be used since this will mean that when the mechanism is not being actuated, the servo itself can carry some of the required reaction moment. The amount of torque required by the mechanism must be determined. This can be done using D'Alemberts principle [17].

$$T = J\alpha'' \tag{4.25}$$

Where T is the required torque, J is the mass moment of inertia of the system about the rotational axis and α is the angular acceleration of the system. First it is possible to determine the required acceleration. If a constant acceleration or deceleration is assumed, then it able to determine the acceleration needed to rotate the system through $\frac{\pi}{2}$ rad in a specified time. The value for time to rotate the system is taken to be 14 seconds. This accounts for 3 seconds to accelerate to maximum rotational velocity, 8 seconds of constant angular velocity and a further 3 seconds to decelerate to a halt.To complete the rotation with these parameters, the required acceleration is $\alpha = 0.0476$ rad/s^2. The accelerations, velocity and displacement graphs for the rotation mechanism are shown in Figure 4.14.

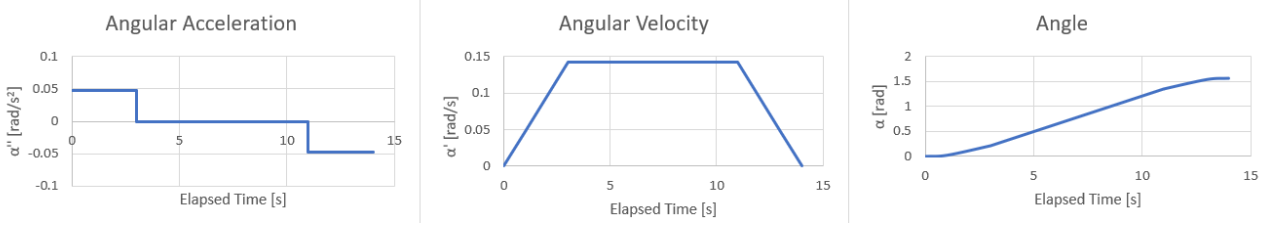

Figure 4.14: Angular acceleration, velocity and displacement graphs for the wing turning mechanism

Next the mass moment of inertia of the rotating part is determined. This is done by assuming a rectangular wing structure with the wing weight as its weight. Point masses are then positioned where the motors and propellers would be allowing for their mass to be accounted for. This is shown in Figure 4.15 and the mass moment of inertia of one wing is calculated as shown in Equation 4.26.

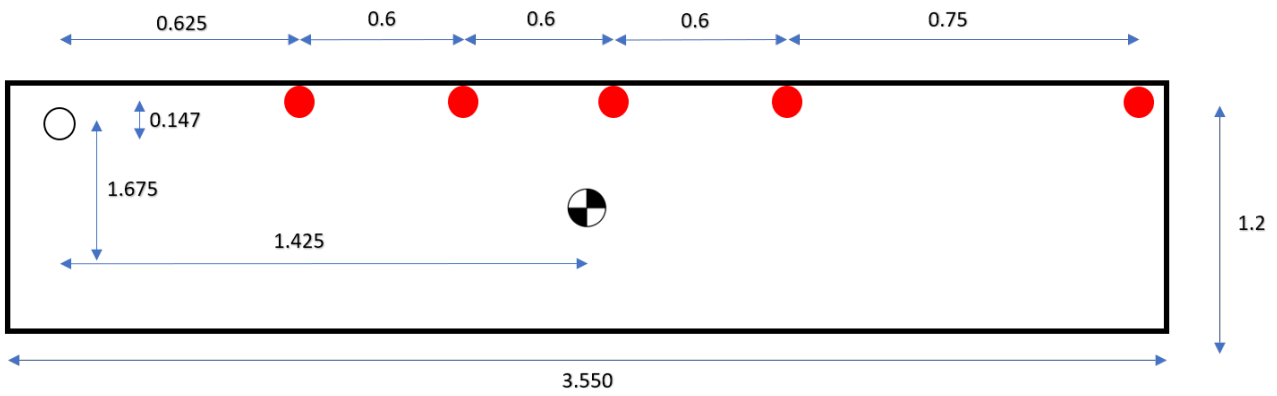

Figure 4.15: Visual representation of the mass moment of inertia of the wing

$$J = \frac{M_{wing}(1.2^2 + 3.55^2)}{12} + M_{wing}(1.675^2 + 1.425^2) + M_{HLP}(0.625^2 + 0.146^2) + M_{HLP}(1.225^2 + 0.146^2) \\ + M_{HLP}(1.825^2 + 0.146^2) + M_{HLP}(2.425^2 + 0.146^2) + M_{CP}(3.175^2 + 0.146^2) = 1246.2\ kgm^2 \tag{4.26}$$

So the mechanism will need to generate a 59.32 Nm of torque in order to rotate in the given time-frame. Firstly a doubling factor is applied to account for friction of the system and an additional 1.5 factor is applied as a safety factor. This gives a total of 177.95 Nm torque required. For this purpose the AKM84-T servo has been selected which will provide 180 Nm of torque and therefore sufficient torque to turn the mechanism.

4.4.3. Locking Mechanism

For the wing in the stowed 'driving position' the loads on the wing will be relatively low, as the only forces will be the weights of the propellers. In this scenario the restive moment of the servo is able to withstand the load and therefore no further locking is required. However for purposes of redundancy, an extra safety measure is applied to the mechanism so as to prevent wing movement in case of servo failure. This is done by adding a single pin for locking in the inside edge of the wing. This pin will need to carry all the potential rotational moment around the z-axis. The maximum moment in this case will be due to the inertia of the wing when the vehicle is accelerating. Since the maximum acceleration of the vehicle is 2.5 m/s^2 then the locking mechanism should be able to withstand $2.5 \cdot 60 = 150$ N . The locking mechanism for the flying configuration is more complicated as it has to withstand all the maximum loads shown in Table 4.6. For this purpose, a new method has been designed. As previously stated, the front spar of the wing is extended through to the centre-line. The roof of the vehicle has an E beam bolted to it. The slots in the E beam are equal to the thickness of the C beam in the wing box which allows the front spar to slot into the E beam when in flying configuration as shown in Figure 4.16 and Figure 4.17.

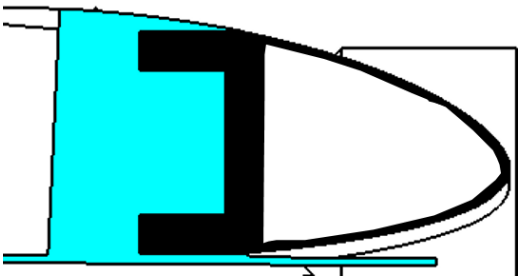

Figure 4.16: Schematic view of E and C beams

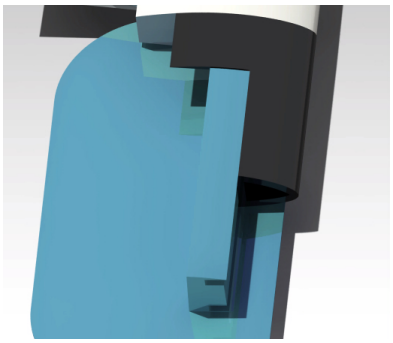

Figure 4.17: Rendered view of E and C beams

In this way, the loads of the wing are spread out across the E beam. To lock the two in place 3 vertical pins are then slid through the contact points between the E and C beams as shown in Figure 4.18. The bolts have to be sized so as to be able to withstand the shear forces that are generated at the hinge since the tensile forces,

the moments around the x-axis, will be carried by the E beam itself. These 3 bolts must be able to generate the force and recreate a moment equal to the maximum reaction force and moments in Table 4.6.

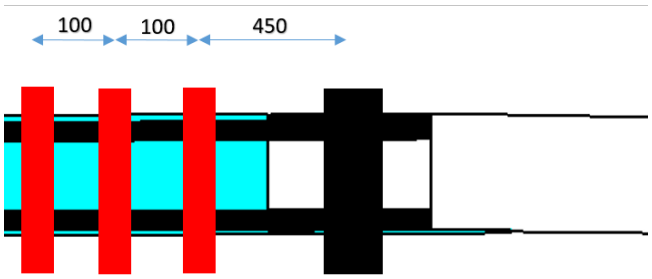

Figure 4.18: The positions and distance of the bolts through the C and E beam

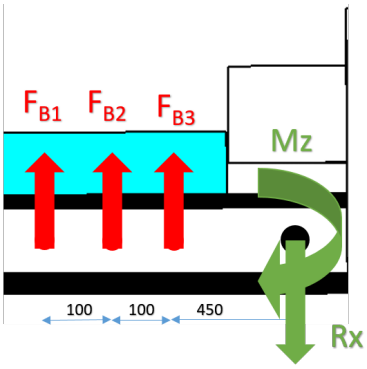

Figure 4.19: Free body diagram of bolts loaded in shear

Since the bolts have to be analysed for redundancy, the case will be tested where 1 bolt is broken, so the inner 2 bolts would carry all the load. For this analysis the assumption will be made that $F_{B1} = 0$. From Figure 4.19 it possible to to generate the static equations to solve for the forces in the bolts.

$$\sum F_z \Rightarrow F_{B2} + F_{B3} = R_x = 1300.8\ N \tag{4.27}$$

$$\sum M_x \Rightarrow 0.450 \cdot F_{B3} + 0.550 \cdot F_{B2} = M_{I_z} = 2081.3\ Nm \tag{4.28}$$

Solving the system of equations leads to reaction forces of F_{B2} = 1551.9 N and F_{B3} = -251.1 N. So the critical shear force is 1551.9 N. In order to size the bolts, the maximum shear will be selected and the bolt will need to withstand this load without reaching the allowable stress. The bolts will be made from titanium since it is strong enough to support the loads but also lightweight. The shear strength of titanium is 550 MPa [18]. Applying a 2.2 safety factor means the allowable shear stress is 250 MPa. Solving for the required diameter is done as by the equation below:

$$\tau = \frac{F_{shear}}{\pi r^2} \Rightarrow r = \sqrt{\frac{F}{\tau\pi}} = \sqrt{\frac{1551.9}{250 \cdot 10^6 \pi}} = 0.00141\ m \tag{4.29}$$

From this calculation it can be seen that the bolts must have a diameter of at least 0.00282 m or 2.82 mm.

4.4.4. Aerodynamic Fairing

In order for the mechanism function, it is physically impossible for the wing to be extended all the way to the centre line. This is due to the fact that doing this would cause the inner corners of the wings to collide during the rotation. Furthermore, to make space for the E beam used by the locking mechanism, an extra portion of the trailing edge of the wing is cut out as seen in Figure 4.12. Both these things lead to very poor airflow over the central portion of the wing. This is not very desirable as it would cause large amounts of drag and negatively impact the lifting performance of the wing. For this reason an aerodynamic fairing is developed and placed over the region. The aerodynamic follows the contour of the top side of the wing. However the fairing must be movable, since it must be able to lift when the wings are folded to prevent collision with the wing itself. Since the fairing is only for aerodynamic purposes, it will be made from the same material and layup as the main wing skin. For this reason it can be actuated by a simple piston which raises and lowers the rear of the fairing by rotating it around a hinge situated at the E beam. The fairing in the open and closed position can be seen in Figure 4.20 and Figure 4.21.

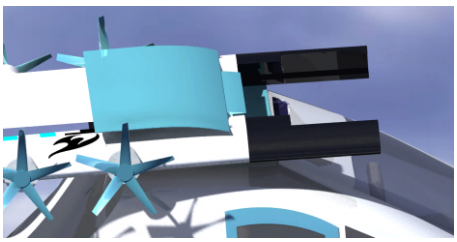

Figure 4.20: Render of the aerodynamic fairing in the open position

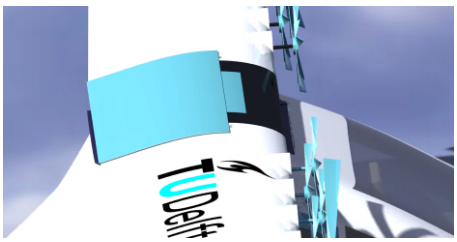

Figure 4.21: Render of the aerodynamic fairing in the closed position

4.5. Aileron Sizing

The aileron is sized based on the aileron roll requirement. The aircraft is considered a small light aircraft and therefore is classified as a class I aircraft. The aileron roll requirement corresponding to a class I aircraft has to satisfy a roll angle of 60° in 1.3 seconds [19]. The aileron sizing method was adopted from [19]. The geometry of the aileron is determined by estimating the position of the inner and outer board of the aileron (y_{a_i}, y_{a_o}), the ratio of the aileron chord to wing chord ($\frac{c_a}{c}$) and the maximum aileron deflection ($\delta_{a_{max}}$). From the aileron chord to wing ratio, the control surface effectiveness (τ_a) can be retrieved from Figure 4.22. Afterwards, the roll damping derivatives ($C_{l_{\delta_a}}$, C_{l_p}) are calculated, which is given by Equation 4.30 and 4.31.

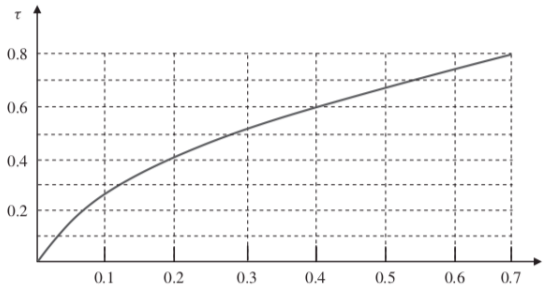

Figure 4.22: Control surfaces effectiveness

$$C_{l_{\delta_a}} = \frac{2C_{l_\alpha}\tau}{S_w b}\left[\frac{y^2}{2} + \frac{2}{3}\left(\frac{\lambda-1}{b}\right)y^3\right]\Bigg|_{y_{ao}}^{y_{a_i}} \tag{4.30}$$

$$C_{l_p} = -\frac{4(C_{l_\alpha}+C_{d_0})c_r}{S_w b_w^2}\left[\frac{y^3}{3} + \frac{1}{2}\left(\frac{\lambda-1}{b}\right)y^4\right]\Bigg|_{0}^{\frac{b_w}{2}} \tag{4.31}$$

Once the roll damping derivatives are calculated, the roll rate can be determined with Equation 4.32 using a maximum deflection of ±20°which is derived from the stall requirement in order to prevent flow separation. The required time in order roll the aircraft with an angle of 60° can be calculated with Equation 4.32. The method that has been used is iterative. If the required time turns out to be > 1.3 seconds, the calculations have to be repeated with updated estimations of the geometry of the aileron until the required time is equal of less than 1.3 seconds. The numerical values that have been used for the calculations are listed in Table 4.9. The final geometry of the aileron will be presented in section 7.1.

$$P = -\frac{C_{l_{\delta_a}}}{C_{L_p}}\delta_{a_{max}}\left(\frac{2V}{b}\right) \tag{4.32}$$

$$\Delta t = \frac{\Delta\phi}{P} \tag{4.33}$$

Table 4.9: Numerical input values for the aileron sizing

C_{l_α} [1/rad]	C_{d_0} [-]	$\frac{C_a}{C_w}$ [-]	y_{a_i} [m]	y_{a_o} [m]	c_r [m]	τ_a [-]	$\Delta\phi$ [rad]
6.3	0.055	0.2	3.256	3.96	1.15	0.41	1.047

5

Main Body Design

In this chapter, it is explained how the main body, namely the fuselage of the HAVIC is designed. This includes an explanation of design methods and trade-offs. An overview of the final results is shown in chapter 7. The structural analysis, which is done in the chassis design is shown in section 5.1. The drivetrain and suspension design is shown in section 5.2, while the aerodynamic characteristics are shown in the body shape design in section 5.3. The arc duct is discussed in section 5.4, while the cabin environment is shown in section 5.5. The control & stability characteristics, including the horizontal and vertical tail, as well as the rudder and elevator design is presented in section 5.6. Finally the materials science of the main body is shown in section 5.7.

5.1. Chassis Design

The chassis design process is initialised by doing a small literature study on similar vehicles. Mass produced cars often use a unibody structure meaning the chassis is integral with the body. This allows for better handling due to higher body rigidity. Heavier cars and trucks often use a ladder frames which support a higher load. However, lighter vehicles often use spaceframes, to save weight. The decided upon structure for the HAVIC is therefore the spaceframe, since the vehicle needs to be as light weight as possible.

Components are fitted to the space frame structure at nodes, meaning the skin itself is not a load bearing part. To minimise weight as well as maximising the rigidity, triangles are made use of in the design. The forces on the beams are kept to tensile or compression loads as much as possible, allowing the beams to be kept thin and therefore lightweight. The structure can be seen in Figure 5.1 and Figure 5.2.

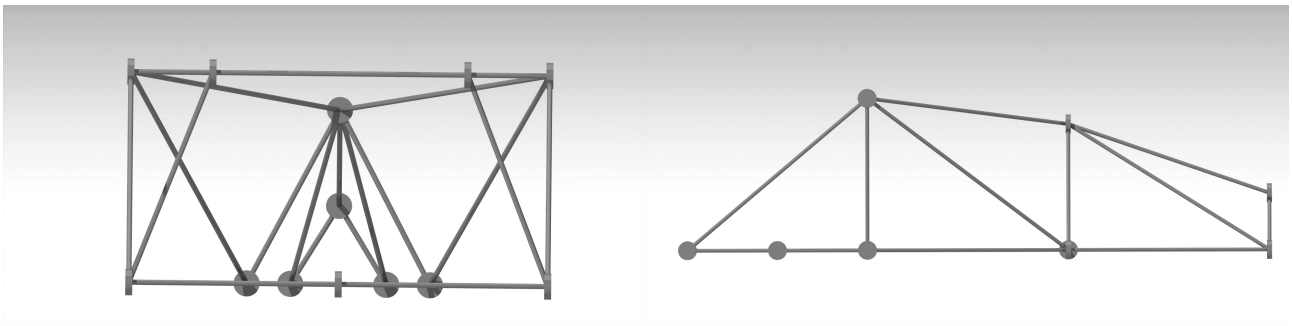

(a) Front view of the space frame

(b) Side view of the space frame

Figure 5.1: The space frame geometry

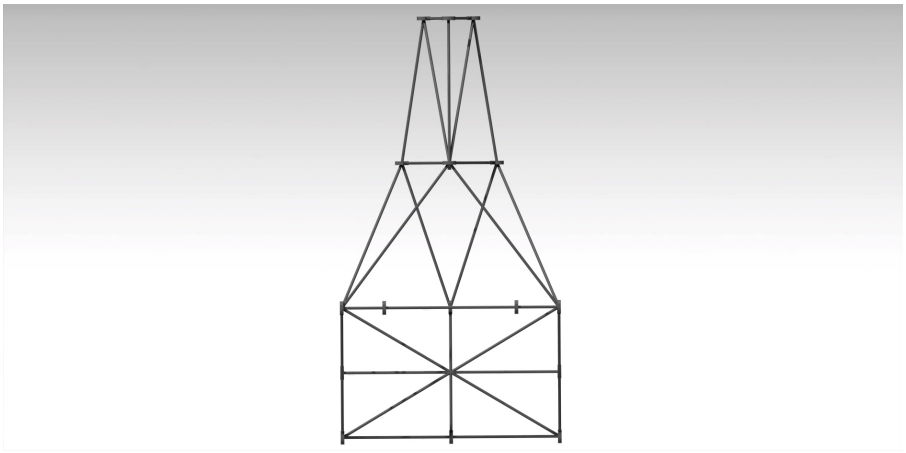

Figure 5.2: Top view of the space frame

The figures above show how the frame is triangulated everywhere but for the front section where the windscreen and front seat will be placed. To further minimise the weight of the structure, ANSYS software is used to find the optimal material and design. A finite element analysis is performed with the forces distributed over the relevant part of the structure. It should be noted that in order to meet regulations the structure is tested in worst case landing condition which means that loads are added at 3g.

The initial analysis takes all of the solid beams to be made out of a titanium alloy, having a diameter of 30 mm. The stress analysis shows that with a safety factor of 1.5 the maximum stress in the beams was lower than the 510 MPa failure stress at 505 MPa. However, the displacement analysis revealed that upon the worst case landing condition there is a displacement of 0.06 m in the middle of the front cross, which is where the passengers sit and the fuel tank resides. Taking these points into consideration, the material is changed to get the lightest possible structure, expanded upon in section 5.7 and the thickness of the beams is increased where the displacement is too high and decreased where it is low. A visual representation of the analysis can be seen in Figure 5.3.

The next step is to optimise topology using displacement as the critical condition. The front of the space where the passengers sit, under the wing, has its radius increased to 30 mm and various trusses on the side of the space frame have a diameter of 15 mm.

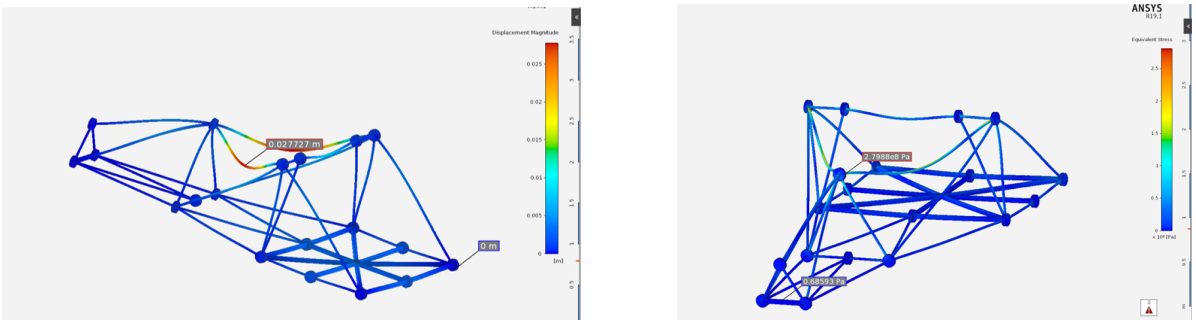

(a) The displacement of the space frame.

(b) The stress in the space frame.

Figure 5.3: Analysis of the space frame

The last step is to perform a buckling analysis under critical landing conditions. In this case, the solid beam with the maximum stress is chosen for the analysis which is located under the wing. The critical landing condition under 3g is calculated by multiplying the mass of the wing and propellers with the gravitational acceleration which yields a load of 14830 N. From Figure 5.4a and Figure 5.4b, it can be concluded that the solid beam with a radius of 30 mm already starts to buckle at 7711 N.

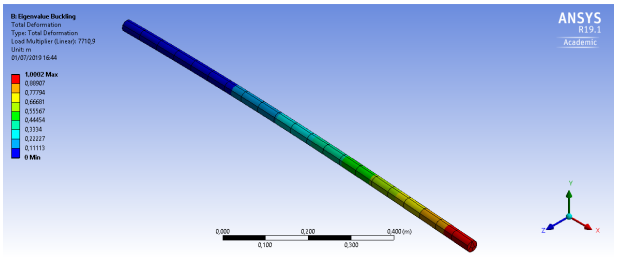

(a) The critical buckling load of the solid beam with a 30 mm radius

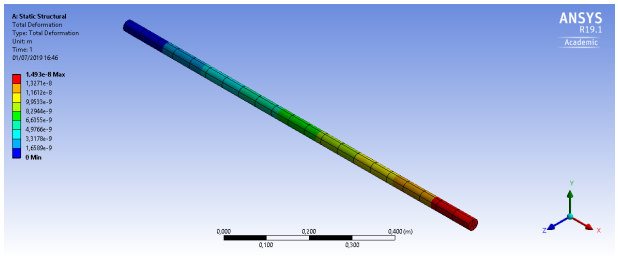

(b) The total deformation in the solid beam with a 30 mm radius

Figure 5.4: Analysis of the 30 mm radius solid beam

In order to prevent buckling at critical landing condition, the radius of the solid beam has to be increased. The same analysis is performed where the radius of the solid beam is increased from 30 to 36 mm. This resulted into a critical buckling load of 16386 N as shown in Figure 5.5a and Figure 5.5b. Therefore, with the increase in radius the structure will not buckle under critical loading conditions.

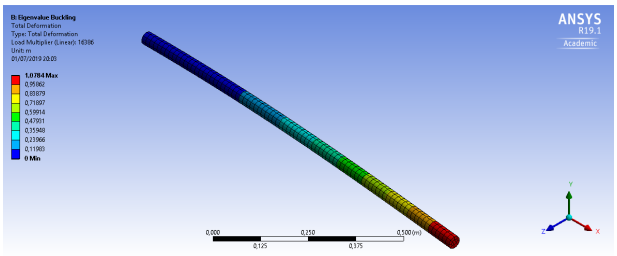

(a) The critical buckling load of the solid beam with a 36 mm radius

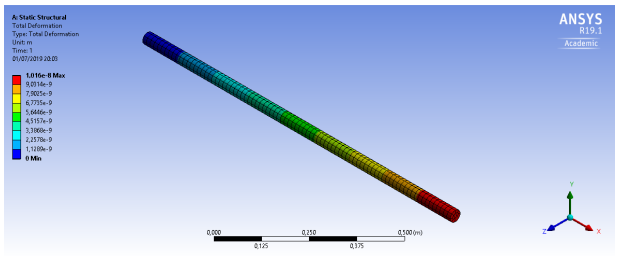

(b) The total deformation in the solid beam with a 36 mm radius

Figure 5.5: Analysis of the 36 mm radius solid beam

5.2. Drivetrain & Suspension Design

The drivetrain of the vehicle begins at the fuel cells. The induction engine requires a three phase alternating current. The direct current produced from the fuel cells will be wired to an inverter, placed next to the motor. The inverter will then provide the required current for the motor. The motor is attached to a gear box which is a single speed transmission. Electric motors are efficient over a large range of speeds compared to an internal combustion engine and so only a single speed transmission is needed. The powertrain will use 17.6 kW of power in order to meet the driving requirements expanded upon in subsection 12.2.1.

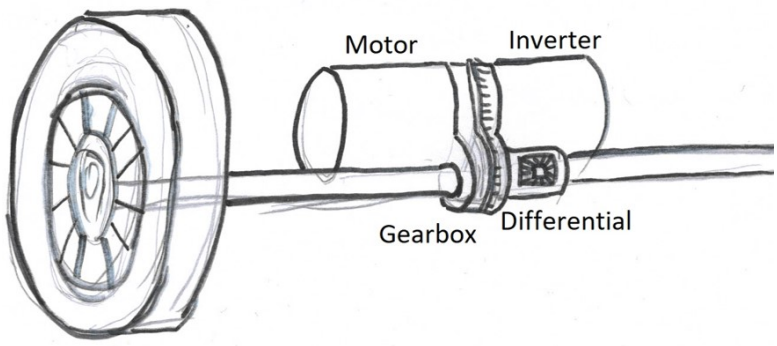

Figure 5.6: The drivetrain on the front axle

To size and design the suspension, the loads are analysed at the critical condition, which is landing. A sizing method from Roskam [20] is used. A schematic for the front and back suspension systems is shown in Figure 5.7.

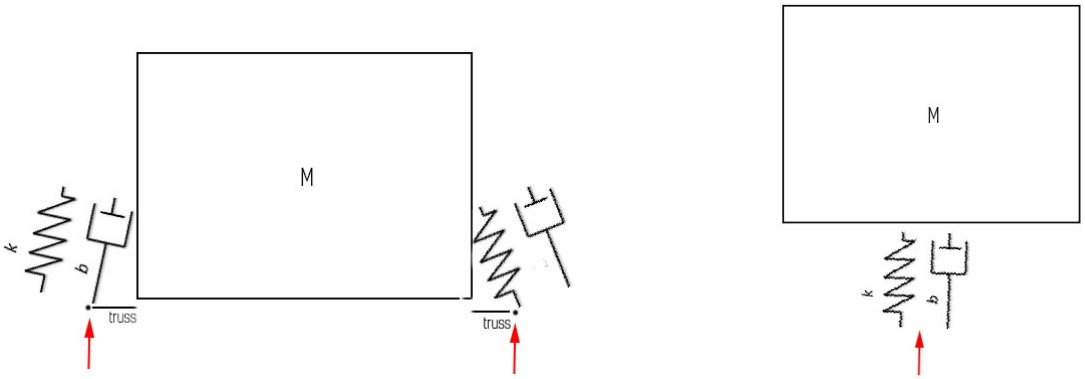

(a) Schematic front suspension system (b) Schematic back suspension system

Figure 5.7: Suspension systems for the front and back

Since there are two front wheels, two spring damper system are placed in the front at an angle of 10° relative to the vertical axis. A steel truss is added to account for the horizontal component of the forces. One spring damper system is places in the back with no angle. FAR23 states that the landing gear load factor is 3.0 for the weight range of the HAVIC [21].

Liquid springs are chosen for the design, which have an energy absorption efficiency of 0.85. The length of the shock absorber is calculated with Equation 5.1

$$s_s = \left[0.5(W_L/g)(w_t)^2/(n_s P_m N_g)) - \eta_t s_t\right]/\eta_s + 2.54 \tag{5.1}$$

Where W_L is the landing weight, for which the MTOW is taken in case the vehicle has to land immediately after take-off. W_t is the touchdown rate, also specified by FAR23 [21]. n_s is number of landing gears, so $n_s = 2$ for the front and $n_s = 1$ for the back. P_m is the maximum load per landing gear, while N_g is the load factor of 3.0. η_t and η_s are the tire and shock absorber efficiency. s_t is the maximum allowable tire deflection which is given by the tire manufacturer. The diameter of the shock absorber is given by Equation 5.2

$$d_s = 0.041 + 0.0025(P_m)^{0.5} \tag{5.2}$$

Finally the horizontal truss has to be sized where aluminium 8091 T6 is used as the material. The truss will be a circular beam, for which the area can be determined by Equation 5.3.

$$A_{truss} = \frac{n_s P_m}{\sigma_y} \tag{5.3}$$

The length of the horizontal truss is dependent on the shock absorber length determined in Equation 5.1.

5.3. Body Shape Design

After determining the chassis and structural body the shape surrounding this framework can be designed. Due to the constraint that specific body types should fit in the cabin, the curvature height is restricted. The shape and streamlining of the exterior body of the vehicle is important to reduce the drag. The drag that occurs is based on two main factors; the frontal area of the vehicle and the drag coefficient. Both should be as low as possible. Various shapes were considered using the wind tunnel models as displayed in Figure 5.8 [22]. From this figure the fifth car was chosen as initial concept shape.

To specify the curvature dimension, research is done on existing cars with a beneficial aerodynamic shape. The Volkswagen XL1 is selected as a reference model because it has the lowest aerodynamic drag coefficient for a production car.[1] This shape is used for the dimensions of the front of the car with an scaling factor of 1.3. Besides the frontal area and bumper dimensions it was not possible to recreate the whole shape. The scale is

[1] https://www.carfolio.com/specifications/models/car/?car=314391 [cited 22 June 2019]

not identical and the back of the HAVIC should converge into the tail. This is done with the shallowest slope possible to create an optimal aerodynamic airflow.

It should be noted that the best shapes are gradually bending down at the back of the car. However, for our vehicle, having a small negative slope would make the effective vertical tail very small, as air is already influenced by the body. Having the top area steeper would cause separation leading to a useless tail, so that is no possibility. It could be chosen to have a small slope at the top surface but a steeper slope for the bottom, as this would cause less separation as the bottom side has a higher pressure. The effective tail would then be below the connection between the body and the tail. This would be most optimal for further design. However, this would cause problems for the other components. For this reason, a compromise had to be made, a steep top surface in combination with a duct to re-energise the flow such that the tail area can be effective and the separation is reduced.

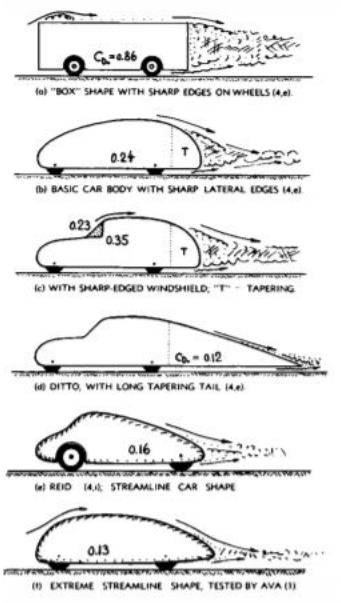

Figure 5.8: Drag coefficients of several smooth wind tunnel models [22]

Deletion and fabrication of parts can be used to reduce parasitic and frontal drag. This is done for specific components, such as the side mirrors. They increase the frontal area and the drag coefficient since they protrude from the side of the vehicle. The mirrors will be replaced with cameras. The rims of the two front wheels will be adapted to reduce the turbulence around the wheel. Smooth wheel covers will be applied, with these hub caps no air can pass through. At the back wheel a fender skirt is used as extension of the body panel to cover the wheel. Because the back wheel will not be able to turn anyways, this is applicable. The underside of the vehicle will be covered with an under tray. No air can be trapped under the vehicle and everything will be closed off.

5.4. Arc Duct

It can be seen in Figure 5.9 that there is a large angle behind the wing where separation of the flow would occur creating a lot of drag as well as a turbulent flow for the tail.

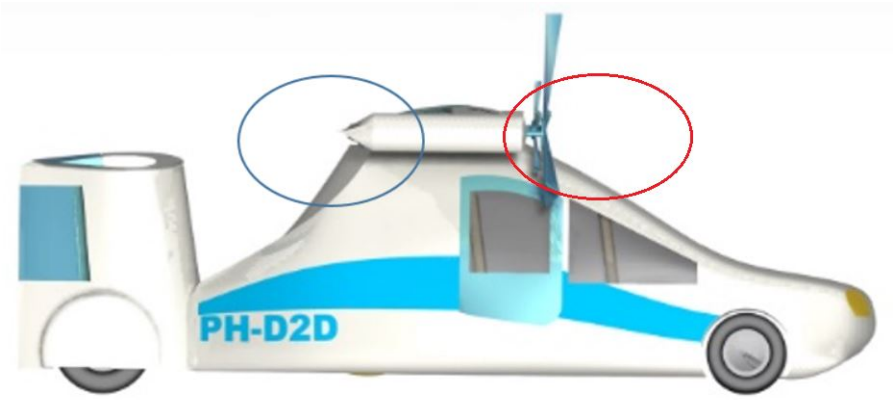

Figure 5.9: Blue circle: separation will occur, Red circle: build up of boundary layer

In order to increase the effectiveness of the tail and reduce the drag, an arc duct is implemented in the car. The arc duct is an inlet of air that compresses and changes the direction of the flow. Firstly, the build up of the boundary layer seen in the red circle in Figure 5.9 causes a lot of drag and pressure problems over the body of the vehicle. The arc duct therefore acts to decrease this pressure build up. Furthermore the arc duct will blow air across to the rear of the main body as seen in the blue circle in Figure 5.9 energising the boundary layer reducing the levels of separation.

In order to provide proof of concept and to size the duct a CFD analysis is performed on both cases, the vehicle having an arc duct and the vehicle without an arc duct. Firstly points were added to the 2D sketch of the vehicle in CATIA. The coordinates of the points are extracted by creating a table of coordinates in a drawing in CATIA. The coordinates are imported into ICEM CFD 19.1. Although structured meshing is simpler to make, an unstructured mesh was required so that it could be refined in areas that had to be looked into in detail such as the arc duct and the area between the body and tail.

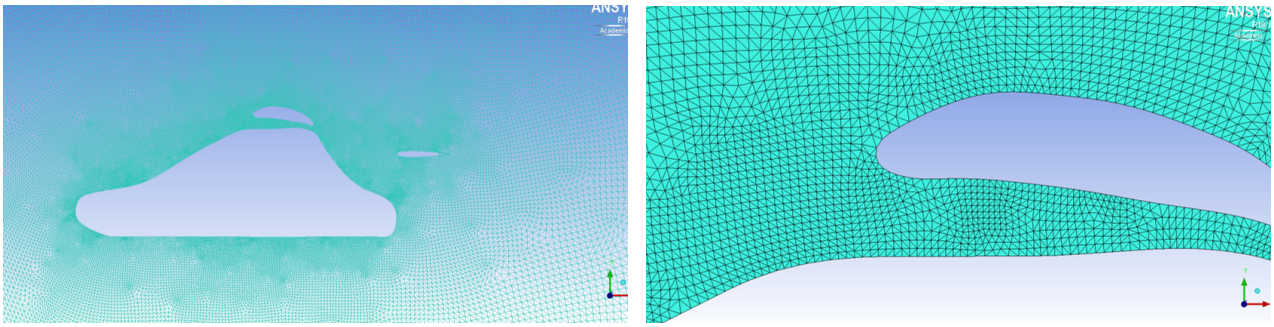

(a) A view of the 2D section surrounded by the mesh.

(b) The refined structured mesh in the arc duct

Figure 5.10: Suspension systems for the front and back

The arc duct should not compress the air enough that it reaches mach 1. Shock waves increase drag and are unwanted. Because the flow is subsonic in the model triangular meshing as seen in Figure 5.10 with 3 sides and 3 vertices rather than quadrilateral meshing is acceptable, saving on computational time. However the mesh was refined in the areas seen in Figure 5.11

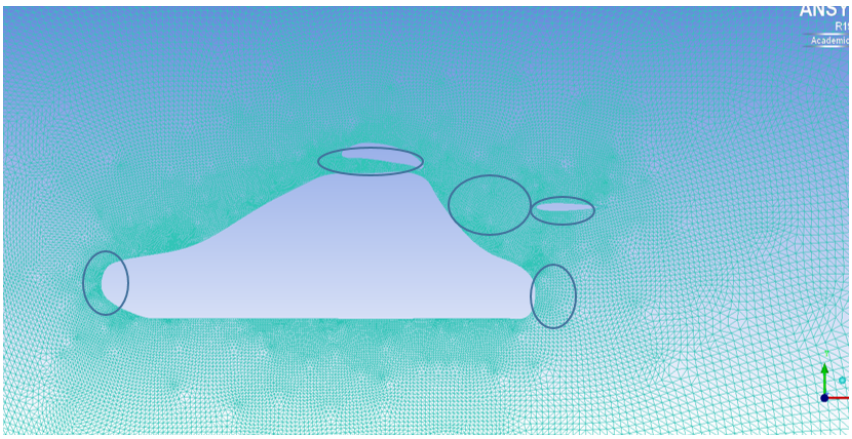

Figure 5.11: The refined locations of the mesh.

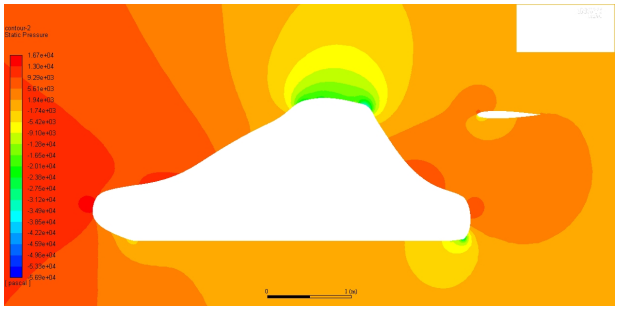

Figure 5.12: CFD computed the static pressure distribution around the body with no duct

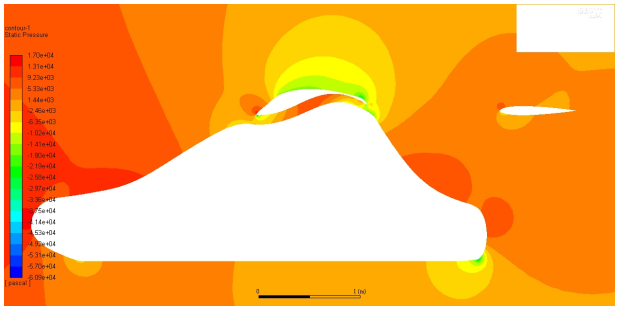

Figure 5.13: CFD computed the static pressure distribution around the body with arc duct

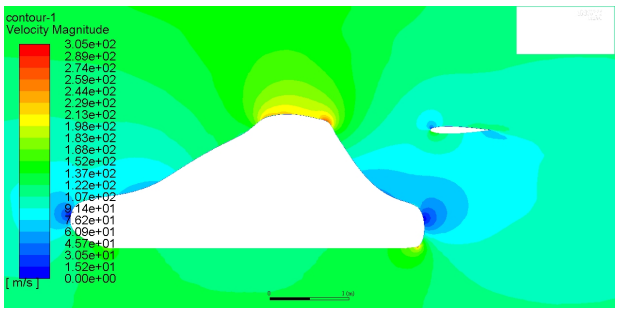

Figure 5.14: CFD computed the velocity distribution around the body with no duct

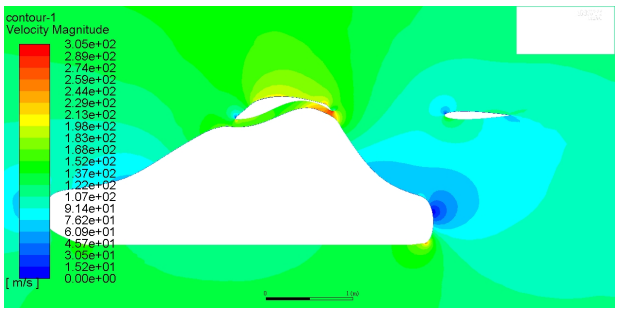

Figure 5.15: CFD computed the velocity distribution around the body with duct

The CFD analysis results regarding static pressure distributions can be seen in Figure 5.12 and Figure 5.13. As you can see, the pressure distributions are very similar, however there are noticeable differences. The first main difference is that the arc duct induces higher pressure at the back, which implies less separation occurs and thus less drag is felt by the vehicle. Furthermore, less separation is beneficial for the use of the tail surfaces as well. The second difference is that the low pressure zone on top is curved more in the shape of the vehicle, such that the pressure does not change rapidly, but rather changes gradually.

The limited accuracy of the mesh used and the fact that turbulence and vortices can not be modelled, the surfaces should be looked at in detail. It is clear to see that there is potential for the arc duct concept. The flow towards the rear of the car is faster once the duct was positioned. This improves the flow towards the rear of the vehicle and allows for much more efficient performance of the rudder and reduction in drag. Furthermore, as seen in Figure 5.15, the increased velocity of the flow adds energy to the boundary layers which will cause it to stick to the surface more than without the duct. Also the high energy air is added to the flow after the fairing on top of the car just before where separation is expected. This can be seen where the orange section ends in Figure 5.14, reducing the level of separation even more.

At this early stage of the development and due to the limited time scale of the DSE project, the CFD analysis could only be used as a proof of concept, due to the time consuming nature of this form of analysis. So from the CFD it is clear that the concept is valid, as the flow is being energised, however for future development of the vehicle, further iterations of the duct design should take place, so as to clean the airflow behind the duct and make the most of this concept.

5.5. Cabin Design

An important interface between passenger and vehicle is the interior. Factors to consider for the interior will be its weight, durability, feel, aesthetics and flame resistance. Since the HAVIC is an aircraft after all, weight plays a large roll in every design choice made.

For larger panels of the interior such as the flooring, honeycomb composite structures can be used, which are lightweight and offer great stiffness. These panels however can form pinholes as the resins outgas during reaction and cure, which necessitates a decorative finish to cover surface flaws. These panels can also be covered in flame retardant carpet.

More complex shapes such as the dashboard are usually made out of PVC, as PVC moulding compounds can be extruded, injection moulded, compression moulded, calendered and blow moulded to form a huge variety of products, either rigid or flexible depending on the amount and type of plasticizers used.

The seating material is an important part of the interior because the seats have to be comfortable for the passenger during the whole mission. Two types of materials are considered, (vegan) leather and fabric seats, both of which have their own advantages. Genuine leather can not be used to comply with the sustainability requirements, however, synthetic leathers have gathered interest from car manufacturers as a replacement for genuine leather. Leathers are easier to clean, are more stain resistant and feel more luxurious to the customer. A leather interior does come at a higher price and higher maintenance costs. Leather interiors also respond more to temperature than fabric interiors, making them less suitable for extreme climates.

In order to make sure that the HAVIC will suit 95th percentile male and 5th percentile female, a proper seat sizing must be done. From the bottom plate of the HAVIC 5 cm of spacing will be kept for structural reasons

and cable management. After these 5 cm the cabin environment will start. The seat will be set with an angle and start from 18 cm from the bottom of the cabin environment with a height of 97 cm. This values will be enough to fit the 95th percentile male. On top of this value, 6.35 cm will have to be added before the cabin environment will end. Adding all these values will give the total height of the cabin environment at the front seat, which is 121.35 cm. To make the HAVIC suit the 5th percentile female, the location of the windscreen, which is 74 cm from the bottom of the cabin environment, is too high. However, when the seat would be able to move upwards and downwards, this would not affect the lateral c.g. position of the HAVIC and would make it suit the 5th percentile female [23]. For the seat pitch, a pitch of 80 cm is found as this number is often used in aircraft.[2] The front seat has got more spacing as the HAVIC needs to be operated from there.

5.6. Tail Design

In order to minimise the drag, the smallest horizontal tail surface area needs to be calculated that corresponds to a certain longitudinal wing position. This is done in a way, where the longitudinal wing positions is adjusted using an iterative process until the smallest horizontal tail surface is obtained that is within the stability region. The surface area is used to obtain the horizontal tail geometry. For the vertical tail, reference data has been used in order to determine the vertical tail geometry. Furthermore, the airfoil is selected for both the horizontal and vertical tail.

5.6.1. Airfoil Selection

As both tail sections should be able to give both negative and positive lift, it is desirable to have symmetric airfoils. Furthermore, it is beneficial to have a high lift curve slope as well as a high range of angles of attack. The reason for this is that the tail size has to increase for lower slopes and a tail should stall at higher angles of attack than the wing. Furthermore, the tail drag should be kept as low as possible. Javafoil is used to model airfoils in different conditions. Parameters such as the aspect ratio, Mach number, Reynolds number, viscosity and density are put into the model and changed per iteration. For the horizontal tail, widely used airfoils for this purpose are looked at. These airfoils and their most important parameters are shown in Table 5.1. In the end, it is decided to go for the NACA 0012, as the lift curve slope and stall angle are significantly higher, having just a slightly higher zero lift drag coefficient. As the wing rests on the tail in driving configuration, the vertical tail should be able to carry high loads. For this reason, the thickness to chord ratio of the vertical tail should be at least 0.26, resulting in a very thick airfoil. As this already leads to high drag values, the thinnest possible airfoil for this thickness ratio is chosen, which is the NACA 0026, for which the same parameters are shown in Table 5.2.

Table 5.1: Horizontal tail airfoil trade-off

Airfoil	α_{stall} [°]	C_{L_α} [-]	$C_{L_{max}}$ [-]	C_{D_0} [-]
NACA 0008	±10	2.41	0.42	0.006
NACA 0009	±8.5	2.70	0.4	0.006
NACA 0010	±11	2.60	0.5	0.007
NACA 0011	±11	2.60	0.5	0.008
NACA 0012	±11	2.71	0.52	0.008

Table 5.2: Vertical tail airfoil parameters

Airfoil	α_{stall} [°]	C_{L_α} [-]	$C_{L_{max}}$ [-]	C_{D_0} [-]
NACA 0026	±25	1.33	0.58	0.013

5.6.2. Horizontal Tail

The c.g. of the HAVIC has to be determined in order to determine the static stability of the vehicle. The position of the c.g. determines the amount of lift that has to be generated by the horizontal tail to counteract the moment by the main wing to ensure static stability. The analysis of the c.g. is done by using the method in [24] where the operational empty weight (OEW) c.g. is determined using Equation 5.4. With the OEW c.g. determined,

[2] https://www.airlinequality.com/info/seat-pitch-guide [cited 19 June 2019]

the loading diagram can be constructed. The location and weight of the components that have been used for the c.g. analysis are listed in Table 5.3 where the nose of the vehicle is used as the reference point.

Table 5.3: Location and mass of the components with respect the nose of the vehicle

Component	Mass [kg]	$x_{position}$ [m]
Tail	22.5	5.0
Chassis	422.5	2.75
Propulsion System	383.9	2.5
Wing	120.0	2.875
Drive Train	158.8	0.51
Fuel Cell	86.0	1.725
Battery	75.0	2.61
Fuel Tank	45.4	3.490
Total	1292	[−]

$$x_{CG_{OEW}} = \frac{\sum_i x_{cg_i} \cdot W_i}{\sum_i W_i} \tag{5.4}$$

The cargo is loaded first, followed by the passengers and the fuel. With this, a loading diagram is constructed for the HAVIC, which is shown in Figure 5.16. From Figure 5.16, the c.g. range can be derived including a safety margin of 2%. The c.g. range has to be within the stability region. The stability region is defined by the stability and controllability curve given by Equation 5.5 and Equation 5.6. The aerodynamic parameters that have been used are derived from the selection of the airfoil for the wing and tail. With these parameters, the scissor plot can be constructed which is shown in Figure 5.17. The numerical values that have been used are listed in Table 5.4.

Table 5.4: Numerical input values for the scissor plot

$C_{L_{\alpha_h}}$ [1/rad]	$C_{L_{\alpha_{A-h}}}$ [1/rad]	C_{L_h} [-]	$C_{L_{A-h}}$ [-]	$C_{m_{ac}}$ [-]	$\bar{x}_{ac}$ [-]	$\frac{d\epsilon}{d\alpha}$ [-]	l_h [m]	$\frac{V_h}{V}$ [-]
4.3	6.3	-0.8	1.5	-0.08	0.25	0.395	2.4	0.8

$$\bar{x}_{cg} = \bar{x}_{ac} + \frac{C_{L_{\alpha_h}}}{C_{L_{\alpha_{A-h}}}}\left(1 - \frac{d\epsilon}{d\alpha}\right)\frac{S_h l_h}{S\bar{c}}\left(\frac{V_h}{V}\right)^2$$

$$\frac{S_h}{S} = \frac{1}{\frac{C_{L_{\alpha_h}}}{C_{L_{\alpha_{A-h}}}}\left(1 - \frac{d\epsilon}{d\alpha}\right)\frac{l_h}{\bar{c}}\left(\frac{V_h}{V}\right)^2}\bar{x}_{cg} - \frac{\bar{x}_{ac} - 0.05}{\frac{C_{L_{\alpha_h}}}{C_{L_{\alpha_{A-h}}}}\left(1 - \frac{d\epsilon}{d\alpha}\right)\frac{l_h}{\bar{c}}\left(\frac{V_h}{V}\right)^2} \tag{5.5}$$

$$\bar{x}_{cg} = \bar{x}_{ac} - \frac{C_{m_{ac}}}{C_{L_{A-h}}} + \frac{C_{L_h}}{C_{L_{A-h}}}\frac{S_h l_h}{S\bar{c}}\left(\frac{V_h}{V}\right)^2$$

$$\frac{S_h}{S} = \frac{1}{\frac{C_{L_h}}{C_{L_{A-h}}}\frac{l_h}{\bar{c}}\left(\frac{V_h}{V}\right)^2}\bar{x}_{cg} + \frac{\frac{C_{m_{ac}}}{C_{L_{A-h}}} - \bar{x}_{ac}}{\frac{C_{L_h}}{C_{L_{A-h}}}\frac{l_h}{\bar{c}}\left(\frac{V_h}{V}\right)^2} \tag{5.6}$$

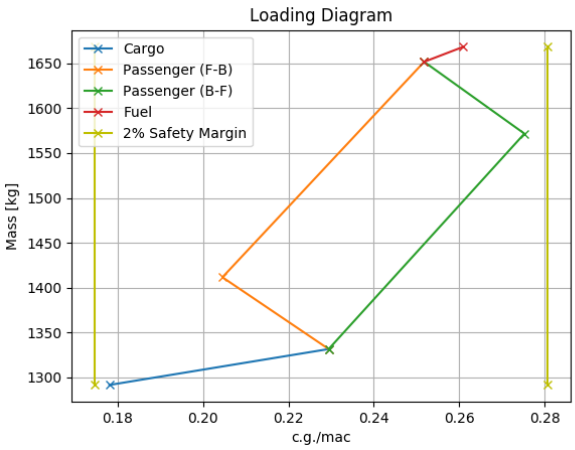

Figure 5.16: Loading diagram for horizontal tail sizing

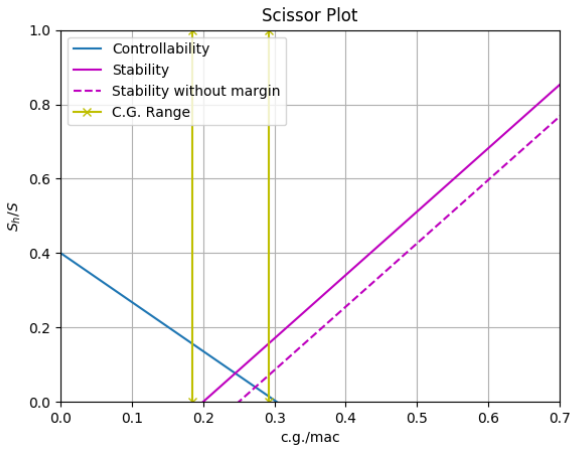

Figure 5.17: Scissor plot for horizontal tail sizing

From Figure 5.17, it can be concluded that at $\frac{S_h}{S} = 0.154$ the minimum horizontal tail surface area is obtained that is within the stability region. With this numerical value, the geometry of the horizontal tail can be determined by computing the aspect ratio (A_h), taper ratio (λ_h), chord length (c_h) and sweep angle ($\Lambda_{h_{0.25c}}$). The final result of the horizontal tail geometry is presented in subsection 7.1.5.

5.6.3. Vertical Tail

The vertical tail is sized based on a different approach compared to the horizontal tail sizing. The vertical tail volume coefficient C_v has to be determined which is obtained from Raymer [25] based on the classification of the aircraft. With this numerical value $C_v = 0.04$, the surface area of the vertical tail can be computed using Equation 5.7.

$$S_v = \frac{C_{vt} b_w S_w}{L_{vt}} \tag{5.7}$$

Again, with the surface area of the vertical tail known, the geometry of the vertical tail can determined by computing the aspect ratio (A_v), taper ratio (λ_v), chord length (c_v) and sweep angle ($\Lambda_{v_{0.25c}}$). The final result of the vertical tail geometry is presented in subsection 7.1.5

5.6.4. Elevator Sizing

The elevator is sized based on take-off conditions, since the aircraft has to generate a pitch up moment. The method that has been used in order to size the elevator is retrieved from [26]. The elevator has to generate a positive as well as negative lift for longitudinal static stability. Furthermore, a moment balance has to be made for take-off conditions to determine the amount of lift that has to be generated by the tail, which can be seen in Figure 5.18. From the moment balance, the lift generated by the tail can be calculated with Equation 5.8. Furthermore, the lift coefficient of the tail can be computed with Equation 5.9, where V_r is the rotational speed which is equal to the stall speed of the aircraft V_{stall}. The numerical values used for Equation 5.8 and Equation 5.9 are given in Table 5.5 and Table 5.6. Furthermore, $Iyy\ddot{\theta}$ is determined to be 2251.31 Nm.

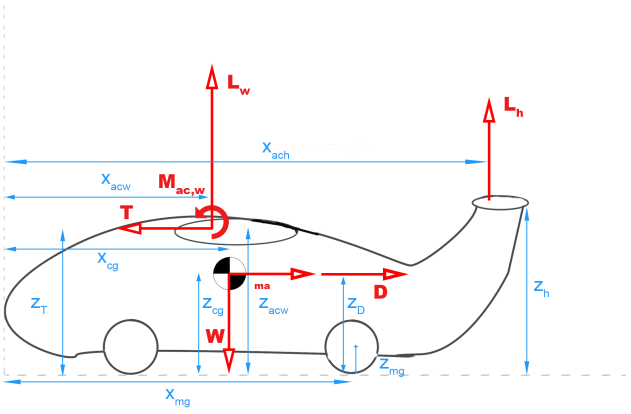

Figure 5.18: Moment balance for take-off conditions

Table 5.5: Position of the forces and component for the moment balance

x_{mg} [m]	x_{cg} [m]	x_{ac_h} [m]	x_{ac_w} [m]	z_D [m]	z_{mg} [m]	z_T [m]	z_{cg} [m]
4.984	2.5092	4.8136	2.4854	1.053	0.15	1.7	1.053

Table 5.6: Input values for the moment generated by different forces

M_{L_w} [Nm]	M_{ac_w} [Nm]	M_a [Nm]	M_W [Nm]	M_D [Nm]	M_T [Nm]
44958.31	-332.66	2463.32	-40481.29	357.25	-4742.76

$$L_h = \frac{M_{Lw} + M_{ac_w} + M_a + M_w + M_D + M_T - Iyy\ddot{\theta}}{x_{ac_h} - x_{mg}} \tag{5.8}$$

$$C_{L_h} = \frac{2L_h}{\rho_0 V_r^2 S_h} \tag{5.9}$$

In order to determine the elevator chord to horizontal tail chord ratio, Equation 5.10 and Equation 5.11 have been used. With this, the control surface effectiveness (τ_e) can be determined which is equivalent to 0.633. From this, the elevator to horizontal tail chord ratio ($\frac{C_e}{C_h}$) can be derived using Figure 4.22 which is equal to 0.4377

$$\alpha_h = \alpha + i_h - \epsilon \tag{5.10}$$

$$\tau_e = \frac{\alpha_h + \left(\frac{C_{L_h}}{C_{L\alpha_h}}\right)}{\delta_{E_{max}}} \tag{5.11}$$

The next step, is to calculate the required elevator deflection in order to trim the aircraft for various velocities and thus ensure longitudinal static stability. Prior to this, the aerodynamic parameters have to be determined which is done by applying Equation 5.12, 5.13 and 5.14. Furthermore, it was assumed that $\frac{b_e}{b_h} = 1$ and the maximum elevator deflection allowed is $\pm 25°$ [26].

$$C_{m_{\delta_e}} = -C_{L_{\alpha_h}} \eta_h \bar{V}_h \frac{b_e}{b_h} \tau_e \tag{5.12}$$

$$C_{L_{\delta_e}} = C_{L_{\alpha_h}} \eta_h \frac{S_h}{S} \frac{b_e}{b_h} \tau_e \tag{5.13}$$

$$C_{L_{h_{\delta_e}}} = C_{L_{\alpha_h}} \tau_e \tag{5.14}$$

With all the aerodynamic parameters known, the required elevator deflection for different velocities can be determined with Equation 5.15. The required elevator deflection with respect to the velocity of the aircraft has been computed for sea level and cruise condition. These plots are displayed in Figure 5.19. From this figure, it can be seen that the required elevator deflection in order to trim the aircraft becomes more positive with increasing velocity. Furthermore, the elevator deflection is negative which means that it creates as positive lift in order to counteract the pitching moment created by the main wing and the thrust generated by the propellers due to high wing configuration. The numerical values used for the computations are given in Table 5.7.

Table 5.7: Input values for the calculation of the elevator deflection

$C_{l_{\alpha_h}}$ [1/rad]	C_{L_c} [-]	C_{L_0} [-]	C_{m_0} [-]	C_{m_a} [-]	$C_{m_{\delta_e}}$ [-]	$C_{L_{\delta_e}}$ [-]	$C_{L_{h_{\delta_e}}}$ [-]
4.3	0.5812	0.24	0.05	-0.575	-0.892	0.402	2.720

$$\delta_e = -\frac{\left(\frac{T(z_T - z_{cg})}{\bar{q}S\bar{c}} + C_{m_0}\right)C_{L_{\alpha_h}} + \left(C_{L_c} - C_{L_0}\right)C_{m_\alpha}}{C_{L_\alpha}C_{m_{\delta_e}} - C_{m_\alpha}C_{L_{\delta_e}}} \tag{5.15}$$

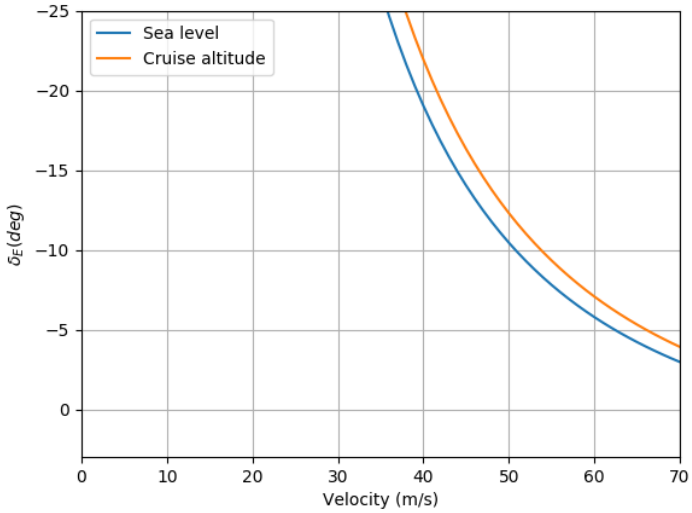

Figure 5.19: Required elevator deflection for longitudinal static stability for different velocities

In order to check that the elevator does not cause stall during take-off rotation, the horizontal tail take-off angle has to be considered which is given by Equation 5.16. The tail angle at take-off has to be less than the stall angle of the horizontal tail which is given by Equation 5.17. If it turns out that this is not the case a redesign should be considered. The angle of attack at take-off for the horizontal tail ($\alpha_{h_{TO}}$) is 0.0258°, whereas the stall angle during take-off of the horizontal tail (α_{h_s}) is 5.1°. Therefore, the horizontal tail satisfies the stall requirement. The final geometry of the elevator is presented in subsection 7.1.6

$$\alpha_{h_{TO}} = \alpha_{TO}\left(1 - \frac{d\epsilon}{d\alpha}\right) + i_h - \epsilon_o \tag{5.16}$$

$$\alpha_{h_s} = \pm\alpha_{h_{s:\delta_E=0}} - \Delta\alpha_{h_E} \tag{5.17}$$

5.6.5. Rudder Sizing

The first step of rudder sizing is to determine the most critical condition for which it should be sized. For a multi-engine normal general aviation aircraft this condition is asymmetric thrust [26]. To size for this most critical condition it is assumed that the right wing is not producing any thrust, and thus that the rudder will be deflected to the left (positive). First, the b_R/b_v ratio and maximum rudder deflection are set at 0.54 and 30° respectively [26]. In accordance with regulations, a minimum controllable speed is defined as follows: $V_{MC} = 0.8V_s$. The total yawing moment generated around the z-axis is computed by Equation 5.18.

$$\sum N_{cg} = 0 \Rightarrow T_L y_t + L_v l_v = 0 \Rightarrow N_A = \sum_{n=1}^{0.5\cdot n_{prop}} -T_n l_n \tag{5.18}$$

Next, the rudder control derivative $C_{n\delta r}$ is computed using Equation 5.19 at maximum rudder deflection. For this equation zero side slip ($\beta = 0$) and zero aileron deflection ($\delta_a = 0$) are assumed. Additionally the aircraft is assumed to be symmetric, hence $C_{n_0} = 0$.

$$C_{n\delta r} = \frac{1}{\delta_r}\left(\frac{N_A}{qSb} - C_{n0} - C_{n_\beta}\beta - C_{n_{\delta_A}}\delta_A\right) = \frac{N_A}{qSb\delta_r} \tag{5.19}$$

From this, the control surface effectiveness (τ_r) can be found using Equation 5.20

$$\tau_r = \frac{C_{n\delta R} b_r}{-C_{L_{\alpha V}} \overline{V}_v \eta_v b_v} \tag{5.20}$$

With the vertical tail coefficient from Equation 5.21.

$$\overline{V}_v = \frac{l_v S_v}{b_w S_w} \tag{5.21}$$

If τ_r is larger than 1, the rudder requirement cannot be fulfilled with the current c.g. position and vertical tail design. In this case the design needs to be adjusted, or the c.g. location needs to be changed and all previous steps are repeated. If τ_r is smaller than 1, one may continue and use it as an input for Equation 5.22 [26].

$$\frac{C_r}{C_v} = \left(\frac{\tau_R \sqrt{0.7}}{0.8}\right)^2 \tag{5.22}$$

If $\frac{C_r}{C_v}$ is larger then 0.5, it is advised to change to a moving vertical tail with $\frac{C_r}{C_v} = 1$. The area can simply be calculated using Equation 5.23. The total yawing moment generated is -4680.41 Nm. With this, the $C_{n\delta R}$ can be calculated which is equal to -0.0404, where a value of 4.5 has been used for $C_{L_{\alpha_v}}$ Next to this, the control surface effectiveness (τ_r) can be computed which is equal to 0.675 and thus the $\frac{C_r}{C_v}$ ratio can be determined from Figure 4.22, which is equivalent to 0.498. The final result of the rudder geometry is presented in subsection 7.1.6.

$$A_R = \frac{C_r}{C_v} C_v \cdot \frac{b_r}{b_v} b_v \tag{5.23}$$

5.7. Material Choice

The main body contains three main components as defined in subsection 3.5.2: the frame, the fuselage/main body skin and the interior. These will be elaborated on in this section.

5.7.1. Frame

A literature study is conducted to choose a best fitting material for the frame. Four materials that are used more often in aerospace structures and are considered for the design are; aluminium, beryllium, composite materials and titanium [13]. In CATIA, a first stress calculation and deflection check is performed. With those values, the best fitting material will be chosen. Next to the mass, the density, the cost, the toxicity, and the manufacturability, the sustainability will be considered. All those factors are seen as important for the choice of the material to be used. In Table 5.8, the most important material properties are mentioned.

Table 5.8: Material properties

	Aluminium 7075 T6	**Beryllium S-200**	**Al(8089) - 20 % SiC MMC powder**	**Titanium alpha - beta alloy**
Mass [kg]	302	155	-	255.2
Density [kg/m3]	2800	1850	2670	4500
Toxicity	Low	High, during manufacturing	Medium, during manufacturing	None
Price [€/kg]	€3,50	€436, -	€211, -	€18, -
Manufacturability	Not weldable	Poor weldability	Limited shaping	Poor weldability
Sustainability	43% is being recycled, excellent durability	10% is being recycled, excellent durability, reacts with oxygen at high temperatures, highly toxic, rare material	3% is being recycled, excellent durability	23% is being recycled, excellent durability

From these four materials, the titanium alpha-beta alloy is chosen as the main material for the frame. The mass and density are not the only criteria, because in this trade-off the sustainability aspect, manufacturability and costs have major impacts on the choice as well. It might seem that beryllium is a best solution considering the mass of the truss structure. However, this material is highly toxic when being manufactured and beryllium is a rare material on Earth. When beryllium gets inhaled, this can lead to serious consequences.[3] [4] Furthermore, beryllium is a difficult to handle metal and very costly [5, 27]. Based on these factors, this material is disregarded. The composite of the four is disregarded as well, due to the price in combination with the manufacturability. The truss structure is not easy to manufacture with composites [5]. In a later phase, composites still might be chosen for the frame material. For this, a better understanding of composite frames should be acquired by the team. Of the two materials left, the titanium alloy has been chosen over the aluminium 7075 T6. The main reason is the manufacturability of the materials. As both can be recycled, both are in the price range that can be afforded and both are non toxic.[5] Titanium is weldable wheras aluminium is not. To weld titanium, certain precautions have to be taken, but that will result in a structure that is more easily changed. If aluminium is to be used, this truss structure should be moulded out of one piece and that would increase the costs a lot as well as the changeability of the design. With titanium, a prototype can be build and tested and changes can be made that are needed.

5.7.2. Fuselage Skin

The material of the skin of the fuselage is assumed to be minimally loaded as the frame takes up all the load. This can be achieved by the fact that the cabin will not be pressurised and that the chassis is a spaceframe structure. The main function of the fuselage skin is that it is the barrier between the vehicle interior with passengers and the environment. This means that several other factors are of importance, such as resisting impact, ability to provide the aerodynamic shape and durability. From literature, it becomes apparent that there are two main contenders for aircraft: aluminium and carbon fibre reinforced composites [28].[6] [7]

One of the potential impact forces on the vehicle is a bird strike. Around 90% of the bird strikes take place at an altitude lower than 1500 m [29], which is exactly the operating altitude of the HAVIC. As there are no bird impact rules for a normal category FAR 23 aircraft [30], this will not be taken into account in this analysis. However, one should realise that a relatively small bird of for example 1.5 kg can result in a significant impact. This is demonstrated by Equation 5.24 and Equation 5.25 [30], which show that a spherical mass with 0.1 m radius of 1.5 kg at 69.4 m/s (cruise speed) will result in a force of 36 kN. This should be taken into account in further analysis.

$$\Delta KE = W = \frac{1}{2} m V^2 \tag{5.24}$$

$$F = \frac{W}{d} = \frac{\Delta KE}{d} \tag{5.25}$$

Another important parameter for the material is its ability to be shaped in double curves as these are required for the aerodynamic shape of the vehicle. Such a shape can for example be formed by stretching or deep drawing for metals. As these processes are not suitable for composites, resin transfer moulding could be used for composites[11]. The materials are pre-selected based on this property.

Finally, the durability of the materials are taken into account. Phenomena such as erosion and corrosion can severely deteriorate the material properties. For this analysis the long term exposure to fresh water and UV light (sunlight) are looked at.

As with all other aircraft components, the mass for the skin should be minimised. With a CATIA model an estimate for the skin area is made. It resulted in approximately 26 m^2. Skin thickness for a light aircraft may be as small as 0.38 mm.[8] However, skin thicknesses for example the Boeing 737 and Boeing 757 are from 1

[3] https://www.lenntech.com/periodic/elements/be.htm [cited 19 June 2019]
[4] https://mmta.co.uk/metals/Be/ [cited 19 June 2019]
[5] https://www.lenntech.com/periodic/elements/ti.htm [5] [cited 19 June 2019]
[6] http://www.keytometals.com/Article95.htm [cited 14 June 2019]
[7] https://www.boeing.com/commercial/787/by-design/-/advanced-composite-use [cited 14 June 2019]
[8] http://www.keytometals.com/Article95.htm [cited 7 June 2019]

mm to 1.6 mm and 0.99 mm respectively.[9] [10] For a mass range, the mass is computed based on a 0.5 mm thickness and a 1 mm thickness. A summary of the relevant properties of the materials considered can be seen in Table 5.9 [5].

Table 5.9: Relevant material properties for potential fuselage skin materials

	Al 2024 T3	**Al 7475 T61**	**Al 8009 RS**	**2024 T3, Al/aramid**	**7075 T761, Al/aramid**	**Epoxy /HS carbon fibre**
Density [kg/m^3]	2770	3532	2930	2380	2350	1570
Mass (max) [kg]	72.3	92.0	76.5	62.1	61.3	41.0
Mass (min) [kg]	36.1	46.0	38.2	31.1	30.7	20.5
Water (fresh)	Excellent	Excellent	Excellent	Excellent	Excellent	Excellent
UV light	Excellent	Excellent	Excellent	Excellent	Excellent	Good
Price [eur/kg]	1.90	3.53	8.53	307.00	307.00	33.45
Price (max) [eur]	136.99	324.27	651.86	19068.03	18827.68	1370.52

From Table 5.9 it becomes clear that the composites containing aramid are by far the most expensive. Even though they are slightly lighter than their aluminium counterparts, they are almost 30 times as expensive, excluding them from further consideration. Because of the aluminium alloys similar durability properties, the lightest and cheapest will enter the final trade-off.

One of the major advantages of using Al 2024 T3 rather than a composite is the existing knowledge about the failure modes of metals. Another advantage is that metals are generally cheaper than composites. A final difference between the two is their durability rating to degradation by UV light. In this case "good" means in the order of years, while "excellent" means decades. In order to improve the UV light durability, several solutions such as absorbers, stabilisers, blockers or coatings may be used [5]. However, the epoxy/HS carbon fibre results in a mass saving of roughly 43%. In the case of the HAVIC the mass saving outweighs the price as long as it fits within the budget. For this reason the epoxy/HS carbon fibre is chosen as the skin material, with examples such as the Boeing 787 and Airbus A350 proving that a composite skin can be done.

One difference between the previously mentioned aircraft and the HAVIC is that the cabin of the HAVIC is not pressurised. This relieves the tensile strength requirement of the material, but makes the structure vulnerable for buckling. Even though, the structure is unloaded, it can can still be loaded when it comes into contact with another object or person. It is undesirable that a dent occurs every time the user touches their HAVIC. This means that prevention of this failure mode might require stiffening elements on the skin. These stiffeners can be composite or metal and be joined through mechanical fasteners or adhesives. For further analysis several load cases can be tested to determine the shape of the stiffeners as this is load dependent. This, however, may cause a significant weight increase, both from the added material and the added joints.

Another option is to make the stiffening elements and integral part of the structure. This might be easier to achieve with metals than with composites as they are more suitable for machining. This has the advantage of lowering the part count. The disadvantage of this, is that it allows for rapid crack growth. Also, it results in a lot of scrap material. The same effect may be achieved by using a composite sandwich structure. This may be beneficial for the mass as it eliminates the need for stiffening elements. Another benefit is that you have a smooth surface on both sides of the panel. On the other hand a sandwich panel might be more difficult to repair and join [31].

In future iterations a detailed trade-off may take place between an unstiffened skin, a stiffened skin or a honeycomb. Based on the different load cases, the mass for each of the options can be determined. Other factors such as maintainability and repair options may also play a role in addition to the factors already mentioned in this section.

[9] https://www.easa.europa.eu/sites/default/files/dfu/CODAMEIN_Report_20120312_highres.pdf [cited 7 June 2019]
[10] https://flightsafety.org/wp-content/uploads/2016/10/asw_oct11_p18-20.pdf [cited 7 June 2019]

6

Power System Design

This chapter discusses the design methods for each power system. To calculate the energy and power needs for the vehicle a model is made using the mission profile shown in section 6.1. The design methods and trade-offs for the resulting power system designs can be found in this chapter, while the final overview is shown in chapter 7. A trade-off between different power sources is explained in section 6.2, while calculated energy budgets are shown in section 6.3. Design choices for the fuel cell are elaborated upon in section 6.4. The design choices for the tank can be found in section 6.5. Finally, the design methods for the Auxiliary Power Unit (APU) system can be found in section 6.6.

6.1. Mission Profile

The vehicle's mission profile is shown in Figure 6.1. The HAVIC is capable of driving for up to 50 km to its take-off location, taking off and climbing to an altitude of 1.5 km, cruising for 400 km (with reserve fuel for an added 45 minutes of cruise), descending and landing, then driving for another 50 km from the landing strip to its final destination. The significant driving range and reserve fuel allow for flexibility within each trip in terms of allowable proximity to airfields.

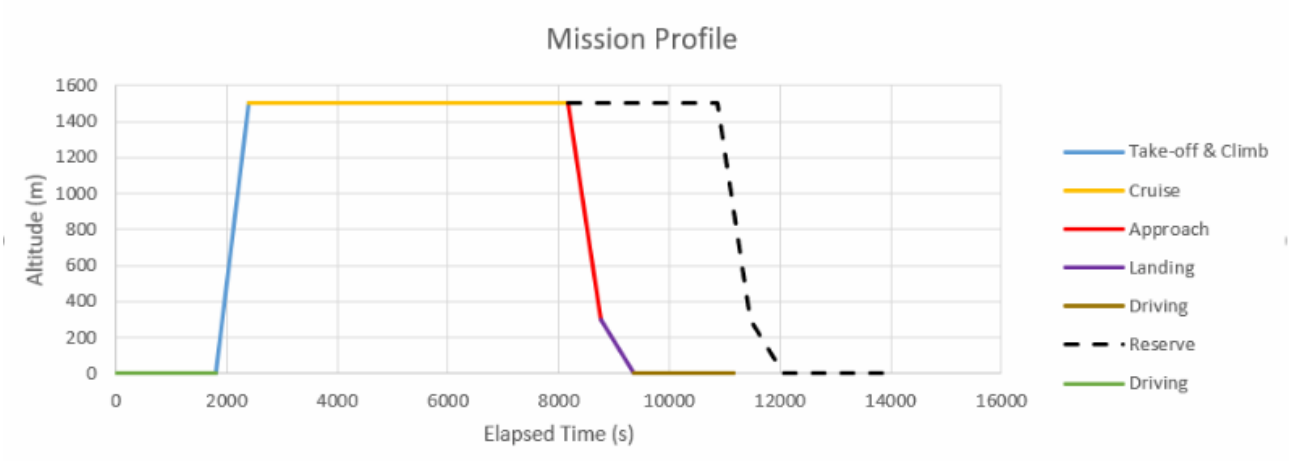

Figure 6.1: An altitude vs time plot representing the mission profile

6.2. Power Source

In search for the best sustainable power source two types are considered: Lithium (Li) ion batteries and hydrogen fuel cells. Two parameters are important to consider: volumetric density and gravimetric density. Values are found in Table 6.1.[1] [2]

[1] https://www.energy.gov/sites/prod/files/2014/03/f12/fcm01r0.pdf [cited 07 June 2019]
[2] https://www.eia.gov/Energyexplained/?page=about_energy_units [cited 07 June 2019]

Table 6.1: Gravimetric and volumetric densities of different fuels

Fuel source	Gravimetric density [Wh/kg]	Volumetric density [Wh/L]
Li-ion battery	100-243	250-730
Hydrogen (1 bar, 15.6°)	39,405.6 (HHV) 33,313.9 (LHV)	3.3 (HHV) 2.8 (LHV)
Hydrogen (690 bar, 15.6°)	39,405.6 (HHV) 33,313.9 (LHV)	1,478.6 (HHV) 1,250.0 (LHV)
Hydrogen (liquid)	39,405.6 (HHV) 33,313.9 (LHV)	2,790.0 (HHV) 2,358.6 (LHV)
Gasoline	12,888.9	9,500
Kerosene	11,944.4	9,722.2

Hydrogen has the highest gravimetric energy when compared to batteries and traditional fossil fuels, however, its volumetric density compared to gasoline and kerosene is much lower. For a required energy, liquid hydrogen will need a volume that is more than four times as high as that of the fossil fuels. Compared to Li-ion batteries it has much higher gravimetric and volumetric densities, but one should take into account that to use hydrogen as an energy source, fuel tanks and fuel cells are needed, which reduces the overall energy density. The main challenge in designing a hydrogen power system therefore lies in designing lightweight solutions to the fuel tank and fuel cell problem. For the power source, liquid hydrogen is chosen over all other forms of hydrogen and batteries because of their excessive weight or volume.

6.3. Power and Energy Budgets

The total power and energy budgets can be divided into two parts. The propulsive and driving power is provided by the primary power source, the hydrogen fuel cell stack. The power for secondary electrical systems such as cabin thermal control, navigation, and avionics is provided by the auxiliary power source, the Li-ion battery. Splitting up the vehicle's power needs as such increases its range and allows for independent operation of the primary and secondary power systems. This allows, for example, for the vehicle's control surfaces and navigation system to remain operational even in the case of an empty fuel tank, which is an indispensable safety feature.

6.3.1. Primary Power and Energy Budgets

For each mission phase, the required propulsive force is calculated via Equation 4.4. This equation takes the MTOW and drag values which have been calculated as described in subsection 3.5.1 and subsection 4.2.2 respectively. In the case of the initial driving phase, this driving force is converted to power required through the simple relation below. The total efficiency involved in the total conversion of energy to driving force $\eta_{driving}$ includes the efficiencies of the inverter, gear box, and single speed transmission. A value of $\eta_{driving} = 0.9$ is taken as a conservative assumption.[3]

$$P_{drive} = \frac{T_{drive} V}{\eta_{driving}} \tag{6.1}$$

Furthermore, the required shaft size for such a power output can be estimated by the simple empirical relation[4] below, where P is the power in kW and N the RPM of the engine.

$$D = \sqrt{\frac{1.33 \cdot 10^6 P}{N}} \tag{6.2}$$

In the case of a flying phase, the power required from propulsion is calculated as described in section 4.1. The throttling of the HLP and CP is decided based on whether or not the vehicle is taking off or landing. The efficiency, power input, thrust, and wake velocity for the HLP and CP are then calculated using the momentum theory propeller efficiency model, and Equation 4.3 and Equation 4.2 from the actuator disk model.

[3] https://www.energy.gov/sites/prod/files/2014/04/f15/10097517.pdf [cited 11 June 2019]
[4] https://www.pumpsandsystems.com/relationship-torque-and-shaft-size [cited 22 June 2019]

The energy required by each phase is calculated by multiplying the phase's duration with its average power required, i.e. $E = Pt$. The following charts in Figure 6.2 and Figure 6.3 detail the system's power and energy budgets for each phase of the mission.

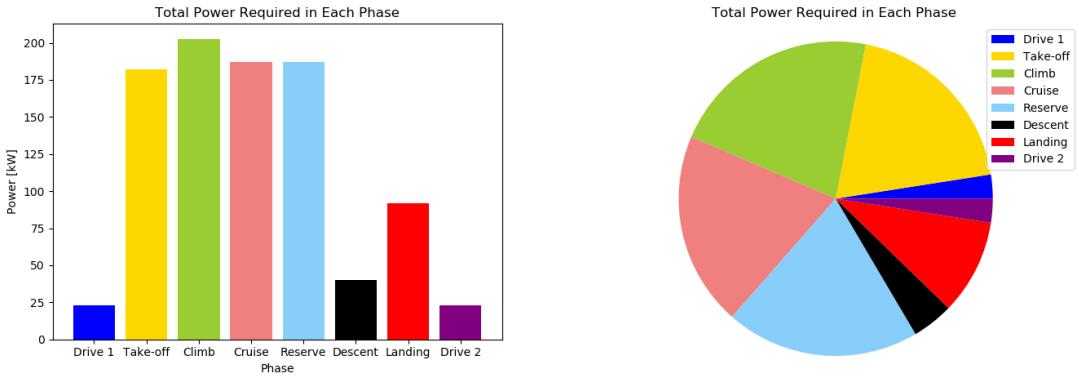

Figure 6.2: A breakdown of the system's power usage over the course of the entire mission

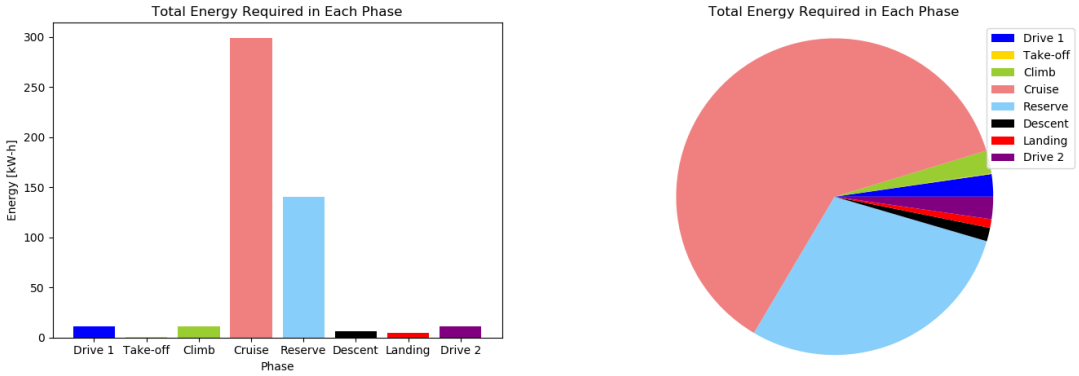

Figure 6.3: A breakdown of the system's total energy usage over the course of the entire mission

The mass of hydrogen used in phase i with duration T_i and average power required P_i is calculated via Equation 6.3. Here, SED_{H2} is the Specific Energy Density of hydrogen (131 MJ/kg [32]) and $\eta_{fuel\ cell}$ is the efficiency of the fuel cell (60%).[5]

$$M_{H2,i} = \int_0^{T_i} \frac{P_i}{SED_{H2} \cdot \eta_{fuel\ cell}} dt \tag{6.3}$$

The total mass of hydrogen required to power N phases then equals: $M_{H2,total} = \sum_{i=0}^{N-1} M_{H2,i}$. For each succeeding phase, the mass of hydrogen used in previous phases is subtracted from the vehicle's total mass when calculating the required thrust. The resulting water is released into atmosphere and thus does not increase the vehicle's mass. This calculation results in a total hydrogen mass of 21.77 kg and, taking a density of 70.8 kg/m^3, a total hydrogen volume of 0.327 m^3.

6.3.2. Secondary Power and Energy Budgets

Additionally to the hydrogen fuel cell, which powers the electric motors driving the propellers and wheels, the vehicle should also carry an APU to provide power to secondary electrical systems. A simple Li-ion Battery was chosen for this application, as options are easily available for the power values required. This APU will also be charged by the regenerative braking described in section 6.6. Also, some of the excess heat generated by the hydrogen fuel cell can be used for cabin thermal control as described in section 6.4, and this is reflected in the secondary power budget. An initial estimate was performed based on reference data so as to size and select an appropriate APU. It can be found in Table 6.2 below.

[5] https://www.energy.gov/sites/prod/files/2015/11/f27/fcto_fuel_cells_fact_sheet.pdf [cited 11 June 2019]

Table 6.2: Power estimate for secondary electrical systems

System	Power [W]	Duration [s]	Energy [kW-h]	Source
Cabin Thermal Control	1700	11000	5.194	[6]
Parking Sensors	3.5	150	$1.458 \cdot 10^{-4}$	[7]
Reverse Driving Camera	5	150	$2.083 \cdot 10^{-4}$	[8]
Radio	200	9000	0.5000	[9]
Phone Charging	6	8000	0.01333	[10]
Windscreen Wipers	60	12918	0.2153	[11]
Lights	250	12918	0.8971	[12]
Flight Management	75	12918	0.2691	[13]
Flight Control	150	12918	0.5383	Estimate
Locking Mechanism	1	5000	0.001389	Estimate
Anti-icing	300	10000	0.833334	Estimate
Communications Radio	300	9000	0.7500	[14]
Anti-lock Breaking System	72	100	$2.000 \cdot 10^{-3}$	Estimate
Total	4522.5		9.21	

6.4. Fuel Cell System

To provide the required power to the engines, a fuel cell system is designed. In this section the design choices for the fuel cell system will be discussed. The fuel cell system consists of three parts, the fuel cell stacks, the oxygen supply and the hydrogen supply.

6.4.1. Fuel Cell Stacks

Designing the fuel cell stack is not included in the scope and time frame of this project. Since attractive solutions for the power requirements already exist on the market, only a choice of fuel cell will be made. Several different types of fuel cell exist, an overview is given in Table 6.3.[15]

Table 6.3: Overview of different fuel cell types

Fuel cell Type	PEMFC	AFC	PAFC	MCFC	SOFC
Qualified Power	1W-500 kW	10W-200 kW	<10 MW	10 MW	100 W- 200 MW
Electricity Efficiency	50-60%	60-70%	37-42%	65%	60%
Operating Temperature	50-100 degree	<80 degree	150-200 degree	600-650 degree	500-1000 degree
Start-up Time	Low	Low	Medium	High	High
Contaminant Sensitivity	High	High	Medium	Low	Low
Cost	Medium	Medium	High	High	High
Durability	High	Low	Medium	Low	Low

From Table 6.3 it is clear there are two feasible candidates, the Proton Exchange Membrane fuel cell (PEMFC) and the alkaline fuel cell. Only the PEMFC will be considered, as its durability is higher and its sensitivity to contaminants is lower, though it's still higher than the other fuel cells [33]. PEMFC's are used in automotive industry, for example in the Toyota Mirai and thus are a proven technology.

[6] https://www.nrel.gov/docs/fy00osti/28960.pdf [cited 22 June 2019]
[7] https://www.globalsources.com/si/AS/Loyal-International/6008832651379/pdtl/Parking-Sensor/1041501637.htm [cited 22 June 2019]
[8] https://www.azdome.hk/news-detail-181.html [cited 22 June 2019]
[9] https://www.caraudioshop.nl/autoradios-alpine-CDE-1787BT [cited 22 June 2019]
[10] http://energyusecalculator.com/electricity_cellphone.htm [cited 22 June 2019]
[11] http://www.irjes.com/Papers/vol2-issue4/Version%20%202/B240714.pdf [cited 22 June 2019]
[12] http://donklipstein.com/d2.html [cited 22 June 2019]
[13] http://www.esterline.com/Portals/17/Documents/en-us/cma9000.pdf [cited 22 June 2019]
[14] https://www.rohde-schwarz.com/nl/product/m3ar-productstartpage_63493-9147.html [cited 22 June 2019]
[15] https://www.energy.gov/eere/fuelcells/types-fuel-cells [cited 19 June 2019]

Powercell is a manufacturer of PEMFC based in Sweden. The Powercell S3 platform is scalable and can deliver up to 125 kW peak power and is chosen for its high power density. The units have an integrated water cooling system to ensure operating temperatures of at most 85°. Two units will be installed to provide the required power. Parameters of the fuel cell are given in Table 6.4.

Table 6.4: Fuel cell parameters

Fuel Cell Model	Max Power [kW]	Dimensions $w \times h \times d$ [cm]	Mass [kg]
Powercell S3	125	$42.0 \times 56.8 \times 15.6$	43
Max continuous temperature (K)	Fuel pressure (bar)	Coolant pressure (bar)	Air pressure (bar)
358	<2.2	<2.5	<2.3

6.4.2. Oxygen Supply

Oxygen is needed for the reactions in the fuel cell to take place. Supplying pure oxygen to the fuel cells would improve their performance, however, carrying pure oxygen on board would lead to excessive fuel mass. Therefore an air intake system needs to be designed. The air intake has several functions: taking in air, purifying, compressing, temperature controlling and humidifying.

Airflow

To calculate the intake area, the airflow required by the fuel cell is first determined. To calculate the required airflow to the fuel cell, Equation 6.4 [33] is used. For this equation it is assumed that air contains 21% oxygen.

$$\dot{m}_a = 3.5710^{-7} \lambda \frac{P_e}{V_c} \tag{6.4}$$

where λ is the stoichiometric multiple, P_e is the power output of the fuel cell and V_c is the average voltage of each cell. Using $\lambda = 1$ provides the exact amount of air to react with the hydrogen. To ensure all reactive sites are utilised, it is advised to use at least $\lambda = 2$ [33].

An estimation of the intake area can be made using Equation 6.5.

$$A = \frac{\dot{m}}{\rho V_a} \tag{6.5}$$

Here A is the intake area in m^2 and v_a is the airspeed in m/s. During idle or low airspeed situations the air needs to be moved by an adequate fan. The airflow calculated in Equation 6.4 needs to be converted to the volumetric flow rate of humid air, since dry air cannot be used. Equation 6.6 is used to calculate the density of the humid air needed.

$$\rho_{humid} = \frac{p_d}{R_d T} + \frac{p_w}{R_w T} \tag{6.6}$$

where p_d and p_w are the partial pressures of dry air and water vapour in pascals, R_D and R_w are the specific gas constants of dry air and water vapour respectively in J/kgK and T is the temperature of the resulting mixture in Kelvin.

p_w is calculated using Equation 6.7, where ϕ is the relative humidity as a fraction and p_{sat} is the saturated pressure, obtained from [33].

$$p_w = \phi p_{sat} \tag{6.7}$$

To calculate p_d, Equation 6.8 is used , where p_f is the fuel cell operational pressure.

$$p_d = p_f - p_w \tag{6.8}$$

Finally, the humid airflow Q in m^3/s to the fuel cell is calculated using Equation 6.9, where $\dot{w}$ is the massflow of water added to the air, calculated using Equation 6.14.

$$Q = \frac{\dot{m}_a + \dot{m}_{water}}{\rho_{humid}} \tag{6.9}$$

Purity

For the fuel cell to function properly, contaminants in the air have to filtered out. Sulphur compounds, nitrogen compounds, carbon monoxide and other volatile compounds are common contaminants found in air, of which sulphur compounds are most damaging to the fuel cell as they adsorb to the platinum catalyst and reduce the number of available reactive sites. The fuel cell's performance is decreased by as much as 30% when exposed to 1 ppm of SO_2 [33].

Temperature

The operational temperature has great influence on the performance of the fuel cell, as in most other chemical reactions. The upper limit to the operational temperature is set to 85°, based on the thermal stability and conductivity of the Naflon membrane.

The fuel cell is of course not 100% efficient, in converting chemical energy to electrical energy, heat is also created. For fuel cells where the water is emitted as a vapour, the heat produced is described by Equation 6.10. This waste heat has to be transported from the fuel cell to prevent overheating. For fuel cells with a power output of more than 5 kW, liquid cooling is needed.

$$P_h = P_e\left(\frac{1.25}{V_c} - 1\right) \tag{6.10}$$

Pressure

Increasing the pressure has a similar effect on the fuel cell as increasing the temperature, the rates of diffusion are enhanced at higher operating pressures and activation over potential is reduced by increasing the site occupancy at the catalyst [33]. The act of pressurising requires power from the fuel cell, so it is only effective if this parasitic power draw is smaller than the power gained from pressurising.

The voltage gain can be calculated using Equation 6.11 [33]. The power gain is simply obtained by multiplying the voltage gain by the current times the number of cells, $\Delta P = \Delta V I n$.

$$\Delta V = C l n\left(\frac{p_2}{p_1}\right) - 3.58 \cdot 10^{-4}\left(\frac{T_1}{\eta_m \eta_c}\right)\left[\left(\frac{p_2}{p_1}\right)^{0.286} - 1\right]\lambda \tag{6.11}$$

Inputting slightly optimistic values [33] found in Table 6.5, we find that the optimum pressure ratio range is between 2 and 4 with a peak at 3, which falls in line with the operating pressure of the Powercell fuel cell.

Table 6.5: Inputs to the voltage gain/pressure ratio equation

Parameter	Value	Unit	Description
C	0.1	[-]	Constant determining voltage gain
T_1	288	[K]	Inlet air temperature
η_m	0.95	[-]	Compressor motor efficiency
η_c	0.75	[-]	Compressor efficiency
λ	1.75	[-]	Stoichiometric multiple

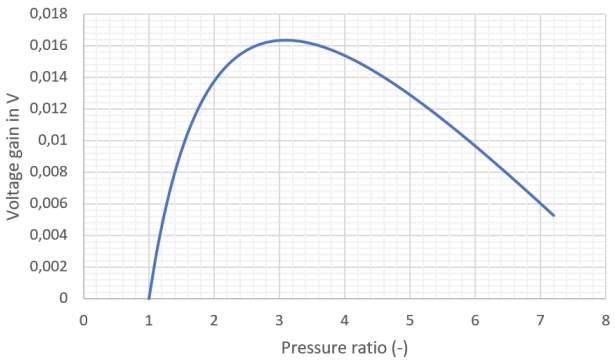

Figure 6.4: Graph showing the relation between the voltage gain and the compressor pressure ratio

And the temperature increase due to compression is calculated using Equation 6.12 [33].

$$\Delta T = \frac{T_1}{\eta_c}\left[\left(\frac{p_2}{p_1}\right)^{\frac{\gamma-1}{\gamma}} - 1\right] \tag{6.12}$$

Finally, the compressor power is calculated using Equation 6.13 [33]

$$P_c = c_p \frac{T_1}{\eta_c}\left[\left(\frac{p_2}{p_1}\right)^{\frac{\gamma-1}{\gamma}} - 1\right]\dot{m} \tag{6.13}$$

Humidity

Water management is a crucial aspect of designing the fuel cell system due to the nature of the Naflon membrane. The membrane needs to be fully hydrated to perform optimally. In fuel cells operating above 60°, dry airflow will dry out the electrodes faster than water is produced by the fuel cell. Humidity must lie between 90 and 100% for the membrane to be hydrated, but humidity above 100% should be avoided to prevent flooding of the electrodes. The required water flow $\dot{w}$ can be calculated using Equation 6.14 [33].

$$\dot{m_{water}} = 0.622 \frac{p_v}{p_f - p_v}\dot{m}_a \tag{6.14}$$

The fuel cell produces essentially pure water, this water can be recirculated to humidify the membrane. The rate of water production $\dot{w}_{FC}$ by the fuel cell is calculated using Equation 6.15 [33]

$$\dot{m}_{water_FC} = 9.34 \cdot 10^{-8}\left(\frac{P_e}{V_c}\right) \tag{6.15}$$

6.4.3. Air Intake Components

To fulfil all the functions of the air intake system, several components are chosen and integrated in the system, namely the following:

1. Inlet, to ensure enough airflow to the fuel cell
2. Air filter, to remove contaminants in the ambient air
3. Fan, to make sure there is airflow when the vehicle sits idle
4. Compressor, to bring the pressure of the air to the operating pressure of the fuel cell
5. Humidifier, to prevent the fuel cell membrane from drying out
6. Temperature controller, to ensure the air is at the correct temperature for the fuel cell

An overview can be seen in Figure 6.5.

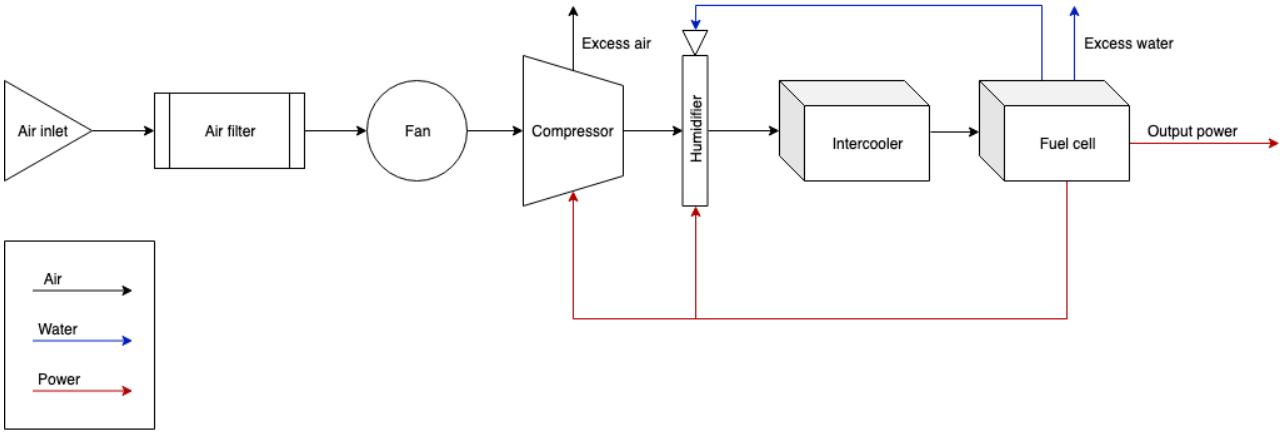

Figure 6.5: Layout of the air intake

To supply the large amount of air needed a whale-mouth design is chosen. Whale-mouth designs have been proven in cars to be able to provide the large airflow needed. Another interesting option is the NACA duct as they are less disturbing to the boundary layer and thus induce less drag. However, they are less likely to provide

the required amount of air without being overly large, as they are not perpendicular to the freestream of the air. Using Equation 6.4 and Equation 6.5 the intake area is calculated with worst case scenario in mind, being ascending to cruise altitude with maximum power settings. The parameters used for the intake area calculated are listed in Table 6.6.

Table 6.6: Parameters for the intake area

Parameter	Value	Unit	Description
λ	2.0	[-]	Stoichiometric multiple
P_e	125	[kW]	FC Power output
V_c	0.7	[V]	Cell Voltage
$\dot{m}$	0.013	[kg/s]	Massflow of air
ρ_{1500m}	1.056	[kg/m^3]	Air density
V_a	39	[m/s]	Inlet velocity
A	0.0033	[m^2]	Intake area
n	2	[-]	Number of inlets

The filter system has two functions, filtering harmful chemical compounds and removing dust particles. For the filtration system a dust filter and an activated carbon filter are chosen, both are chosen for their design versatility and lifetime. Both are also chosen for their ability to let the airflow through without pressure drops [33].

For the compression of the air, screw compressors are chosen for their compact size and ability to provide the required pressure ratio without pulsation. Lysholm[16] provides performance maps of their superchargers and show they can create a pressure ratio of 2.2 at around 60% compressor efficiency. The maximum power used and temperature increase by the compressor can be calculated using Equation 6.12 and Equation 6.13. The parameters used for the calculations are listed in Table 6.7.

Table 6.7: Parameters for the maximum power and temperature calculations by the compressor

Parameter	Value	Unit	Description
T_1	288	[K]	Inlet air temperature
η_c	0.6	[-]	Compressor efficiency
η_m	0.95	[-]	Compressor motor efficiency
$\frac{p_2}{p_1}$	2.2	[-]	Maximum pressure ratio
γ	1.4	[-]	Heat capacity ratio
ΔT	121.3	[K]	Temperature increase
c_p	1004	[J/kg/K]	Specific heat of air
$\dot{m}$	0.013	[kg/s]	Massflow of air
P_c	16.7 kW	[kW]	Max power compressor
P_c %	13.3%	[-]	Parasitic power usage of the compressor

To humidify the air, water must be added to the air after compressing, that way the humidification also acts as a method of cooling the air. The water flow that needs to be added is calculated using Equation 6.14. The water that is produced by the fuel cell can be recirculated to the humidifier. This amount of water is calculated using Equation 6.7 and Equation 6.15, with the parameters listed in Table 6.8. p_{sat} comes from [33]. Pentair is a manufacturer of fuel cell humidifiers that make use of the water exhaust from the fuel cells.[17]

[16] `http://www.lysholm.us/pdf/diagram_lys1200ax.pdf` [cited 17 June 2019]

[17] `https://engineeredfiltration.pentair.com/en/products` [cited 18 June 2019]

Table 6.8: Parameters for the calculations of water produced by the fuel cell

Parameter	Value	Unit	Description
ϕ	1.0	[-]	Relative humidity
p_w	0.4739	[bar]	Required water pressure 85°
p	2.2	[bar]	Fuel cell operating pressure
$\dot{m}$	0.023	[kg/s]	Maximum waterflow needed to keep 100% relative humidity
$\dot{m_{water_{FC}}}$	0.018	[kg/s]	Maximum water production by fuel cell
$\dot{m_{water,FC_{total}}}$	0.041	[kg/s]	Total waterflow out of FC
Water recycle	57	[%]	Percentage of water out of FC that can be recycled

To cool the air after compression and humidification, two options exist. Air to liquid intercoolers and air to air intercoolers. Air to air intercoolers have the advantage of being simpler in design and requiring no power to operate. The advantages of air to liquid intercoolers includes being smaller in size and being more effective in cooling, controlling the temperature is also easier, due to being able to vary the liquidflow through the heat exchanger. The latter is the reason that an air to liquid intercooler is chosen, as it's important to operate the fuel cell near 85° at all times to ensure maximum efficiency. A smaller heat exchanger also means the intake can be smaller, which is of importance for aerodynamic performance. A thorough analysis needs to be done to validate the choice of intercooler and its capability to control the temperature of the air.

6.5. Hydrogen Tank

This section will describe the design choices made for the hydrogen tank and other components related to hydrogen supply. The hydrogen supply consists of a hydrogen tank, pressure valves, pressure regulators, sensors and piping.

The first step in designing the hydrogen tank is to calculate the tank volume based on the energy requirements from the mission profile. During liquefaction of normal hydrogen, ortho-hydrogen is spontaneously converted to para-hydrogen under exothermic conditions. This leads to considerable boil-off rates in long term storage. Triggering the conversion during liquefaction, which requires a certain amount of extra energy input, avoids this conversion afterwards. Therefor, para-hydrogen will be referred to as LH2. LH2 is considered in saturated state under associated cryogenic temperature to reduce the disadvantage in the density of GH2. The fluid pressure corresponds to the saturation pressure and their relationship can be seen in figure Figure 6.6. From Figure 6.7 can be seen that increasing the pressure leads to a drop in density of the saturated LH2 density, while GH2 behaves in the opposite way.

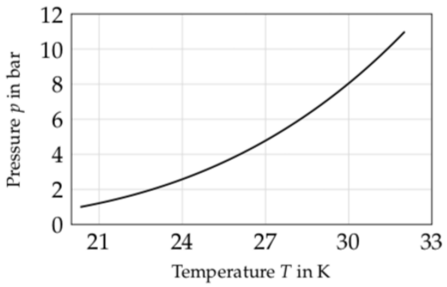

Figure 6.6: Saturation curve para-hydrogen [34]

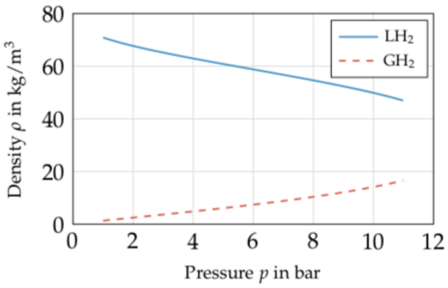

Figure 6.7: Density of liquid and gaseous para-hydrogen [34]

Resulting from heat-input pressure in the tank will rise due to boil-off of LH2. Once the maximum allowable tank pressure is reached, venting might be necessary to decrease or maintain the pressure level. Therefor p_{vent} is denoted as the maximum allowable pressure. In the case of venting, at least 3% of the volume should be available for gaseous hydrogen, making the maximum liquid volume fraction y_{max} = 0.97. Figure 6.8 shows that the mean density of the fuel decreases with pressure. To operate safely, the pressure in the tank has to be greater than ambient pressure as operating below ambient pressure can cause oxygen to flow into the tank, creating an explosive mixture in the case of structural failure. The filling pressure p_{fill} is set equal to this

minimum pressure. To decrease pressurisation efforts before the fuel cell, the operational pressure should be above, but close to the operating pressure of the fuel cell. The venting pressure should be chosen so that it is always higher than the operating pressure of the fuel cell, or the tank will vent at a pressure lower than the fuel cell's operating pressure. Minimising the venting pressure is preferred, as the amount of LH2 available increases with decreasing p_{vent}, shown in Figure 6.9

The minimum pressure is chosen to be 1.2 bar, in accordance with C. Winnefeld [34]. The maximum allowed pressure is 2.3 bar and the venting pressure is 2.2 bar. From Figure 6.7 a density of 64.0 kg/m^3 is interpolated.

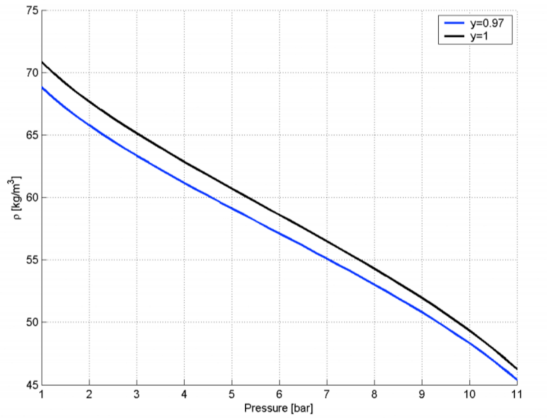

Figure 6.8: Average LH2 density for different pressure range [35]

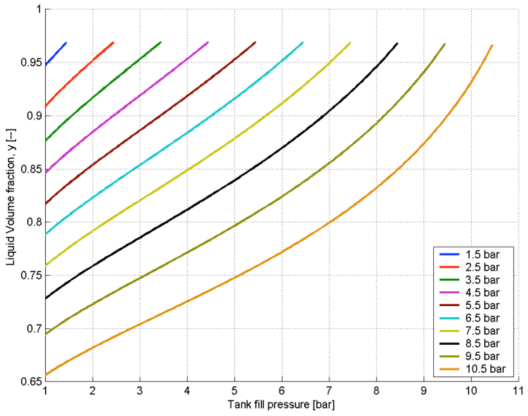

Figure 6.9: Liquid volume fraction vs. pressure for varying venting pressure [35]

In this report only one type of cryogenic tank will be considered as it is unfeasible within the scope and time frame to make an analysis of all the different types. Hydrogen can be stored in several forms, but only liquid hydrogen will be considered. All other forms appear to impractical for the type of aircraft that is to be designed. Two possible types of liquid hydrogen storage exist: supercritical liquid or a saturated liquid. The latter is the only possibility as storing supercritical liquid hydrogen requires tank pressures over 13 bar [35].

6.5.1. Integral vs. Non-integral

A choice has to be made between integral and non-integral tank designs. Non-integral tanks only serve as fuel containers and are supported by a conventional skin/stringer/frame structure. They only have to bear the loads associated with the fuel containment, i.e. pressurisation, fuel slosh and thermal stresses.

Integral tanks form an integral part of the aircraft structure. In addition to the loads described before, they must withstand the usual fuselage axial, bending and shear stresses resulting from the critical aircraft loading conditions. Compared to non-integral tanks, integral tanks have higher structural efficiency, which yields a direct weight saving for the aircraft.

In the HAVIC's case, a non-integral design is chosen. A tank shape in the form of the aircraft's body would be too complex for manufacturing and structural analysis. Being able to remove the tank from the aircraft is also an advantage, in case of maintenance.

6.5.2. Tank Shape

For the tank shape, a few options are considered. Spehrical tanks offer the highest volume to surface ratio which minimises heat flux to the tank, thus the boil-off of LH2. A second option is the cylindrical tank, which offers a lower volume to surface ratio than the cylindrical tank. An advantage compared to the spherical tank is that it is easier to manufacture and it can have a higher volumetric efficiency in normal passenger aircraft. In the case of the HAVIC, no cylindrical shape is present, thus reducing this advantage. A third option is the multisphered tank [36]. Its volume to surface area ratio lies between that of the spherical and cylindrical tank, however in certain geometries it can offer the highest volumetric efficiency. This tank geometry is the hardest to produce however, a spherical design was chosen for the tank. Due to the dimensional constraints it was determined that the spherical shape has the highest volumetric efficiency. Multisphere tank design was considered to be too complex for the scope of this project, but should be considered in future design phases.

6.5.3. Material Choice

In the material selection for the fuel tank, there are multiple factors to be considered. As with any pressure vessel, (specific) strength and stiffness, but also its thermal properties because of the cryogenic storage of LH2.

In order to maximise the strength and stiffness properties but minimise the mass, the specific strength and specific stiffness are shown in Figure 6.10. Materials in the top right corner are desirable for their high specific properties. From this figure, composites, metals and plastics rank the best. Even tough plastics have good specific properties, generally their stiffness is not high enough, they are therefore excluded from further analysis.

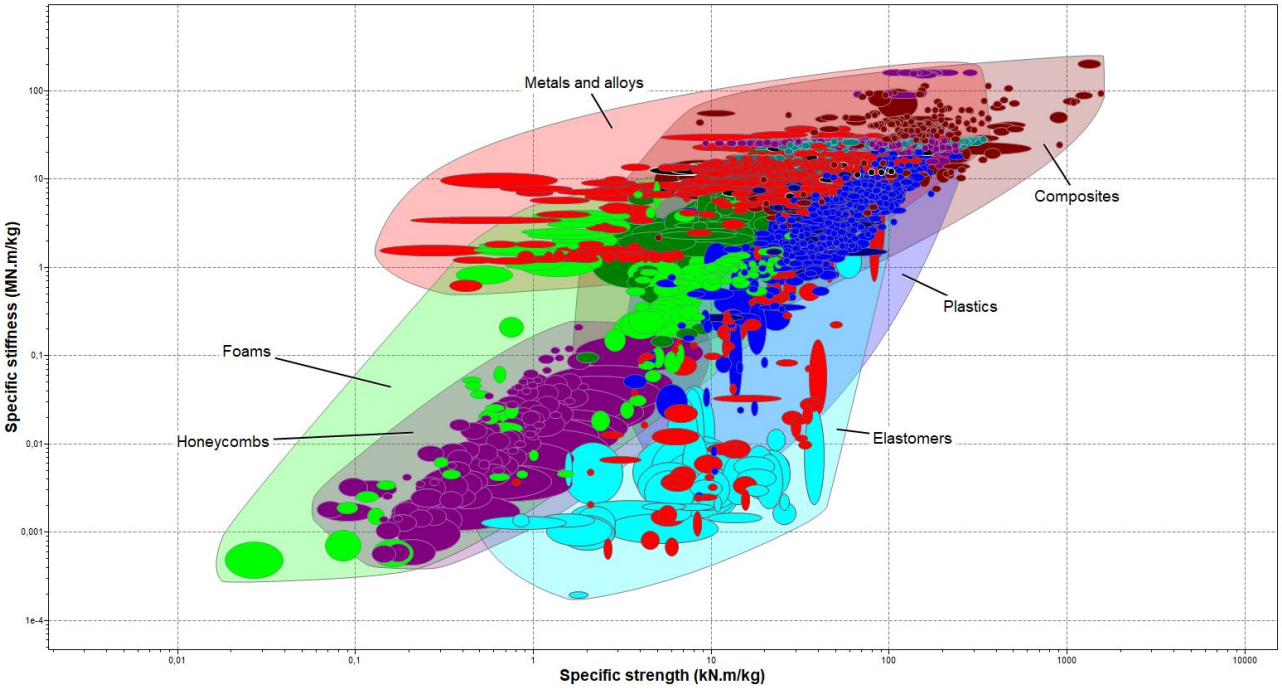

Figure 6.10: The specific strength and stiffness

Two key indices in designing a pressure vessel are the yield-before-break ($\frac{K_{1c}}{\sigma_f}$) and the leak-before-break ($\frac{K_{1c}^2}{\sigma_f}$). The first ensures stable deformation such that it can be detected and repaired, the second allows for stable crack growth such that it can be detected and the pressure is released in a safe manner. For this pressure vessel yield before break is preferable, as this reduces the risk of highly flammable LH2 being released into the air. This approach means that $\frac{K_{1c}^2}{\sigma_f}$ needs to be maximised. The material group ceramics will be excluded based on their low fracture toughness and brittle failure, meaning they will almost not yield at all before failing.

Another challenge that arises is the permeability. Hydrogen molecules are very small and thus capable of permeating through many materials. Metals could be a solution to this, but will most likely not be beneficial for the tank mass. Another suggestion could be using a metallic liner, with a lighter composite shell, however, this may cause thermal stresses due to the difference in thermal expansion coefficient. This may cause separation of the layers or even cracking [37]. In the NASA X-33, a polymer/phenolic sandwich structure was used without any additional liner. Microcracking in the polymer allowed for hydrogen to reach the core material. Once the liquid there has turned into gas, there was a pressure build-up and the sheets delaminated [38].

Hydrogen embrittlement should also be taken into account. This may occur in iron, steel and alloys [39]. It occurs in materials that are susceptible to it and that are under stress [35]. The tank would be under tensile stress as the hydrogen will be pressurised at 2 bar to aid the pumping of the hydrogen. Hydrogen embrittlement may be reversed by applying a certain heat treatment (baking) to diffuse the hydrogen out of the material.

Another important facet to consider are the insulation properties of the material, since liquid hydrogen needs to be stored at 20 K in order to prevent the boiling off of the hydrogen. In this case the hydrogen will only be cooled

passively, so the thermal conductivity and thermal expansion are important parameters. These parameters can be plotted as shown in Figure 6.11.

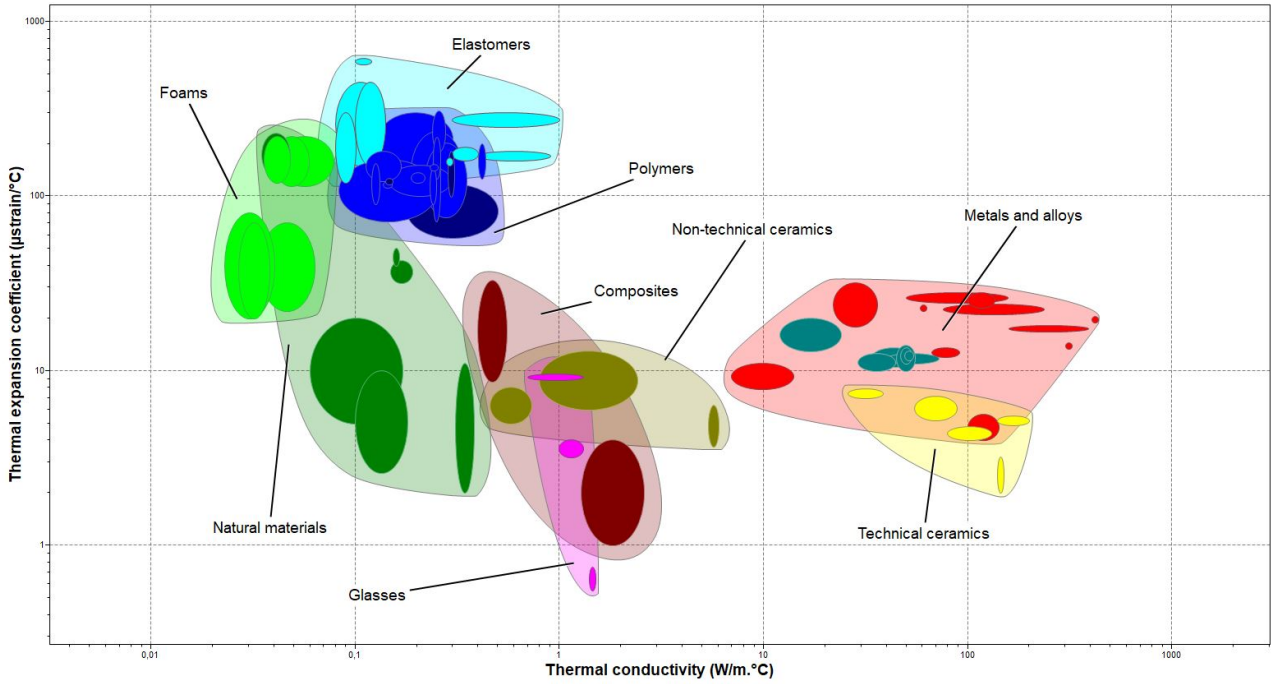

Figure 6.11: The thermal coefficient and the thermal conductivity [5]

For the tank design it is desired for the material to have a low thermal expansion coefficient, to minimise deformation. Additionally, the material should be an insulator, so thermal conductivity should be low. From this figure if becomes clear that foams, elastomers and polymers fit those criteria best. Natural materials are also shown to fit these criteria, but are not considered due to durability concerns. These groups are considered for liner material, as they do not meet the stiffness requirement.

From the literature study in combination with the diagrams three main material categories seem feasible for the tank design, they are summarised in Table 6.9. Specifically mentioned are: Carbon-Fibre-Reinforced Polymer (CFRP), Discontinuous Reinforced Aluminium (DRA) and aluminium [35, 37, 40]. For a first iteration of the tank thickness, three materials are taken into consideration, they are listed in Table 6.10. Note that this first iteration is based on a single walled spherical tank and does not account for mechanisms such as Multi-Layer Insulation (MLI) or vacuum insulation.

Table 6.9: Main tank material groups and their advantages and disadvantages, adapted from NASA [37]

	Metals	**Composites**	**Hybrids**
Advantages	Well established technology Low manufacturing cost Minimal permeation	Lower mass High specific properties Adjustable properties	Optimise for lowest mass
Disadvantages	Higher mass Higher conductivity	Higher cost Complex & costly manufacturing Differing CTE Hydrogen may permeate Liner is required	Complex & costly manufacturing Differing CTE

Table 6.10: Materials properties for the first tank wall thickness iteration [5]

	Epoxy/ HS carbon fibre	**Al-65%Al2O3(Nextel fibre)**	**Aluminium 8091, T6**
Density [kg/m^3]	1550-1580	3400	2560-2610
Young's modulus [GPa]	49.7-60.1	158-179	77-81
Specific stiffness [MNm/kg]	31.7-38.4	46.4-52.8	29.7-31.4
Yield strength [MPa]	603-738	183-252	440-550
Specific strength [kNm/kg]	385-472	53.9-74.2	170-195
Thermal conductivity [W/mK]	1.28-2.6	51	75-79
CTE [$\mu_{strain}/C°$]	0.36-4.02	10.4-12.2	21.3-22.3
Notes	UD prepreg QI lay-up	QI laminate	Solution heat-treated and artificially aged

From the structural analysis it is clear that the epoxy/HS carbon fibre results in the minimum structural mass. In order to prevent hydrogen diffusion a metallic or plastic liner will be implemented. This material should minimise the Coefficient of Thermal Expansion (CTE) difference to prevent cracks from forming in the liner. For more material choices for the insulation, it was decided that the insulation will not be load bearing, but will be located on the outside of the tank. This allows for all components to fulfil their respective purpose.

For the insulator, two foams and an aerogel blanket[18] are compared, their relevant properties are listed in Table 6.11. From the analysis as in subsection 6.5.4, the decision was made to use the aerogel blanket. For the liner 2 metallic and 2 plastics are shown in comparison with the epoxy/HS carbon fibre in Table 6.12. The NiFe alloys are excluded based on their high density, which would result in a significantly higher mass. Because there is a gap in the data considering the liner material, the preliminary estimate is the same as in "Multi-Spherical Composite-Overwrapped Cryogenic Tanks for Hypersonic Aircrafts" by Ilias Tapeinos [36]. This results in a liner made out of PA12 with a thickness of 6.5 mm. However, this still leaves the challenge of the differing CTE coefficients.

Table 6.11: Relevant properties of insulation materials

	Melamine foam	**Expanded PS foam**	**Aerogel blanket**
Density [kg/m^3]	9-12	18-22	70
Thermal conductivity [W/mK]	0.032-0.035	0.033-0.036	0.011

Table 6.12: CTE of liner materials compared to the epoxy/HS carbon fibre

	Epoxy/ HS carbon fibre	**NiFe alloy**	**NiFe alloy**	**LCP (45%)**	**LCP (30%)**	**PA12**
CTE	0.36-4.02	0.5-2.0	1.25-2.0	5-30	2-50	140-180
Density [kg/m^3]	1565	8200	8200	1770	1500	1030
Notes	-	Cold worked, hard	Soft, annealed	-	-	Flexible

6.5.4. Wall Thickness

The thickness of the load-bearing, structural wall is done by using the hoop-stress equation below. A safety factor S_t of 2.0 is used, and the liquid hydrogen must be stored at 2.2 bar pressure.

$$t_{wall,s} = \frac{S_t p r}{2\sigma_{yield}} \tag{6.16}$$

The thickness of the insulating wall is calculated by modelling the heat transfer through the wall as conduction through a straight wall of an area equal to the surface area of the spherical tank ($A = 4\pi r^2$). The liquid hydrogen is stored at $T_{cold} = 16$ K, and for the limiting case a temperature inside the vehicle of $T_{hot} = 273.15 + 80.0$ K is considered.

[18] `http://www.buyaerogel.com/product/thermal-wrap-8-mm/` [cited 12 June 2019]

$$t_{wall,i} = \frac{KA\left(T_{hot} - T_{cold}\right)}{\dot{Q}} \tag{6.17}$$

The allowable heat transfer rate $\dot{Q}$ is calculated via the specific heat formula. As the boiling point of liquid hydrogen is 20.32 K, it is decided that a temperature increase of up to $\Delta T = 3.5$ K over the course of the entire mission (including reserve fuel) is allowable. In reality the vehicle is not expected to travel its maximum range including reserve fuel at a temperature of 80° C, but this value is chosen for safety.

$$\dot{Q} = \frac{Q}{t_{mission}} = \sum_{phase} \frac{m_{H2} C(T) \Delta T}{t} \tag{6.18}$$

Here the heat flow over the course of the mission is approximated as the sum of the heat flow of each of the phases. Clearly the mass of hydrogen in the tank does change within a given phase but a conservative assumption is made by taking the lowest hydrogen mass (at the end of each phase), and therefore calculating the lowest heat flow and highest thickness. The specific heat capacity of liquid hydrogen is calculated as a function of temperature as follows:[19]

$$C(T) = 14.43877 - 1.691T + 0.10687T^2 - 0.00174T^3 \tag{6.19}$$

Based on these equations and the materials taken into consideration for the structural wall and insulation, the total tank masses and thicknesses were calculated for each material combination. These are represented in Figure 6.12 and Figure 6.13 below. The tank masses and thicknesses are grouped by insulating material, as this choice has the greatest effect on the total values. The differences between the structural materials are difficult to make out from this chart, as the insulating wall makes up a much larger percentage of the tank wall's thickness and weight. The numerical values relevant to tank sizing are therefore also provided in Table 6.13. The Carbon fiber and Epoxy composite allows for the lightest and thinnest structural wall, due to its high yield stress and relatively low density.

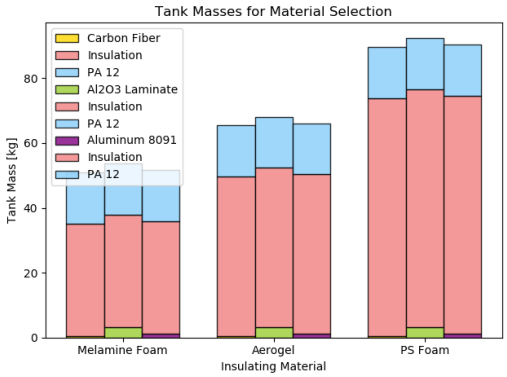

Figure 6.12: Tank masses for each combination of structural and insulating material

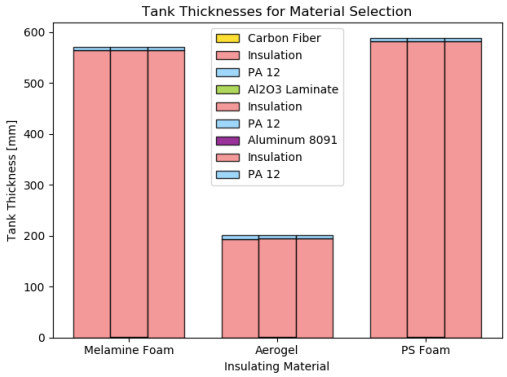

Figure 6.13: Tank thicknesses for each combination of structural and insulating material

Table 6.13: Masses and thicknesses for the structural layer of the tank wall for the different materials considered

Material	Structural Mass [kg]	Structural Thickness [mm]
Carbon Fiber / Epoxy Composite	**0.484**	**0.129**
Al203 Laminate	3.05	0.379
Aluminium 8091	1.17	0.189

It can be clearly seen in Figure 6.12 that the melanine foam insulator results in the lightest fuel tank, followed closely by the aerogel. However, Figure 6.13 shows that the aerogel allows for a much thinner insulating wall than either of the foam materials. This is due to the aerogel material's higher density. The weight of

[19] https://inis.iaea.org/collection/NCLCollectionStore/\protect\T1\textdollar2DPublic/36/045/36045728.pdf?r=1&r=1 [cited 22 June 2019]

the hydrogen fuel tank is not as much of a limiting factor in its design as its volume; the HAVIC's fuselage size is limited by road regulations and the hydrogen fuel tank takes up a considerable fraction of the cabin volume even with the thinnest choice of insulating wall. Therefore the combination of a carbon fiber and epoxy composite material for the structural wall and an aerogel for the insulating wall is chosen for the hydrogen fuel tank. Lastly, the PA12 polymer material is chosen for the inner lining wall to decrease the permeability of the tank wall. A visualisation of the final tank design is presented in Figure 6.14, including all three layers of the tank wall.

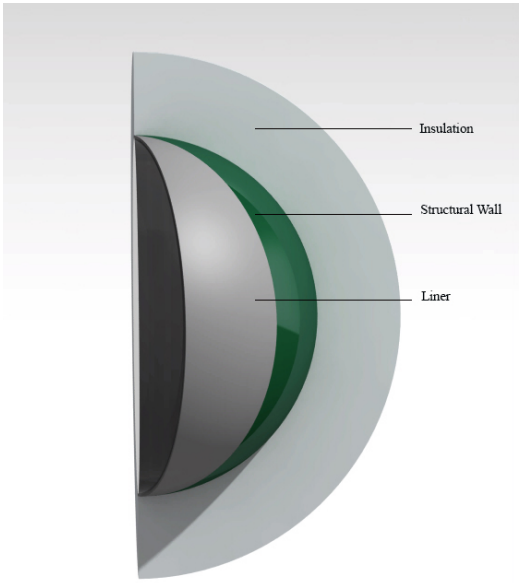

Figure 6.14: 3D model of the final tank design, to scale. The labels point to the separate layers of the tank wall

The final specifications of the hydrogen tank can be found in Table 6.14.

Table 6.14: Final specifications for the hydrogen fuel tank

	Mass [kg]	Thickness [mm]
Liner Layer (PA12)	15.621	6.5
Structural Layer (Carbon Fiber / Epoxy Composite)	0.484	0.13
Insulating Layer (Aerogel)	49.026	194.93
Total	**65.132**	**201.56**

6.5.5. Hydrogen Supply

Several sensors for measuring temperature, pressure and fuel level are required for safe operation and monitoring the LH2 tank. The combination of electrical power in the environment with air and hydrogen obligates appropriate precautions. The sensors have to be designed in compliance with intrinsic safety guidelines. For the proper function of a liquid hydrogen storage system, several valves, heat exchangers and pumps have to be implemented. An overview of the system is seen in Figure 6.15.

During refuelling, valves SV01 and SV02 are opened, so fuel can flow from the filling station to the tank. Some LH2 will be vaporised immediately and can leave the tank via SV02 back to the filling station. At a tank pressure close to venting pressure, gaseous hydrogen flows through the opened SV02 and CV02 through the HE01 and finally to the fuel cell through SV03 [41].

At lower tank pressures, LH2 flows directly through the open SV01 the same way as described. In case the tank's pressure decreases to a defined margin, heated hydrogen will be pumped by IPG1 into the tank to increase the pressure. A redundant pressure relieve valve is installed. Designing or choosing and analyzing every component is not within the reach of this project, therefore a weight margin of 1.3 will be added to the tank mass, which is based on data from similar LH2 tanks designed for vehicles [41].

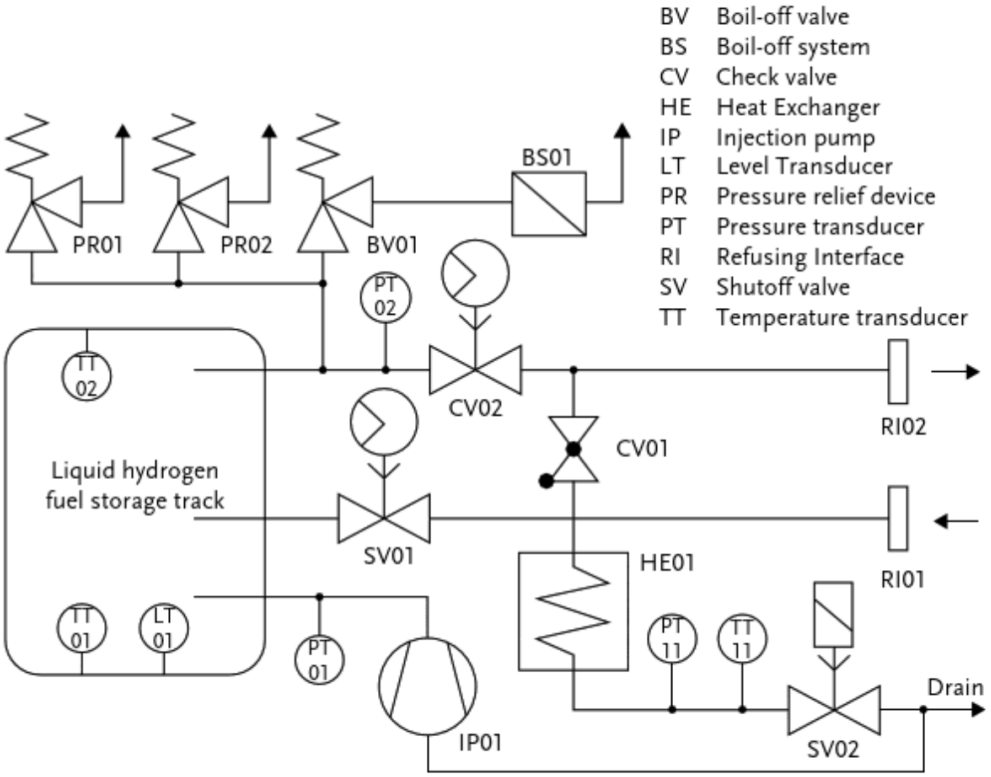

Figure 6.15: Layout of the tank auxiliary system [41]

6.6. APU System

The vehicle's APU should be able to provide sufficient power to secondary electrical systems, as detailed in subsection 6.3.2. A simple Li-ion battery is chosen for this application, as options are easily available for the power values required. This is also capable of being used to drive the vehicle for a short distance in case of severe hydrogen boil-off during parking.

To limit the size and weight of the APU, regenerative braking is used whilst driving and a similar system, regenerative drag, will be used in the landing stage of flying. The regenerative drag works using drag to turn the two CPs that are not providing any thrust in the landing stage just like a wind turbine. Using the python library windpowerlib[20] the power and energy that is generated by the CPs is simulated.

As the propellers convert kinetic energy into electrical energy, the kinetic energy equation is the start of the derivation. The equation is differentiated in terms of time, as power is the rate of change of the energy.

$$E = 0.5mv^2 \qquad (6.20) \qquad P = 0.5v^2\frac{dm}{dt} \qquad (6.21)$$

$$\frac{dm}{dt} = \rho Av \qquad (6.22) \qquad P = 0.5\rho Av^3 C_p \qquad (6.23)$$

Equation 4.3 gives the power output of a single propeller with ρ being the density of air, A being swept area of the propeller and C_p being the power coefficient which exists due to the slowing of air behind the propeller. As there is a wing behind the propeller, the power coefficient was taken as 0.1, conservatively lower than the power coefficient of a normal wind turbine which is between 0.35-0.45.

[20] https://windpowerlib.readthedocs.io/en/stable/modelchain_example_notebook.html [cited 22 June 2019]

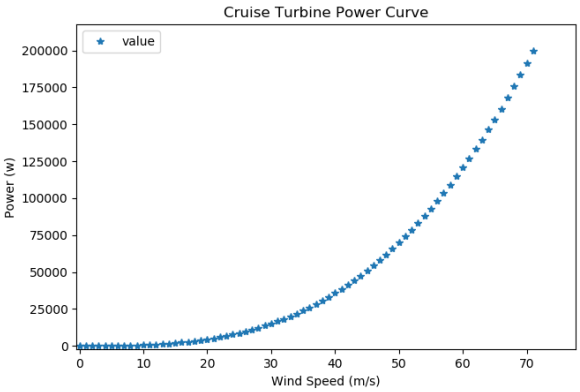

Figure 6.16: The power generated by a single cruise propeller

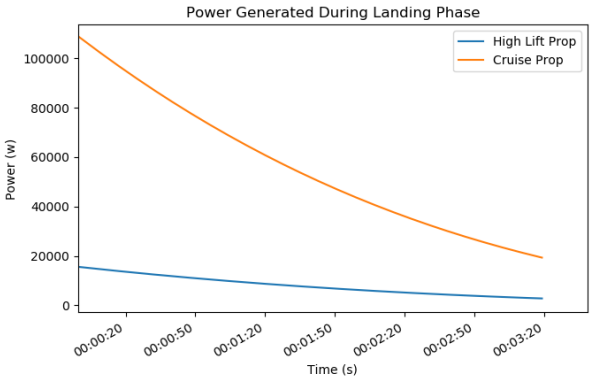

Figure 6.17: The power generated during landing phase

Figure 6.16 shows how the power generated changes as the windspeed through the propellers change. Figure 6.17 shows the power that would be generated by a CP and a high lift propeller during the landing phase of a journey. The area under the CP curve gives the total energy generated in the 200 seconds landing phase as 3.1 kWh per propeller.

The structure of this system is seen below in Figure 6.18.[21] Batteries recharge at a slower rate than they discharge. The charge time can be decreased but this is to the detriment of the battery life. To keep the life of a battery as long as possible the current from the motor will be dumped into a super capacitor which does not have the charge time problem.

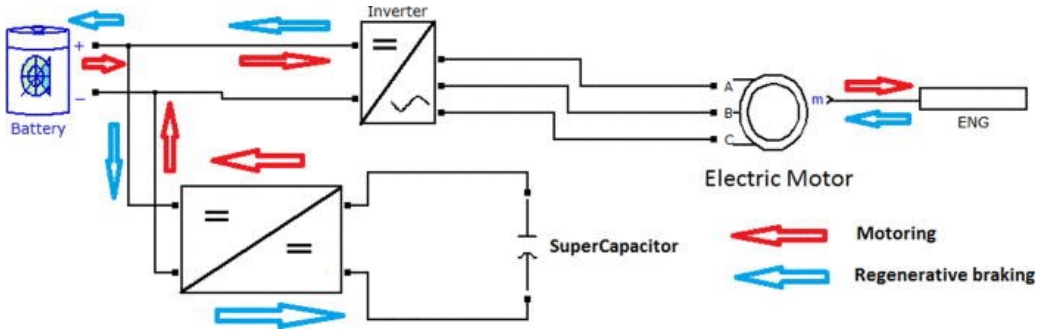

Figure 6.18: The circuitry of the regenerative drag

Additional power can be recuperated via regenerative braking during the driving phases. This recuperated energy can be expressed as follows, where η_{motor} is the efficiency of the electric motor (0.9), p is the braking proportion (0.49 in urban areas), η_{recup} is the recuperated proportion of braking energy (assumed to be 0.6), and $E_{driving}$ is the energy used in the driving phase.

$$E_{recup} = \eta_{motor} p \eta_{recup} E_{driving} \tag{6.24}$$

Each of the two driving phases uses 24.7 kWh of energy, and therefore 3.41 kWh can be recuperated during each of these phases. This power is also routed to a supercapacitor first, then discharged into the APU.

Taking a 90% discharge efficiency for the supercapacitor, roughly 5.6 kWh of energy should be recovered from the regenerative drag process during landing and roughly 6.14 kWh should be recuperated from regenerative braking in the two driving phases together. Assuming that the battery is fully charged before departure, the power gained from regenerative braking during the first driving portion can keep the battery at maximum power for the duration of this first drive. The battery's energy must then be able to keep the secondary power systems online for the entire flying portion. Lastly, power is regained from landing and the final driving phase to power the vehicle during this last stretch. The vehicle's APU can then be plugged into the grid upon arrival at its location.

[21] https://aip.scitation.org/doi/full/10.1063/1.4759457 [cited 22 June 2019]

Given this mission profile, the power budget in Table 6.2, and a safety margin of 20%, the LG Chem 48 V RESU 9.8 kWh Li-ion battery[22] is chosen for the vehicle's APU. This battery weighs 75 kg and has a size of 452 x 483 x 227 mm, which is consistent with early estimations of the vehicle's APU.

6.7. Subsystem Interfaces

The interfaces between the different electrical systems which make up the HAVIC are represented in an electrical block diagram shown in Figure 6.19. The hydrogen fuel cell produces a high-voltage direct current which is used to power a total of 11 electrical induction motors: 1 for powering the drivetrain, 8 for driving the HLPs, and 2 for driving the CPs. These induction motors can also be used to charge the Li-ion battery (both directly and indirectly through a capacitor) whenever energy is being recuperated by the processes of regenerative drag and regenerative braking as described in section 6.6. Here the secondary electrical systems powered by the Li-ion battery are placed into categories for ease of representation.

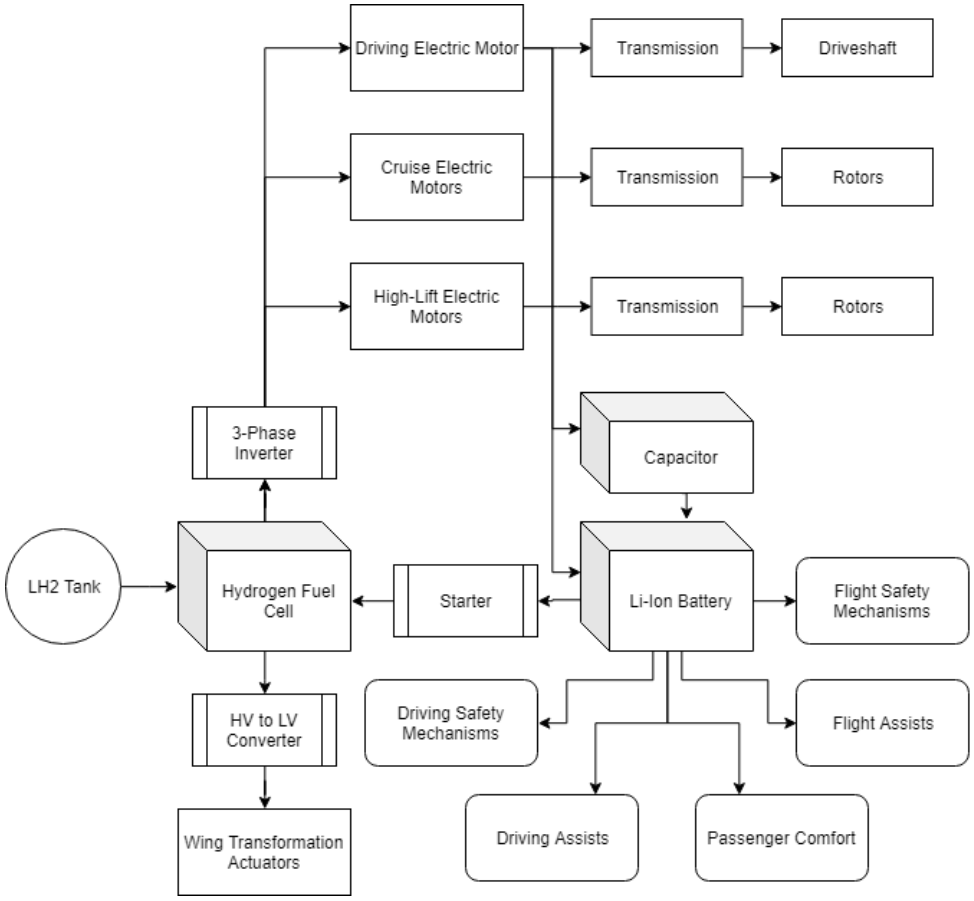

Figure 6.19: Electrical Block Diagram showing the interfaces between different electrical systems

[22] https://www.cclcomponents.com/lg-chem-48v-resu-9-8kwh-lithium-battery [cited 22 June 2019]

7

Final Design Overview

This chapter gives an overview of the final design. The most important parameters can be found in section 7.1. This section gives an overview of the main body, wing, tank, propulsion, empennage, control surfaces, drive train and suspension design. It also shows the existing parts bought on the market. In section 7.2 the systems that are used to operate all these parts is shown by hardware and software block diagrams. The data transfer from the vehicle with the outside world is also shown by a data handling block diagram. Finally a sensitivity study is performed in section 7.3, which looks into what model inputs and outputs should be allocated more or less resources in further development.

7.1. Final Sizing Results

After the iterative design program, explained in subsection 3.5.1, will run, it will provide the mass budget and all the relevant sizes of the vehicle. The HAVIC MTOW converges after 4 iterations with a threshold of 0.5 kg in maximum take-off weight, to a *MTOW of 1668 kg* which corresponds to a *OEW of 1292 kg*. The final design is shown in Figure 7.1.

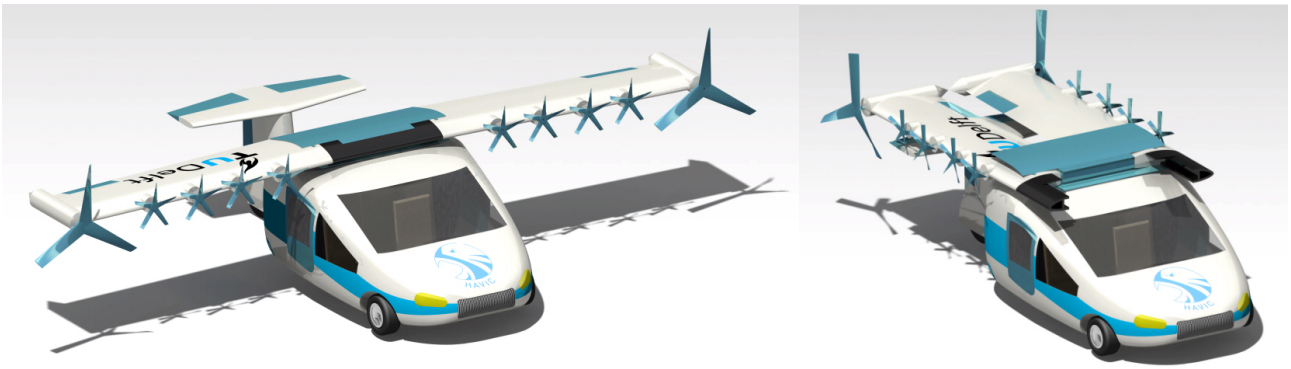

Figure 7.1: Render of the final design of the HAVIC

Since the HAVIC uses various parts that are bought from the market and not custom made, specifications of these parts are not changed in the iteration, it is just checked if the parts work in the design or need to be replaced. Existing parts also influence the design of the parts and subsystems that are custom made for the HAVIC, such as the fuel tank and wing.

7.1.1. Final Main Body Design

The final results of the main body are shown in Table 7.1. It should be noted that the length of the main body is measured from the front to the most aft point of the tail. However, in driving conditions the wing will be sticking out by 45 cm. The width of the vehicle is from side to side on the widest part of the vehicle, which is nearby the wheels. The largest contributor to the weight is the truss structure, which takes up most structural loads. Other main contributors to the weight are the skin and windows. A schematic drawing of the main body can be found in Figure 7.2.

Table 7.1: Results main body design

Parameter	Value	Unit
Total main body length	5.45	[m]
Total main body width	2.40	[m]
Total main body height	1.52	[m]
Truss structure mass	255.20	[kg]
Skin mass	21.00	[kg]
Total windows mass	11.16	[kg]

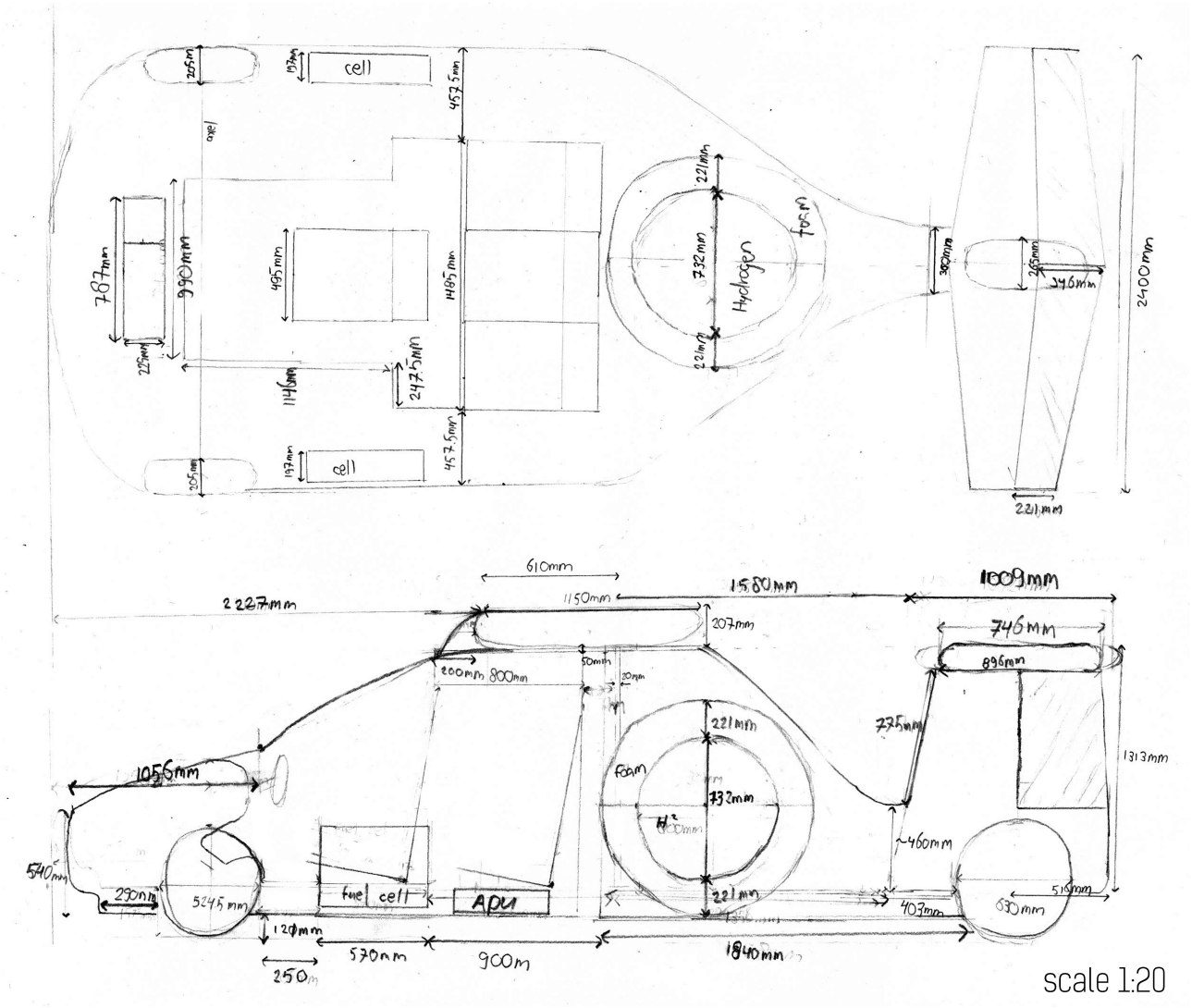

Figure 7.2: Schematic drawing of the main body

7.1.2. Final Wing Design

The final wing design is shown in Table 7.2. It should be noted that the total wing span is from tip to tip. The root chord is the chord at the location where the wing touches the side of the car. The flap area is the area of a single flap. Also, the weight of the wing skin and wing box is the weight at a single wing. A schematic drawing of the wing on the vehicle can be found in Figure 7.3.

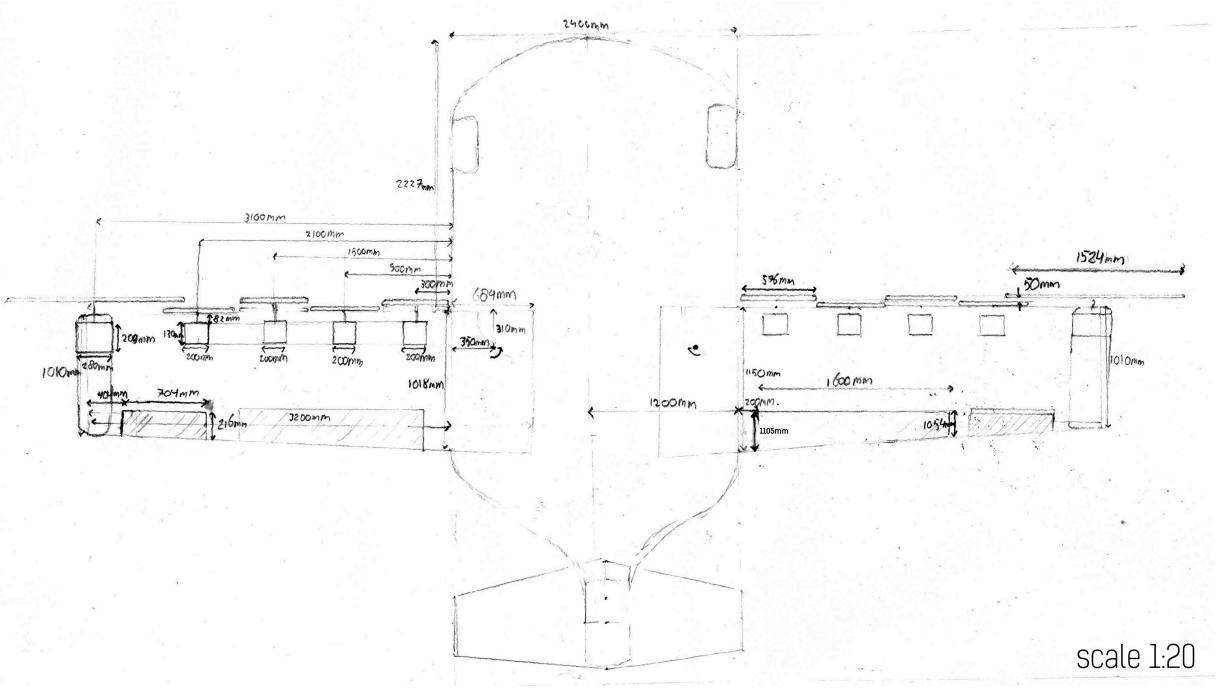

Figure 7.3: Schematic drawing with wings in fly mode

7.1.3. Final Propulsion System Design

The final values for the propulsion system can be found in Table 7.3. The location of the propellers and engines can be found in Figure 7.3. The mass of the propulsion system is including the propellers, engines, shafts, gears and power cables.

Table 7.2: Result wing design

Parameter	Value	Unit
Total wing span	8.80	[m]
Distance root to tip	3.20	[m]
Root chord	1.11	[m]
Tip chord	1.01	[m]
Wing area	9.53	[m^2]
Flap area	0.52	[m^2]
Wing skin mass	24.26	[kg]
Wing box mass	35.74	[kg]

Table 7.3: Results propulsion system design

Parameter	Value	Unit
Mass propulsion system	353.880	[kg]
Number of CPs	2	[−]
Number of HLPs	8	[−]
Diameter CPs	1.524	[m]
Diameter HLPs	0.576	[m]

7.1.4. Final Tank Design

The final results for the tank design can found in Table 7.4. It should be noted that the tank diameter starts from the outside of the structural wall.

Table 7.4: Results fuel tank design

Parameter	Value	Unit
Tank diameter	1.174	[m]
Liner thickness	6.500	[mm]
Structural wall thickness	0.129	[mm]
Insulating wall thickness	195.000	[mm]
Tank volume	327.000	[L]
Fuel mass	21.800	[kg]
Empty tank mass	65.100	[kg]
Inlet area	0.033	[m^2]
APU mass	75.000	[kg]

7.1.5. Final Empennage Design

The final empennage design can be seen in Table 7.5. Most sizes of the empennage are limited by the sizes of other components. For example, the height of the horizontal tail is limited by the height of the wings, since in driving configuration, the wings have to rest on the horizontal tail, which then further limits the height of the vertical tail. Also, the horizontal tail span is limited by the width of the vehicle. For more dimensions and locations of the empennage can be found in figure Figure 7.2.

7.1.6. Final Control Surface

The final control surfaces design is shown in Table 7.6. The sizes of these control surfaces were constantly changed in the iteration process. More dimensions and the locations of the control surfaces can be found in Figure 7.2 and Figure 7.3.

Table 7.5: Result empennage design

Parameter	Value	Unit
Horizontal tail surface area	1.467	[m^2]
Horizontal tail surface span	2.400	[m^2]
Horizontal tail taper ratio	0.640	[m]
Horizontal tail aspect ratio	3.930	[−]
Vertical tail surface area	1.290	[m^2]
Vertical tail surface hieght	1.350	[m^2]
Vertical tail taper ratio	0.820	[m]
Vertical tail aspect ratio	1.420	[−]

Table 7.6: Results control surfaces design

Parameter	Value	Unit
Aileron surface area	0.300	[m^2]
Aileron span	0.704	[m]
Rudder surface area	0.340	[m^2]
Rudder height	0.730	[m]
Elevator surface area	0.770	[m^2]
Elevator span	2.400	[m]

7.1.7. Results Drivetrain and Suspension System Design

The final drivetrain results are shown in Table 7.7. It should be noted that 2 struts are located in the front, which make an angle of 10° with the vertical axis to prevent tip over of the vehicle in a steep turn. Only 1 strut is located at the rear aligned with the vertical axis.

Table 7.7: Results drivetrain design

Parameter	Value	Unit
Strut length rear wheel	18.00	[cm]
Strut diameter rear wheel	27.10	[cm]
Strut length front wheel	8.80	[cm]
Strut diameter front wheel	20.30	[cm]
Truss diameter front wheel	3.75	[mm]
Truss length front wheel	1.52	[cm]

7.1.8. Existing Parts

In the design, some existing parts are bought from the market which are used in the HAVIC. It should be noted that the Tesla Model S Drive unit includes the motor, invertor and gears. 2 front wheels are used, 1 back wheel, 8 HLP motors, 2 CP motors, 2 fuel cells, 1 APU and 2 rotation servos.

Table 7.8: Existing parts

Part	Model Name	Mass [kg]	Price
Front wheel	Continental HTR 205/70 R15 V124/122J	8.5	270.15 EUR[1]
Back wheel	Dunlop SP 344 265/70 R17.5 V139/136M	9.6	361 EUR[2]
Drivetrain	Tesla Model S Drive unit	158.75	10,613 EUR[3]
HLP motor	Custom H20 (20 kW)	8.2	requested[4]
CP motor	Custom H60 (60 kW)	30	requested[4]
Fuel cell	Powercell S3	43	70,279.72 EUR[5]
APU	48V RESU 9.8 kWh Li-ion Battery	75	5,293.16 EUR[6]
Rotation servo	AKM84-T Powerservo	14.5	3,999.99 EUR[7]

7.1.9. Mass breakdown

A final breakdown of the weight of all the subsystems is shown in Figure 7.4.

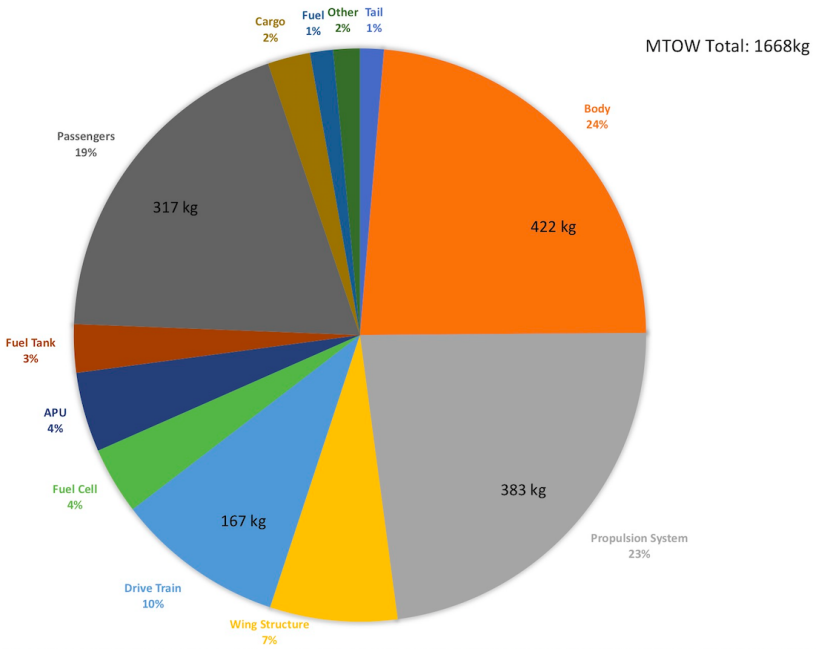

Figure 7.4: Final overview of the mass of all the subsystems

7.2. System Interfaces

The software and hardware block diagrams in Figure 7.5 and Figure 7.6 respectively show the interfaces between the pilot and different software and hardware components required to operate the vehicle.

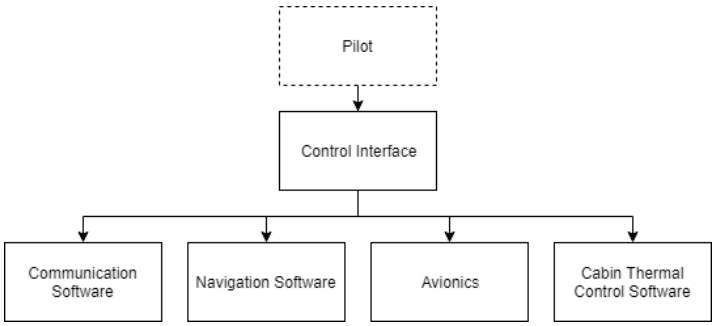

Figure 7.5: Software block diagram showing the interfaces between the pilot and different electronic systems

The pilot's cockpit must include a total of 4 throttle sticks in order to control the CP and HLP on either side of the wing separately. The cabling for these engines must travel through the wing (in the wing box), then exit through the bottom of the wing box, and enter the cabin through an opening on the roof of the cabin. This opening must be semi-circular in shape and protected by a rubber material to account for the rotation of the wings between driving and flying modes. The actuators for the control surfaces on the wings must also be linked to the controls in the cabin in this manner, as they also operate on the basis of electrical signals in a fly-by-wire system. The driving engine and wheel controls are easier to implement, as they work similarly to

[1] https://www.autobandenmarkt.nl/rshop/Banden/Continental/HTR/205%2D70%2DR15%2D124%2D122J/D%2D101489 [cited 10 June 2019]
[2] https://www.tirendo.nl/dunlop-sp-344-265-70-r17.5-139-136m-r-266068.html [cited 10 June 2019]
[3] https://www.evwest.com/catalog/product_info.php?products_id=476 [cited 22 June 2019]
[4] https://meggittpower.com [cited 24 June 2019]
[5] https://www.energy.gov/sites/prod/files/2016/07/f33/fcto_battelle_mfg_cost_analysis_pp_chp_fc_systems.pdf [cited 21 June 2019]
[6] https://www.cclcomponents.com/lg-chem-48v-resu-9-8kwh-lithium-battery [cited 22 June 2019]
[7] https://www.kollmorgen.com/en-us/products/motors/servo/akm-series/ [cited 22 June 2019]

the control interfaces in a typical automobile. The yoke will double as a steering wheel, and the switch between controlling the wheels and controlling the aerodynamic control surfaces can be made on the fly by the pilot through a simple switch in the cockpit.

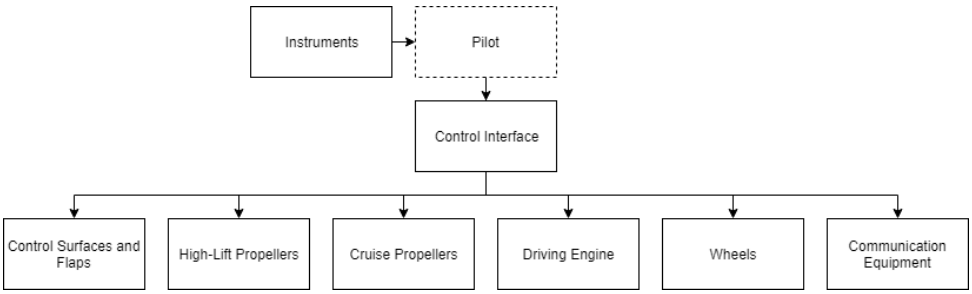

Figure 7.6: Hardware block diagram showing the interfaces between the pilot and different physical systems involved in the vehicle's operation

Figure 7.7 details the interfaces for data transfer both within the vehicle and between vehicle and outside world. Data transfer within the vehicle includes for example the transmission of relevant aircraft data to the pilot for controlling of the vehicle through a CAN bus, which is a light-weight and robust bus standard that has been widely used in both the automotive and aerospace industries.[8] Other signals such as activation of the wing transformation and door-locking mechanisms or the transfer and display of reversing camera footage would also be implemented in a similar way, but are not included in the diagram for brevity. Data transfer between the vehicle and the outside world for the purpose of navigation is achieved through a range of receivers and transponders. For example, GPS positioning information is received through a GPS receiver and ADS-B information from nearby vehicles is received through a Very High Frequency (VHF) receiving subsystem such as an Universal Access Transceiver or a simple 1090 MHz extended squitter [42]. Such an ADS-B system would enable HAVIC vehicles to receive information directly from nearby aircraft and be capable of flying with minimal ATC interference [43]. One potential solution is to use a battery-powered GPS and ADS-B dual receiver, such as the dual XGPS170D.[9] Such a lightweight solution would enable the pilot to receive both GPS and ADS-B information. All relevant navigation information is displayed in one datalink control and display unit screen in the cockpit.

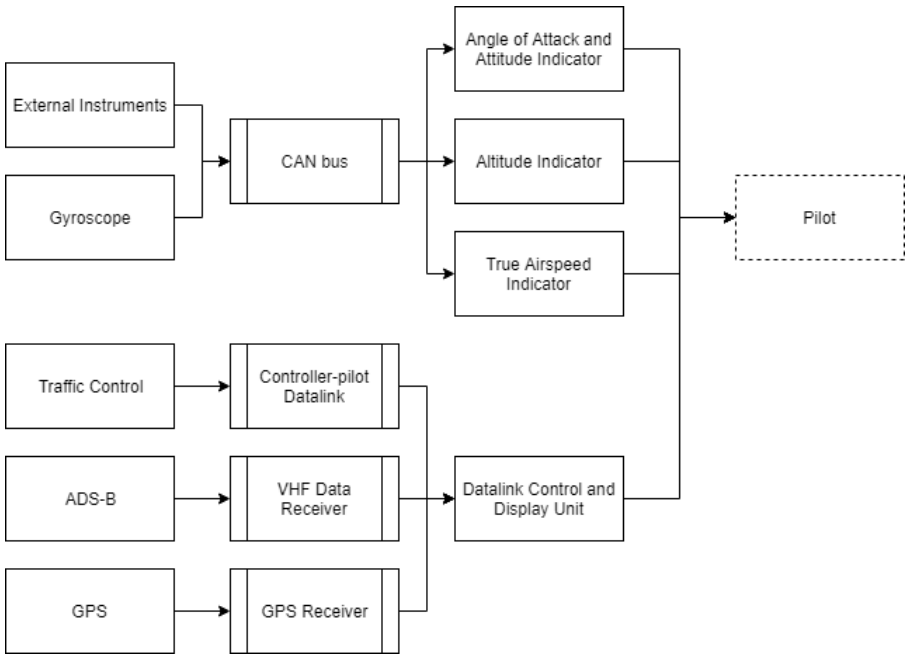

Figure 7.7: Data Handling Block Diagram showing some of the interfaces for data transfer both within the vehicle and between vehicle and outside world

[8] https://www.can-cia.org/can-knowledge/ [cited 22 June 2019]

[9] https://www.pilotmall.com/collections/gps-receivers/products/dual-xgps170d-dual-band-gps-ads%2Db-weather-receiver [cited 22 June 2019]

7.3. Sensitivity Study

The purpose of the sensitivity study is to estimate what impact the inputs of the model have to the outcome of the model, this way the reliability of the outputs can be determined. The importance of certain inputs can be determined by doing a sensitivity study as well. If it shows that changing a certain input does not affect the outcome of the model by a great amount, less resources can be allocated to that input, while more resources can be allocated to other issues.

In order to asses this project's sensitivity, 3 input parameters are chosen to be investigated. These parameters are:

- MTOW, which could change in case of passengers that are heavier than 80 kg, which is stated in the requirements or when more than 40 kg cargo is desired. The MTOW will increase from 1668 kg to 1835 kg.
- Lift coefficient (C_L), since the increase in C_L by distributed propulsion is based on new research, it can be lower than in experimental cases and thus lower than the expected C_L for the HAVIC. The C_L will decrease by 10%. The value of C_L depends on the flight phase.
- Fuel cell efficiency ($\eta_{fuelcell}$), since this value is based on research on fuel cells, which is still at an early stage, this value can be lower than anticipated. $\eta_{fuelcell}$ will be decreased from 60% to 50%.

The outputs tested for sensitivity are the range, take-off length and fuel tank weight. It is checked how all of these values change relative to its original value. A change lower than 1% is considered negligible, a change between 1% and 10% is considered acceptable and a change of more than 10% is considered significant. The results of changing these input parameters can be seen in Table 7.9.

Table 7.9: Sensitivity analysis for chosen parameters

	Range decrease	Take-off length increase	Fuel tank weight increase
Increase of 10% in MTOW	8.5%	10.1%	1.97%
Decrease of 10% C_L	7.5%	26.3%	0.43%
Decrease of 10% in $n_{fuelcell}$	37.5%	26.3%	4.13%

As can be seen the from the table, a lower than expected in put value of $n_{fuelcell}$ will have the most severe consequences, where the range decrease and take-off length increase are affected significantly. For further development, resources should be invested in obtaining an as high efficiency as possible for the transfer from hydrogen energy to usable energy. A decreased effect of the distributed propulsion on the C_L will have the greatest effect on the take-off length. In considering airfields, the potential increase in required take-off length should be taken into account. The output parameter that is influenced the least is the fuel tank weight. It should be noted that the fuel tank is a lightweight subsystem anyways, so in further development, not much more resources have to be allocated to the optimisation of the fuel tank weight.

8

Design Performance

Now an overview of all the subsystems and the final design is given, the design performance of the HAVIC can be analysed in this section. This analysis is done for the lift and drag respectively in section 8.1 and section 8.2. The noise is analysed in section 8.3 and the TOL performance is looked into in section 8.4, while the climb and glide performance are given in section 8.5 and section 8.6. Finally the payload range diagram is given in section 6.1.

8.1. Lift Estimation

In section 4.2 the lift needed for take-off and landing is calculated as 1.1 times the MTOW. To determine the specific C_L at a given angle of attack, a wing lift curve is needed. This curve can be computed with the DATCOM method which is based on five parameters: aspect ratio, taper ratio, sweep angle, airfoil type and compressibility. To create this curve three things are required: the slope $\frac{dC_L}{d\alpha}$, the $C_{L_{max}}$ and the stall angle α_s. The slope can be calculated with Equation 8.1.

$$\frac{dC_L}{d\alpha} = \frac{2\pi A}{2 + \sqrt{4 + \frac{A\beta}{\eta}^2 (1 + \frac{tan\Lambda^2_{0.5c}}{\beta^2})}} \tag{8.1}$$

The airfoil efficiency factor η is assumed to be 0.95 and $\Lambda_{0.5c}$ is the sweep angle measured at half chord length. The Prandtl-Glauert compressibility correction factor is stated as β and can be determined with Equation 8.2.

$$\beta = \sqrt{1 - M^2_\infty} \tag{8.2}$$

After the slope is determined, the focus can be shifted to the $C_{L_{max}}$. Within the DATCOM method, there are two different approaches: one for high and one for low aspect ratio wings. The approach required to apply can be determined with Equation 8.3.

$$A > \frac{4}{(C_1 + 1)\cos\Lambda_{LE}} \tag{8.3}$$

C_1 can be deduced from Figure 8.1. The result concludes that the high aspect ratio approach has to be used for the HAVIC. From this, the maximum lift coefficient can be determined which follows from Equation 8.4

$$C_{L_{max}} = \left[\frac{C_{L_{max}}}{C_{l_{max}}}\right] C_{l_{max}} + \Delta C_{L_{max}} \tag{8.4}$$

The fraction $\frac{C_{L_{max}}}{C_{l_{max}}}$ is a function of the sweep angle and the thickness. To find the corresponding stall angle of attack Equation 8.5 is used. Combining all of this, results in the lift curve shown in Figure 8.2.

$$\alpha_s = \frac{C_{L_{max}}}{C_{L_\alpha}} + \alpha_{L=0} + \Delta\alpha_{C_{L_{max}}} \tag{8.5}$$

It should be noted that the lift due to the body is approximated by the part of the area of the wing that is on top of the HAVIC. In later stages of the design, the body of the HAVIC should be tested in either simulations or

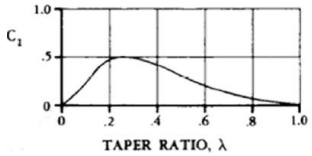

Figure 8.1: C1 determination with the taper ratio λ

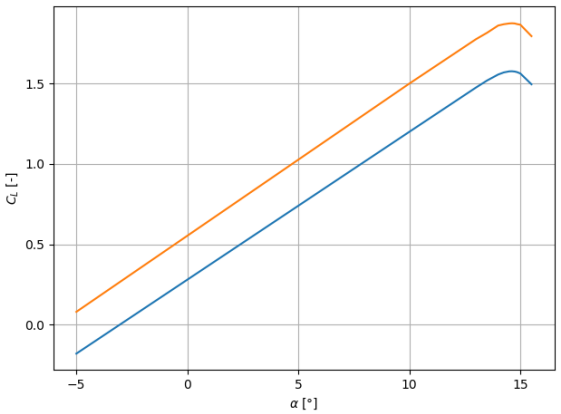

Figure 8.2: Lift curve

wind tunnels to achieve the actual lift values, but for now this assumption is close enough.

8.2. Drag Estimation

The drag estimation is performed using various methods. This is done to converge to an accurate value. The total drag can be divided into the zero-lift drag and induced drag due to lift, elaborated in the next sections.

8.2.1. Zero-Lift Drag

Two methods are available to calculate the zero-lift drag of the vehicle. From skin-friction drag or from the individual drag of the components.

Skin-Friction Drag

The first method uses the aircraft geometry to estimate the zero-lift drag D_0 with the aid of an equivalent skin-friction coefficient C_{fe} This results in Equation 8.6.

$$D_0 = qC_{fe}S_{wet} = qC_{D_0}S_W \tag{8.6}$$

The C_{fe} used in the equation differs from the skin-friction drag coefficient C_f, as the equivalent skin-fraction coefficient takes into account the form drag, interference drag, trim drag and additional drag. This list contains the other forms of drag contribution to the zero-lift drag. The constant is set at 0.0045 what can be estimated for an light aircraft type with twin engines. From Equation 8.6, Equation 8.7 can be derived.

$$C_{D_0} = C_{fe}\frac{S_{wet}}{S_W} \tag{8.7}$$

The wetted area is specified for every component: fuselage, wing, horizontal and vertical tail plane and can be found in Equation 8.8 and Equation 8.9. Adding the values of the wetted area of the individual components the total wetted area can be calculated.

$$S_{wet,F} = \pi d_f l_f (0.5 + 0.135\frac{l_n}{l_F})^{\frac{2}{3}}(1.015 + \frac{0.3}{\lambda_F^{1.5}}) \tag{8.8}$$

$$S_{wet,W,H,V} = 2S_{exp}(1 + 0.25\frac{t}{c_r}\cdot\frac{1+\tau\cdot\lambda}{1+\lambda}) \tag{8.9}$$

These calculations resulted in a C_{D0} of 0.027, seeming to be a bit low. This method simplifies a lot. For this reason the method with the individual drag of components is used for a more detailed estimation of C_{D_0}.

Individual Drag of Components

The second method is based on the calculation of the polar of the individual components. This zero-lift drag coefficient can be determined with the following factors: the skin friction drag coefficient C_f, a Form Factor (FF) which includes the pressure drag of the component, an interference factor Q which includes the interference drag, the factor S_{wet}/S_{ref}. With this the zero-lift drag coefficient can be calculated with Equation 8.10.

The factors that are used can be found in Table 8.1 and are based from theory [44].

$$C_{D_O} = \sum_{c=1}^{n} C_{f,c} FF_c Q_c \frac{S_{wet,c}}{S_{ref}} \tag{8.10}$$

Table 8.1: Input for the zero-lift drag coefficient estimation

Re_{wing}	$4.56 \cdot 10^6$	$C_{f_{wing}}$	0.000397	FF_{wing}	1.369	Q_{wing}	1.00	$S_{wet,W}$	19.91 m
$Re_{horizontal}$	$2.58 \cdot 10^6$	$C_{f_{horizontal}}$	0.000438	$FF_{horizontal}$	1.226	$Q_{horizontal}$	1.04	$S_{wet,H}$	3.023 m
$Re_{vertical}$	$4.02 \cdot 10^6$	$C_{f_{vertical}}$	0.000405	$FF_{vertical}$	1.226	$Q_{vertical}$	1.04	$S_{wet,V}$	2.77 m
$Re_{fuselage}$	$23.18 \cdot 10^6$	$C_{f_{fuselage}}$	0.000305	$FF_{fuselage}$	6.525	$Q_{fuselage}$	1.00	$S_{wet,F}$	32.10 m

This method results in a total C_{D_0} value of 0.008. This value is too low and not reasonable. The main factor that is off, is the drag coefficient of the wing. Therefore the C_{D_0} of the wing is subtracted and the value found in Javafoil is added. This results in a total zero-lift drag coefficient of 0.016 that is closer to reference data of a small aircraft. But because the HAVIC has no normal fuselage the zero-lift drag coefficient should be higher as the body is wider and has various curvatures. For this reason the individual drag of components method is not used in the estimation of the total drag.

8.2.2. Total Drag

As it seems there is no suitable empirical estimation method for this type of aircraft and modelling should not be used in this phase of the design, a very simplified method is used. For the wing, vertical and horizontal tail this is done with the graphs in Javafoil, where the C_D is determined for a range of lift coefficients for the chosen airfoil. The drag coefficient for the flap can be found using Equation 8.11. The drag coefficient of the fuselage and nacelle are estimated with the use of theory [22]. Various shapes are displayed as a wind tunnel model. From this a range can be found. After some research on existing cars with a beneficial aerodynamic shape, the Volkswagen XL 1 was seen as an inspiration. The shape of this car and the other example car shapes in literature have a drag coefficient in the range of 0.2-0.4. Our vehicles body is assumed to have a coefficient within this range. With those coefficients, the drag can be calculated with Equation 8.12. The zero lift drag coefficient is found by adding all components and dividing by the reference area, giving approximately 0.055. As a first estimate, the induced drag is assumed to be coming only from the wings, leading to the drag polar shown in Figure 8.3. The induced drag due to the body is approximated by the part of the wing that is on top of the body (the same as for the lift). In later phases, models should be ran to verify and optimise.

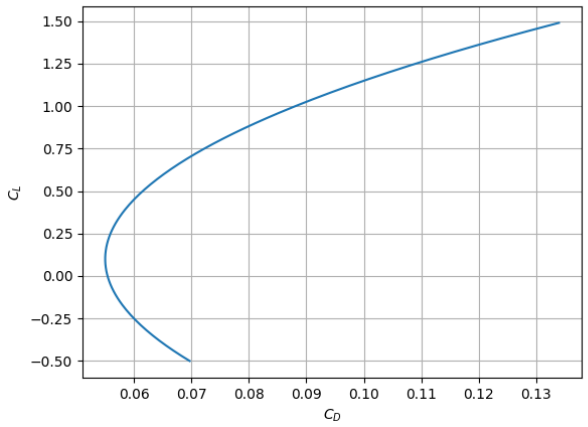

Figure 8.3: Drag polar

$$\Delta C_{D_{flap}} = F_{flap} \frac{c_f}{c} \frac{S_{flap}}{S_{ref}} (\delta_{flap} - 10) \Longrightarrow F_{flap} = 0.0144 \tag{8.11}$$

$$D = \sum C_D \frac{1}{2} \rho V^2 S \tag{8.12}$$

The input is listed in Table 8.2 and the output of the drag for the components in Table 8.3. It should be noted that the induced drag due to lift is all accounted for by the wings, as the drag coefficient of the fuselage is assumed to stay the same. For this reason, the wing drag is very high at take-off, as the angle of attack is high.

Table 8.2: Input total drag

ρ_{to} [kg/m^3]	1.225	ρ_{cr} [kg/m^3]	1.090
$C_{D_{W_{to}}}$	0.103	$C_{D_{W_{cr}}}$	0.0290
$C_{D_{h_{to}}}$	0.0450	$C_{D_{h_{cr}}}$	0.0110
$C_{D_{v_{to}}}$	0.0130	$C_{D_{v_{cr}}}$	0.0130
$C_{D_{fus_{to}}}$	0.300	$C_{D_{fus_{cr}}}$	0.300

Table 8.3: Output total drag

$D_{w_{to}}$	1247.4	$D_{w_{cr}}$	816.6
$D_{h_{to}}$	38.4	$D_{h_{cr}}$	42.4
$D_{v_{to}}$	9.8	$D_{v_{cr}}$	44.02
$D_{fus_{to}}$	533.4	$D_{fus_{cr}}$	2410
$D_{nac_{to}}$	7.200	$D_{nac_{cr}}$	32.30
$D_{flap_{to}}$	342.4	$D_{flap_{cr}}$	0.0

$$C_D = C_{D_0} + k(C_L - C_{L_{minD}})^2 \Longrightarrow k = \frac{1}{\pi A e} \tag{8.13}$$

8.3. Noise

The noise production of an aircraft is vital to estimate as a lot of airfields have noise restrictions. When considering noise characteristics of a vehicle, first the origins of the noise production have to be located. After literature study it became clear that the propeller, wing, tail, landing gear and electric motor are the main components of noise production [45]. These components are analysed in more detail in this section. Furthermore, there is fuel cell noise, ground configuration noise and installation effects.

There are several requirements relating to noise set for the HAVIC. 'REQ-TR-GEN-4-3: The noise level inside the cabin of the vehicle shall not exceed 80 dB' is affected by the noise production as is the sustainability aspect. 'REQ-CR-REG-3-1: The vehicle noise level on ground shall be <68 dB'. However, coming back to the cabin noise, Bose is developing a noise cancelling car system.[1] Such a system might be implemented in the cabin of the HAVIC, making sure the noise inside the cabin is minimal.

Identifying origins of the noise was done with a literature study [45]. First all the noisy subsystems of an aircraft were found and those applicable to the HAVIC were taken into account. Afterwards some hydrogen car specific subsystems were added to the list of noisy systems, which is displayed below:

- Fuel cell noise
- Installation effects
- Electric motor noise
- Aerodynamic noise
- Propeller noise

Fuel Cell Noise

The fuel cell noise can be neglected, as a fuel cell will produce about 50 dB noise at maximum.[2] This is below the noise production of humans and therefore can be left out of the noise equation. About the installation effects, no elaborate information has been found so far. Apart from the information that interaction of motor sounds with the surface of the wing might have influence on how the sound is perceived on the ground [46]. This is a detail that could be further explored during a later design stage.

Electric Motor Noise

Noise produced by an electric motor is harder to predict than noise production by a fuel cell. The origins of noise produced by an electric motor are brush noise, shaft noise, clearance sound, resonance, thrust sound and wind.[3] For a first estimation, Equation 8.14 was found.

$$PWL = 27 + 10Log(kW) + 15Log(RPM) + 10Log(CSA) \tag{8.14}$$

[1] https:www.theverge.com [cited 16 May 2019]
[2] https://energies.airliquide.com/resources-planet-hydrogen/fuel-cell [cited 16 May 2019]
[3] https://studyelectrical.com [cited 16 May 2019]

For using Equation 8.14 [47] some parameters need to be estimated as well. The cruise propellers chosen are the largest propellers on all three concepts. These would need an input power of around 40 kW, which has 2200 RPM.[4] The conformal surface area term is neglected as it will be a small area and since a newer electric motor is considered 10 dB can be subtracted from the final outcome as these newer motors are less noisy. A first predicted outcome would be a sound power level of 83 dB when standing next to the moter. On the ground, when the HAVIC is flying at an altitude of 1219.2 m this results in a noise level of 23 dB.

Propeller Noise

There was a lack of information in the prediction of the propeller noise. However, the propeller noise is highly dependent on the wing tip speed [48], as such it was chosen not to predict the sound power level. The trade-off is performed based on the diameter of the propellers. The wing tip speed is dependent on the diameter as can be seen in Equation 8.15 [49]. Hence, no final values have been obtained yet for the propeller noise. For further analysis the following tools might be used: PANAM-tool and NIROS-tool [46].

$$M_t = \frac{\pi D n_p}{60c} \tag{8.15}$$

The noise produced while in ground configuration and driving is another aspect of the noise characteristics. However, the only noise producing sources that will be added are the driving transmission and the tyre noise production [50]. For the tyre sound power level, a number of 70 dB was assumed. This sound power level is based on a medium speed and medium grip [51]. On the ground the noise level would be 8.28 dB.

Airframe Noise

The last major aircraft noise contributing factor is the airframe noise. This noise is estimated by use of a NASA research [52] on airframe noise. Equation 8.16 shows that the sound pressure radiated from the wing has a 4.8 power dependence on aircraft velocity and is linearly proportional to the drag coefficient for the wing and wing area. The solution is given in dBA. Input parameters that have been used for the calculations are given in Table 8.4.

$$OASPL = 10\log \frac{K_W C_{D_W} \rho^2 U^{4.8} S_W \cos(\frac{\theta}{2})^2 \cdot \sin\phi \cos\psi^2}{p_{ref}^2 (\frac{c}{v})^{0.2} a R^2} \tag{8.16}$$

Table 8.4: Input airframe noise

$10\log K_W$	-29	θ	270°	ν	$1.8 \cdot 10^{-5}$ m^2
C_{D_W}	0.029	ϕ	270°	a	334.4 m/s
ρ	1.09 kg/m^3	ψ	−1.8°	R	1219.2 m
U	69.4 m/s	p_{ref}	20 μPa		
S_w	9.504 m	c	1.08 m		

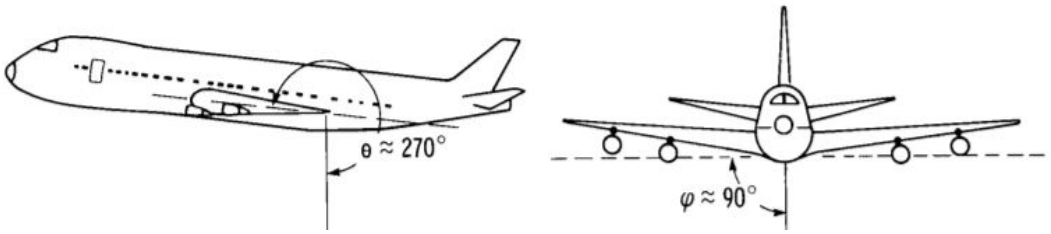

Figure 8.4: Direction of angles quadruple trailing-edge diffracted noise sources

The aerodynamic noise on the ground results in a value of 50.37 dB. From this a conclusion can be drawn that the aerodynamic noise of the airframe contributes to most to the noise level on the ground.

[4] https://www.pipistrel-usa.com/electric-propulsion/ [cited 21 May 2019]

Total Noise

Adding the noise of each component results in the noise of the aircraft that can be compared with the limit that is stated in the requirement. Three noise levels should be added up, the 23 dB of the electric motor, the 8.28 dB of propeller and the 50 dB of aerodynamic noise. The result is given in Equation 8.17.

$$SPL = 10 \cdot log(10^{23/10} + 10^{8.28/10} + 10^{50/10}) \tag{8.17}$$

The calculated value, 50.009 dB lays within the constrained range.

8.4. TOL Performance

The runway length of the HAVIC is an important aspect of its performance, as having a long runway length decreases the flexibility of the vehicle. To assess take-off performance an analytical calculation is done. Ground effect, runway slope and wind are neglected in this calculation. The runway length is calculated using Equation 8.18 - Equation 8.21. The required input values for the calculation and the outputs are listed in Table 8.5.

Table 8.5: Performance parameters for ground run distance

V_{stall} [m/s]	V_{LOF} [m/s]	$\bar{T}$ [N]	$\bar{D}$ [N]	$\bar{D}g$ [N]	g [m/s^2]	W [N]	$\bar{a}$ [m/s^2]	s_{ground} [m]
29.0	30.5	4063.66	184.2	373.1	9.81	16363.1	2.4	220.6

$$s = \frac{V_{LOF}^2}{2\bar{a}} \tag{8.18}$$

$$\bar{a} = \frac{g}{W}(\bar{T} - \bar{D} - \bar{D}_G) \tag{8.19}$$

$$\bar{V} = \frac{V_{LOF}}{\sqrt{2}} \tag{8.20}$$

$$V_{LOF} = 1.05 V_{stall} \tag{8.21}$$

Next to the ground run distance, an airborne distance needs to be calculated using Equation 8.22. A minimum screen height of 15.2 m has to be cleared at the end of the runway. For this calculation it is assumed that the climb is stationary, meaning the climb angle and airspeed are constant. During this phase the HLPs provide a lifting multiplier, it is assumed this increase in effective C_L has no influence on the induced drag of the wing. The parameters used for the airborne distance calculations can be found in Table 8.6.

Table 8.6: Performance parameters for airborne distance

T [N]	D [N]	$s_{airborne}$ [m]
4022.2	843.2	207.9

$$s_{airborne} = \frac{W}{T - D}\left[\frac{1}{2g}\left(1.2V_{stall}\right)^2 - V_{LOF}^2\right) + 15.2\right] \tag{8.22}$$

The total runway length is equal to s_{ground}+$s_{airborne}$ = 428.6 m. This calculation serves as an indication of the minimum runway length for the HAVIC, however, assumptions are made regarding coefficients of rolling resistance, propeller efficiency and the effect of the HLPs on the lift and drag. Further analysis is required to validate these calculations.

The landing performance is done in similar fashion to the take-off performance. A screen height of 15.2 m has to be cleared at the start of the runway. Landing consists of an airborne phase and a ground phase, Equation 8.23-Equation 8.26 are used to calculate the landing ground run distance. For this analysis it is assumed no thrust is generated, the flaps are fully deployed and the coefficient of rolling resistance μ = 0.5. Furthermore the approach angle γ_a is taken to be 3°and Δn = 0.15, taken from empyrical data [53]. The performance parameters can be found in Table 8.7 and Table 8.8

Table 8.7: Performance parameters for airborne distance for landing

$C_{L_{Landing}}$ [-]	W [N]	ρ [kg/m^3]	S [m^2]	R [-]	$s_{airborne_L}$ [m]
1.7	16363.0	1.225	9.53	2720.5	361.3

$$s_{airborne_L} = R\sin\gamma_a + \frac{15{,}2 - (1-\cos\gamma_a)R}{\tan\gamma_a}; \gamma_a = 3° \qquad (8.23) \qquad R = 1.3^2 \frac{\frac{2W}{S\rho C_L}}{\Delta n \cdot g}; \Delta n = 0.15 \qquad (8.24)$$

Table 8.8: Performance parameters for ground distance at landing

V_{min_L} [m/s]	$\bar{T}$ [N]	$\bar{D}$ [N]	μ [-]	W [N]	L [N]	$s_{transition}$ [m]	s_{brake} [m]
37.4	0	3882.0	0.5	16363.03	3456.7	97.3	191.1

$$s_{transition} = 2.6 V_{min,L} \qquad (8.25) \qquad s_{brake} = \frac{W^2}{2gS}\frac{2}{\rho}\frac{1}{(\bar{T} - \bar{D} - \mu(W-L))} \qquad (8.26)$$

From these calculations a landing ground run distance of $s_{airborne_L} + s_{transition} + s_{brake} = 649.8$ m is found.

8.5. Climb Performance

The climb performance of the aircraft is important, since it has to climb from ground level to cruise altitude. The climb performance for the HAVIC can be calculated based on the equation of motion in steady state condition. All equations in this section are taken from a Flight Mechanics course taught at Delft University of Technology [53]. The change in velocity is assumed to be zero and thus the equation of motion reduces to Equation 8.27. Multiplying both sides with the velocity V and rearranging the terms result into the rate of climb (RC) in steady state condition as a function of the power available (P_a), power required (P_r) and the weight (W) and is given by Equation 8.28. Note that $P_a = TV$, $P_r = DV$ and $RC_s = \mathrm{V}\ \sin(\gamma)$.

The RC for a light aircraft lies between 800-1000 ft/min [54]. In the climb performance analysis, it was considered to use the average value of 900 ft/min (274 m/min) for the RC calculations. In this analysis, an air density of 1.225 kg/m^3 was considered. The velocity range in which the aircraft has to fly in order to obtain a RC of 274 m/min or above is calculated using Equation 8.28. The velocity is varied and the corresponding RC is calculated. Based on this, the velocity range can be found. The optimal RC can be obtained by calculating the optimal C_L and using this value for the RC calculations. From the performance diagram, the optimal RC is obtained at the point where the difference between P_a and P_r is maximum.

$$T - D - W sin(\gamma) = 0 \qquad (8.27) \qquad RC_s = V sin(\gamma) = \frac{Pa - Pr}{W} \qquad (8.28)$$

The maximum RC can be found using the theory explained in previously. From this, the optimum lift coefficient ($C_{L_{opt}}$), velocity (V_{opt}), RC and climb angle (γ) can be calculated. These values are listed in Table 8.9. Furthermore, the climb velocity (V_{climb}) range can also be calculated in order to maintain a safe climb rate for a light aircraft. Next to this, the performance diagram and RC graphs are plotted as shown in Figure 8.5 and Figure 8.6. The optimum climb velocity can be found from Figure 8.5, which is the point where the difference between the power available P_a and power required P_r is maximum. The V_{climb} range can be found in Figure 8.6, the part above the intersection indicates the RC required for a light aircraft in order to maintain a safe climb.

Table 8.9: Performance parameters for optimum rate of climb

$C_{L_{opt}}$ [-]	V_{opt} [m/s]	RC [m/min]	γ [°]	V_{climb} [m/s]
1.87	37.5	430.8	11.03	17-63

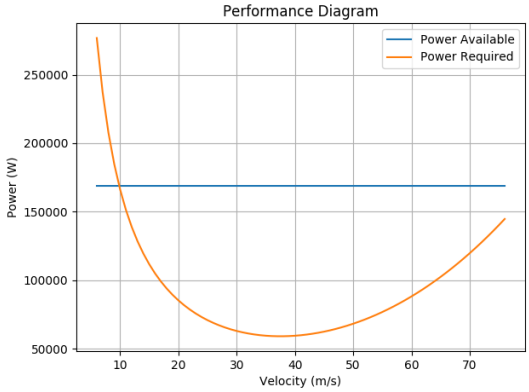

Figure 8.5: Performance Diagram HAVIC

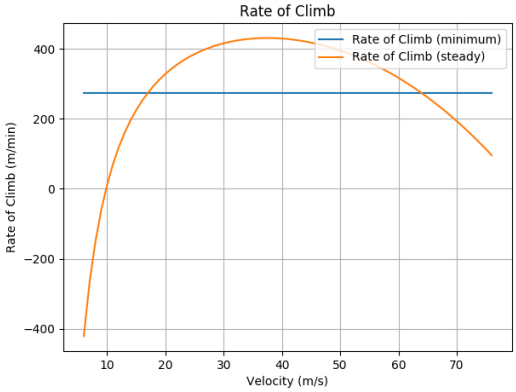

Figure 8.6: Climb Performance HAVIC

8.6. Glide Performance

When an emergency situation occurs where the engines are not giving any thrust, the airplane must be able to glide. The glide ratio is defined by the amount of units can be crossed horizontally, while only descending 1 unit vertically. This ratio is equal to the lift coefficient divided by the drag coefficients, which is the highest for the C_L found in Equation 8.29. The glide ratio turns out to be 11.3 for this design, which is comparable to similar vehicles: a Cessna 172 has a glide ratio of 9.

$$C_{L_{opt}} = \sqrt{\frac{C_{D0}}{k}} \tag{8.29}$$

8.6.1. Payload Range Diagram

The payload-range diagram in Figure 8.7 below was generated by calculating the cruise range with different payload configuration and the same amount of hydrogen fuel. The plot shows the vehicle's range from the maximum payload case, where all 4 passengers are present and the aircraft weighs the MTOW of 1668 kg, to the minimum payload (or ferry) case, where no passengers are present and the aircraft therefore weighs 1348 kg. This 20% mass decrease yields a 15% range increase, i.e. the ferry range is 460 km. The increase in range is linear with the decrease in payload, as is typical for a payload-range diagram. But contrary to some other aircraft, there is no possibility to increase the fuel weight when decreasing payload weight and further increase range in that way. The maximum capacity of the hydrogen fuel tank is designed for the full payload case and no extra fuel can be taken due to volume constraints.

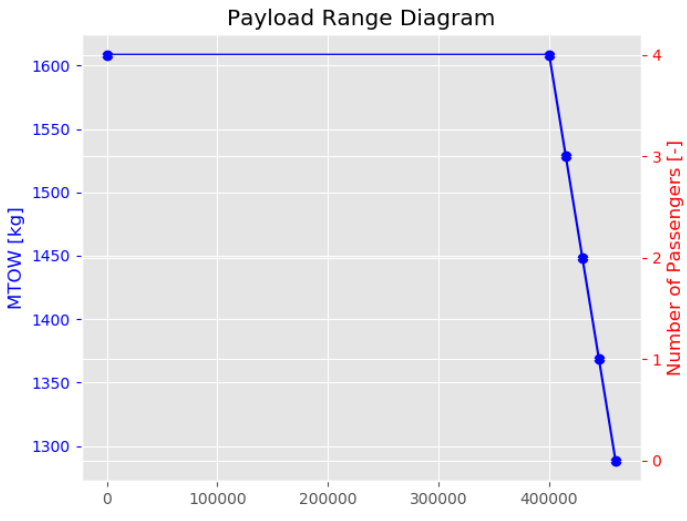

Figure 8.7: The payload range diagram, showing the cruise range for different payload configurations

III

Further Development

9

Sustainable Concept Development

As stated in the introduction of this report, sustainable engineering is placed high on the to-do list of the Door2Door project. Our mission and requirements both reflect that one of the main tasks of the project is the sustainable aspect. This was done by making one person the sustainability officer and set up a sustainable development approach. This chapter will elaborate on the process and main outcomes of the sustainable development.

9.1. Plan Do Check Act - Structure

A Plan Do Check Act - Structure is chosen as the basic model for the sustainable development. This circle is an always developing circle, as can be seen in the Figure 9.1. The terminology 'Plan Do Check Act' is also widely known in the industry as the model has proven its outcomes. It logically contains 4 phases, which shall be explained both for the model explanation and how it was established in the sustainable development of the Door2Door project. It starts with a Plan phase in which the process is studied in more detail and a plan is determined. The Door2Door project started with identifying what sustainability exactly is. During this phase the three pillars and the UN agenda were identified as applicable. Next comes the Do phase, in which the requirements have been set and implemented in the concept design. This concept must than be checked if the requirements are met. This will happen in the Check phase. The circle's last phase is the Act phase. During this part of the process, new ideas on how to improve must be observed. Those ideas can than be implemented in the next Plan phase, to continue the circle.

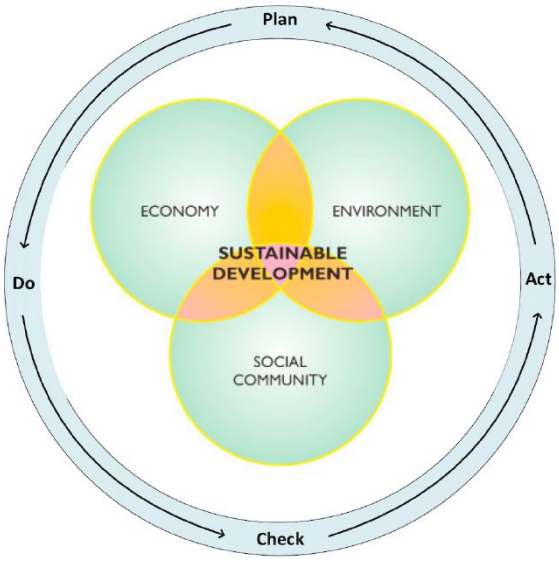

Figure 9.1: Pillars of sustainable development [55]

Three Pillars of Sustainability

First the definition of sustainability has to be determined and requirements and trade-off criteria have to be established accordingly. To do so, the UN agenda is used, as will be explained on a short notice. During the conceptual design phase, these shall be implemented as best as possible. These results must be analysed and new goals for the detailed design phase should be set up. Let's first answer the question: what is sustainability?

The world is set to become increasingly more sustainable. Organisations worldwide have set goals to reduce emissions, but sustainability is much broader than just reducing emissions. Sustainable development is divided into three main pillars: social community, economy and environment. This is depicted in Figure 9.1. These pillars together show a complete overview of where sustainability can have an impact. Only when all three pillars are taken into account, will the final product contribute to sustainability optimally. Therefore the Door2Door project shall not work out a product, but a complete process for the future development. The three pillars are there, because in this way the global sustainability can be explained from different perspectives, but the pillars can never be completely isolated from each other.[1] Only when all aspects are taken into account a design can be called sustainable. The UN agenda is used as a guideline, because it splits these pillars into multiple sections.

The UN Sustainable Agenda and the Set Requirements

The UN agenda describes 17 sustainable topics that should be addressed by the world. This agenda is depicted in Figure 9.2. The HAVIC is not able to comply with all agenda points due to time constraints. Therefore has the team chosen to select a couple of the agenda points. That will be the numbers: 7,12 and 13. This selection will be used to limit the vision on sustainability aspect to achieve more realistic goals. For each of the chosen agenda points the Door2Door project shall have a requirement to help attain sustainability. Below is each topic together with the set requirements described.

Figure 9.2: The UN sustainable agenda[2]

In order to comply to the clean energy requirements set by our clients, the Door2Door project has taken these requirements in the process. Affordable and clean energy is also number 7 on the UN sustainability agenda. The following requirements are attached to this aspect. A more elaborate analysis of the use of solar panels can be found in section 15.3.

- REQ-TR-GEN-7-1: The range of the vehicle shall be extended by $< tbd >$ through the use of solar energy *
- REQ-TR-GEN-5-1: The vehicle shall produce only water as its waste product *

Next to this, the project team would like to educate our client and customers about the sustainable aspects of the final product and process. This allows for a more sustainable use of the HAVIC during its lifetime. As not all power suppliers have a fully developed sustainable approach, the project team would like to share this kind of information about subcontractors and suppliers. Listed at number 13 on the UN sustainability agenda, this aspect has been transferred in the below described requirement and the project team has set the goal to distribute this information.

[1] https://www.e-education.psu.edu/eme807/node/575 [cited 2 May 2019]
[2] https://www.un.org/sustainabledevelopment/sustainable-development-goals/ [cited 2 May 2019]

- REQ-TR-GEN-7-9: The vehicle shall only be charged with hydrogen made through a process which emits no greenhouse gases

The materials and manufacturing methods should comply with 'durable design'. This means the materials and manufacturing methods should have low cost and a positive or minimally negative social and environmental impact. To ensure environmental sustainability on this aspect, only cooperation with ISO 14001[3] or similarly certified companies is allowed. Furthermore, recycling batteries and circular design are considered. "Ensure sustainable consumption and production patterns" is placed at number 12 on the UN sustainability agenda. The requirements below reflect that the project group will take this into account during designing:

- REQ-TR-GEN-7-3: Subcontractors shall be certified as an ISO 14001 company or have a similar certification
- REQ-TR-GEN-7-4: The vehicle shall be circular in use for at least $< tbd > \%$
- REQ-CR-RS-1-1: The lithium of the batteries shall be recyclable
- REQ-CR-RS-1-2: The metals shall be completely reusable

9.2. Sustainable Aspects of the HAVIC

With the help of this set of requirements, the HAVIC is developed for sustainability. The focus has been placed on the The three main sustainable findings shall be presented in this section. The project group would like to elaborate on the sustainable usage, the end-of-life aspect and the emissions of the HAVIC. After those aspects are explained, a comparison between the HAVIC and the current market shall be presented.

Sustainable Use of the HAVIC

To look at the usage of the car and develop an educating system for the clients, could greatly contribute to the sustainable level of the HAVIC. As the 'use' phase of a product related to transport, this phase has the most environmental impact during the lifetime of the product. Therefore it is of importance to look at how a client can be using the HAVIC. This will start with analysing the power core of the HAVIC, the fuel cell. The two fuel cells in the HAVIC act as powerful electric generators, which use hydrogen to generate electricity. The output of the fuel cell is pure water vapour, which is more sustainable than the output of gasoline engines. However, hydrogen needs to be manufactured as it is not found on the Earth on a large scale. This production of hydrogen is not always as sustainable as one might think.

Electrolysis is a method of splitting water molecules into hydrogen and oxygen that can be done in a sustainable fashion. This is only possible if the electric energy needed for electrolysis is also created without emissions, such as wind, water or solar energy. Two new methods of hydrogen production are under investigation, namely photoelectrochemical and photobiological hydrogen splitting, which split water into hydrogen by making use of sunlight and algae respectively. Users of the HAVIC should be informed of how their hydrogen is produced, that way it can be ensured that the use of hydrogen is fully sustainable.

There is also a new way of making hydrogen without the use electricity being research at the moment. This method isolates hydrogen from industrial waste water with the use of solar. This would make the production more sustainable, but not a large amount can be made using this method. However, it does show that there is an evolution happening regarding the production techniques of hydrogen. In the near future, when the fuel cell technologies becomes more widely accepted and cheaper, the production techniques regarding hydrogen will mature as well.[4]section 15.3 contains more information on the future production of hydrogen.

The APU battery must also be charged for the use of electronic instruments during operation. The charging of the APU can take place via the use of a solar array, which can be placed on top of the wing of the HAVIC. This is elaborately described in chapter 15. The use of these solar array and how to use them, must be explained and researched. This shall take place in the future development phase. This will make sure that the customer knows from which energy source the APU is charged, as this information might be unclear to get when the APU would be charged from the grid.

[3] https://www.nen.nl/NEN-Shop/Vakgebieden/Managementsystemen/Milieumanagement.htm [cited 25 April 2019]

[4] https://www.waterworld.com/industrial/wastewater/article/14004886/princeton-univ-researchers-pull%2Dhydrogen-from-wastewater-using-sunlight [cited 22 June 2019]

As stated earlier the operations phase of a transportation product is the phase which has the highest impact on the overall sustainability of the product. This implies by making this phase only a little more sustainable, the overall sustainability of the product increases by a lot. For example, the owner can choose to let other people use his HAVIC at the moments the vehicle is not in use by the owner. There are already various apps helping in connecting owners and people wanting to pay per trip. This is becoming more common as youngsters are not in need of owning a own product, but rather want to pay when the product is being used by them. The HAVIC can be used in both markets and is therefore designed for the current times as well as the future [56].

End of Life of the HAVIC

Products are not designed to be operative forever and thus should have an end of life plan. The Door2Door project determines what will happen with the various components of the HAVIC after the vehicle will no longer be used. Due to time constraints, three parts are chosen to perform this end of life analysis upon. The frame, the wing and the tank will be considered. A full end of life analysis shall be performed before the product launch. The end of life phase is also the last part of a life cycle assessment as depicted in Figure 9.3 as 'Disposal', this could also mean recycling or circular use.

Figure 9.3: An example describing the topics a life-cycle analysis[5]

The frame, which is made from titanium which is recyclable, is designed to last for a long time. When taking a look at the frame as described in chapter 5, it consists of titanium bars welded together. This might not be the optimal way for larger series designs, but for the HAVIC it is. Not only will it result in a cheaper first batch, it will also make the design changeable and therefore circular in use. Whenever the HAVIC will come to the end of its use, the bars of the frame can be taken out and inspected. These positively inspected bars can than be used for another frame or other purpose. The bars that have a negative outcome during inspection, will undergo a recycling process. There are possibilities of recycling titanium using less energy than refining titanium ore. This is obviously a promising new technology for HAVIC's titanium parts to be processed to become usable again for new high-tech purposes.[6]

Carbon is used in the wing as well as the hydrogen fuel tank and the fuselage skin. These parts together are a significant part of the HAVIC and must therefore have an appropriate end of life plan. Especially since the production of carbon parts, requires vasts amount of energy. When the recycling of carbon is not as energy demanding as virgin fibres, this would greatly increase the sustainability. There are three main methods for recycling carbon fibres, mechanical, chemical and thermal [57]. Each with its shortcoming, as the knowledge on recycling of composites is still not at a high level. In a scenario where the fibres of old HAVICs will be used for new highly engineered vehicles, there is only one recycling method that can be used. This is the chemical recycling, where chemicals are used to remove the resin to leave the fibres. This method will result in fibres showing a tensile strength of up to 97% compared to virgin fibres .

Unfortunately, these chemicals are not yet sustainable. They are costly and complex in use, and might not yet be the right solution for HAVIC. By using one of the other methods, the deterioration of the material is far worse compared to chemical recycling. These recycled materials cannot be used for high engineered complex structures, but these recycled parts can be used for products where costs plays a huge factor, for example sport related items can be made from recycled carbon fibre. The best option is to use the components of a old HAVIC for their same purpose. This can be achieved by making the design somewhat modular, but this might prove

[5] https://www.innovationservices.philips.com [cited 2 May 2019]

[6] https://medium.com/eib-connect/titanium-recycling-gives-europe-a-valuable-new-metal-supply-27d9fe0e836d [cited 24 June 2019]

difficult in reality. For the tank that is a complete different story. The tank is with a spherical design not as specifically designed for the HAVIC and may be re-purposed.

Hydrogen Fuel and Emissions

As explained, a hydrogen fuel cell will emit water vapour. Storing this water mass in flight is completely unfeasible as this would almost double the MTOW of the vehicle. The HAVIC will output 36 grams of water at full thrust per second, which might not seem a lot. However, when a full hydrogen tank is used, the amount of water being released into the atmosphere is 196 kg. Therefore, the only option is to release the water vapour mid flight. Water vapour is in some cases considered a greenhouse gas, but it is less harmful than the emissions of standard jet-powered aircraft. Under the circumstances, and due to the limitations in place, it was concluded that this is an appropriate strategy.

When water vapour gets released in the air, contrails might be transformed in to cirrus clouds. This transformation depends on the temperature and humidity of the air. These factors also determine if a cirrus cloud formed by water vapour will last for seconds, minutes or days. The temperature of the air decreases when the altitude increases, until an altitude of 18 kilometres. Cirrus clouds affect the climate by reflecting the radiation and heat from the Sun. This is similar how carbon dioxide is contributing to global warming. One major difference will be that the carbon dioxide will last for about 5 decades in the atmosphere, while water vapour will have a maximum of a couple of days. This obviously has to be noted as a difference as comparing emissions with fossil fuel emissions can not be done on amount of emissions only.[7]

The right conditions for cirrus clouds to occur only start from an cruising altitude of 7500 metres on most flight paths. This is far beyond the cruising altitude of the HAVIC and therefore it is safe to assume that the water vapour released from the HAVIC is not contributing to the global warming. Only in cold and moist conditions this transformation might still occur. A solution can be to change flight paths into slower climbing ones. This makes sure that the amount of time flying at the cruising altitude is limited.

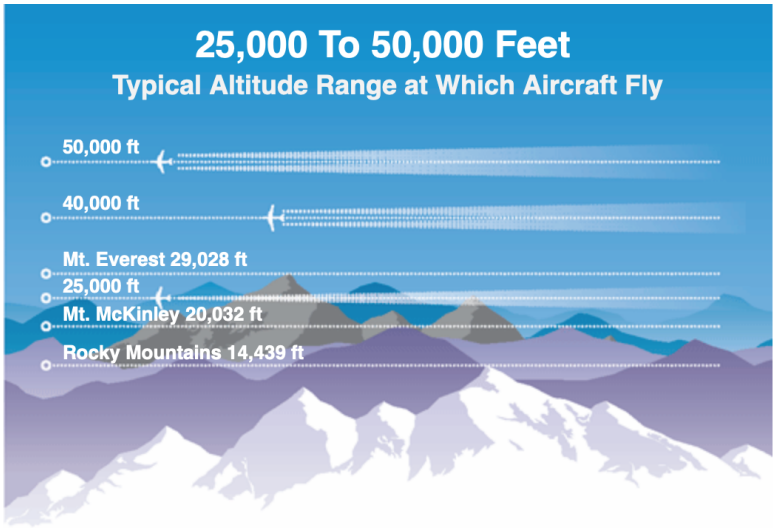

Figure 9.4: An illustration on contrail forming at different altitudes[8]

There is a minor issue regarding the water vapour that gets released by the HAVIC. The water is slightly acid after being processed by the fuel cell, as it will have a pH value of around 5-6. A similar value is found in acid rain, but a solution can be to add a filter in the exhaust system for increasing the pH value. In this way, no acid rain will be occurring and the water will be returned to Earth in its old form with no harm to the environment.[9] [10]

[7] https://www.faa.gov/about/office_org/headquarters_offices/apl/noise_emissions/contrails/ [cited 24 June 2019]
[8] https://www.faa.gov/ [cited 24 June 2019]
[9] https://www.autonews.com/article/20141124/OEM06/311249952/toyota-fuel-cell [cited 24 June 2019]
[10] https://www.healthline.com/health/ph-of-drinking-water[cited 24 June 2019]

Comparing the HAVIC to Current Market

To measure the sustainability of this project, the vehicle needs to be compared to existing vehicles in the current market. It will be compared to regional aeroplanes and conventional cars and should perform better or at least similar in emission.

For a preliminary comparison the emissions in kg from a car and a charter jet are used. As can be read from Figure 9.5, aircraft and cars do already emit water vapour as well. The HAVIC will emit a lot more, but won't emit any CO_2. As Figure 9.6 shows, the life-cycle of hydrogen production nowadays using electrolysis, is the least CO_2 emitting fuel of all the ones listed. As explained CO_2 will remain in the atmosphere longer than water. This difference, together with the knowledge that the water vapour is released at low altitude, means it does not contribute to the global warming. The HAVIC is the best option regarding the emissions. Hydrogen production rates are currently limiting the number of HAVIC that can be taken in operation. As the Door2Door project aims for a first batch of 50 HAVICs, this is not a problem for now. In the near future the knowledge on sustainable hydrogen production is expected to grow and solve the availability issue of hydrogen.[11] [12] [13]

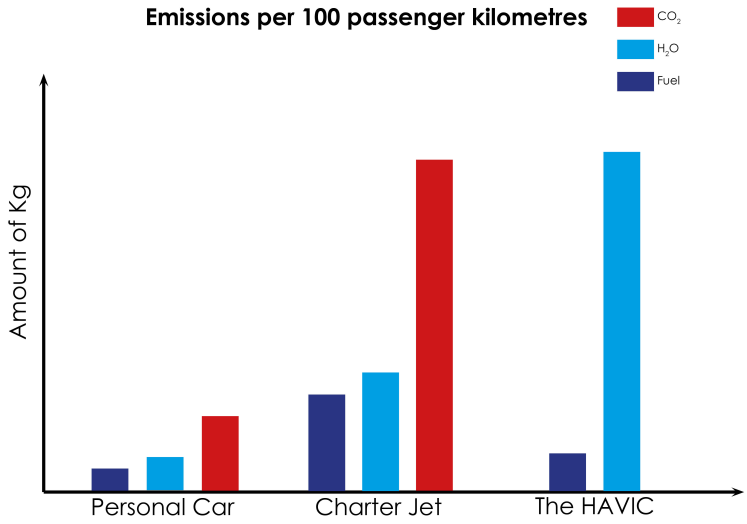

Figure 9.5: Illustrating the CO_2 and water emissions per transport method

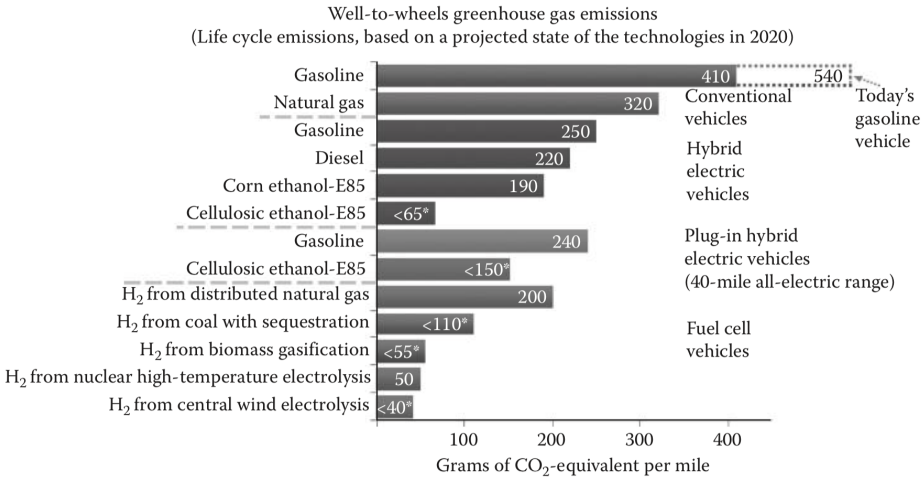

Figure 9.6: Illustrating the CO_2 life cycle emissions [58]

[11] https://micpohling.wordpress.com/2007/05/08/math-how-much-co2-released-by-aeroplane/ [cited 2 June 2019]
[12] https://blog.openairlines.com/how-much-fuel-per-passenger-an-aircraft-is-consuming [cited 2 June 2019]
[13] https://agupubs.onlinelibrary.wiley.com/doi/epdf/10.1029/2002JD002623 [cited 2 June 2019]

10

Financial Analysis

In this chapter, a financial analysis is performed for the HAVIC. This includes the resource allocation and budget breakdown which is discussed in section 10.1, the cost breakdown structure in section 10.2 and the return on investment and operational profit in section 10.3.

10.1. Resource Allocation & Budget Breakdown

Technical Performance Measurement (TPM) is a process during the project to measure the risks, where a set of parameters are chosen. These parameters are design specific. The TPM values are implemented at the start of the project in order to keep track throughout the whole process. These TPM values are constantly updated for each phase of the project and must be within an acceptable tolerance range. The TPM parameters chosen are the cost, mass, power, emission and range. For each phase of the design a contingency margin is reserved in order to account for unforeseen circumstances that may be encountered during the project phase. The contingency margins for the TPM parameters are listed in Table 10.1 for each design phase. The contingency margins are taken from [59–61] and adapted with respect to the risk of exceeding the target value.

Table 10.1: Resource allocation including contingency margin for each design phase

Design Phase	Cost [%]	Mass [%]	Power [%]	Emission [%]	Range [%]
Conceptual Design	20	25	25	15	50
Preliminary Design	15	20	20	5	25
Detailed Design	9	12	12	0	10
Testing Design	7	5	5	0	5
Production	0	0	0	0	0

From Table 10.1, it can be seen that the contingency margins set for the TPM parameters decrease as the project approaches the production phase. The contingency margin for emission starts at 15% and reduces to 0% at the detail design phase. This can be explained due to the fact that one of the key requirements of the design is to design a vehicle that produces zero emissions. Furthermore, it can be seen that at the conceptual design the contingency margin for the range is 50%. This is because, during this phase three use cases were established with different ranges. Upon this stage, it was not decided which use case will be chosen for the detailed design. Once the use case is selected, the contingency margin for the range decreases to 10% at the detailed design phase.

10.2. Cost Breakdown Structure

The cost break down structure is shown in Figure 10.1 and is divided into the development, manufacturing and testing cost. The development cost consists of the main components of the HAVIC, whereas the manufacturing cost includes the main components and takes into account the final assembly. Moreover, the testing cost consists of the windtunnel testing, system testing, structural testing, propulsion testing and simulation. In order to estimate the cost of development and manufacturing, a cost estimation method was used from Markish [62]

based on statistical relationship from reference aircraft's. The cost estimation for development and manufacturing of the components of the HAVIC takes into account inflation and are given in $/kg and listed in Table 10.3 and Table 10.4. Furthermore, the mass of the main components are given in Table 10.2. In this case the mass of the fuel, payload and cargo are excluded.

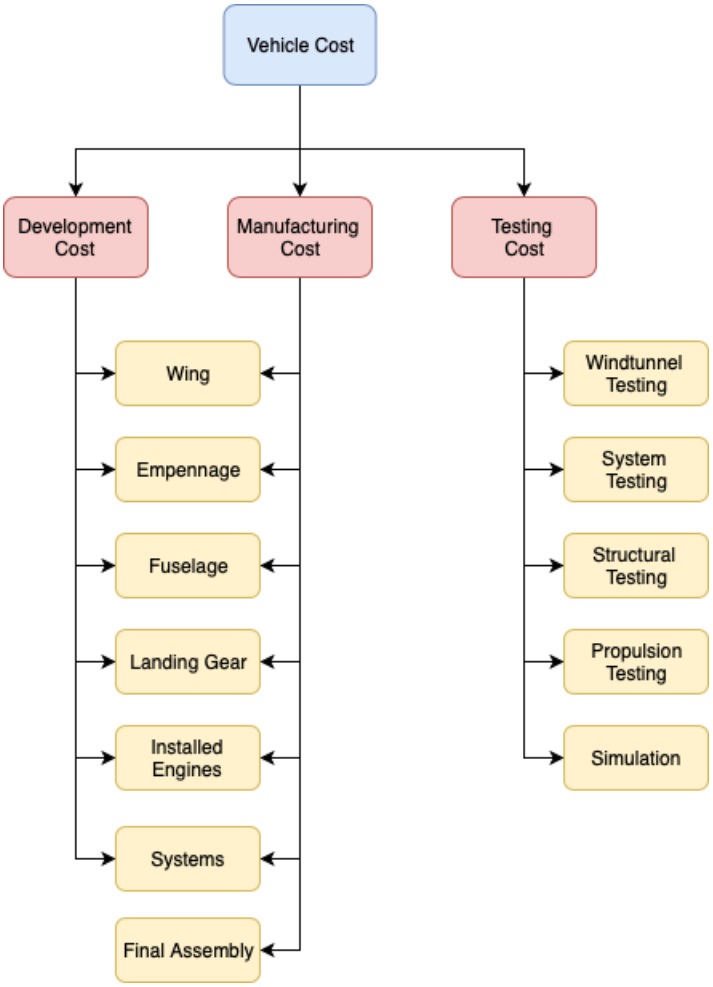

Figure 10.1: Cost breakdown structure of the HAVIC

Table 10.2: Mass estimation of the main components

Wing [kg]	Empennage [kg]	Fuselage [kg]	Landing Gear [kg]	Installed Engines [kg]	Systems [kg]	Total [kg]
120	22.5	422.5	158.8	383.9	183.7	1291.4

Table 10.3: Development cost estimation for main components of an aircraft in USD 2019

	Engineering [$/kg]	Material & Equipment [$/kg]	Tool Design [$/kg]	Tool Fabrication [$/kg]	Support [$/kg]	Total [$/kg]	Cost [$]
Wing	22190	5547	5825	19305	2606	55470	6656784
Empennage	65265	17131	17131	56781	7668	163166	1248147
Fuselage	40160	10039	10543	34941	4718	100400	23437427
Landing Gear	3125	782	820	2719	366	7818	8806371
Installed Engines	10878	2719	2856	9463	1276	27189	21296162
Systems	42931	10734	11269	37350	5043	107327	10190427

Table 10.4: Manufacturing cost estimation for main components of an aircraft in USD 2019

	Labour [$/kg]	Materials [$/kg]	Other [$/kg]	Total [$/kg]	Cost [$]
Wing	1905	638	275	2819	338245
Empennage	5049	1514	729	7292	164078
Fuselage	2124	594	307	3025	1278141
Landing Gear	335	307	50	691	109791
Installed Engines	776	285	113	1173	450376
Systems	985	285	144	1414	259760
Final Assembly	13	13	9	34	44441

The total development and manufacturing cost can be found by summing up the total cost of all components listed in Table 10.3 and Table 10.4. However, since this statistical data is solely based on reference aircraft's and the HAVIC is classified as a car and aircraft, a factor has been applied to account for this. This factor is derived based on the manufacture price of the HAVIC and scaled down with respect to the mass of the AeroMobil 4.0. Therefore, after calculating the development and manufacturing cost a factor of 0.8138 was applied. Furthermore, the cost for testing the HAVIC is calculated based on a statistical relationship from Roskam [63] and is given by Equation 10.1. In this case W_{ampr} = 953.21 kg, V_{max} = 134.99 knots, N_{rdte} = 2, CEF[1] = 6.6 and F_{diff} = 2. This resulted into a testing cost of $591856. The final development cost, manufacturing cost and investment are listed in Table 10.5. From Table 10.5, it can be concluded that the investment and manufacturing cost are 59 and 2.2 million USD, respectively.

$$C_{test} = 0.008325(W_{ampr})^{0.873}(V_{max})^{1.890}(N_{rdte})^{0.346}(CEF)(F_{diff}) \tag{10.1}$$

Table 10.5: Development and manufacturing cost

	OEW [kg]	Development Cost [$]	Manufacturing Cost [$]	Testing Cost [$]	Investment [$]
HAVIC	1291.4	58291915	2152258	591856	58883771

The price in order to manufacture the HAVIC is 2.2 million USD, which exceeds the initial cost requirement discussed in section 2.2. This can be explained due to the fact that in the early stage of the project a lot of uncertainties were encountered during the conceptual phase. This leads to a underestimation of the manufacturing price of the HAVIC. Furthermore, a lot of design choices were made which has a signification impact on the cost of the HAVIC.

10.3. Return on Investment and Operational Profit

The amount of money that has been invested into the development of the HAVIC has to be returned. The first vehicle that will be produced will be sold to the client with no profit, therefore the price is set at 2.2 million USD. When the first vehicle is launched and proven to be successful, the roll out of the first batch of vehicles will be in 2034. A total of 50 vehicles will be produced in 2034, where a profit margin of 15% is considered. The manufacturing price and the amount of time to delivery a vehicle is related to the learning curve, where a reduction factor of 0.9 is used every time the number of vehicles produced is doubled. The two learning curves are shown in Figure 10.2 and Figure 10.3. Furthermore, from Figure 10.3 the number of vehicles produced each year can be derived, which is shown in Figure 10.5. It was assumed that only one factory is responsible for the production and the number of vehicles produced in year 2034 is 50 due to the highly advanced technology.

[1] Cost Escalator Factor

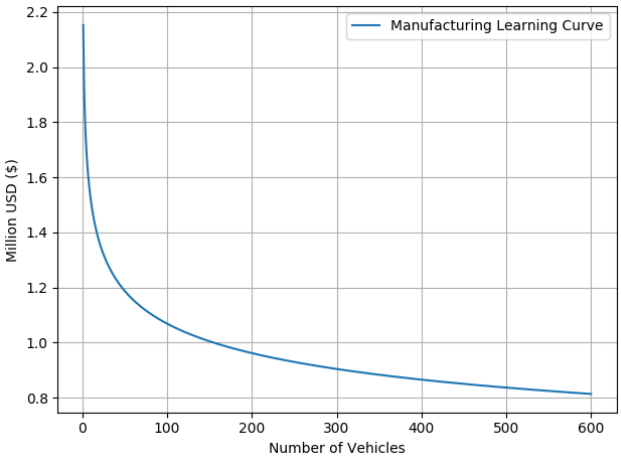

Figure 10.2: Manufacturing price learning curve

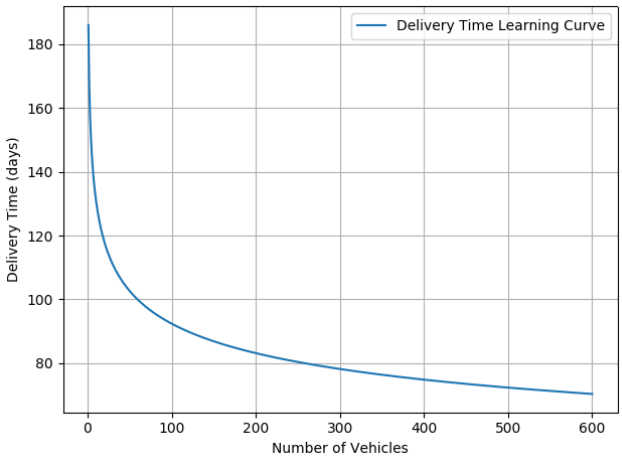

Figure 10.3: Learning curve for the manufacturing price and delivery time

In order to obtained the invested money of 59 million USD back, the vehicles have to be sold to customers with a profit margin starting in 2020. Taking into account the learning curves from Figure 10.2 and Figure 10.3. The invested money in this case are the development and testing cost which can be considered as non-recurring costs, whereas the manufacturing costs of the vehicle can be considered as the recurring costs. The total cost and total revenue as function of the number of vehicles are shown in Figure 10.4. From Figure 10.4, it can be concluded that after the 382nd produced vehicle, the company is starting to make profit and the return on investment is accomplished. Therefore, the amount of money invested is returned in year 2023 according to Figure 10.5.

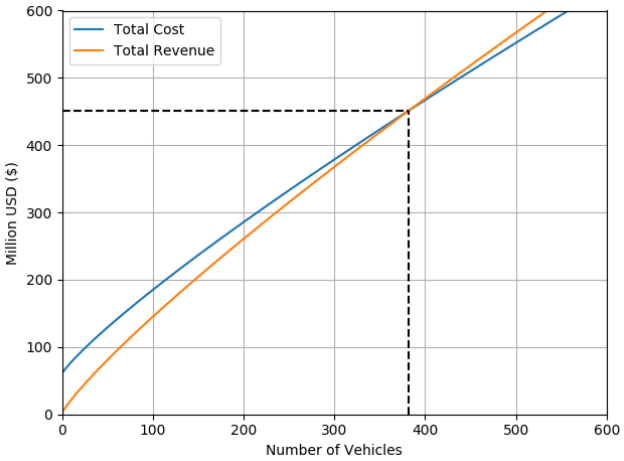

Figure 10.4: Total cost and total revenue

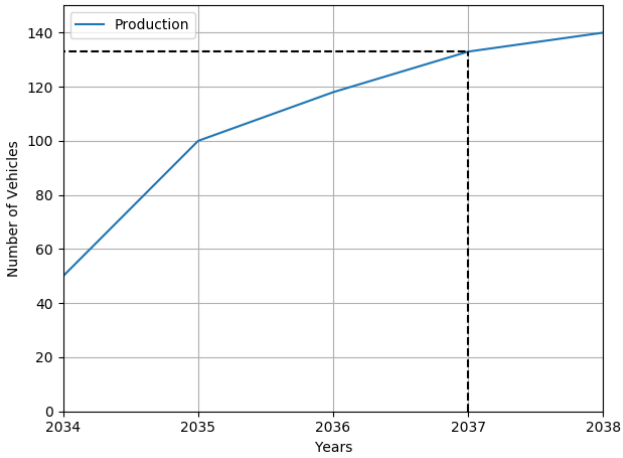

Figure 10.5: Number of vehicles produced in each year

11

Compliance and Feasibility

In this chapter the compliance matrix is generated, which is shown in Table 11.1. In this compliance matrix all the requirements are checked whether they are fulfilled.

Table 11.1: The compliance matrix, detailing the compliance status for all requirements in the Door2Door project

Requirement ID	Requirement	✔ / ~ / X	Relevant Sections and Comments
REQ-TR-GEN-1-1	The vehicle shall be capable of carrying 4 persons with an average mass of 80 kg	✔	Chapter 4, chapter 5, and chapter 6. The subsystems have been designed with the required payload in mind.
REQ-TR-GEN-1-2	The vehicle shall be capable of carrying an additional 10 kg of luggage per person	✔	Chapter 4, chapter 5, and chapter 6. The subsystems have been designed with the required payload in mind.
REQ-TR-GEN-1-3	The vehicle shall have a luggage volume of at least 350 liters	X	Not enough cabin space given for the power system's volume chapter 6
REQ-TR-GEN-1-4	The vehicle shall not require a pressurised cabin	✔	Cabin pressurisation not required at the maximum planned flight level of the vehicle section 6.1
REQ-TR-GEN-3-1	It shall be possible to convert the vehicle to 'flight ready' condition in at most 10 minutes	✔	The wing transformation itself only lasts a few seconds (chapter 4). Besides this, testing of the control surfaces and propellers must also be done. The entire conversion to flight-ready condition should in fact take less than 5 minutes.
REQ-TR-GEN-3-2	The vehicle shall have a flight navigation system accurate to 4 m	✔	section 7.2
REQ-TR-GEN-3-3	The vehicle shall have a ground navigation system accurate to 4 m	✔	section 7.2
REQ-TR-GEN-4-1	The vehicle shall be designed to suit the 95% percentile male and 5% percentile female	✔	section 5.5

REQ-TR-GEN-4-2	The internal temperature of the vehicle shall remain between 15-25° Celsius during all operations	✔	Thermal control has been sized accordingly (chapter 6)
REQ-TR-GEN-4-3	The noise level inside the cabin of the vehicle shall not exceed 80 dB	✔	section 8.3
REQ-TR-GEN-5-1	The vehicle shall produce only water as its waste product	✔	chapter 6
REQ-TR-GEN-5-2	The vehicle shall produce no more than 70 dB of noise at an altitude of 152 m (500 ft)	✔	section 8.3
REQ-TR-GEN-6-2	The vehicle shall have a fully redundant power delivery system	✔	The power system contains two hydrogen fuel cells, reserve fuel, and an APU (chapter 6)
REQ-TR-GEN-6-3	The vehicle shall have a fully redundant propulsion system	✔	The vehicle's 10 propellers are each powered by individual electrical motors for maximum redundancy (chapter 4)
REQ-TR-GEN-6-4	The vehicle shall have an airbag	~	This will be developed at a later stage in the design
REQ-TR-GEN-6-5	The vehicle shall have a fail-safe control system	~	This will be developed at a later stage in the design
REQ-TR-GEN-7-1	The range of the vehicle shall be extended by <tbd> through the use of solar energy	X	Solar panels have been considered for the preliminary design (section 15.3), but cannot be used to significantly extend the range of the vehicle. They would instead be used for recharging the APU.
REQ-TR-GEN-7-2	There shall be an expected outline for the infrastructure up to <tbd> years from 2019	✔	An initial plan for the required infrastructure and operations is laid out in chapter 14
REQ-TR-GEN-7-3	Subcontractors shall be certified as ISO 14001 company or similar	~	Specific contractors would be defined at a future stage of the development
REQ-TR-GEN-7-4	The vehicle shall be circular in use for at least <tbd> %	~	Discussed in chapter 9, but the final percentage of circular use is still unknown
REQ-TR-GEN-7-9	The vehicle shall only be charged with hydrogen made through a process which emits no greenhouse gases	~	It is possible to produce hydrogen in a clean way through electrolysis, but it is unclear whether this will be feasible in a large enough scale. Industrial partnerships could be made to ensure clean hydrogen refuelling facilities. Discussed in chapter 9.
REQ-TR-DRI-1-1	The vehicle shall have a minimum driving range of 80 km (50 miles)	✔	chapter 6
REQ-TR-DRI-1-2	The vehicle shall have a maximum driving speed of at least 105 km/hr (65 mph)	✔	subsection 12.2.1

REQ-TR-DRI-2-1	The vehicle shall have a maximum stopping distance when driving of 40 m at 80 km/h (50 mph)	✔	subsection 12.2.1
REQ-TR-DRI-2-2	The vehicle shall be able to accelerate at 2.5 m/s^2	✔	subsection 12.2.1
REQ-TR-DRI-2-5	The vehicle shall have reverse driving capability	✔	subsection 12.2.1
REQ-TR-FLY-1-1	The vehicle shall have a flying range of 400 km (248.5 miles) in addition to the driving range	✔	chapter 6
REQ-TR-FLY-1-2	The vehicle shall have a maximum flying speed of 241 km/hr (150 mph) at cruising altitude	✔	chapter 4 and chapter 6
REQ-TR-FLY-1-3	The vehicle shall have a cruising altitude of between 0.9 and 1.5 km (3000-5000 ft)	✔	chapter 4 and chapter 6
REQ-TR-FLY-2-1	The propulsion system shall generate a thrust of 4.5 kN	✔	chapter 6
REQ-TR-FLY-2-2	The vehicle shall be able to perform a rate one turn in all flying conditions	✔	Ailerons were sized to meet this requirement (chapter 4)
REQ-TR-IDL-1-1	The vehicle shall have a top-down footprint no larger than 4.8 x 2.3 m	✔	section 7.1
REQ-TR-IDL-2-1	The vehicle shall be able to recharge its battery fully in no more than 30 minutes	~	The specifics of liquid hydrogen refuelling must still be investigated further
REQ-TR-TOL-1-1	The vehicle shall have a top down footprint of no more than 8.6 x 5.4 m in take-off configuration	✔	section 7.1
REQ-TR-TOL-2-1	The vehicle shall be able to take off and land with 108 km/hr longitudinal speed	✔	section 8.6
REQ-CR-CST-1-1	The market price shall not exceed 750,000 dollars	X	The latest estimates can be found in section 10.2
REQ-CR-CST-1-2	The profit gained shall be zero	✔	section 10.3
REQ-CR-CST-2-1	The maintenance cost shall be in the range of 700-900 dollar annually	~	This will be defined at a later stage in the design
REQ-CR-CST-2-2	The electrical charging cost shall be in a range of 0.025-0.062 dollars per km (0.04-0.10 dollars per mile)	✔	The Li-ion battery could be charged entirely via solar panels (section 15.3)
REQ-CR-CST-3-1	The vehicle shall be able to use the current infrastructure facilities	✔	chapter 14

REQ-CR-CST-4-1	It shall be possible to produce at least 500 vehicles in the first 5 years	✔	As discussed in chapter 10, 50 vehicles should be produced in the first year. Assuming one factory, every subsequent year would see a production of roughly 133 vehicles per year (totalling around 580 vehicles produced in the first 5 years).
REQ-CR-REG-1-1	The airplane design and capabilities shall be in agreement with the applicable aviation regulations (EASA CS23)	~	Regulations have been taken into account through the conceptual design process chapter 13 and chapter 3. However, compliance with all EASA CS23 regulations cannot yet be assured at this stage.
REQ-CR-REG-1-2	The MTOW shall not exceed 5670 kg	✔	section 7.1
REQ-CR-REG-1-3	The stall speed shall be no more than 31.38 m/s	✔	chapter 4
REQ-CR-REG-1-4	The rate of climb shall be no less than 274 m/min	✔	section 8.5
REQ-CR-REG-1-5	The take-off speed shall be no less than 1.2 times the stall speed	✔	chapter 4
REQ-CR-REG-1-6	The airplane shall always operate 305 m (1000 ft) above the highest object in the surroundings when utilising forward facing propulsion	✔	Given current airfield locations, the vehicle's rate of climb, and the cruise altitude, this requirement should be achievable
REQ-CR-REG-1-7	The vehicle shall have a minimum reserve fuel/power of 30 min	✔	chapter 6
REQ-CR-REG-2-1	The vehicle shall pass the periodic vehicle inspection according to European Directive 96/96/EC	~	This will be determined during a later stage of development
REQ-CR-REG-2-2	The driver shall have a valid driver licence	✔	This will be ensured during a later stage of development
REQ-CR-REG-2-3	The vehicle shall be inspected every year	✔	This will be ensured during a later stage of development
REQ-CR-REG-3-1	The vehicle noise level on ground shall be <68 dB	✔	section 8.3
REQ-CR-TM-1-1	The conceptual design shall be finished within 10 weeks	✔	-
REQ-CR-TM-2-1	The assembly time shall be no more than 2 months	X	As discussed in section 15.2, the entire production cycle would take 6 months
REQ-CR-RS-1-1	The Li-ion of the batteries shall be recyclable	~	This will be investigated further in the preliminary design phase
REQ-CR-RS-1-2	The metals shall be completely reusable	X	Complete reusability is not feasible in this case
REQ-CR-RS-2-1	The preliminary design shall be completed with the Door2Door project group	✔	-

12

Verification and Validation

To check if the models used work properly and if they model reality to a high enough extent, verification and validation is performed. The models and programs used in chapter 4, 5, 6 and 8 are verified and validated in section 12.1, 12.2, 12.3 and 12.4.

12.1. Wing Design

Verification and validation for the propulsion system, aerodynamic characteristics, wing box design and wing folding mechanism are done in the following subsections.

12.1.1. Propulsion

The momentum disk analysis to calculate the wake velocities is verified by unit tests. For several input values, the output is checked to be the same as a hand calculation. Validation for further research should be done with CFD models of the propeller wake over the wing behind the different type of propellers. Wind tunnel tests should also been done to validate in the end. NASA has done research and ran models on their design, which uses a very similar configurations to the HAVIC configuration. For this reason, it is referred to their findings.[1]

12.1.2. Aerodynamic Characteristics

For the airfoil choice and performance estimation of the vertical tail, horizontal tail and wing, firstly the NACA database was used to make a first selection of most suitable airfoils. After this, DATCOM methods and Javafoil were used to estimate the wing lift curve drag polar depending on the aircraft and mission parameters, such as: aspect ratio, Reynolds number and Mach number. It is assumed that both the NACA database and Javafoil are verified and validated. Furthermore, the DATCOM methods used are unit tested using known aircraft wings to check outputs to known outputs. Next to this, in calculations it was assumed that the tail down force never exceeds 0.1MTOW, such that L=1.1MTOW. This was found to be true.

12.1.3. Wing Box Design

The loading diagram created for the wing is made using a python program to analyse the effect of the forces acting on the wing and interpret the reaction forces and inner shear and moments. These are straightforward calculations which were all verified by performing the calculations on paper and matching the results. The design of the wing box is verified by using readily available software CATIA and ANSYS. Firstly a model of the wing box is created in CATIA to the exact specification as the wing box design chapter. The model is assigned the material properties as defined from the material selection. The model is then imported into ANSYS where the forces and loads are applied in the correct positions. The software is then able to determine the displacement and stresses in the wing-box as seen in Figure 12.1 and Figure 12.2 which can be compared to the calculated values.

[1] `https://aero.larc.nasa.gov/files/2012/11/Distributed-Electric-Propulsion-Aircraft.pdf` [cited 22 June 2019]

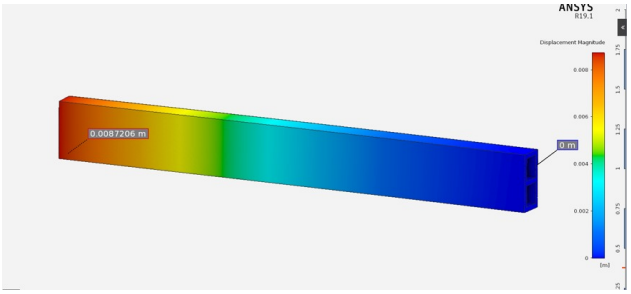

Figure 12.1: ANSYS analysis of the wing box showing displacement

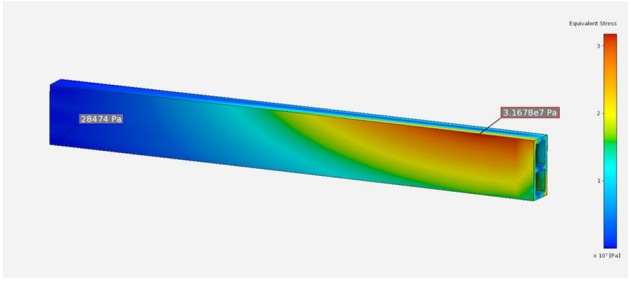

Figure 12.2: ANSYS analysis of the wing box showing stresses

It can be seen from this analysis that the calculations were accurate. Given that the displacement is similar to the calculations done by the python program. Furthermore the analysis on ANSYS proves that the design is suitable since the stress in the wing box is lower than the allowable stress and the displacement is lower than the maximum allowable displacement.

12.1.4. Wing Folding Mechanism

The static equilibrium equations which are required for the analysis are calculated by solving a set of simultaneous equations. The program can be confirmed by first setting all the input forces to 0 and ensuring that all the reaction forces equate to 0. Furthermore, it is possible to replicate the equations by hand for one of the load cases. This will allow the program to be verified. To verify the fail-safe requirement for the rotating mechanism, the analysis is repeated with a broken bolt, but the bolt that was broken is changed. This is tested for each of the 3 bolts. Finally the analysis is performed but with no bolts broken to confirm that the forces acting in the system are in fact lower.

12.2. Main Body Design

Verification and validation for the ground system, tail design and control surfaces, general structures and material and manufacturing are detailed in the following sections.

12.2.1. Ground System

In order to verify the ground system, calculations are done by hand and the driving performance of the vehicle is looked into in detail. All driving requirements are met with the current design.

The maximum force the car has to provide is 4966.517 N. this is taken at a speed of 104 km/h accelerating to 105 km/h with 105 km/h being requirement REQ-TR-DRI-1-2. F_r is the rolling resistance force using a rolling resistance coefficient of 0.02.[2] F_d is the drag force at sea level using the vehicle's C_D0 of 0.3. F_c is the force needed to accelerate at the 2.5 m/s^2 which is requirement REQ-TR-DRI-2-2.

$$F = F_r + F_d + F_c \quad (12.1) \qquad F_r = \mu \cdot weight \quad (12.2)$$

$$F_d = 0.5\rho C_D A v^2 \quad (12.3) \qquad F_c = ma \quad (12.4)$$

Using Equation 12.5 it can be seen that the required maximum power to meet the requirements REQ-TR-DRI-1-2 and REQ-TR-DRI-2-2 is 145 kW using force as 4966.517 N and velocity of 105 km/h.

$$P = Fv \quad (12.5)$$

Taking an average speed of 50 km/h the force that needs to be provided by the drive train using Equation 12.1, Equation 12.2, Equation 12.3, Equation 12.4 and Equation 12.5 again the average power needed is 17.6 kW making the assumption that acceleration occurs 0.2% of the time.

Using Equation 12.6 the total energy needed to meet requirement REQ-TR-DRI-1-1: The vehicle shall have a minimum driving range of 80 km, is 27.2 kWh, ad-hearing to the power and energy budgets.

$$E = Pt \quad (12.6)$$

[2] https://www.engineeringtoolbox.com/rolling-friction-resistance-d_1303.html [cited 23 June 2019]

REQ-TR-DRI-2-1: The vehicle shall have a maximum stopping distance of 20 m at 80 km/h (50 mph) is solved easily. Stopping distance regulations state that a frictional coefficient of 0.7 must be used. The disc brakes used in the HAVIC plus the regenerative braking system have a larger friction coefficient with normal values ranging between 0.45 - 0.65 but multiplied by 2 as there are two pads either side of the wheel. The equation for stopping distance is seen in Equation 12.7 giving a value of 35.96 m.

$$D = \frac{v^2}{2\mu g} \tag{12.7}$$

The final driving requirement REQ-TR-DRI-2-5: The vehicle shall have reverse driving capability, is completed as there is a camera on the back of the vehicle that projects the view onto the console in the cockpit.

12.2.2. Tail Design & Control Surfaces

The calculations for the horizontal and vertical tail can be verified by performing a unit test. In this case, a test is performed where an example problem is used as an input, the output of the example problem is known. When the calculations give the correct outputs corresponding to the example problem, the program is verified. This was the case and therefore the program for sizing the horizontal and vertical tail is verified.

In order to validate the results, the geometry of the horizontal and vertical tail are compared with reference aircraft's. The tail geometry of different aircraft's can be found in Table 12.1. Comparing the geometry, it can be concluded that the surface area ratio of the horizontal tail is below the reference aircraft's. This can be explain due to the fact that the HAVIC is not only an aircraft but also a car. The variation in c.g. during operation is significantly smaller when compared to a regular small aircraft, therefore a smaller tail size can be obtained. For the surface area ratio of the vertical tail it can be seen that it is within the range of the reference aircraft's. Furthermore, the aspect ratio for both the horizontal and vertical tail are close to the values of reference aircraft's.

Table 12.1: Tail geometry comparison with reference aircraft

Aircraft	M_{TO} [kg]	S_h/S [-]	A_h [-]	S_v/S [-]	A_v [-]
HAVIC	1668	0.154	3.93	0.135	1.42
Cessna 177	1100	0.202	4.0	0.107	1.41
Cessna Citation I	5375	0.260	5.2	0.192	1.58

For the calculations and sizing of the aileron, elevator, and rudder, the same unit test was performed as for the calculations for the tail size. An example problem was implemented into the program in such a way that it gives the correct outputs and therefore verified. To validate the results obtained, the geometry of the control surfaces are compared to reference aircraft, which is shown in Table 12.2. It can be seen that the aileron chord to wing ratio is similar within a certain extent with reference aircraft's. The same can be said about the elevator chord to horizontal tail ratio and the control surface area ratio. Furthermore, the rudder chord to vertical tail ratio is significantly higher compared to reference aircraft's. This can be explained due to the fact that the back wheel of the HAVIC is placed underneath the vertical tail, which limits the span area of the rudder. In order to compensate for this, the chord of the rudder has to be increased in order to provide the same yaw stability.

Table 12.2: Control surface geometry comparison with reference aircraft

Aircraft	M_{TO} [kg]	C_a/C_w [-]	C_e/C_h [-]	S_e/S_h [-]	C_r/C_v [-]	S_r/S_v [-]
HAVIC	1668	0.2	0.44	0.52	0.5	0.26
Cessna 182	1406	0.2	0.44	0.38	0.42	0.38
Cessna 650	9979	0.3	0.37	0.37	0.27	0.26

12.2.3. General Structures

The masses of all designed components have to be verified to ensure that the weight estimation is accurate. This is done using CATIA models. Accurate recreations of the wing, wing box, fuselage skin, and empennage are made using the modelling software and the correct material properties are assigned to each part. At this point it is possible to generate a mass estimate for the part using the software. The outcome of this test is shown in Table 12.3

Table 12.3: Table showing comparisons of masses from calculations and from CATIA estimates

Component	Calculated Mass [kg]	CATIA Mass [kg]
Wing Box	35.74	33.2
Wing Skin	24.26	25.1
Fuselage Skin	21.00	23.9
Empennage	22.50	24.0

12.2.4. Materials & Manufacturing

The material selection can be verified by analysis by implementing the materials into the various Python programmes and the CATIA model. This goes hand in hand with the structural verification. If one would like to verify purely the materials only, they could be modelled using a finite element method. Also, verification by testing is important. Materials can be tested on various levels as can be seen in Figure 12.3. When applying novel materials it is important to perform tests at all levels and both nondestructive and destructive tests. These tests take place during the complete development and production.

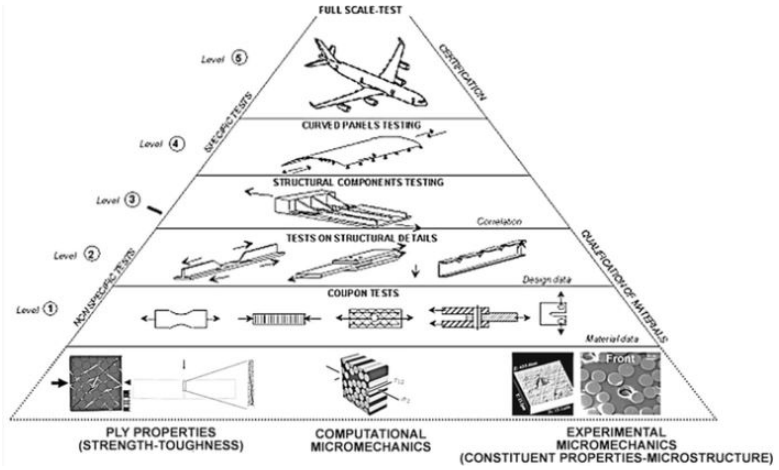

Figure 12.3: Pyramid schematic to show the different levels of material testing, with an extra layer with a proposed testing method for composites [64]

This testing for verification is continued throughout the manufacturing as a form of quality control. Special attention is reserved for the quality of the composites as their flaws are often not traceable with visual inspection. In order to detect flaws such as delamination and voids in the actual skin panels, nondestructive testing can be used. Methods based on sound waves and heat emission can be used, while methods based on electric current cannot be applied, because composites are non-conducting. The manufacturing can also be verified using a computer model. Additionally, a model can be made to verify the production line and optimise it for the HAVIC.

In terms of validation of the materials, reference data from similar materials functioning under similar circumstances can be used. While the use of composites in aircraft is not new, the use for the skin panels as extensively as is done in the HAVIC is less than 10 years old. Therefore, it is essential to keep track of the aircraft that do apply similar composites in that fashion. Also, as time goes by, experience is gained in designing with composites, this can also be used as a form of validation.

12.3. Power

In this section verification and validation is done for the power subsystem. This includes the hydrogen fuel cell in subsection 12.3.1, air intake system in subsection 12.3.2 and the fuel tank in subsection 12.3.3.

12.3.1. Hydrogen Fuel Cell

In order to verify the performance of the vendor's hydrogen fuel cell, the power generated by a given cell area can be estimated through the fuel cell's polarisation curve. Many empirical models have been developed for estimating a fuel cell's polarisation curve [65]. They all calculate the cell potential $V(i)$ as a function of current density i (in A/cm^2). This can be represented as the theoretical cell potential E_{rev} minus the cell voltage drop E_{irrev} due to irreversible loss mechanisms. This voltage drop E_{irrev} can be described as the sum of voltage losses due to species crossover from one electrode through the electrolyte and internal currents, which can be further classified into three major groups:

- Activation Polarisation ($v_{act,anode}$ and $v_{act,cath}$)
- Ohmic Polarisation (v_{ohmic})
- Concentration Polarisation ($v_{conc,anode}$ and $v_{conc,cath}$)

All empirical models therefore follow a similar formula:

$$V(i) = V_{rev} - v_{act,anode} - v_{act,cath} - v_{ohmic} - v_{conc,anode} - v_{conc,cath}$$

The Fraser and Hacker model [66] is used here because it has been considered to be one of the most accurate models in previous validation efforts [65]. In this model, the cell potential $V(i)$ as a function of current density i is calculated through Equation 12.8.

$$V(i) = V_{rev} - \mathbf{b} \cdot \log\left(\frac{i + \mathbf{i_{loss}}}{\mathbf{i_0}}\right) - \mathbf{R} \cdot i - \mathbf{m} \cdot exp(\mathbf{n} \cdot i) \tag{12.8}$$

The supplier of the Powercell S3 hydrogen fuel cell provides the polarisation curve seen in Figure 12.4 for their 55 cm^2 unit cell, of which there are 43 in the S3 model.[3]

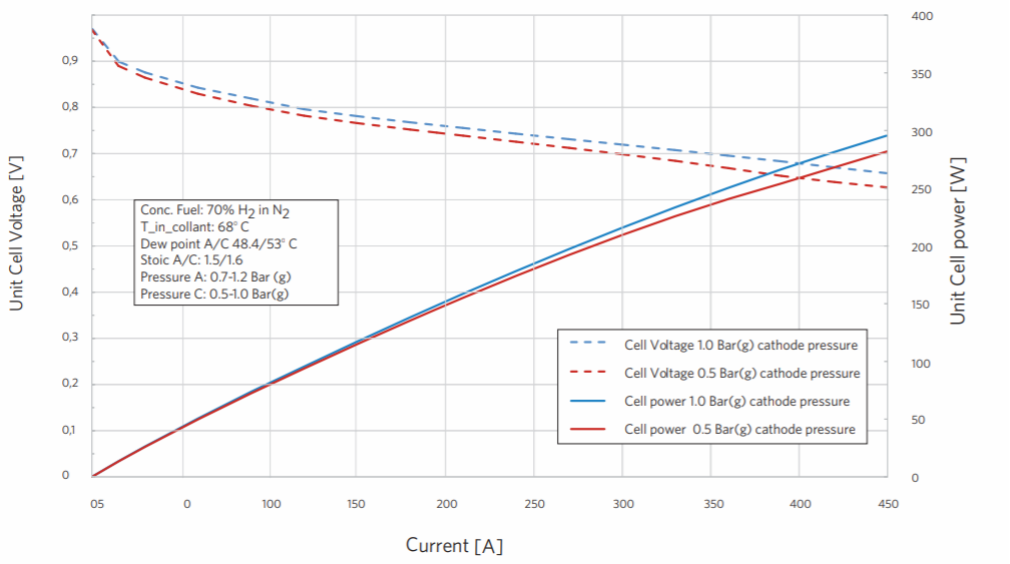

Figure 12.4: Powercell's unit cell polarisation curve

A polarisation curve was then produced using the Fraser and Hacker model from Equation 12.8, specifications on the Powercell unit cell operational parameters, and fitting parameters which should be similar to values

[3] https://www.powercell.se/wordpress/wp%2Dcontent/uploads [cited 22 June 2019]

present in literature. If a polarisation curve can be produced by this method which matches the curve provided by the vendor, then this voltage-current relationship can be trusted to be reproducible and thus will be used in further power and cell area calculations. The polarisation curve produced can be seen in Figure 12.5 below, and the fitting parameters used can be seen in Table 12.4 together with some fitting parameters from bench test data available in literature [65].

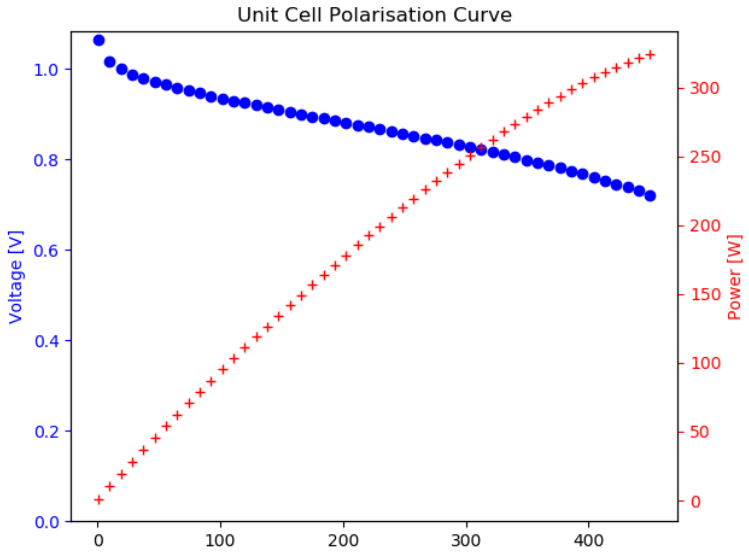

Figure 12.5: Polarisation curve fit to Powercell's unit cell data

Table 12.4: Fitting parameters for the polarisation curve model

	b [V/decade]	R [Ωm^2]	i_{loss} [Acm^2]	i_0 [$10^{-7} Acm^2$]	m [V]	n [cm^2/A]
Literature	0.06642	0.1083	0.001225	3.7980	0.005248	2.2421
Powercell Unit Cell	0.02501	0.0320	0.000715	3.7980	0.002105	0.6133

Clearly the cell potential and power values provided by Powercell can be achieved with realistic fitting parameters. However, this does require assuming e.g. a lower electrical resistant than what was measured in previous tests. Also, as Powercell has not provided sufficient data on their fuel cell stacks themselves, it is at this point impossible to validate the efficiency of the fuel cell stack assembly. It is possible that the fuel cell stack incurs further power losses and therefore does not provide as much power as 43 individual unit cells.

12.3.2. Air Intake System

To validate the air intake system simulation, testing needs to be used, as the specific air intake layout has not yet been fully employed for aviation purposes. However, making CFD simulations and prototypes of the air intake are out of the scope of the project and similar solutions to air intakes already exist in the automotive industry, thus partly validating the design choices made. Validation is also done by comparing the design to that of T. Diepenhorst et al. where a similar intake was designed for a 100 kW fuel cell [67].

12.3.3. Fuel Tank

Tank validation can be accomplished by building a prototype tank and checking its ability to withstand the required pressure and insulate the inside from temperature changes. In case running this test is not possible until far too late into the design or if this is too costly to perform, validation could also be performed through computational models for the structural wall and insulating walls respectively.

12.4. Performance

In this section the performance in terms of lift and drag will be verified and validated.

12.4.1. Lift

The calculation that uses DATCOM methods will be tested by unit tests on similar wings for which the wing lift curve is known. If the results appear to be close to the actual values, then the program is implemented correctly.

12.4.2. Drag

The drag polar is verified by looking at the shape and its parametric values. Looking at drag polars of other aircraft shows similarities. As an example, the Cessna 172S is taken. It can be seen that the drag polar parameters are similar. It should be noted that the zero lift drag coefficient of the HAVIC is higher, due to the fact that the Cessna body has a better aerodynamic shape. The difference in the factor k is due to the difference in aspect ratio and Oswald efficiency. Furthermore it should be noted that the drag polar is always an estimation, as the quadratic relation is usually a fitted curve to real data points.

Table 12.5: Drag polar comparison

Aircraft	C_{D_0} [-]	k [-]
HAVIC	0.055	0.040
Cessna 172S[4]	0.033	0.035

Minimum drag coefficients of more aircraft were found online and the HAVIC's drag coefficient is comparable to the others.[5] It should be noted that in later design phases, CFD models should be used to verify and optimise the current design, shape and aerodynamic estimates.

[4] https://www.researchgate.net/figure/Figure-A10-Drag-polar-for-the-Cessna-172S-This-plot-is%2Dcreated-for-NACA-2412-airfoil_fig25_328578766 [cited 22 June 2019]

[5] http://www.aerospaceweb.org/question/aerodynamics/q0184.shtml [cited 22 June 2019]

13

Technical Risk Assessment & R.A.M.S.

In this chapter the technical risk analysis and R.A.M.S. analysis is performed. The first is done in section 13.1 and the latter is done in section 13.2.

13.1. Technical Risk Assessment

Having an overview of the potential risks is important for the design of a product. Preventing catastrophic risks by mitigation is better than not identifying these risks and having the chance of losing a design. Therefore potential risks associated to this project are identified and a risk map is shown in subsection 13.1.1. Section 13.1.2 discusses the risk mitigation plan. Implementing this, a posterior risk map is generated in subsection 13.1.3.

The technical risk assessment follows the structure described in Figure 13.1. This five step approach will be integrated to generate the technical risk map, find a technical approach to minimise the risk and create a 'posterior' risk map that shows the effect of the mitigation. The risk assessment approach will be used throughout the duration of the project in an integrated way, where the risk map is updated at each phase.

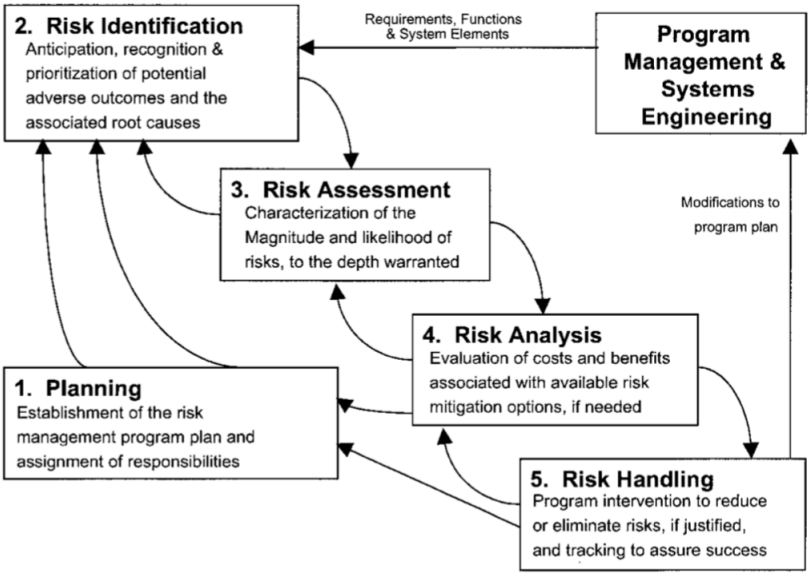

Figure 13.1: Technical risk assessment approach [60]

13.1.1. Risk Identification

In this section, the risks associated with the project are identified using the approach mentioned. As there are many risks, the focus is put on the ones that are special for our project. In Table 13.3, the risks can be categorised into five parts: general risk (1), detailed design risk (2), manufacturing risks (3), operational risk (4) and organisational risk (5). Furthermore, the severity and level of probability before and after mitigation are indicated in Table 13.3. The level of probability is categorised into four parts: very likely (I), likely (II),

unlikely (III) and very unlikely (IV). The terms linked to the level of probability in Table 13.2 are defined as follows. For design risk, the TRL[1] is used as a measure of probability, while for all other risks, a reasonable estimate in percentage range is used. 'Very Likely' has a high level of probability in the range of 75-100%, or a TRL of 1-3. 'Likely' has a medium-high level of probability in the range of 50-75%, or a TRL of 4-5. 'Unlikely' has a low-medium level of probability in the range of 25-50%, or a TRL of 6-7. 'Very Unlikely' has a low level of probability in the range of 0-25%, or a TRL of 8-9. The severity are categorised into four parts, for which the definitions depend on the type of risk, as can be seen in Table 13.1. After identifying the risks, a risk map is generated, which is displayed in Table 13.2. Risk mitigation is discussed in the next section. However, there are some risks that are not mitigated but are important to discuss:

1.2 & 3.4) While trading off material choices, toxicity is always taken into account as it invokes risks on manufacturing, assembling, maintenance personnel and customers.

4.5 & 4.8) Take-off in severe weather conditions may impose a problem and can cause termination of the flight. This risk can not be mitigated as there are already simple regulations on when you can and can not take off. The skin of the vehicle can withstand rain and hail, but not sun. For this reason, a coating referred to in subsection 5.7.2 is to be used to protect against sun degradation.

Table 13.1: Description of the severity for each risk category

Severity Risk type	**General**	**Detailed Design**	**Manufacturing**	**Operational**	**Organisational**
Negligible	No impact on project	Meeting all requirements	No injuries or cost increase	No repair required	No delay
Marginal	Minor impact on project	Meeting all key requirements	Minor injuries or minor cost increase	Direct maintenance required after planned stop	Minor delay
Critical	Decent impact on project	One key requirement is not met	Major injuries or significant cost increase	Emergency landing	Significant delay
Catastrophic	Project is forced to stop	Multiple key requirements are not met	Fatalities or extreme cost increase	Crash	Extreme delay

Table 13.2: Technical risk map

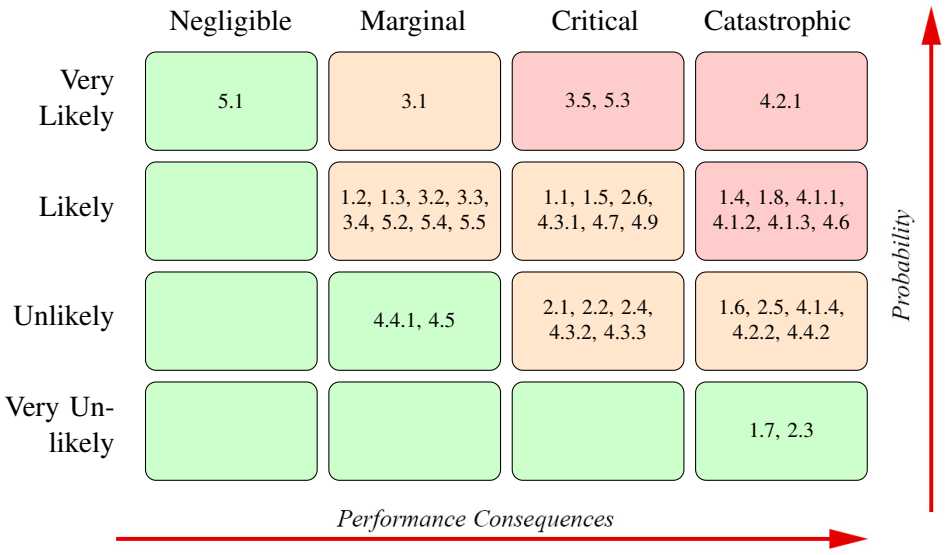

[1] https://www.nasa.gov/directorates/heo/scan/engineering/technology/txt_accordion1.html [cited 23 June 2019]

Table 13.3: Risk identification

		Severity		Probability	
Identifier	Risk	Before	After	Before	After
1.1	Lack of hydrogen tank stations	Critical	Critical	II	III
1.2	The use of toxic materials due to not having sufficient alternatives	Marginal	-	II	-
1.3	No sufficiently sustainable subcontractors/suppliers can be found	Marginal	-	II	-
1.4	Government bans final product after release on the market	Catastrophic	Catastrophic	II	IV
1.5	Not enough customers to have globally relevant impact	Critical	Critical	II	III
1.6	Concept not marketable	Catastrophic	Catastrophic	III	IV
1.7	Client break-up	Catastrophic	-	IV	-
1.8	Concept not feasible	Catastrophic	Catastrophic	II	IV
2.1	Power source too heavy	Critical	Critical	III	IV
2.2	Too much power needed for take-off	Critical	Critical	III	IV
2.3	No static stability	Catastrophic	-	IV	-
2.4	No dynamic stability	Critical	Critical	III	IV
2.5	Exceeding size constraints	Catastrophic	Catastrophic	III	IV
2.6	Rotating mechanism exceeds size or mass constraint	Critical	Critical	II	III
3.1	Increase in material cost	Marginal	Marginal	I	III
3.2	Employee strike	Marginal	-	II	-
3.3	Wage increase	Marginal	-	II	-
3.4	Incidents while manufacturing	Marginal	-	II	-
3.5	No access to certain parts of the design	Critical	Critical	I	IV
4.1	On-board fire	-	-	-	-
4.1.1	Hydrogen tank catches fire	Catastrophic	Critical	II	III
4.1.2	Electrical systems catch fire	Catastrophic	Critical	II	III
4.1.3	APU fire	Catastrophic	Critical	II	III
4.1.4	Hydrogen valves catch fire	Catastrophic	Critical	III	IV
4.2	Collision with harzardous objects	-	-	-	-
4.2.1	Bird strike	Catastrophic	Marginal	I	II
4.2.2	Other aircraft	Catastrophic	Catastrophic	III	IV
4.3	Propeller shutdown in flight	-	-	-	-
4.3.1	Power shutdown due to fire detection	Critical	Critical	II	III
4.3.2	Wire failure	Critical	Critical	III	IV
4.3.3	Propeller failure	Critical	Critical	III	III
4.4	Rotation mechanism failure	-	-	-	-
4.4.1	Mechanism is stuck in place	Marginal	-	III	-
4.4.2	Mechanism moves while in flight/on road	Catastrophic	Catastrophic	III	IV
4.5	Damage due to weather condition	Marginal	-	III	-
4.6	Lightning strike hits aircraft	Catastrophic	Marginal	II	II
4.7	Component not repairable on short notice	Critical	Critical	II	III
4.8	Too dangerous weather conditions to takeoff/fly	Criticial	-	II	-
4.9	Vehicle runs out of hydrogen	Critical	Critical	II	III
5.1	Absence due to illness or obligations	Negligible	-	I	-
5.2	Miscalculation in time management	Marginal	-	II	-
5.3	IT Problems	Critical	Marginal	I	II
5.4	Missing out on specific specialist knowledge	Marginal	-	II	-
5.5	Unavailability of tutors and coaches	Marginal	-	II	-

13.1.2. Risk Mitigation

From Table 13.2, it can be seen that a few risks appear in the top right corner of the risk map. These have a catastrophic impact on the design and a high level of probability. Therefore, these risks should be mitigated as much as possible. The mitigation process of each risk identified in Table 13.3 is described below.

1.1) A lack of hydrogen tank stations has a large impact on the project, as it would make the vehicle impossible to use. It is assumed that hydrogen will be used widely in the future, so the probability of this occurring lowers. Furthermore, a good marketing campaign will convince the general public opinion towards the use of hydrogen.

1.4) The potential of a government ban on the final product after release on the market has a huge impact to the whole project. In order to mitigate this risk, compliance with regulations for both air and ground vehicles is of utmost importance from the beginning of the design process. As the current design meets these requirements, probability of the final design being banned will be very low.

1.5) One of the objectives of this project is to introduce a more sustainable type of transport and with this lowering the emissions all over the world. Global impact of the project is relevant for this. To higher the probability of having a global impact, a marketing campaign should be started, aiming to shift the global public towards the use of hydrogen and other green energy and to introduce them to this vehicle.

1.6) It would be catastrophic if the concept would not be marketable. In the early stages of the project, the chances of this happening are the highest. To mitigate this, market research has been done to decrease the chance of the product not being marketable.

1.8) The whole project would fail if the final chosen design is not feasible. As the different concepts are worked out by now, the chances that they are not feasible have been heavily decreased and will decrease even more in the following design stage. Furthermore, in all trade-offs the feasibility is heavily taken into account, making the outcomes more feasible.

2.1) Calculations are done on the mass of the power system, which resulted in a mass being acceptable with the mass budget. The probability of having a too heavy power system in the detailed design phase will thus decrease.

2.2) The power needed at take-off is calculated for this design phase and the power system is able to produce this. For this reason, the probability of the power system not being able to give enough power for take-off for the detailed design has decreased.

2.4) Dynamic stability is checked for during this phase of design and the requirements on this are met. The chance of the detailed design being dynamically unstable has thus decreased.

2.5) In early stages of design, it is hard to keep the size between certain limits. Having a too large size would be catastrophic for the design phase as the driving capability would then be useless as the car size exceeds the legal size limits to drive on the road. In this design phase, the vehicles is within the size constraints, so the probability of exceeding the constraints in the detailed design has decreased.

2.6) The rotating mechanism of the vehicle is complex to design. This induces a high risk of exceeding size and mass constraints of this subsystem. An increase in size will lead to a design that is not able to drive on the road. Furthermore, an increase in mass has the same effect on its flying capabilities. In order to reduce the likelihood of occurrence, the size and mass should have constantly been iterated and checked throughout the design process until they converge. As the mechanism mass and size in this phase is within the constraints, the chances of exceeding the constraints during the detailed design phase have decreased.

3.1) In early stages of design, it is hard to estimate the material cost for manufacturing the vehicle. To keep track of the material cost and make sure they do not keep increasing heavily, the most important material choices have been made early in the design phase. As the material cost are approximately known, the chance of occurrence of this risk has decreased.

3.5) The risk of not being able to reach certain parts of the vehicle during manufacturing can be decreased by lowering the probability by strictly following the production plan.

4.1) Fire on board is a serious risk, as a non conventional power system is used. Different sources of fire are distinguished. Oxygen together with a significant amount of hydrogen in the air can cause dangerous situations,

because it can catch fire easily with the help of a small spark. There are two ways this mixture could occur within this vehicle. Firstly, the tank/valves can leak hydrogen out into the cabin air. Secondly, the air can go into the tank/valves via a gap. For the first case, this would lead to a too low concentration of hydrogen to cause serious problems. However, the second case can easily cause fire/explosions. For this reason, tank/valve pressure is designed to be higher than the ambient pressure. Furthermore, pressure is measured in the tank and mass flow is measured at the start and end of the valves to be able to handle quickly in case of pressure drop due to a leak somewhere in the system. Next to this, a hydrogen sensor is used to measure the presence of levels of hydrogen in the cabin that are well below the tolerance[2]. When these sensors detect a leak either in the tank or valves, the hydrogen flow to the valves directly stops, as the valves run through the bottom of the cabin possibly leading to dangerous situations. In this case, the vehicle has to glide to a safe spot to have an emergency landing. The tank is behind the three back seats with a firewall in between. The potential fire in the tank is blocked until emergency landing. Furthermore, sensors are placed close to wires, the APU and other electrical systems in combination with small local sprinklers, so a potential fire can directly be extinguished. Furthermore, for significant fires, a fire extinguisher is placed in the cabin.

4.2) The collision with hazardous objects can only be partially mitigated. A flight radar is implemented to monitor air traffic in the surroundings in order to avoid any potential collisions. However, bird strikes are inevitable, as 90% of all bird strikes happen below 1500 m [29], and all of our flight is below this altitude. The severity of occurrence is reduced by implementing a system that is able to deal with an inoperative propeller and that is robust to bird impacts. This is taken into account for material selection.

4.3) Propeller shutdown in flight can lead to dangerous situations. Propellers are connected in parallel and are fail safe, having multiple wires running to the same propeller. Furthermore, both fuel cells can separately power both left and right side propellers. However, in the rare situation that all wires towards one wing fail, the rudder and aileron(s) are able to counteract the occurring moments. In case of fire the vehicle has to glide.

4.4) The rotating mechanism is a non conventional and very fragile part, specific to this vehicle. The mechanism connects the wings with multiple pins to the fuselage in both driving and flying configuration. Having redundant pins, the mechanism can not be moved in flight or in driving configuration unless multiple pins fail simultaneously, for which chances are very low. There also is a risk of the mechanism not rotating when it should. This could occur when one or multiple pins are stuck in place. It is very inconvenient as you can not continue your journey as the vehicle can either not drive or fly. The danger related to this is very low, as you are on the ground when this problem occurs.

4.6) An aircraft can be hit by a lightning strike during operation in the air. This may cause catastrophic damage to the aircraft and thus failure. However, this risk is mitigated by designing a vehicle that is protected against lightning strikes. The wings are made of composites that has a metal strip within. Furthermore, the fuselage has a lightning rod. In this way the likelihood that a lightning strike causes failure is reduced heavily.

4.7) The components that have to be replaced or checked the most have been placed close to a door or in a clear open area. The components that have to be checked less frequently have been placed behind or under these parts. This strategy should be followed for further design, decreasing the risk of not being able to access crucial parts The risk will be decreased by doing this.

4.9) Running out of hydrogen is a serious and special risk related to this design. Liquid hydrogen becomes gaseous quickly compared to for example kerosene, the so called boil off. Tanks are designed such that the temperature does increase only a few Kelvin over the mission time, having negligible boil off. However, when you leave your vehicle in your garage for a week, all hydrogen have changed to gas and you will not be able to drive to the tank station anymore. For this reason, the APU is designed to have enough energy to drive towards the closest hydrogen tank station. However, this is still very inconvenient and expensive. A solution to this problem will have to be found in the future, which is out of the scope of this project.

5.3) IT issues are a potential risk for all design phases of the vehicle and can cause delays and difficulties in the work-flow. However, this risk can be mitigated by simply taking into account the possible problems and formulate a contingency plan in case of one of the problems occur. For example in case of Wi-fi disconnection a different work location should be booked in order to continue working. Furthermore, a group member is put on IT problems and this is advised for further design phases as well.

[2] `https://www.fuelcellstore.com/senseh2-hydrogen-sensor` [cited 22 June 2019]

13.1.3. Posterior Risk Map

The risks that were identified in the top right corner in Table 13.2 are mitigated using the approach mentioned in subsection 13.1.2. This mitigation helps to reduce the the severity and the level of probability. After implementing the mitigation strategies, a posterior risk map make can be generated and is shown in Table 13.4. In this posterior risk map no risks are in the top right corner and of all identified risks, only risks acceptable to take are left.

Table 13.4: Technical posterior risk map

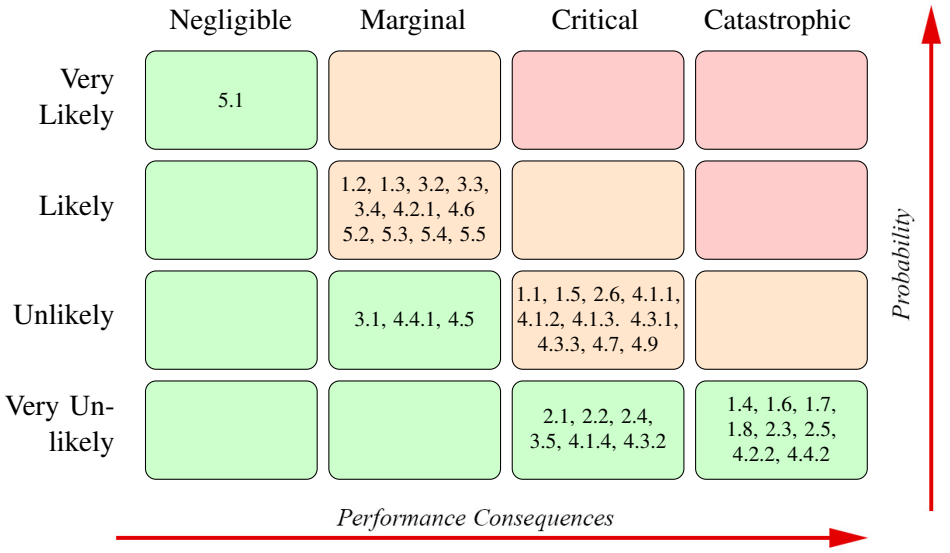

13.2. R.A.M.S.

Once the design is finalised, it is important to estimate the performance in terms of Reliability, Availability, Maintainability and Safety (R.A.M.S.) of the design, which is done in subsection 13.2.1 to 13.2.4. With this, the focus should be put on the systems that are special to this design, the unconventional systems. For the conventional systems these performance characteristics can be assumed to be similar to the ones of these systems in other aircraft's and cars.

13.2.1. Reliability

Reliability is the ability of the vehicle to perform its specific functions. This will be discussed for the unconventional systems below.

Hydrogen Tank

The hydrogen tank is an important subsystem as failure of this would lead to an emergency landing or even a crash. Liquid hydrogen tanks have been used in the car industry, but not the aircraft industry [68]. This low TRL decreases the reliability of the vehicle.

Fuel Cells

As one fuel cell is not enough to continue flying in cruise conditions, single fuel cell failure would force the vehicle to glide to an airfield, with propellers still giving some thrust. The fuel cell that is still working, powers both wings propellers equally, but not giving enough to maintain cruise. Not being able to continue reduces its reliability. Furthermore, there are not many aircraft's or cars using fuel cells. This low TRL also decreases the reliability of the vehicle.

Rotating Mechanism

Failure of the rotating mechanism can happen in two ways: the mechanism undesirable rotates in flight due to multiple pin failure, or the mechanism is stuck in place when transformation is required. Both failures lead to the system not fulfilling its functions. As rotating mechanisms are not widely used, and the companies that use it are not sharing their findings, the TRL is very low. For this reason, the probability of failure has increased, decreasing the reliability.

Distributed Propulsion
Distributed propulsion is not widely used in the aircraft industry, so the TRL is relatively low. However, the propellers are connected in parallel, so failure would mean only one propeller stops working. This would not be dramatic, as control surfaces are designed for total shutdown of propellers on one side of the wings and can thus easily compensate for it. Having a single failed HLP would still make it possible to fulfil its function and have a repair directly after. CP failure would result in a forced landing, decreasing reliability.

13.2.2. Availability
The availability describes the portion of the time the vehicle is actually available for use. Taken into account are the scheduled maintenance and checks, refuelling and repairs

Maintenance & Checks
Scheduled maintenance and checks will lead to a significant portion of the unavailability of the vehicle. The time it takes and how frequent the checks occur is stated in subsection 13.2.3.

Refuelling
Refuelling has to be taken into account, as the vehicle can not be used in this time. Refuelling this vehicle will surely take less than 10 minutes, according to research [69]. This will have influence on availability to travel long distances, because it requires a waiting time of 5-10 minutes every 250 km flying. However, the vehicle is meant to be used mostly to travel medium range distances, intercity. Furthermore, it is assumed that the vehicle can be refuelled at or close to these stops.

Starting Fuel Cells
The fuel cells need time to heat up and have a high enough pressure to have optimum performance. Without a compressor, the air and hydrogen will start to react, slowly increasing to the desired level in six minutes. However, since the vehicle has a compressor that runs on APU energy, it reduces the fuel cell starting time to one minute [33].

Repairs
Repairs will only occur when a part of the vehicle is malfunctioning in any way. Doing strict maintenance checks regularly decreases the chances of this happening. The repairing time is very hard to estimate in this design phase.

13.2.3. Maintainability
Maintainability is the ability to be maintained easily without spending a lot of time. Again, for the conventional components it is assumed that the results are similar to the ones for conventional aircraft. Furthermore, the unconventional systems are explained and indicate which maintenance checks are required.

Maintenance Checks
The aircraft maintenance checks are required for each subsystem and can be categorised into four groups: A, B C and D. Maintenance check A is performed every 200-300 flight cycle and requires approximately 50-70 man hours to perform the maintenance check. Maintenance check B is performed every 6-8 months and takes about 1-3 days to complete. Maintenance check C is more extensive compared to check B and is performed every 20-24 months. Inspection will be done for the majority of the components and takes 1-2 weeks to complete. The last maintenance is check D, which is the most extensive one and is performed every 6-10 years. During the maintenance the whole aircraft is taken apart to perform detailed inspections and requires 2 months to complete depending on the number of technicians. Furthermore, whenever there is damage to the aircraft direct maintenance should take place after operation, check O.

Hydrogen Tank
The hydrogen tank is a critical system since it is used as storage for the fuel. A leaking hydrogen tank can lead to dangerous situations in flight and on ground, since hydrogen is explosive. It is important to perform maintenance checks on a regular basis in order to ensure that the hydrogen tank is able to carry the fuel without problems. Therefore, it is chosen for the hydrogen tank to perform a maintenance check A next to the mandatory check D.

Fuel Cells
The fuel cell is used to convert chemical energy directly into electrical energy. This energy is required to power the vehicle. It is important that the fuel cell is working properly otherwise the vehicle can not be used. Maintenance checks should be performed on a regular basis and therefore check A is chosen next to the mandatory check D.

Rotating Mechanism
As the rotating mechanism is a safety critical system, it should be checked regularly. The rotating mechanism failing in flight would lead to a crash. Even though the mechanism is designed to be redundant, the connection pins have to be checked often and have to be replaced if failure of one of them has occurred. So, the rotating mechanism needs to have an A check next to the mandatory D check for all subsystems.

Distributed Propulsion
The distributed propellers are connected in parallel such that they are redundant. The aircraft is designed to be able to do an emergency landing with all propellers on one side of the wings shut down. With one of the CPs failing, the vehicle should also make an emergency landing. However, with single HLPr failure, the vehicle would still be able to fulfil its mission. This makes the distributed propulsion subsystem a little less critical than the others. Thus, the distributed propulsion system needs a B check next to the mandatory D check for all subsystems.

Table 13.5: Maintenance checks per (sub)system

(Sub)system	Check
Hydrogen tank	A, D, O
Fuel cells	A, D, O
Rotating mechanism	A, D, O
Distributed propulsion	B, D, O

13.2.4. Safety
Safety is about not harming users or the environment during the full life cycle. The safety for the conventional systems is assumed to be similar to the safety of these parts in conventional aircraft's. The safety of the unconventional systems is discussed below.

Hydrogen Tank
The hydrogen tank has many safety concerns. Leakages can lead to serious problems such as an emergency landing or even a crash, as already discussed in subsection 13.1.2. This makes the system a safety critical system. Possible fires could start, for which measures are taken: a firewall is put between the tank and the passenger seats, sprinklers are installed and a fire extinguishers is located in the cabin. Furthermore, appropriate sensors are installed to ensure the probability of fire in the cabin decreases. When sensors detect a leak, all valves are closed such that no hydrogen runs through the valves in the cabin. Proper maintenance checks will further decrease the risk.

Fuel Cell
The fuel cells are a dangerous part of the vehicle, as the combustion takes place here. The fuel cells are already existing and used widely and tested, so the chances of failing are low. Furthermore, if failure occurs, the hydrogen and air flow towards the fuel cell can be directly blocked to decrease the severity.

Rotating Mechanism
The rotating mechanism is a fragile part of the vehicle. As already explained, failure could happen due to undesired movement in flight or the mechanism being stuck in place when moving is required. The second failure mode does not lead to safety concerns. However, the first failure mode in flight directly leads into a crash, so the system is a safety critical system. There should be no way the wings can rotate without being on the ground and with permission. For this reason, multiple redundant connectors are used. Furthermore, higher safety factors than usual have been used, as the TRL is low.

Distributed Propulsion

As the propellers are connected in parallel, chances are low that more than one propeller fails at the same time. Even though there is one propeller less in this case, it does not influence the safety of the passengers or the environment and the aircraft is able to still fulfil its mission. Furthermore, the control surfaces are designed for propeller shutdown of one side of the wing. In the occurrence of propeller shutdown of one side of the wing, still no harm is done to the passengers. However, the vehicle must glide towards the nearest location to have an emergency landing, possibly damaging its surroundings.

Skin

Another note should be made: the skin is made from composites. As composites are non conducting materials, it can invoke dangerous situations in case of lightning strikes, since it would give rise to high temperatures. For this reason, metals are used to protect the vehicle from reaching too high temperatures in case of lightning. Metal conducts electricity and the lightning can easily escape again.

14

Operations and Logistics

Since the HAVIC is neither a standard aircraft, nor a standard car, non-standard procedures will have to be followed for operation. Three modes of operation will be considered, driving operations in section 14.1, ground operations in section 14.2 and flight operations in section 14.3. Furthermore the logistics will be discussed in section 14.4.

14.1. Driving Operations

The driving operations consist of two parts, namely the standard car procedures and the specialised procedures. Standard car procedures include loading of the payload and pre-driving checks such as checking lights, mirrors, tyre pressure and fastening seat belts. Non-standard procedures are related to the specific subsystems and mechanisms such as the fuel cell and the wings.

Before driving is initiated, all driving electrical systems are activated. A check on the wings needs to performed. The wings should be retracted and fastened to the empennage. The engines need to be turned off and the propellers must be stationary.

Since boil-off is an unavoidable consequence in LH2 systems, the tank's LH2 level needs to be checked. All pressure and temperature sensors are then checked to ensure no leaks are present. In case fuel levels are sufficient, the fuel cells are initiated. The fuel cells perform optimally at 85° and it is preferred to bring the fuel cells up to operating temperature before driving, during the first minute of driving the fuel cells should heat up adequately.

Refuelling LH2 is done in comparable fashion to refuelling gasoline. Refuelling times should be comparable, however, specialised refuelling stations are needed. LH2 is stored at 20 K and should therefore be professionally handled to prevent spillage and cold burns. In case fuel levels are not sufficient for driving to the nearest refuelling location, the vehicle needs to be initiated by using the APU and regular refuelling procedures can follow. Recharging the APU can be done in similar fashion as recharging an electric car.

To cease driving operations the vehicle should come to a halt and standard car procedures should be followed. The fuel cells are then turned off by closing the hydrogen supply. A check on the tank's LH2 level should be performed to ensure there is enough fuel for the next trip. After the fuel cells are turned off, standard car procedures can be followed again.

14.2. Ground Operations

Ground operations include all procedures starting from arrival at the airport up to and including pre-flight checks, vacating of the runway and including leaving the airport. Upon arrival at the airport, a flight plan should already have been submitted at least six hours before the flight. Passengers and payload are loaded at the parking position if they are not already present in the vehicle and refuelling should be performed before taxiing to the runway. The wing mechanism should be initiated and a wing and empennage inspection should be performed, Propellers are also checked for damage. Electrical flight systems should be activated before taxiing to the runway. Once arrived at the runway, just like during driving operations, tank and fuel cell checks

should be performed to ensure the fuel cells are at operating temperature and enough fuel is available for the mission. Power can then be directed to the propulsion engines, a check is performed to see whether the engines are operational. Just before flight the brakes can be released and flight operations can follow.

Post-flight operations start after vacating the runway. A taxi manoeuvre to the parking position is performed and the vehicle is put to a halt. The brakes are applied once arrived at the parking position. The fuel cells can be turned off if the mission is terminated, but can be left running if further driving operations are required the power is then directed to the drive train. A check is performed on the engines and propellers to ensure they are idle, then the wing mechanism can be activated. Once the wing is retracted, it needs to be fastened to the empennage. If the mission is terminated, all electrical systems can be turned off and passenger unloading can begin. If the mission is continued by road, driving operations can be performed.

14.3. Flight Operations

Flight operations include all manoeuvres described in the mission profile described in Figure 6.1. Before take-off is performed, the go/no-go velocity should be reached with enough runway left, else take-off should be terminated. Climbing to cruise altitude can be performed in two ways, fastest RC or largest climb angle. Fastest RC is preferred for passenger comfort and least time to reach cruise altitude. In kerosene powered aircraft the fuel fraction is substantially higher than in hydrogen powered aircraft, therefore usually a step climb is performed during cruise to ensure optimal flying conditions. For hydrogen powered aircraft this fuel fraction is much lower and as such a step climb is less effective. During descent, the HLPs are turned on and the CPs are set to a lower thrust. The flaps are activated to ensure enough lift is still created. During landing the flaps are fully extended and the engines are set to the lowest thrust setting possible. After a successful landing the vehicle is brought to taxiing velocity and ground operations can continue.

14.4. Logistics

Logistics of the HAVIC concern the infrastructure for Operations and production of hydrogen and will be discussed in the following sections.

Infrastructure for Operations

Infrastructure for operations already exists in the form of airports and roadways, however, if aircraft/car hybrids become widely used, more suitable runways will have to be built to increase the flexibility of these vehicles. These runways should be well connected to the roadways to decrease travel times, again increasing flexibility. Also, with the increase in demand for hydrogen vehicles, refuelling stations will have to be deployed as this is a significant market barrier to the successful introduction of fuel cell electric vehicles. A study [70] was done by M. Melaina and M. Penev comparing cost estimates for hydrogen refuelling stations. For larger stations $3370/kg/day, including development, construction and operation was estimated, resulting in a station cost of $5.05 M for a capacity of 1500 kg/day. A layout of the refuelling station is seen in Figure 14.1 [71].

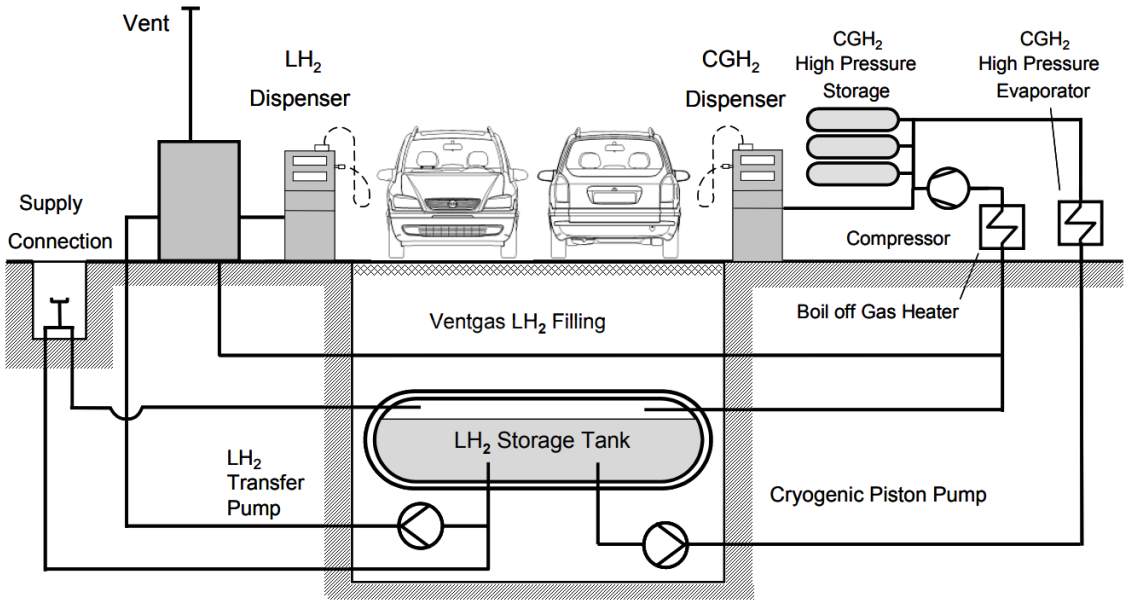

Figure 14.1: Layout of the hydrogen refuelling station [71]

Hydrogen Production

Instead of directly forming liquid hydrogen, gaseous hydrogen is formed and then liquefied. Hydrogen can be formed through multiple processes, the main form of production being steam reforming where hydrocarbons are split into hydrogen gas and CO_2. However, this production method does not conform to the sustainability requirements of the Door2Door project and therefore can't be used. Electrolysis is a method of producing hydrogen and oxygen as byproduct through direct decomposition of water by electric energy. This method produces very pure hydrogen and can be made green if the supplied electric energy is also produced in a sustainable fashion.

Liquefaction of hydrogen is done in two ways, via the helium Brayton cycle and the hydrogen Claude cycle. The helium Brayton cycle is more suitable for small production sites due to its less expensive and complex compressor system. This makes it usable for on-site production of hydrogen where fuel production requirements are lower and less economic investment is preferred, similar to the gas stations we have today. Local production also reduces the environmental impact of hydrogen transport. The hydrogen Claude cycle lends itself more to larger centralised production sites where production requirements are higher, since production efficiency is higher. In the future, where hydrogen powered vehicles will take a larger market share, more of these sites will have to be built to supply the growing liquid hydrogen demand for aviation and other industries. It is advisable to transport hydrogen in liquid form to overcome the inherent limitations of uneconomic road transport.

15

Long Term Vision

To fulfil the whole design of the vehicle before applying it to the market, different phases should be accomplished. Within those phases, tasks are identified and will be carried out in a real-world process. In section 15.1 the development after the DSE will be elaborated with a flow diagram and Gantt-chart. Followed up with the production plan in section 15.2 where a chronological overview is given of the manufacturing and assembly activities. The last section lists future technologies that can be used for an improved model of the HAVIC.

15.1. Post DSE Approach

A design process can be divided in three-stages, consisting of the conceptual design phase, the preliminary design phase an the detailed design phase. These stages have their own time frame and need a different group of engineers to accomplish the stage. After the design stages the vehicle should be certified and adhere to all the regulations before it can be sold to the market. All the subsequent phases are displayed in Figure 15.1.
This report and design process cover the conceptual design phase. The following stages will be performed after the DSE and will be explained in this section.

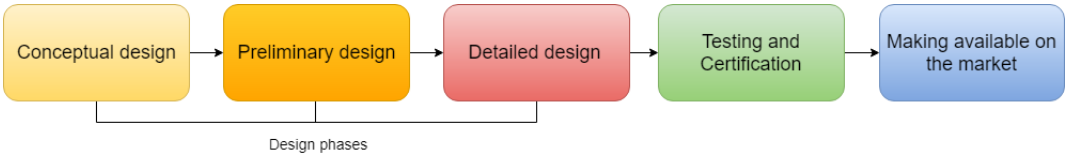

Figure 15.1: Development stages of the HAVIC

Conceptual Design

The conceptual design is the beginning of the design process with rough sketches of the HAVIC configuration. The requirements are taken into account while designing the subsystems including structures, aerodynamics, propulsion, power system, materials and control systems. Fundamental aspects such as fuselage shape, wing configuration and location, engine size and type are all determined with use of basic equations and assumptions. The final product of this stage is a conceptual layout of the vehicle configuration found in this report. Because of the limited time, the conceptual design phase should be extended to increase the confidence level and include the future technologies elaborated in section 15.3.

Preliminary Design

The second stage includes the preliminary design where the chosen concept will be developed and improved. The product shall fit all the imposed parameters of the regulations. In this stage the control stability analysis, structural analysis and the detailed hydrogen fuel cell analysis are the main focus points.
After this, wind tunnel tests and fluid dynamic calculations will be performed to find flaws in the design, resulting in a correction of the design problems. When all changes are made an updated technical drawing will be made. With this drawing and finalisation of the design an discussion can be started with the designer and client about going ahead with the production of the HAVIC. This choice will be based on the economical feasibility.

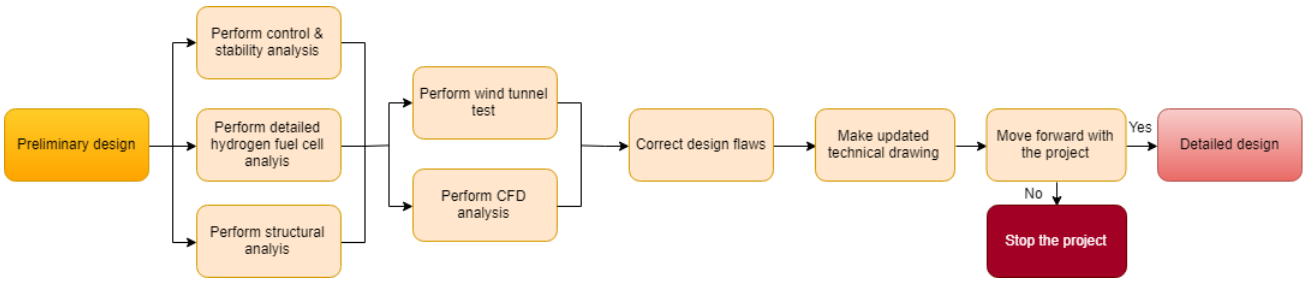

Figure 15.2: Preliminary design phase of the HAVIC

Detail Design Phase

The final phase of the design process will use the longest time frame as every part of the HAVIC will be designed in the smallest detail possible. Besides the subsystems this phase includes the fabrication aspect of the vehicle and the manufacturing method. The tools and jigs will be selected and when necessary designed for the assembly of the vehicle. All the numbers of the ribs, spars, sections and other structural elements are determined and placed.

In parallel with this, a flight simulator will be developed. When the final design is finished the test can be performed with the prototype. However, it is likely that first testing procedures would already begin before having the finalised design, for instance in a smaller technology demonstrator aircraft. Because the HAVIC will fly with use of hydrogen, the testing period and detailed design phase can take longer than for a conventional aircraft that has a time frame of a minimum of 5 years. For this reason a time frame of 7 years is chosen.

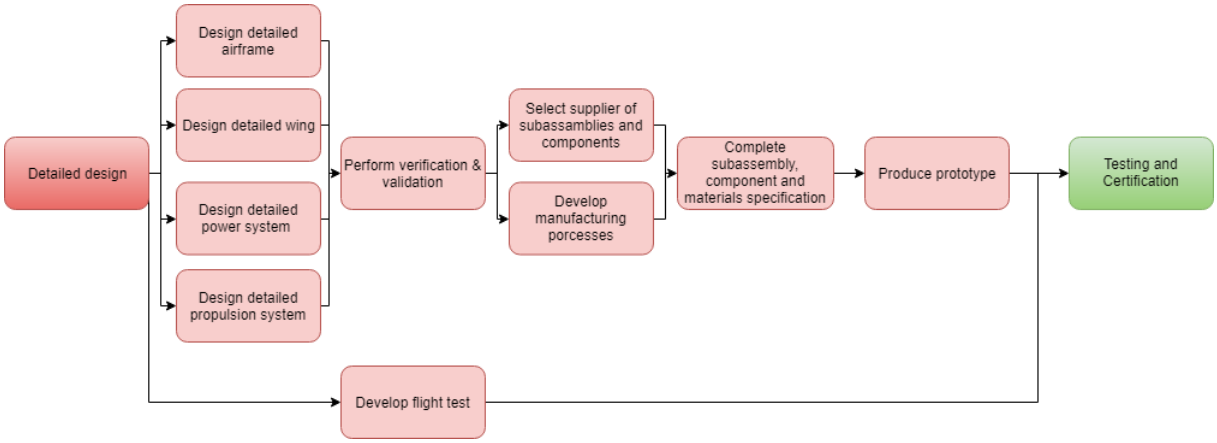

Figure 15.3: Detailed design phase of the HAVIC

Testing and Certification

After designing the vehicle, certification is necessary to meet all the requirements on regulations and to have an approved vehicle to make available on the market. As the HAVIC should be capable of driving on the road and flying in the air, the certification process should be done twice. This will be performed parallel with various prototypes. Multiple prototypes are required to perform different functions simultaneously to save time. All configurations will be tested to take the critical situations into account; take-off, cruise, landing and driving.

The certifications of the aircraft configuration are set up by EASA[1] and include 4 steps. First the EASA certification team will do a research on the HAVIC and set up a list of rules. When the manufacturer agrees with all the requirements, the compliance demonstration can start. This will be the longest period to complete. The HAVIC needs to demonstrate the compliance of all the requirements of all the subsystems. This analysis will be done on the ground and during flight. When the EASA is satisfied with the results, the investigation is closed and a certificate will be issued. For the car configuration this is more basic as a certification and confirmability test will be done. After those separate paths, the production assembly line and the fuel and emissions will be tested. A conventional aircraft uses 9 months for this certification phase. As the HAVIC is a

[1] `https://www.easa.europa.eu/easa-and-you/aircraft-products/aircraft-certification` [cited 18 June 2019]

very new concept that can fly and drive, the time frame will be extended. Thereby, more time is needed for the testing of the hydrogen power system as this is a new technology in this field, a defect would be catastrophic.

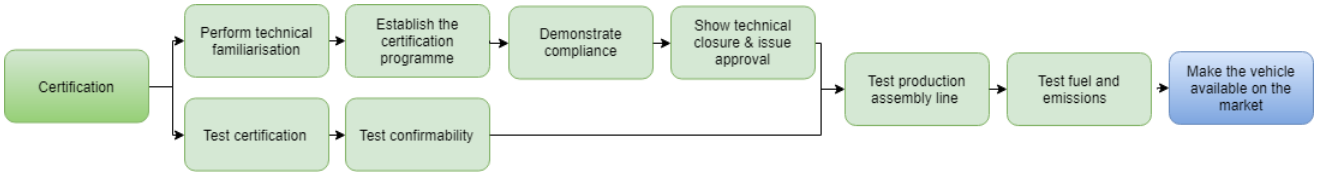

Figure 15.4: Certification phase of the HAVIC

15.1.1. Gantt Chart

In the previous section the design- and after DSE phases are determined. A time frame for these stages is determined and is displayed in Figure 15.5.

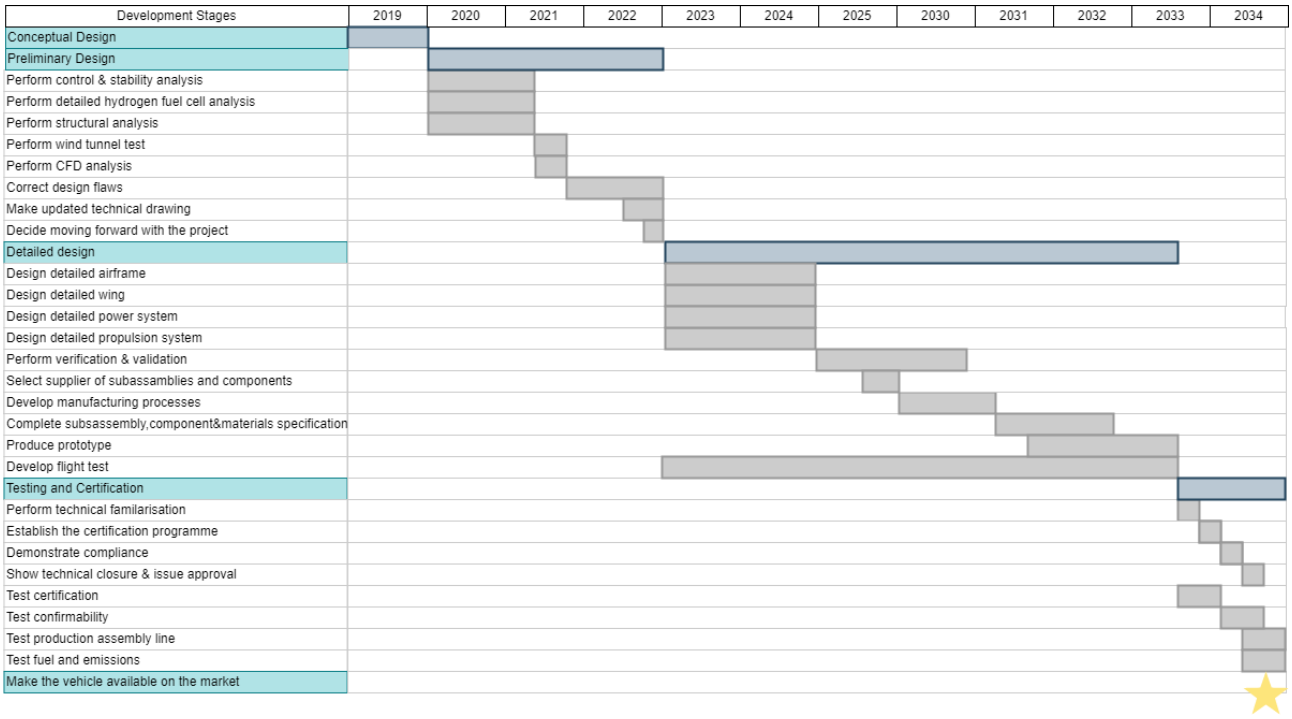

Figure 15.5: Gantt Chart development stages

15.2. Production Plan

The production plan is an overview of the manufacturing and assembly activities of the HAVIC. The aim of the Door2Door project is to have an assembly time of 6 months from the final design. Production rates for aircraft can differ quite a bit, the B737 & A320 series produce about 40-60 aircraft per month, while the B747 & A380 only produce about 30-50 a year [72]. Compare this to Tesla's Model 3 production rate, which is 1000 cars a day.[2] The manufacturing plan of the main individual components will be discussed in subsection 15.2.1. The assembly of the different parts will be elaborated in Table 15.2.1.

15.2.1. Manufacturing

The manufacturing of the main components is dependent on material features such as the weldability and machinability and on product features such as shape and size. Sometimes materials can be pre-treated to increase their manufacturability. Composites and metals cannot always be manufactured using the same processes. Generally speaking the manufacturing of composites is more expensive, however the operational and maintenance costs may be lower [73].

[2] `https://www.cnbc.com/2018/11/30/tesla-reportedly-achieves-model-3-production-rate-of-1000-a-day.html` [cited 18 June 2019]

LH2 Tank

The manufacturing is complicated due to the fact that composites are used and the tank is spherical, which is a double curved shape. Manufacturing will be separate for the liner, structural and insulation wall. First, for the production of a spherical liner tank it is suggested to use rotational moulding [36]. This process allows for the production of one-piece hollow parts with uniform thickness, this is beneficial as a welding line or knitline might lead to an unequal stress distribution. A negative metallic mould of the sphere is produced. The resin is put into the mould in powder form. The mould is heated and spinned causing the resin to disperse over the mould and adhere to the walls. A schematic overview of the process is shown in Figure 15.6. The holes for the piping may be included in this mould or drilled after moulding.

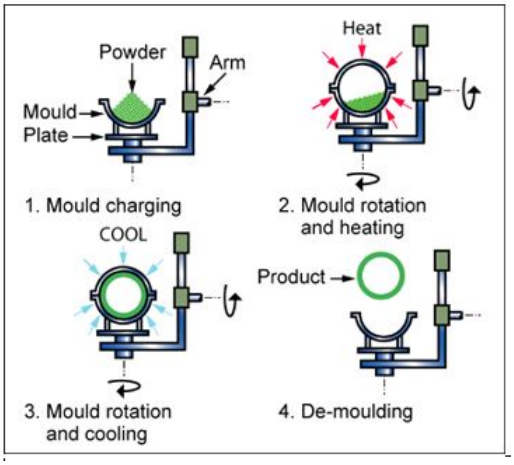

Figure 15.6: A schematic overview of rotational moulding [5]

The liner material can then serve as a positive mould for the composite over wrapping process. The liner might be supported through the pipe holes. The composite overwrapping might be done using Automated Tape/Tow Placement (ATP). Automation allows for precision, which is favourable for the quasi-isotropic lay-up that is desired. Because of the spherical shape the pressure distribution will be equal throughout the whole tank and the material and manufacturing flaws should be kept to a minimum. The epoxy will not only act as a resin for the carbon fibres, but also as an adhesive between the liner and the structural wall. The tank might is cured using an autoclave with a temperature of 115-180 °C at 6-7 bar [5]. During this process the hollow inside may be reinforced to prevent thermal stresses from damaging the liner.

The final insulation layer is the final wall of the tank. This layer is currently selected from a commercially available model, so they are readily available. This layer may be added during the production of the tank or at a later stage. The insulation layer does not need to be bonded to the tank, but the insulation layer should be sufficient all around.

An important note is that the joining of the liner of the tank with that of the pipes should be water and air tight. The pipes that lead the hydrogen into the tank should also be manufactured in such a way that boil-off is limited. They require less insulation materials as the hydrogen will only be contained in the pipes for limited time. If they use the same materials as the tank itself, they are manufactured in a similar manner. If the structural material is changed to a metal, there are other cheaper, easier processes to form them, however, they have their own disadvantages such as extra weight.

Skin Panels

The skin panels are made out of sheets of epoxy/HS carbon fibre composite. An important factor to take into account is that the sheets should be formable into double curved surfaces with large and small bend radii. For metals it is possible to use the principle of bending for the formation of such surfaces, but composites behave differently when in bending. A possible process to form these skin panels is through Resin Transfer Moulding (RTM). RTM is a process that allows for both low and high performance parts which is still relatively cheap compared to other processes as can be seen in Table 15.1 [74].

Table 15.1: The costs of RTM compared to other composite processes adapted from the TU Delft Production of Aerospace Systems

Cost component	Relative to other processes
Machinery	Low
Moulding	Low to moderate
Labour	Moderate
Raw material	High

The reinforcement is placed in the mould and subsequently the resin in injected. It has the advantage that the carbon can be placed in exactly the right orientation before resin is allowed to flow in. Usually the polymer

is pressurised to ensure the flow. For RTM is is important to ensure that all areas are sufficiently infused with resin to prevent dry spots. To prevent the part from sticking to the mould, a release agent should be be applied in advance. To reduce porosity a variant called vacuum assisted resin transfer moulding can be used [75].

Wing
The wing consists out of five main part to be produced, the leading edge, the wing box, the trailing edge, the control surfaces and finally the ribs.

With the help of lay up technique and moulds designed specifically for the HAVIC, sandwich panels can be constructed that will have the required specifications. These panels will be attached at the next stage to form the spars, top and bottom of the wing box. In the other parts, except for the ribs, no honeycomb core is being used. These parts will have to be attached to the main wing box structure. To remain the accessibility at the electric motors, the LE will be riveted after the electric motors are fastened to the front spar of the main wing box. This fastening of the electric motor will use a metallic inserts for the composite. In these metallic inserts, the bolts for fastening the electric motors can be threaded. The holes that will occur shall be analysed in a more detailed way in the further development. The holes can be part of the integral design when applying these inserts [76, 77].

At the TE side, the flaps and ailerons should be fastened via hinges. These are operative during flight. The hinges will have to be attached to the main wing box structure to support these control surfaces. The location of the ribs is not yet defined, but these should go near the electric motor positions. Along these locations there will be have to be openings for the power and hydraulic cables, so some reinforcement will be on its place. In further development this should be elaborated upon.

Frame
For the manufacturing of the frame first the individual rods will be produced. Titanium has several forming options, one of them being rolling. Rolling is a process that can form uniform shapes with simple cross sections. In a further design stage when the frame might have varying thicknesses or shapes a different process such as casting might be a better fit. Rammed graphite casting is a process that can be applied on large titanium castings such as the space-frame [5]. This will also maybe allow the frame to be produced in one integral part, as this would eliminate weak spots due to joining operations.

To create an almost integral strong part welding is chosen as the joining process rather than adhesives or mechanical fasteners. The disadvantage of welding is that there is an affected area in which the material properties are decreased. This area can be minimised by for example using laser beam welding or electron beam welding, as the area actually affect by the beam is small. Both these processes are already used in the aerospace and automotive industry [5]. One difference will be that titanium welding should take place in an Argos gas environment as oxygen will affect the titanium welds.[3]

Assembly
An essential part of assembly is the joining of the different elements into sub-assemblies and the sub-assemblies into the final assembly. There are two types of divisions: mounting divisions and production divisions. Mounting divisions are required by the function of the aircraft (moving parts), such as the door or control surfaces. Production divisions are done for ease of manufacturing or structural reasons. The advantages of joining are that they allow for moving parts and can provide structural security such as the prevention of the propagation of a crack. Also it may ease the maintainability significantly as it may allow for easier access to a part for repairing operations or the replacement of a part. One of the disadvantages of joining is that is adds weight. This is caused by the fact that you add extra material such as rivets and bolts and that the material needs to be thicker is areas with a joint. The latter is because a joint introduces a structural weak spot, because of for example the deterioration of material properties due to thermal effects.

The joining of composites remains a difficult process as they are not suited for welding. Some types of mechanical fasteners can be used. Solid rivets, however, can not be used in combination with laminate composites as they will cause the material to delaminate. Another alternative is the use of adhesives. The disadvantages are that an adhesive bond requires extensive pre-treatment and is very weak when a peel force is applied. This type of joining is also not suitable for the joining of plates/sheets, for which bolts, hi-loks or inserts can be

[3] `https://www.dynamicfab.com/titanium-welding-argon/` [cited 20 June 2019]

used [78]. There are already (threaded) inserts commercially available. They provide different types of inserts, such as bonded, bonded mechanical or non metallic, all with their own specific application [79]. A hi-lok is a titanium fastener. For a proper load transfer the fit between the whole and fastener should be of high quality. As hi-loks can be pre-loaded the fatigue life of the joint can be improved.[4]

Similar to aircraft assembly the assembly system of the HAVIC is a line production, meaning that the sub-assemblies will be worked on at workstations. The general assembly plan can be seen in Figure 15.7. The arrows in this diagram represent joining operations. For now the plan only specifies the major components and sub-assemblies, in a further design stage the assembly plan can include more elements and sub-assemblies.

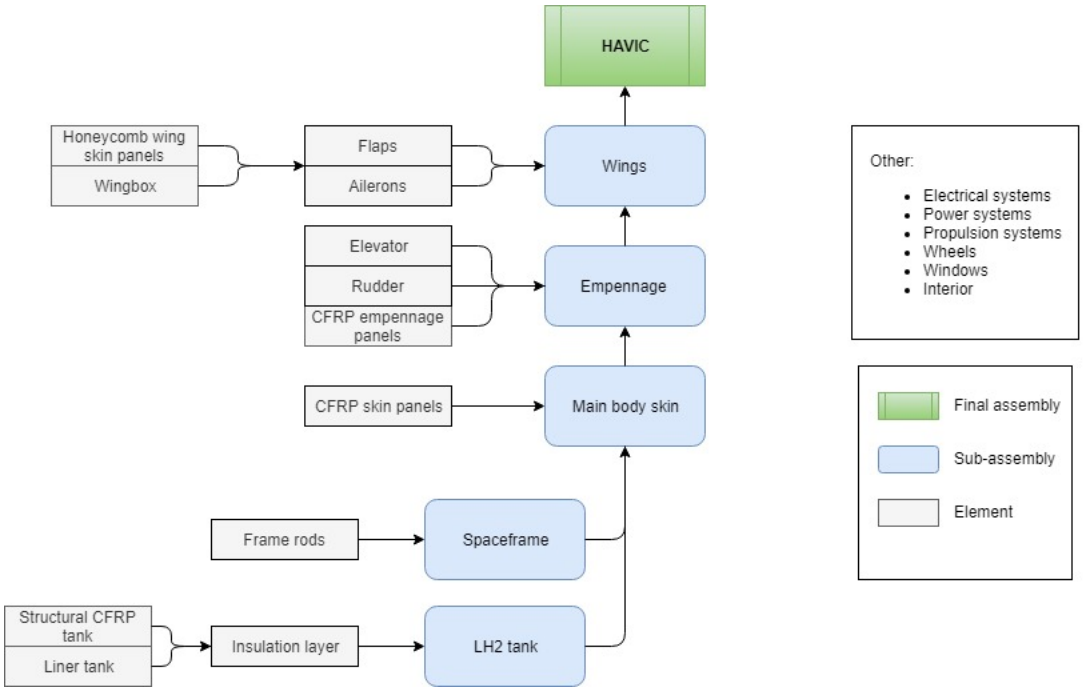

Figure 15.7: General overview assembly plan

15.3. Future Technologies

In the extended conceptual design phase more technologies can be explored and in further development improved systems can be used. These technologies are given in this section.

Solar Panels

It might be possible to charge the Li APU through solar power, both during the vehicle's operation (to extend battery life) and when idle (to cut down on power required from the grid). If the solar cells can be made light enough, this might be a practical and sustainable way to charge the HAVIC's APU. This possibility is explored further here. Research has been done into various solar cells, where the solar mono-crystalline silicon cell was deemed favourable for its lightness, flexibility and efficiency. The specific values of this type are displayed in Table 15.2. Furthermore, the wing including the solars cells is displayed in Figure 15.8

Table 15.2: Monocrystalline silicon cells values [80]

Efficiency	22.7 %
Weight density for solar cells	0.18 kg/m^2
Weight density for interconnected matrix	0.24 kg/m^2
Power density	175 W/m^2

[4] https://jet-tek.com/product-specialties/hi-lok-fasteners-hi-lok/ [cited 18 June 2019]

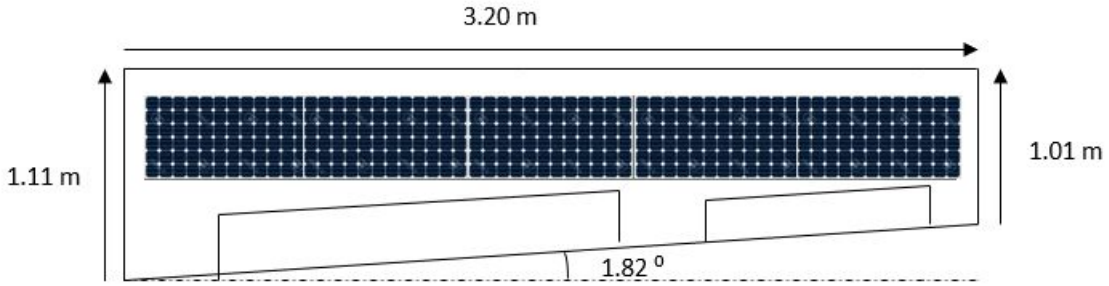

Figure 15.8: Wing platform with solar panels

The solar panels can be applied on the wings where a clean surface of 3.456 m^2 is available. This area is limited as the flaps, ailerons and nacelles are included in the wing. There could be a possibility to add more solar panels on the top of the main body, but this will be for further development as the wings are folded back in driving configuration.

With this area, specific power density and efficiency, an effective power value of 604.8 W is found. This is very low in comparison with the needed power during cruise which is around 175 kW. For this reason the power generated will not be feasible to use for the propulsion. From an energy point of view, it might still be beneficial to implement solar cells. At the moment a battery of 10 kWh is included in the vehicle, which will require to be plugged in and charged from the grid. Instead of fully charging using grid power, it could be recharged with the use of solar panels.

In the next design phase this option should be explored extensively as advantages are applicable. The solar panels should be foldable and thin so the aerodynamic shape will be followed.

Hydrogen Technologies

With the world's growing awareness regarding the environmental impact of fossil fuels, energy alternatives are extensively being researched, hydrogen being one of the promising solutions. As of now, more than 95% of hydrogen is won by steam reformation, a method which is not emission free, as hydrocarbons are split into hydrogen and CO_2. To see a fully emission free hydrogen vehicle, the hydrogen production also needs to be emission free. One way hydrogen production can be truly emission free is by electrolysis powered via solar/water/wind energy. The production costs of hydrogen via electrolysis are still expensive, cost savings can be made by reducing plant costs through technological developments.

Two new methods of low/zero emission hydrogen production are photobiological and photoelectrochemical approaches. The first approach uses sunlight and algae to split water atoms into hydrogen and oxygen. The second approach uses semiconductor materials and sunlight to split the water atoms. Both approaches are suitable for local on-sight hydrogen production and might allow use of wastewater instead of pure water.[5] [6]

Since hydrogen fuel cell systems are likely to take a greater marketshare in the future, more research and development will be done regarding these systems. One way of making hydrogen powered aircraft more feasible is by reducing the weight of the fuel cell and tank system. Since most fuel cells systems are not yet specifically being designed for aviation purposes, more research and development will undoubtedly make these systems much lighter and much more suitable for aviation use.

[5] https://www.energy.gov/eere/fuelcells/hydrogen-production-photobiological [cited 20 June 2019]

[6] https://www.energy.gov/eere/fuelcells/hydrogen-production%2Dphotoelectrochemical-water-splitting [cited 20 June 2019]

Composite Technologies

One of the first aerospace application of composites was roughly 45 years ago. They started out with replacing aluminium and titanium components with boron/epoxy composites [81]. In case of the U.S. F15 fighter plane, which was introduced in the 70's, only 2% of its weight was made out of composites. Throughout the years, with ever improving knowledge, this percentage has steadily risen. Currently, there are the B787 and A350 XWB with half their weight made up of composites. Figure 15.9 shows the increased use of composites by Airbus[7], a similar increase can be seen in automotive industry.

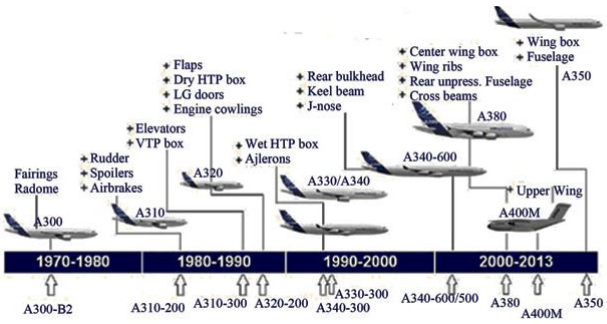

Figure 15.9: The use of composite materials by Airbus

Currently, there is a lot of research being done into the further application of composites in the aerospace industry. Not only are researchers looking for new better materials, but also into the manufacturing methods. There are still some safety concerns surrounding the use of composites, for example the Boeing 787 composite fuselage was called unsafe by one of its former employees.[8] Boeing instated a special programme to perform specialised maintenance and repairs on the Boeing 787.[9] By improving the knowledge of composites and training specialised personnel the safety should not be an obstacle in the advancement of composites in aerospace. For the HAVIC this could possibly mean that further mass reductions might be possible because of the replacement of titanium with a lighter composite for the space-frame for example. Another development will be that the cost of the manufacturing of composites may reduce significantly.

Automation

Possible room for development can be found in the automation of transportation. Automation can range from instruments assisting in flight or drive to completely autonomous cars and drones. NASA is already working on a set of Autonomous Flight Rules (AFR) [82] which will co-exist with IFR and VFR. This technology is quickly developing and more tests show that is possible to have an autonomous vehicle. This technology, however, may be held back by a human factor. Studies show that not everybody is willing to fly on a pilot-less aircraft. Suggestions to reduce this unwillingness are to educate people about automation and to first build up a great safety record with for example cargo aircraft.[10] Another important question is if people would require a license for an autonomous vehicle. Currently, you are still required to have a license even if the vehicle is autonomous, it is expected that this will still remain as such for some time. For the HAVIC it would mean that a pilot's and driver's license is required. These licenses might not be obtainable for everybody. As a middle ground an adapted license could be suggested for the HAVIC, which would have less strict requirements than a normal pilot's license.

Propulsion Technologies

The propulsion of the HAVIC is modelled after NASA's distributed propulsion system. This system is not yet fully developed, as it is still in the prototyping phase. The first prototype was successful but not to scale and unmanned. For this reason there is still time required for development. It is expected that by the time the HAVIC will enter the detailed design phase, this technology will be sufficiently developed to incorporate it in the design. This technology is crucial for the HAVIC, as it allows for a significant reduction in wing size, which is necessary due to road size constraints. If this technology is not ready in time, this might cause a delay in the production of the vehicle.

[7] http://content.icicidirect.com/mailimages/composites.htm [cited 19 June 2019]
[8] https://www.theregister.co.uk/2007/09/19/dreamliner_allegations/ cited 19 June 2019
[9] https://www.boeing.com/commercial/aeromagazine/articles/2011_q1/4/ [cited 19 June 2019]
[10] https://www.forbes.com/sites/stephenrice1/2019/01/07/would-you-fly-on-a-plane-without-a-human-pilot/3e15e8142518 [cited 19 June 2019]

Conclusion and Recommendations

In this chapter, a conclusion is given which is followed by recommendations for further development and research.

Conclusion

To this day, both ground and air transport are still major contributors for worldwide carbon emissions. Industry's transition from fossil fuels to more sustainable forms of energy is moving slowly, while at the same time more and more roads are being built to deal with congestion. Therefore there is a need for a viable alternative.

A new sort of vehicle which can travel on roadways and fly, while generating zero harmful emissions is introduced to reach this goal. This vehicle is called the HAVIC. The HAVIC uses state of the art technologies such as liquid hydrogen as a power source and distributed propulsion for optimal performance. The design of the subsystems of the HAVIC are extensively looked into, using an iterative design method, and are then extensively verified and validated. This lead to an integrated design with the required performance. An overview of the specifications of this vehicle is presented in Table 15.3.

Table 15.3: Specification overview of the HAVIC

OEW	1292 kg
Payload	360 kg
Max. Fuel Weight	21.8 kg
Vehicle Length	5.45 m
Vehicle Width	2.40 m
Capacity	3 passengers + 1 pilot
HLPs	8 props (574 mm diameter)
CPs	2 props (1524 mm diameter)
Engines	8 × Custom H20 (20 kW) and 2 × Custom H60 (60 kW)
Powerplant	2 × Powercell S3 Proton Exchange Membrane Fuel Cell (125 kW)
Fuel Type	Liquid hydrogen
Unit Cost	2.2 million USD
Cruise Speed	250 km/h
Stall Speed	92.4 km/h
Driving Speed	80 km/h
Maximum Acceleration	2.5 m/s^2
Flying Range	400 km
Driving Range	100 km
Cruise Altitude	1219.2 m (4000 ft)
Take-Off Length	428.6 m
Optimum RC	430.8 m/min

The HAVIC is a concept design which needs further development and research. Distributed propulsion and hydrogen fuel cell technology is still at an early stage. It has been found that the design of the HAVIC is very sensitive to the efficiency of these technologies. It is expected that these technologies will both be developed further by the industry in the future.

As of right now, current infrastructure is not yet designed for hydrogen-powered flying cars. Liquid hydrogen refuel stations cannot be found at many locations, and in fact the production of liquid hydrogen must still be optimised in order to meet the increasing demand in a sustainable manner. Current airports would need some minor adjustments to allow for smooth take-off and landing of several HAVIC vehicles in a given day. Should the flying car be widely accepted, significantly more small airfields have to be build. At the same time,

regulations still form a limitation to the HAVIC. For example, the requirement to submit a flight plan before every flight limits the flexibility of the HAVIC. However, with a wider acceptance of the flying car, regulations will adjust.

Although the HAVIC concept by itself might not be a complete solution to the transportation problems we are facing today. The group believes that the HAVIC vehicle shows what is possible with current day technologies. The HAVIC shows a sustainable concept that poses creative, alternative solutions to current day problems with infrastructure, using the state of the art technology from the aviation and automotive industry.

Recommendations for Further Development

As this design stage holds preliminary design, improvements and better simulations can still be made in further design phases, which are mentioned here. For all structural elements, topology optimisation should be used to reduce mass. The most important subsystems for which this should be done are the wing box, vertical tail structure, and chassis. For ground performance, it would be beneficial for controllability purposes to try to move the c.g. down as much as possible and decrease the length of HAVIC, or at least keep this values as low as they are right now. For the body shape, wing shape, and air intake of the fuel cell, Computational Fluid Dynamics (CFD) models should be ran in late stages of design to verify and optimise. The models should also analyse the performance of the High-Lift and Cruise propellers and give a load distribution along the wing. The modelled load distribution can then be used to do a torsion analysis on the wing box. The fuel cell should be further verified and validated as the cell is not yet in production. For control and stability, simulations such as for example a state space model should be used to check for longitudinal static stability using a given pitch input. The same analysis holds for yaw and roll stability, using rudder and aileron inputs.

Bibliography

[1] Working Group III. “Climate Change 2014: Mitigation of Climate Change”. In: (2014).

[2] Airbus. “Global Market Forecast”. In: (2018).

[3] Vladislav Borodulin Vitaly S. Guzhva Tamilla Curtis. “Market Analysis for Small and Mid-Size Commercial Turboprop Aircraft”. In: (2013).

[4] Amsterdam Airport Schiphol. “Airport Charges and Conditions”. In: (2019).

[5] *CES Edupack*. Ver. 18.1.1. Cambridge, UK: Granta Design Limited, 2018.

[6] Aerospace Productions Department TU Delft. *Chapter 1: Introduction*. TU Delft.

[7] Aerospace Productions Department TU Delft. *Chapter 9: Quality system in Aerospace industry*. TU Delft.

[8] R. Carriveau. *Fundamental and Advanced Topics in Wind Power*. 1st. InTech, 2011. ISBN: 9789533075082.

[9] S. Gudmundsson. “The Anatomy of the Propeller”. In: *General Aviation Aircraft Design* (2014).

[10] D. Scholz M. Nita. “Estimating The Oswald Factor From Basic Aircraft Geometrical Parameters”. In: *Hamburg University of Applied Sciences* (2012), p. 4.

[11] O.K. Bergsma, J. Sinke, and C.A.J.R Vermeeren. *Materials & Manufacturing 2*. TU Delft, 2006.

[12] Dr C. Rans and Dr S. Teixiera de Freitas. “Bending Deflection”. In: *TU Delft Lecture Slides* (2007).

[13] W. Callister Jr. and D. Rethwisch. *Materials Science and Engineering*. 9th. Wiley, 2015.

[14] Gurit Company. “Guide to Composites”. In: (2010).

[15] M. Ashby. *Materials Selection in Mechanical Design*. 4th. Elsevier, 2011.

[16] Scott Whitney. “Vibration of Cantilever Beams”. In: (1999).

[17] Queen Mary’s University London. “Lagrange Equations and D’Alemberts Principle”. In: (2004).

[18] Aerospace Specification Metals Inc. “Titanium Ti-6Al-4V (Grade 5), Annealed Data Sheet”. In: (2015).

[19] Dr. Fabrizio Oliviero. *Aerospace Design & System Engineering Elements II - Lecture Slides*. Delft University of Technology. 2018.

[20] J. Roskam. *Airplane Design IV: Layout of Landing Gear and Systems*. 6th. DARcorporation, 2010. ISBN: 978-1-884885-53-2.

[21] Federal Aviation Registration. “FEDERAL AVIATION REGULATIONS”. In: Part 23 - AIRWORTHINESS STANDARDS: NORMAL, UTILITY, ACROBATIC, AND COMMUTER CATEGORY AIRPLANES ().

[22] S.F. Hoerner. *Fluid - dynamic drag*. Hoerner Fluid Dynamics, 1965.

[23] Henry Dreyfuss Associates Alvin R. Tilley. *The Measure of Man and Woman: Human Factors in Design, Revised Edition*. 1st. John Wiley & Sons, Inc., 2001.

[24] Dr. Fabrizio Oliviero. *AE3211-I System Engineering and Aerospace Design - Lecture Slides*. Delft University of Technology. 2019.

[25] Daniel P. Raymer. *Aircraft Design: A Conceptual Approach*. 1st. American Institute of Aeronautics and Astronautics, Inc., 1992. ISBN: 0930403517.

[26] Mohammad H. Sadraey. *Aircraft Design. A Systems Engineering Approach*. John Wiley & Sons, 2013.

[27] Materials Advisory Board - Division of Engineering. *Trends in Usage of Beryllium and Beryllium Oxide*. 1st. National Academy of Engineering, 1972.

[28] Jens Bachmann, Carme Hildago, and Stéphanie Bricout. “Environmental analysis of innovative sustainable composites with potential use in aviation sector - A life cycle assessment review”. In: *Science China Technological Sciences* 60 (Sept. 2017).

[29] S.M. Satheesan. “Bird-aircraft collision at an altitude of 2424 m over the sea”. In: *Journal of the Bombay Natural History Society* 87 (1990), pp. 145–147.

[30] Transport Canada. *Sharing the Skies*. Government of Canada, 2013.

[31] R.C. Alderliesten. *Structures: Aircraft & spacecraft shell structures*. Nov. 2011.

[32] J. Ramage. *Energy: A Guidebook*. 1st. New York Oxford University Press, 1983.
[33] J. Larminie and A. Dicks. *Fuel Cell Systems Explained*. John Wiley and Sons, 2000.
[34] Christopher Winnefeld et al. "Modelling and Designing Cryogenic Hydrogen Tanks for Future Aircraft Applications". In: (2018).
[35] Dries Verstraete. "The Potential of Liquid Hydrogen for long range aircraft propulsion". PhD thesis. Cranfielf University, Apr. 2009.
[36] Ilias Tapeinos. "Multi-Spherical Composite-Overwrapped Cryogenic Tanks for Hypersonic Aircrafts". PhD thesis. Delft University of Technology, 2019.
[37] Subodh K. Mital et al. *Review of Current State of the Art and Key Design Issues With Potential Solutions for Liquid Hydrogen Cryogenic Storage Tank Structures for Aircraft Applications*. NASA, 2006.
[38] T.S. Gates et al. "Facesheet delamination of composite materials at cryogenic temperatures". In: *Composites Science and Technology* 66 (2006), pp. 2433–2435.
[39] M.B. Djukic et al. "Hydrogen damage of steels: A case study and hydrogen embrittlement model". In: *Engineering Failure Analysis* 58 (2015), pp. 485–498.
[40] S.M. Arnold et al. "Spherical Cryogenic Hydrogen Tank Preliminary Design Trade Studies". In: (2007).
[41] A. Godula-Jopek, W. Jehle, and J. Wellnitz. *Hydrogen Storage Technologies, New Materials, Transport and Infrastructure.* Wiley-VCH, Oct. 2012.
[42] ICAO. *Technical Provisions for Mode S Services and Extended Squitter*. 2nd. International Civil Aviation Organization, 2012. ISBN: 9789292490423.
[43] RTCA. *Minimum Operational Performance Standards for Universal Access Transceiver (UAT) Automatic Dependent Surveillance – Broadcast*. 1st. RTCA, 2004.
[44] Dieter Scholz. "Aircraft Design". PhD thesis. Hamburg University, 2015.
[45] L. Bertsch, D. Simons, and M. Snellen. "Aircraft Noise: The major sources, modellÈng capabilities, and reduction possibilities". In: (2015).
[46] S.M. Haasdijk. "Aircraft Noise Prediction". In: (2016).
[47] Dr. B. Henderson and D. Huff. *Electric Motor Noise Status*. NASA Acoustics Technical Working Group. 2017.
[48] J.E. Marte and D.W. Kurtz. "A Review of Aerodynamic Noise From Propellers, Rotors, and Lift Fans". In: (1970).
[49] G.J.J. Ruijgrok. *Elements of Aviation Acoustic*. 2004.
[50] S. Mahajan and R. Rajopadhye. "Transportation Noise and Vibration-Sources, Prediction, and Control". In: (2013).
[51] E. Hammer and E. Bühlmann. "The noise reduction potential of "silent tyres" on common road surfaces". In: (2018).
[52] P. Lasanga et al. "Landing Approach Airframe Noise Measurements and Analysis". PhD thesis. NASA, 1980.
[53] Dr. Ir. M. Voskuijl. *Flight Mechanics - Lecture Slides*. Delft University of Technology. 2012.
[54] Steve Quinn. "General Aviation - Climbing". In: (2011).
[55] M.M. Shah. "Sustainable Development". In: *Encyclopedia of Ecology* (2008), pp. 3443–3446.
[56] S. Corwin et al. "The Future of Mobility". In: *Deloitte University Press* (2015).
[57] S. Melendi-Espina1 et al. "RECYCLING OF CARBON FIBRE COMPOSITES". In: (2016).
[58] x.l. yan and R. Hino. "Nuclear Hydrogen Production Handbook". In: (2011).
[59] NASA. "Resource Management and Contingencies in Aerospace Concurrent Engineering". In: (2019).
[60] W. Verhagen and E. Mooij. *Project Management and System Engineering in the DSE - PMSE Lectures*. Delft University of Technology. 2019.
[61] U.S. Department of Energy - Technical Report. "Cost Estimating Guide". In: (2011).
[62] J. Markish. "Valuation Techniques for Commercial Aircraft Program Design". In: (2002).
[63] J. Roskam. *Airplane Cost Estimation: Design, Development, Manufacturing and Operation*. Roskam Aviation and Engineering Corporation, 1990.
[64] C.S. Lopes et al. "Multiscale virtual testing: the roadmap to efficient design of composites for damage resistance and tolerance". In: *CEAS Aeronautical Journal* 7.4 (Dec. 2016), pp. 607–619.

[65] D. Hao et al. “An Improved Empirical Fuel Cell Polarization Curve Model Based on Review Analysis”. In: *International Journal of Chemical Engineering* (2016).

[66] S. Fraser and V. Hacker. “An empirical fuel cell polarization curve fitting equation for small current densities and no-load operation”. In: *Journal of Applied Electrochemistry* 38 (2008).

[67] T. Diepenhorst et al. *Fuel Cell Air Intake System*. Tech. rep. Michigan Engineering, 2009.

[68] G. Arnold and J. Wolf. “Liquid Hydrogen for Automotive Application Next Generation Fuel for FC and ICE Vehicles”. In: *Journal of Cryogenics and Superconductivity Society of Japan* Vol. 40 No. 6 (2005).

[69] Franz-Josef Wetzel. “Improved Handling of Liquid Hydrogen at Filling Stations: Review of Six Years Experience”. In: 23 (1998).

[70] M. Melaina and M. Penev. *Hydrogen Station Cost Estimates*. NREL, Sept. 2013.

[71] G. Arnold and J. Wolf. “Liquid Hydrogen for Automotive Application”. In: *TEION KOGAKU* (2005).

[72] Jos Sinke. *Production of Aerospace Systems: Assembly*. Mar. 2019.

[73] N. Shama Rao et al. *Carbon Composites Are Becoming Competitive and Cost Effective*. 2018.

[74] TU Delft. *Chapter 5: Processes for thermoplastic and thermoset composites*. TU Delft.

[75] J.S. Hayward and B.Harris. “The effect of vacuum assistance in resin transfer moulding”. In: *Composites Manufacturing* 1 (Sept. 1990).

[76] S. Milton and S.M. Grove. “Composite Sandwich Panel Manuacturing Concepts for a Lightweight Vehicle Chassis”. In: *ACMC, University of Plymouth* ().

[77] Shur-Lok Cooperation. “Advanced Composites Catalog”. In: *Shur-Lok catalog* ().

[78] Aerospace Productions Department TU Delft. *Chapter 7: Riveting and Bolting*. TU Delft.

[79] Shur-Lok. *Advanced Composites Catalog*.

[80] A. Mehta1 et al. “Solar Aircraft: Future Need”. In: *International Journal of Advanced Engineering Technology* 1 (Dec. 2012).

[81] *Flight international: Boron composites*. June 1973.

[82] David J. Wing and William B. Cotton. “For Spacious Skies: Self-Separation with “Autonomous Flight Rules” in US Domestic Airspace”. In: (2019).